Thermo-hydro-mechanical characterisation of London clay

A thesis submitted to the Imperial College London in partial fulfilment of the requirements for the degree of Doctor of Philosophy

by

Sihua Chen

Department of Civil and Environmental Engineering

Imperial College London

March 2022

Declaration

The work presented in this thesis was carried out in the Department of Civil and Environmental Engineering at Imperial College London. This thesis is the result of my own work and any quotation from, or description of the work of others is acknowledged herein by reference to the sources, whether published or unpublished. This thesis is not the same as any that I have submitted for any degree, diploma or other qualification at any other university. No part of this thesis has been or is being concurrently submitted for any such degree, diploma or other qualification.

Sihua Chen

London, March 2022

Abstract

Geothermal energy has been increasingly utilised in recent years to meet the sustainability targets of civil engineering structures. Ground Source Energy Systems (GSESs) that make use of low enthalpy geothermal energy have been shown to be efficient in providing low carbon heating and cooling to structures. To better understand the impact of the Ground Source Energy Systems on the surrounding ground, it is important to obtain high-quality laboratory testing data regarding the thermo-hydro-mechanical (THM) behaviour of soils.

Three pieces of temperature-controlled testing equipment designed at the Imperial College Geotechnical Laboratory were used in this research. i) The existing isotropic apparatus was enhanced with the installation of a mid-height pore pressure probe, to enable accurate monitoring of pore water pressure changes at different locations of the soil specimen during multiple cycles of heating and cooling. ii) A new thermal triaxial apparatus with a double load-cell measuring system was developed to enable the shearing of soil specimens at both ambient and elevated temperatures. iii) A new oedometer apparatus with a thermal bath was developed for the measurement of compression properties of London clay under different temperature levels.

Thermal and mechanical calibrations have been performed on the instrumentation and are presented in this thesis. Procedures of how the measured and calculated values are obtained and how the calibration curves are determined are explained. Trail tests with dummy samples and real soil tests have been performed to validate the calibration and to assess the calibration errors. Consistent protocols for thermal testing of clays are developed and documented here. Corrections are applied to the data where appropriate. The assumptions and expressions used for corrections are presented. The design of the equipment, thermal and mechanical calibrations, testing procedures and corrections for data processing presented in this thesis can be used as a reference to perform thermal testing on soils in the future.

The effect of temperature on the behaviour of London clay has been investigated and presented. Some key aspects of the soil behaviour, including compression characteristics, preconsolidation pressure, volume change, strength, stiffness and pore water pressure, have been evaluated. Soil behaviour observed in this research have been compared with that from the same or other clays in published work. Results obtained in this research could be used to calibrate appropriate constitutive models, for example, the fully coupled thermal model in the Imperial College Finite Element Program (ICFEP).

Acknowledgements

First of all, I would like to thank my supervisors, Prof. Lidija Zdravković and Dr. J. Antonio H. Carraro, for their patient guidance, constructive comments and suggestions for each and every progress that I have made, for their support and encouragement to me along the way.

I am grateful to Steve Ackerley, who inspired me with lots of ideas on the design and improvement of the equipment. This project would not have been running smoothly without his help. I would also like to express my gratitude to Graham Keefe and to Stef Karapanagiotidis, who provided me with technical support.

Special thanks to Prof. Jamie Standing, for always encouraging me and always being very nice.

Meanwhile, I am thankful to other staff and PhD students in the Geotechnics research group, for generously sharing their knowledge and expertise, for the great time we had together.

The research presented in this thesis was funded by Chinese Scholarship Council. This financial support is greatly acknowledged.

Table of Contents

List of Figures

List of Tables

List of Symbols

Abbreviations

$ASTM$	American society for testing and materials
$BPVG$	Back pressure volume gauge
BS	British standard
$GSES$	Ground source energy system
LL	Liquid limit
$LVDT$	Linear variable differential transformer
NC	Normally consolidated
NCL	Normal compression line
OC	Overconsolidated
OCR	Overconsolidation ratio
PI	Plasticity index
PL	Liquid limit
THM	Thermo-hydro-mechanical

Alphabet

Greek characters

α_s	Thermal expansion coefficient of soil skeleton
α_w	Thermal expansion coefficient of water
ε_a	Axial strain
ε_v	Volumetric strain
$\varepsilon_{v,T}$	Thermal volumetric strain
ρ_d	Dry density

Latin characters

e	Void ratio
p'	Mean effective stress
p'_c	Preconsolidation pressure
q	Deviatoric stress
v	Specific volume
E_{sec}	Secant stiffness
G_s	Specific gravity
T	Temperature
V	Volume of the sample
V_{dr}	Volume of drained water
V_s	Volume of soil skeleton
V_w	Volume of water

Chapter 1: Introduction

1.1 Research background

The design of buried thermo-active structures, such as foundations, retaining walls and tunnel linings, depends on the thermo-hydro-mechanical behaviour of the surrounding soil under temperature changes imposed by their operation (Gawecka et al. 2017, Sailer et al. 2018). Below a certain depth (usually 10-15 m, depending on the local climate), the soil temperature remains nearly constant throughout the year (Busby et al. 2009, Banks 2012). Therefore, there is a difference in temperature between the ground and buildings above. The ground can act as a heat source during the winter and as a heat sink during the summer. The interface between the thermo-active structures and the surrounding soil is subjected to heating-cooling cycles from ambient temperature up to 40 °C (Brandl 2006, Hamada et al. 2007, Wood et al. 2009, Yavari et al. 2014, Li et al. 2018). Abuel-Naga et al. (2007) found that normally consolidated and lightly over-consolidated soft Bangkok clay contracted upon heating, while heavily over-consolidated specimens of the same soil dilated. In addition, the thermally induced pore water pressure was affected by the magnitude of the applied mean effective stress and stress history. A range of results for other clays is available from Hueckel and Baldi (1990) (Pontida clay, Pasquasia clay), Sultan et al. (2002) (Boom clay), Cekerevac and Laloui (2004) (kaolin), and Martinez-Calonge (2017) (London clay), with often contradicting evidence on the effect of temperature on the mechanical properties of the clays tested. Such uncertainties are stalling the more widespread application of thermo-active structures for heating and cooling of buildings. Consequently, there is a need for a systematic experimental investigation of clay soils with a range of innovative geotechnical testing equipment to develop a consistent framework of clay behaviour under temperature changes, in order to unlock the great potential of ground heat as a renewable energy source.

1.2 Research objectives

This research aims to characterise the thermo-hydro-mechanical behaviour of reconstituted London clay for the design of thermo-active structures. The research addresses the following issues:

-Thermally-induced pore water pressures: The existing isotropic apparatus is enhanced with the installation of a mid-height pore pressure probe, in addition to conventional pore water pressure measurement at the base of the specimen, to enable accurate monitoring of pore water pressure changes during multiple cycles of heating and cooling.

-Effect of temperature on strength and stiffness: A new thermal triaxial apparatus with a double load-cell measuring system (to compensate for temperature effects) is developed to enable the shearing of London clay specimens at both ambient and elevated temperatures.

-One-dimensional compression: A new oedometer apparatus with a thermal bath is developed for the measurement of London clay compressibility under temperature changes.

-Testing protocols: Consistent procedures for thermal testing of clays are developed and documented.

-Temperature-based calibrations: Procedures for temperature-based calibration of instrumentation are established and validated.

1.3 Thesis layout

This thesis has seven chapters. Chapter 1 introduces the research background, research objectives and explains the layout of the thesis.

Chapter 2 reviews the relevant literature on thermal testing of soils. The first section presents a bibliographical review of the testing equipment that has been used in research internationally to characterise the thermo-hydro-mechanical behaviour of saturated soils. It also provides information on temperature-based calibrations of the equipment and types of soil tested in these schemes. The second section presents some key findings of soil behaviour using equipment described in the previous section.

Chapter 3 presents the methodology applied in this research. First, three pieces of temperature-controlled equipment are presented, including the temperature-controlled triaxial cell, isotropic cell and oedometer cell. The need for temperature-based calibrations of instrumentation is presented. Secondly, the source, geological history, mineralogy and some of the mechanical properties of London clay, as the main testing material, are described. Thirdly, the sample preparation process is presented. This includes the preparation of slurry-consolidated London clay and the reconstituted London clay cake. Finally, experimental procedures for tests using each of the equipment are described.

Chapter 4 presents the results of laboratory tests performed on specimens of isotropically consolidated reconstituted London clay, to investigate the thermally-induced pore water pressures under undrained conditions. The focus of this chapter is to quantify the mobilisation of excess pore water pressure in a saturated clay, following cycles of heating (from ambient temperature, $T_{am} = 20^{o}\mathrm{C}$, to a maximum of $T_{max} = 40^{o}\mathrm{C}$) and cooling (back to ambient

temperature). The importance of understanding the evolution of excess pore water pressure is the effect that this has on reducing the effective stresses in the ground in the short term.

Chapter 5 investigates the effect of temperature change on the volumetric strains, strength and stiffness of the saturated reconstituted London clay. Laboratory tests were performed in the temperature-controlled triaxial apparatus on specimens trimmed from reconstituted London clay cakes.

Chapter 6 elaborates on the programmes of oedometer tests performed on slurry-deposited London clay and on specimens from a reconstituted London clay cake. Temperature, ranging from ambient to 60 °C, was applied during virgin consolidation, unloading / reloading cycles and creep periods. The temperature effect on the compression characteristics of the clay was interpreted from these experiments. The compression characteristics discussed in this chapter include compression and swelling indices (C_c and C_s) and pre-consolidation pressure (σ'_{vc}).

Chapter 7 summarises the main conclusions of this research and gives suggestion for future research.

Chapter 2: Literature review

2.1 Introduction

This chapter introduces a focused overview of existing experimental laboratory set ups, used for the investigation of thermal characteristics of saturated soils. The review addresses in particular temperature controlled oedometer and triaxial apparatus, as this type of equipment was used in the research presented in this thesis. The second focus of the review is on the interpretation of the thermo-hydro-mechanical behaviour of soils from such experiments and difficulties involved with the temperature effects on both the soil but also on the equipment and instrumentation.

2.2 Testing equipment for characterising the thermo-hydro-mechanical behaviour of saturated soils

This section presents a bibliographic review of the testing equipment that has been used in research internationally to characterise the thermo-hydro-mechanical behaviour of saturated soils. The focus is on how heating and cooling were achieved in the testing equipment and what special design the equipment had in order to accommodate the elevated temperature in a controlled manner, compared to the conventional testing equipment. Many of the experimental studies relied on temperature-controlled triaxial or isotropic apparatus (e.g. Campanella and Mitchell, 1963, 1968; Hueckel and Baldi, 1990; Martinez-Calonge, 2017), while a few researches used thermal and hydraulic conductivity cells or oedometer apparatus (e.g. Eriksson, 1989; Boudali et al., 1994). Temperature-controlled triaxial or isotropic apparatus and oedometer apparatus are discussed in this section, as they are more relevant to the research discussed in this thesis.

2.2.1 Temperature-controlled oedometer apparatus

During the early stage of characterisation of the thermo-hydro-mechanical behaviour of soils, oedometer cells were used for laboratory testing by placing heating elements in the water surrounding soil specimens (Gray, 1936; Finn, 1951; Paaswell, 1967; Plum and Esrig, 1969). Oedometer tests were performed to investigate the effects of temperature on the one-dimensional compression characteristics of soils. These can be used as design parameters for evaluating settlement of soils under vertical load. Temperature variations of 5°C to 80 °C were principally applied, avoiding the phase changes at freezing and boiling points of water. Subsequently, further developments have taken place to conventional oedometer devices to accommodate tests on unsaturated soils, for the purpose of investigating compacted clays used in nuclear waste disposal (Romero, 1999; Romero et al., 2001; Villar, 2004; Romero et al.,

2005). Due to the expansion and contraction of oedometer rings with temperature changes, together with the thermal deformation of soil samples, the usual assumption of zero lateral strain may not hold (Casagrande 1936; Becker et al. 1987; ASTM 2004; Duffy, 2012). Interpretation of the experimental data relies on temperature-based calibrations and further assumptions (Finn, 1952; Towhata et al. 1993; Romero, 1999; Abuel-Naga et al., 2005; Frąncois and Laloui, 2010; Shariatmadari and Saeidijam, 2011; Ye et al., 2012; Vega and McCartney, 2015; Favero et al., 2016; Ng et al., 2017). In this section, the equipment, tested soil and temperature-based calibration are presented, while test results are summarised in Section 2.3.

Gray (1936) pioneered in performing probably the first isothermal consolidation tests on a fine-grained soil, at two temperature levels, 10 °C and 22 °C. Few details can be found in the literature regarding the equipment or the soil.

Finn (1952) at the University of California (USA) described temperature-controlled oedometer tests performed at four temperature levels, 4.4°C (40°F), 10°C (50°F), 21.1°C (70°F) and 26.7°C (80°F). Accuracy of the temperature control system was not explicitly stated. The oedometer cell could accommodate a soil specimen with 50.8 mm (2 in) in diameter and 12.7 mm (½ in) in height. The maximum pressure that could be applied was 861 kPa (8 tons per sq ft). The tested soil was described as 'slightly organic silt or clay with high compressibility' with a liquid limit of 64% and a plastic limit of 38%. It was remoulded to a saturated condition and then put into a consolidometer ring made of stainless steel. For tests that were not performed at ambient temperature, equipment and the soil was precooled to temperature below ambient temperature or preheated to the desired temperature that the tests would be performed at, before they were placed in temperature-controlled rooms for testing. Since the consolidation tests were performed under isothermal loading, no further thermal expansion or contraction of the equipment would occur during the consolidation tests. Due to the size of these rooms, only small and portable oedometer cells could be used.

Towhata et al. (1993) at the University of Tokyo (Japan) presented a temperature-controlled consolidation apparatus, as shown in Figure 2-1. Temperature varied from 20 to 90 °C. Temperature of the soil specimen was controlled by the temperature of the water circulated in a water bath around the sample, which was heated by a thermostatically controlled heater inserted in the water bath, with an accuracy of ±2 °C. A glass plate was put on top of the water bath to reduce water evaporation. Water was stirred continuously by an electrical propeller to make water temperature more homogeneous in the bath. The bath was connected to a larger

tank that compensated for the water lost by evaporation. Calibration was performed by measuring the thermal deformation of the apparatus after a long time elapsed in hot water. Details of what exactly were measured, and after what time, for what temperature changes, were not specifically stated by Towhata et al. (1993). The transient thermal deformations of the apparatus could not be calibrated precisely, but this was considered adequate for the purpose of characterising consolidation behaviour of soil in a steady state of temperature field. It was found that the radial deformation of the confining ring was negligible for calculating the radial strain of the soil. Two fine-grained soils were tested. The first type of soil was called 'MC clay' (LL = 70%, PL = 41%, IP = 29%, Gs = 2.751, WC = 160%), which had a similar mineral composition as kaolin clay. The second type of soil was bentonite (LL = 450%, PL = 29%, IP = 421%, Gs = 2.785, WC = 700%).

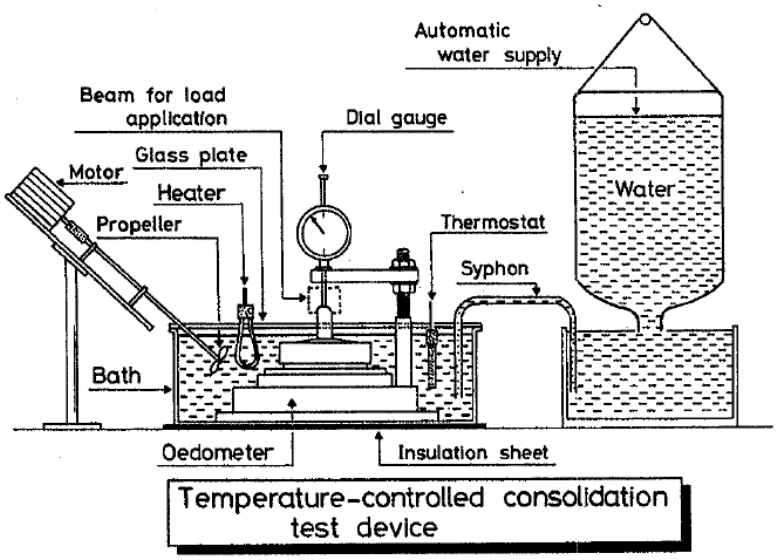

Figure 2-1: Schematic view of a temperature-controlled consolidation apparatus at the University of Tokyo (from Towhata et al. 1993)

Romero (1999) at the Polytechnic University of Catalonia (Spain) developed an oedometer cell where both temperature and suction could be controlled and measured. A schematic view of the apparatus is shown in Figure 2-2. Temperature of the cell was increased by a thermostatically controlled heater, to give better control of the temperature. The heater of 500W at 200V was submerged in a silicone oil bath that surrounds the oedometer cell. Silicone oil was chosen as the cell fluid due to its low electrical conductivity. Deformation of the apparatus with changes in temperature was calibrated, at net vertical stresses of 26 kPa and 85 kPa, by measuring the thermal deformations of ceramic disc and porous stone, loading head, measurement frame and dial gauge. It was found that thermal deformations of the apparatus did not have significant effect on the lateral strain or the volumetric response of the specimen, and that the transient thermal deformations during heating or cooling could not be calibrated

accurately, similar to what was reported by Towhata et al. (1993). Radial deformation of the confining ring was quantified. The internal diameter of the confining ring was measured using a bore gauge and then related to an equivalent vertical displacement of the soil specimen. Details of this correction is shown in Section 3.8.4. Tests were performed at 22° C and 80° C. Axis translation technique was applied using a ceramic porous disc with an air entry pressure of 0.5 MPa. A constant air pressure of 0.5 MPa was maintained while water pressure was varied to achieve the target value of suction. Soil tested was unsaturated Boom clay (LL = 56%, PL = 29%, IP = 27%, G_s = 2.70). Romero (1999)'s work focused more on the effect of temperature on coefficient of permeability, water retention and swelling capacity. These are not the focus of this research and will not be discussed in Section 2.3.

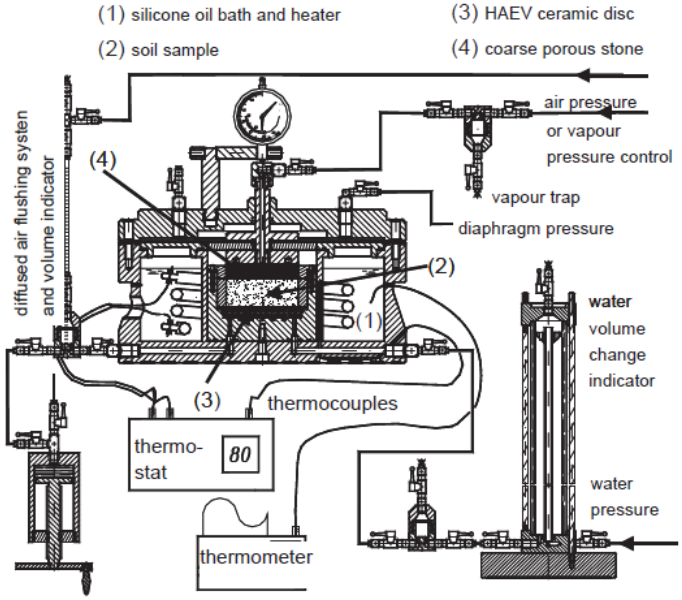

Figure 2-2: Schematic view of a temperature-controlled oedometer cell at the Polytechnic University of Catalonia (from Romero et al. 2005)

Abuel-Naga et al. (2005) at the Asian Institute of Technology, Thailand, described an oedometer cell to study the thermo-mechanical behaviour of soils. A schematic view of the apparatus is shown in Figure 2-3. A 600W ring heater was attached to the outer ring of the oedometer. The heater was designed to be in a ring shape with the aim to heat the specimen evenly, although the homogeneity of the temperature field was not presented by Abuel-Naga et al. (2005). Heating of the soil specimen was achieved by heating the water between the outer ring and the inner ring confining the specimen. A thermocouple placed in the annular space in the water was used for measuring the temperature and providing feedback to the control unit. After temperature in the water bath reached and maintained a constant value, the centre of the soil specimen could reach the target temperature in 25 minutes, measured by a thermocouple

embedded in the specimen centre. Hot water at the same temperature as that in the water bath was supplied to the oedometer cell to compensate for water evaporation during the test. Difference in the readings between that from the thermocouple place in the annular space in the water, and that placed in the specimen centre, was measured and calibrated. Specimen could be heated to 90° C with an accuracy of ±0.1°C. Calibration tests were performed to quantify the thermal deformation of the apparatus. The vertical deformation of the apparatus was tested at different temperature and stress levels, without soil specimens. The radial deformation of the oedometer ring made of stainless steel was measured directly after placing the ring in an oven at tested temperature for a long time. The measurements showed that the radial deformation of the ring was negligible in calculating the radial strain of the soil, similar to what was presented by Towhata et al. (1993). The material tested was soft Bangkok clay (LL = 103%, PL = 43%, IP = 60%, Gs = 2.68, WC = 90 to 95).

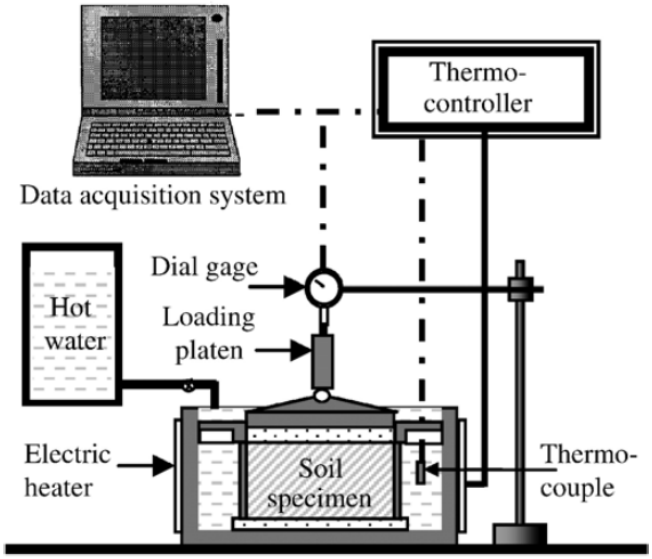

Figure 2-3: Schematic view of a temperature-controlled oedometer cell (Abuel-Naga et al. 2005)

Di Donna and Laloui (2015) at the Swiss Federal Institute of Technology (Switzerland) described a temperature-controlled oedometer cell that was capable of both heating and cooling, with a temperature range from 5 to 60 °C. Annotated photos of the apparatus are shown in Figure 2-4. Change in temperature was imposed by spiral tubes around the specimen. A thermostatically controlled heater was used to heat the water in the bath to the desired temperature. A pump circulated the heated or cooled water from the water bath to spiral tubes. Temperature inside the cell was monitored by a thermocouple. The cell was insulated with a polystyrene box. Water loss due to evaporation was compensated by a large water tank connected to the apparatus. Temperature-based calibration was performed on this apparatus. In this design, oedometer rings made of invar with a coefficient of thermal expansion of

5.5×10^{-7}°C were used to minimise thermal deformation of the cell in the radial direction. Therefore, the assumption of one-dimensional compression in standard oedometer tests was still valid. The tested soil was a saturated, medium-plasticity clay, referred to as Geneva clay (LL = 31.4% to 42.6%, PL = 20.1% to 24.2%, IP = 11.1% to 18.4%, Gs = 2.71 to 2.78, WC = 22.3% to 27.9%).

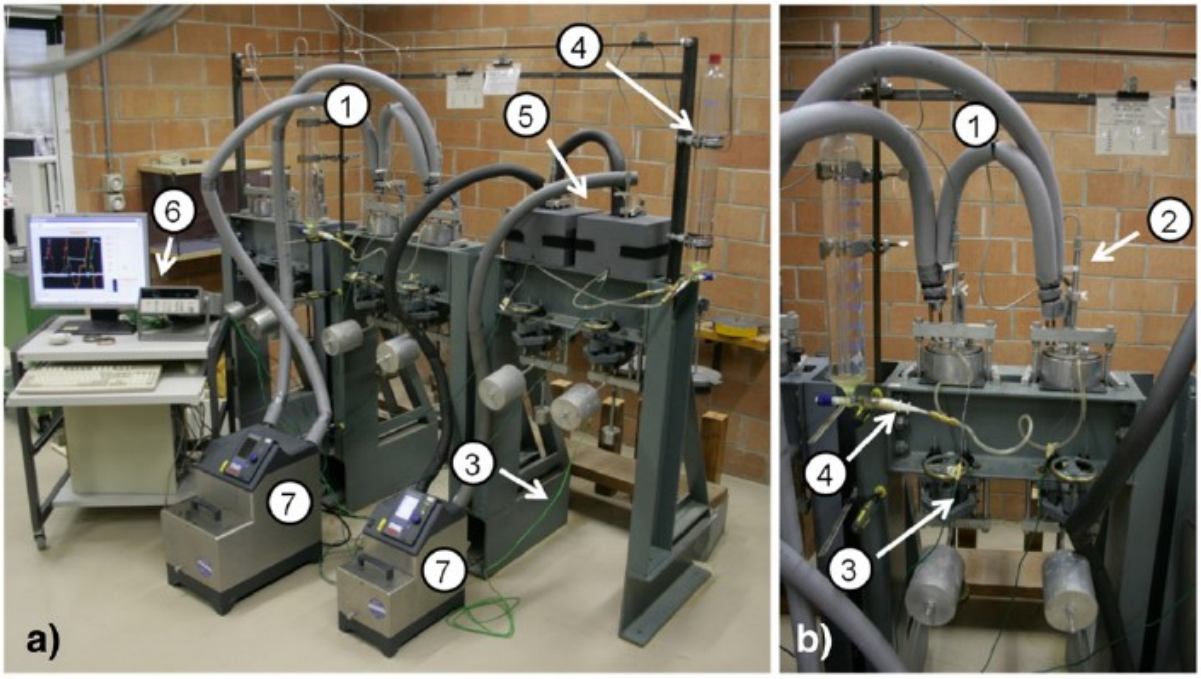

Figure 2-4: Schematic view of a temperature-controlled oedometer cell at the Swiss Federal Institute of Technology (a) global view and (b) detail. 1: tubes with circulating water at the desired temperature, 2: LVDTs, 3: thermocouples, 4: water supplier, 5: insulation, 6: acquisition system, 7: heaters. (Di Donna and Laloui 2015)

Vega and McCartney (2015) at the University of Colorado presented a temperature-regulated single-drainage oedometer cell, as shown in Figure 2-5. A special design of this cell is that it was contained within a pressure cell that was designed to saturate the soil specimen using back pressure before the consolidation process. A 4500W tubular coiled heater surrounding the stainless-steel confining ring was used to heat the specimen. A circulation pump helped to circulate the cell fluid and homogenise the temperature inside the cell. Temperature can be controlled from 18 to 91°C with an accuracy of ±0.5 °C. Another feature of this cell that differentiates it from other cells is that pore water pressure could be measured at the bottom of the specimen, using a differential pressure transducer. Free drainage was allowed at the top, but no drainage occurred at the bottom. Deformation of the apparatus under mechanical and thermal loading was evaluated. Thermal axial displacement of the apparatus was measured during a heating/ cooling cycle, with a steel dummy sample. The deformation of the dummy

sample was calculated based on its material properties and dimensions. This was subtracted from the measured axial displacement, to give the thermal axial displacement of the apparatus itself. Thermal radial displacement of the confining ring was also evaluated. Unlike previous researchers (Towhata et al., 1993; Romero, 1999; Abuel-Naga et al., 2005; Abuel-Naga et al., 2005), Vega and McCartney (2015) stated that the effect of thermal expansion of the confining ring may be significant, especially during cooling phase. During cooling, the contact between the ring and the soil increased, resulting in greater effect of the expansion of confining ring on the volume change of the soil. In addition, the heating/ cooling rate of the soil and confining ring might be different during transient stage and this effect could not be ignored. No direct measurement of the thermal expansion of the ring was presented by Vega and McCartney (2015) but theoretical calculation based on material properties was used. Material tested was Bonny silt (LL = 25 %, PL = 21 %, IP = 4 %, Gs = 2.63).

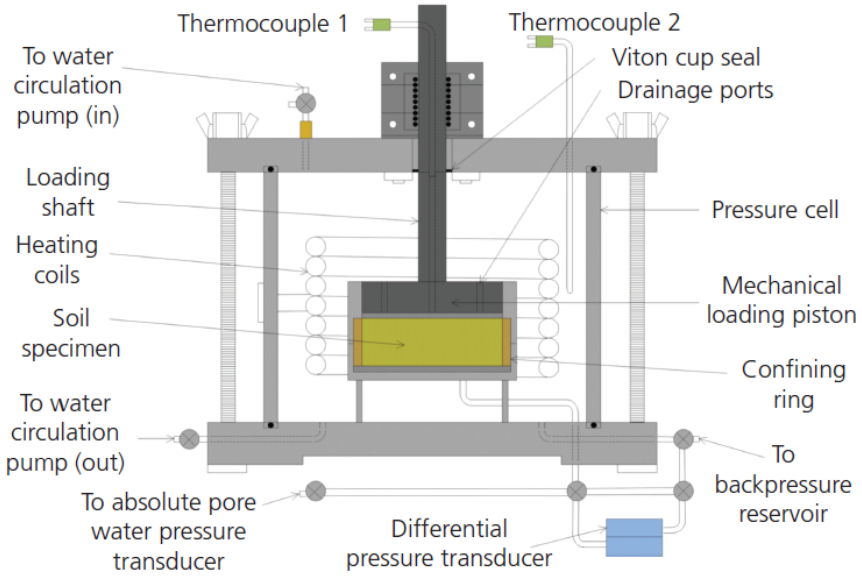

Figure 2-5: Schematic view of a temperature-controlled oedometer cell at the University of Colorado (Vega and McCartney 2015)

Favero et al. (2016) at the Ecole Polytechnique Fédérale de Lausanne described a temperature-controlled high-pressure oedometer cell, as shown in Figure 2-6. Heating was achieved using a 3 mm thick silicon heating mat that wrapped around the cell and was fixed in place with steel rings. The heating mat was composed of an electrical resistance placed between two layers of fibreglass impregnated with a silicon elastomer. Temperature was controlled in the range of 23 to 80 °C by changing the voltage level of the power supplier that connected to the heating mat. Three thermocouples with a resolution of 0.1 °C were used to measure the temperature. Two of them were located at the interface between the heating mat and the oedometer cell, and the

third one was inserted through the drainage line to be in contact with the soil specimen. Calibration tests were performed to obtain the relationship among the voltage level, the heater mat temperature and the cell temperature. The heating system was insulated from the environment with a layer made of silicone foam. Thermal deformation of the apparatus in the vertical direction under load at temperatures from 20 to 80 °C was measured using a steel dummy sample. It was found that the magnitude of the vertical stress did not have significant effect on the thermal deformation of the device. Radial deformation of the confining ring during heating was measured using four strain gauges. The measured thermal deformation of the apparatus was deducted from the total deformation when evaluating the volume change of the soil during non-isothermal paths. Drainage conditions at the top and bottom of the specimen were controlled using valves connected to drainage lines. Pore water pressure at the top and bottom of the specimen could be controlled and measured. Material tested was Opalinus clay (LL = 38%, PL = 23%, IP = 15%, G_s = 2.75).

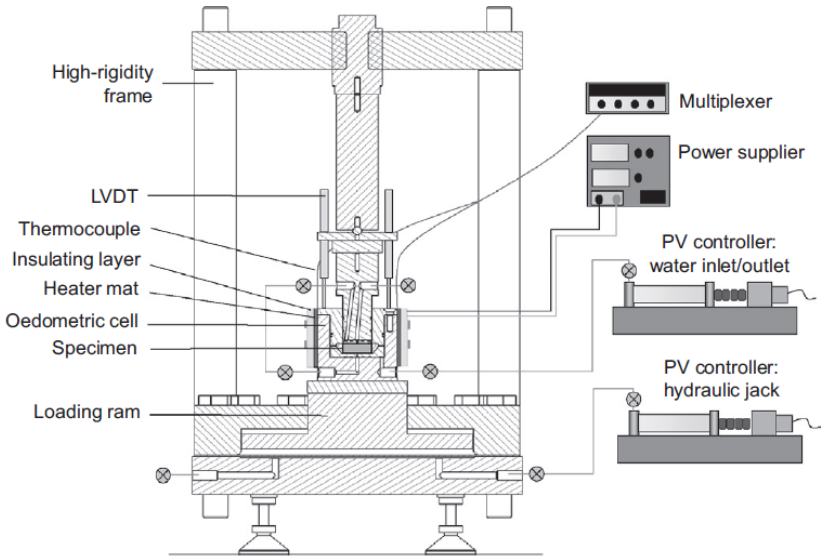

Figure 2-6: Schematic view of a temperature-controlled high-pressure oedometer cell at the Ecole Polytechnique Fédérale de Lausanne (Favero et al. 2016)

Sittidumrong et al. (2019) at the Kasetsart University (Thailand) described a temperature-controlled oedometer, as shown in Figure 2-7. The oedometer cell was placed in a water bath that circulated heated or cooled water to the inlet using a peristaltic pump. A thermistor was placed in the centre of the specimen during the calibration stage and the other thermistor was in the water bath. An Arduino microprocessor was used to regulate the flow of hot or cold water, depending on the target temperature set in the system and the current temperature measured by the thermistor. A special design of this system is that the water overflow from the cell was collected in a water storage which was pumped back to the water bath to maintain the

water level in the oedometer cell. The oedometer apparatus was insulated using expanded polystyrene (EPS) foam. Temperature can be controlled in the range of 28 to 50 °C. Accuracy or stability of the thermal performance of the system was not presented by Sittidumrong et al. (2019). A 15 mm thick steel dummy sample was used to calibrate the vertical thermal deformation of the apparatus and the diametrical thermal expansion of confining ring, at 22 °C, 55 °C and 85 °C. Hysteresis in the vertical thermal deformation was observed but it was not stated how this was accounted for in calculation. Diametric thermal expansion of the confining ring was not considered by Sittidumrong et al. (2019). Material tested was reconstituted and undisturbed Bangkok sand from a block sample (WC = 15.2%, G_s = 2.68). The soil was classified as a poorly graded sand with mainly quartz, small traces of mica, feldspar and kaolinite.

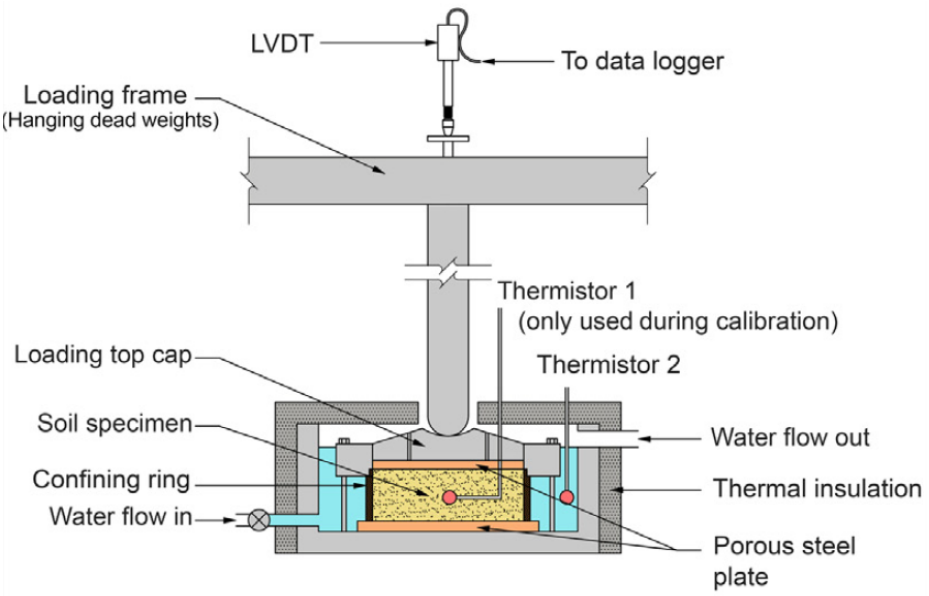

Figure 2-7: Schematic view of a temperature-controlled oedometer at the Kasetsart University (Sittidumrong et al. 2019)

2.2.2 Temperature-controlled triaxial and isotropic cells

Temperature-controlled triaxial and isotropic cells have been used in characterising the thermo-hydro-mechanical behaviour of soils. Compared to oedometer tests, drainage of the specimen can be controlled, and pore water pressure can be measured in triaxial tests. With an appropriate instrumentation, triaxial tests can also be used to evaluate the strength and stiffness of the specimen. Based on the manner in which the heat is applied to the specimen, Cekerevac et al. (2005) distinguished the temperature-controlled triaxial and isotropic cells into three categories, including circulating the confining fluid, lateral and/or external heaters and internal heaters.

Heating by circulating the confining fluid

Heating can be applied by circulating the confining fluid, for example water, for achieving temperatures up to 100 °C, or silicon oil for higher temperature. Campanella and Mitchell (1963) at the University of California (USA) developed the first temperature-controlled triaxial cell, as shown in Figure 2-8. The equipment allowed temperature variations ranging from 4.4 °C to 60 °C (40°F to 140°F) with an accuracy of ±0.27 °C (±0.5°F), by precooling or preheating water in the reservoir and circulating that water around the specimen (Figure 2-8 (a)). A thermocouple encased in a stainless-steel tube was inserted through the base pedestal to measure the temperature of the specimen. The triaxial cell units were placed in an air-filled insulation chamber with the temperature controlled by an air control thermostat (Figure 2-8 (b)). This heating system enabled the specimen to reach the target temperature in 20 minutes. Temperature was measured with an iron-constantan thermocouple encased in a 1/16-inch diameter stainless-steel tube inserted about 1/2-inch into the base of the specimen. Pore water volume could be measured to the nearest 0.01 cm^3 using a volume change measuring device, as shown in Figure 2-8 (c). Changes in the dimension of the specimen was measured by the linear variable differential transformer and a displacement dial gauge on top of the apparatus, with a resolution of 0.0001 inch. Load could be applied to the specimen either using a dead weight or by a pneumatically operated piston. Material tested was saturated, remoulded Illite.

Temperature-based calibrations were performed on the major components of the apparatus. Pipettes were calibrated to indicate the true volume at temperatures other than 20 °C (68 °F), the ambient temperature that was used as reference temperature for the pipettes. The water volume in the porous stones and transmission lines was calibrated as a function of temperature. The effect of temperature on the electrical output of pressure transducers was investigated. Campanella and Mitchell (1963) found that the slope of calibration curve did not change with temperature, but the intercept (zero point) changed.

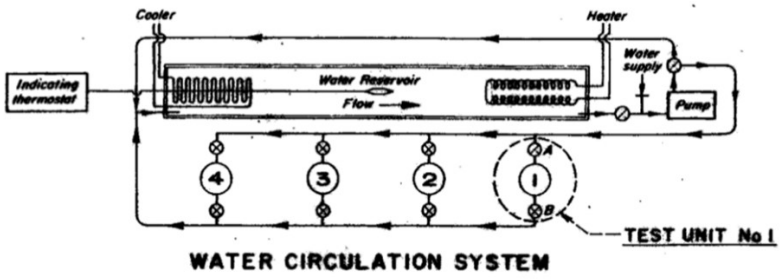

(a)

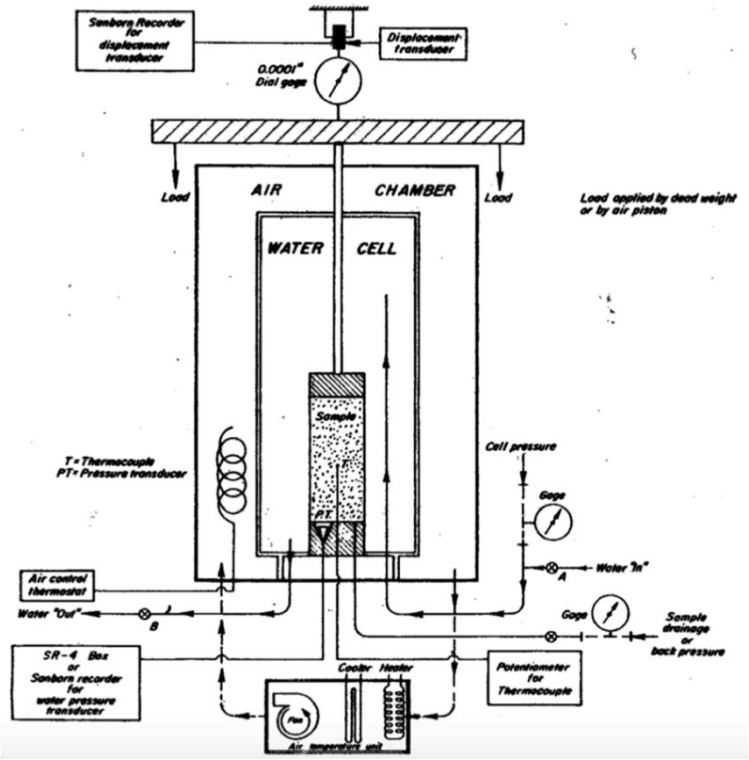

(b)

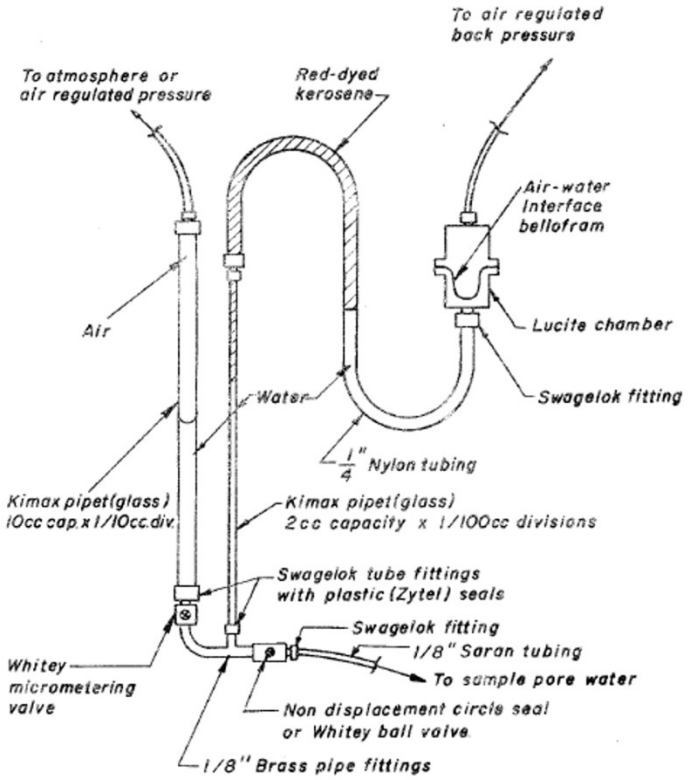

(c)

Figure 2-8: Schematic view of a temperature-controlled triaxial apparatus at the University of California. a) water circulation system; b) triaxial cell; c) volume change measuring device (Campanella and Mitchell, 1963, 1968)

Savvidou and Britto (1995) at the University of Cambridge designed a temperature-controlled triaxial apparatus adopting a similar heating mechanism to that described by Campanella and Mitchell (1963), but with a slightly different heating system, as shown in Figure 2-9. The heating system was mainly composed of a temperature controller, a centrifugal pump and a heat exchanger. Heating of the cell water from ambient to 80 °C was achieved by a thermostatically operated heater unit and cooling water connection on the heat exchanger. Temperatures of the soil specimen and cell water were measured using semiconductor temperature sensors. Two polycarbonate plates were placed at the top and bottom of the specimen for insulation purpose. In this case, water functioned as the confining fluid and as heat exchanger. Only tests under isotropic conditions were reported using this cell. Miniature pore pressure transducers calibrated at different temperatures were used to monitor pore water pressure in the specimen. Details of temperature-based calibration and resolution of instrumentation were not presented by Savvidou and Britto (1995). Material tested was kaolin clay. The major drawback of this cell is that the maximum cell pressure that could be achieved during tests was constrained by circulating the heated confining fluid and affected by the pumping capacity of the centrifugal pump. In addition, temperature and pressure sensors were placed at two different locations, leading to disturbance to the specimen. Their tests results were plotted as pore water pressure or temperature versus time, to be compared to the predicted scenario given by finite element program. Details presented were not sufficient to draw a conclusion on the soil behaviour. Therefore, their results will not be presented in Section 2.3.

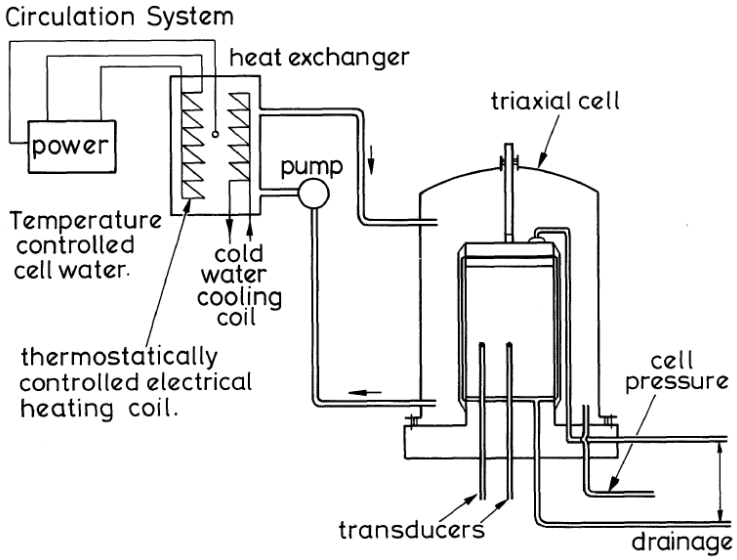

Figure 2-9: Schematic view of a temperature-controlled triaxial cell at the University of Cambridge (Savvidou and Britto 1995)

Heating by lateral and/or external heaters

Temperature-controlled triaxial and isotropic cells that heat the specimen by lateral or external heaters were usually designed as high-pressure cells, as heating could be achieved independently without interfering with the cell pressure controlling system. One of the earliest high pressure, high temperature triaxial cells was presented by Baldi et al. (1987) at the Applied Research Institute for Structural modelling in Italy, as shown in Figure 2-10. Heating was initiated externally to the cell, using a flexible silicon rubber 1700 W heater laterally attached to the outside of the triaxial chamber and two 500 W heating elements located in the base pedestal. These heaters were driven independently by programmable temperature controllers, based on the feedback from thermocouples next to each heater. Another thermocouple was placed close to the specimen to measure the soil temperature. An insulation chamber was designed to reduce heat dissipation to the atmosphere and to maintain a constant temperature with maximum variation of 0.5 °C. The cell and all lines were made of steel to withstand pressures up to 20 MPa and temperature to 200 °C.

Thermal expansion of pressure tubings, porous stones, and water contained within them was determined at different temperature and pressures. For drained tests, these expansions were subtracted from the volume of expelled water measured to correct for the data (Baldi et al. 1987).

Three different clays were tested by Baldi et al. (1987), including a natural soil (Boom clay, taken in blocks from a shaft 250 m deep in Belgium) and two reconstituted soils (commercial kaolin and Pontida silty clay).

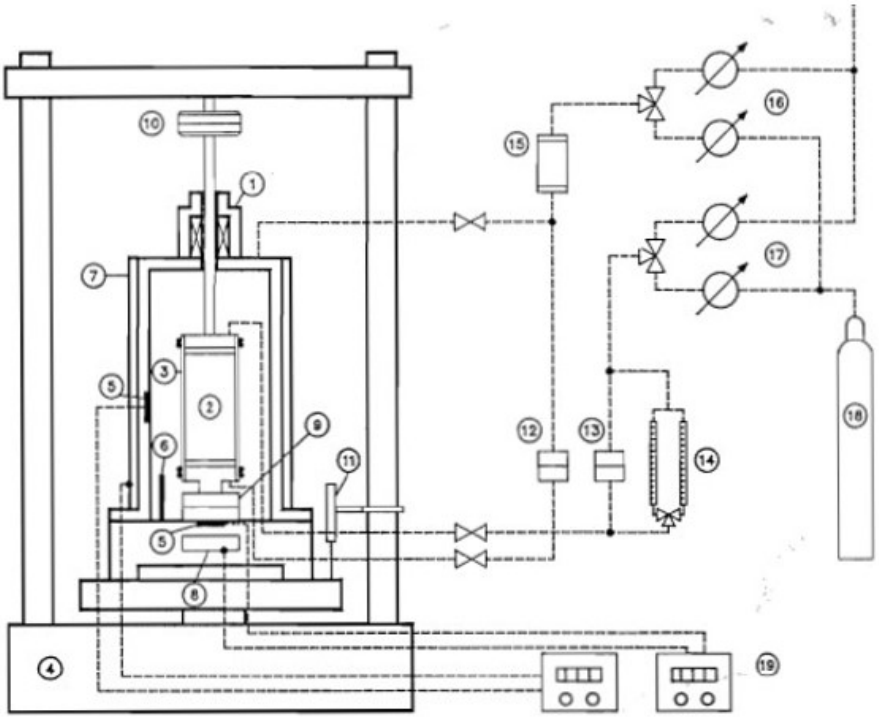

Figure 2-10: Schematic view of a high pressure, high temperature triaxial cell at the Applied Research Institute for Structural modelling in Italy. 1) triaxial cell; 2) specimen; 3) membrane; 4) press (load and speed controlled); 5) heater thermocouples; 6) main thermocouple; 7) lateral heater; 8) bottom heater; 9) internal load cell; 10) external load cell; 11) LVDT (axial deformation measurements); 12) differential pressure transducer (effective stress); 13) differential pressure transducer (volume change); 14) burette (volume-change measurements); 15) air-water interface; 16) cell pressure regulator; 17) back pressure regulator; 18) nitrogen bottle; 19) data acquisition set (Baldi et al., 1987)

Another high pressure, high temperature cell (HITEP) was presented by Lingnau et al. (1996) at the University of Manitoba (Canada), as shown in Figure 2-11. Temperature was controlled using programmable proportional integral differential (PID) controllers and measured on the surface of membranes, using platinum resistance thermal devices (RTD). Silicon oil was used as the circulating fluid as it had lower electrical conductivity, inertness and higher flash point compared to water. Specially designed silicone rubber membranes were used in the heating test to prevent degradation of membranes under elevated temperature. Specimens were consolidated at effective stresses up to 9 MPa and temperatures up to 100°C. Instruments including the internal load cell, lateral displacement gauge, pressure transducers and linear variable differential transducers were calibrated for temperature and pressure effects (Lingnau, 1995).

Temperature-based calibrations were performed on instrumentation. The LVDTs were calibrated at 26, 36 and 94 °C against Mitutoyo and Lufkin vernier micrometre. The calibration

factor of the LVDTs decreased with elevated temperature but this was not relevant for HITEP tests as the LVDTs were mounted externally. Load cell was calibrated at atmospheric pressure and temperature from 26 °C to 100 °C, by submerging the load cell into a controlled temperature bath of silicone oil while loading. It was indicated that temperature only changed the intercept (zero point) but not the slope (calibration factor) of the calibration curve. The zero readings were usually taken at the start of shearing. Therefore, no corrections were needed for the load cell readings. Temperature was shown to have effect on both the intercept and the slope of calibration curves of pressure transducers and volume gauges. Corrections were applied to the pressure data based on the calibration.

Dense sand-bentonite buffer made as a 1:1 mixture by weight of silica sand and sodium bentonite (LL=230-250%, PI=200%). The behaviour of the mixture was clay-dominated.

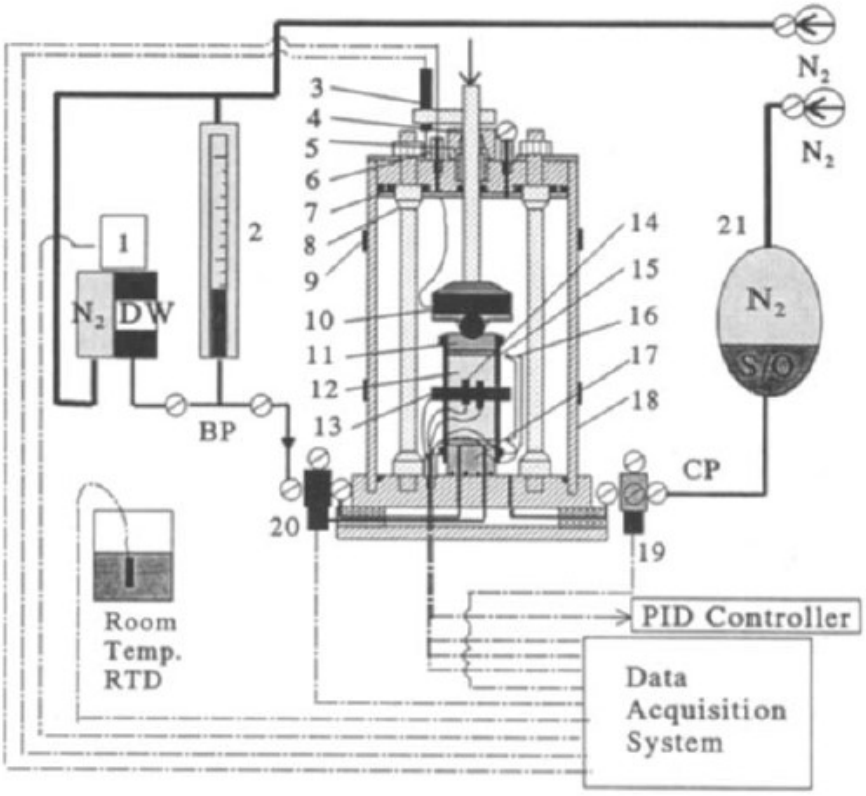

Figure 2-11: Schematic view of a high pressure, high temperature cell at the University of Manitoba. 1) differential pressure transducer; 2) burette; 3) linear variable differential transducer; 4) piston; 5) piston clamp; 6) bulkhead; 7) U-cup seal; 8) tie rod; 9) heat band; 10) load cell; 11) top cap; 12) specimen; 13) lateral displacement gauge; 14) resistance thermal devices; 15) membrane; 16) thermocouple; 17) pedestal; 18) sleeve; 19) cell pressure transducer; 20) back pressure transducer; 21) accumulator. CP: cell pressure, BP: back pressure, DW: deaired water, PID: proportional/ integral/ differential, S/O: silicone oil (Lingnau et al., 1996)

A high pressure, high temperature isotropic cell (Figure 2-12) with a similar heating system to that presented by Lingnau et al. (1996) was employed by Delage et al. (2000), at the Ecole Nationale des Ponts et Chaussées (France). The specimen was heated by a heating coil located on the outer wall of the cell and a thermocouple was installed to monitor the cell water temperature. The temperature regulation system had a capacity of up to 200 °C with an accuracy of ±0.05°C. The isotropic pressure could reach 60 MPa and the back pressure could be raised up to 2 MPa. Most components of the cell were metallic and stiff with repeatable and reversible response to pressure cycles. According to authors, the main advantage of this system was that the measurement of volume changes of the specimen could be performed independently while pressure was applied. This provided an additional measurement of volume change of the specimen compared to the standard triaxial test where only drained water was monitored. The metal tubes connecting to the cell to pressure controllers were immersed in water baths maintained at 20 °C to minimise changes in temperature gradient in the water in ducts connecting controllers. It was implied that no compression of the internal part of this cell occurred in heating tests performed under a constant cell pressure, due to the nature of external heating.

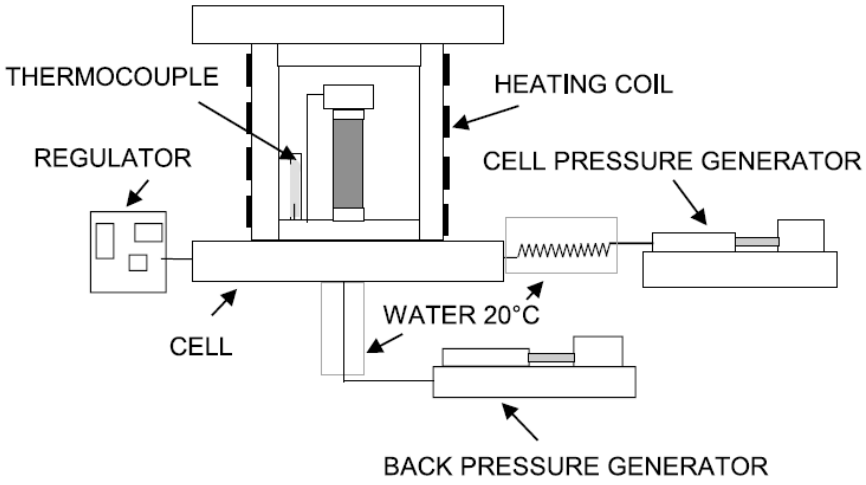

Figure 2-12: Schematic view of a high pressure, high temperature isotropic cell at the Ecole Nationale des Ponts et Chaussées (Delage et al. 2000)

Heating by internal heaters

This heating mechanism usually involves either heaters located inside the cell, or spiral tubes filled with heated water surrounding the soil specimen. Demars and Charles (1982) at the University of Delaware (USA) presented an insulated isotropic cell using such heating mechanism, as shown in Figure 2-13. Heating was achieved by interior copper circulating coil and water bath surrounding the soil specimen. The apparatus allowed heating of the specimen

from 25 °C to 50 °C with an accuracy of ±2 °C. In trial tests where a thermocouple was placed in the centre of the specimen, it was reported that a circulation time of about 35 minutes was required for the specimen to undergo a temperature change of ±25°C. Temperature measurements relied on a thermometer in the water bath. This was adequate as authors followed the same temperature history as in trial tests, and temperatures of the water bath and specimen were equal once a steady state condition had been reached, after 35 minutes of circulation time. The main advantage of this system is that heating was achieved independently of the pressure system. In addition, as heaters were located inside the cell, heat loss of the system was reduced. A more uniform temperature profile could be obtained along the height of the specimen before a steady state was reached. Two layers of latex membrane separated by silicone grease were used outside the soil specimens to minimise osmotic flow. No details of temperature-based calibration were presented by Demars and Charles (1982).

Six soil specimens of marine origin from the North Atlantic were tested. They included two deep-water (4000 m depth), two shallow-water (450 m depth) clays of high to low plasticity, a uniform fine to medium beach sand and one deep-water (4000 m depth) marine clayey silt of low plasticity.

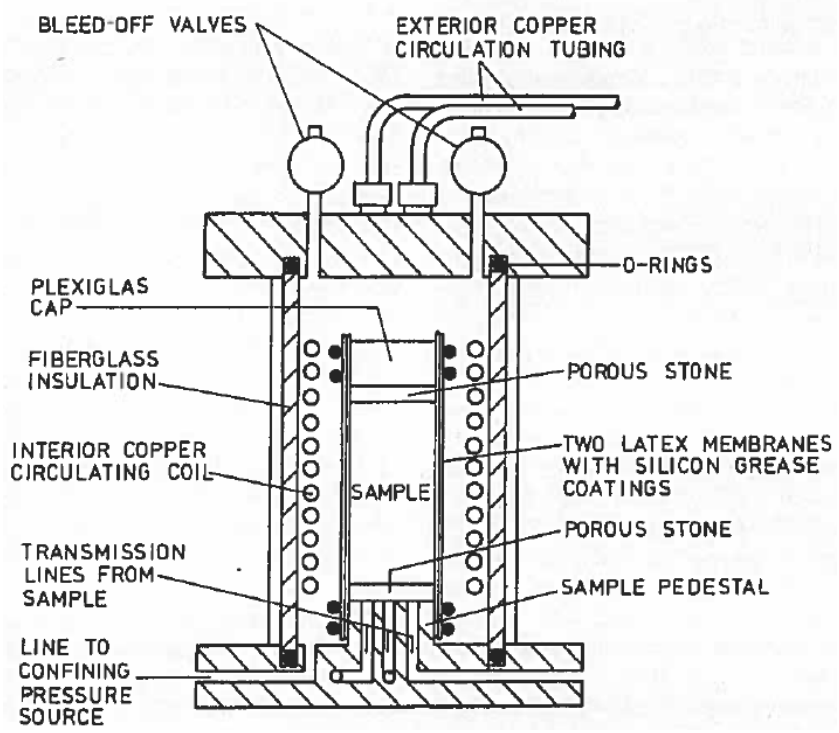

Figure 2-13: Schematic view of a temperature-controlled isotropic cell at the University of Delaware (Demars and Charles 1982)

Kuntiwattanakul et al. (1995) at the University of Tokyo (Japan) presented a temperature-controlled triaxial apparatus that consisted of an inner and outer cell, as shown in Figure 2-14. Heating was achieved by a variable power heater submerged in the water in the inner cell. The amount of power supplied to the heater was automatically adjusted by a control unit to balance the amount of heat loss from the cell to the environment. An air-filled chamber located in between two cells acted as a medium to transfer pressure from a control unit to water in the inner cell and as an insulator. The base of the inner cell was insulated by a plastic disc. The temperature could be controlled from 20 °C to 90 °C, with an accuracy of ±0.1°C. Specimens were 5 cm in diameter and 10 cm in height with lubricated sheets on both ends.

Specimens tested were trimmed from a clay cake. The reconstituted clay cake was prepared by mixing kaolin powder (LL=70%, PI=29%) with distilled water to a slurry, at a water content of 160%, and then preconsolidated to a vertical stress of 98 kPa.

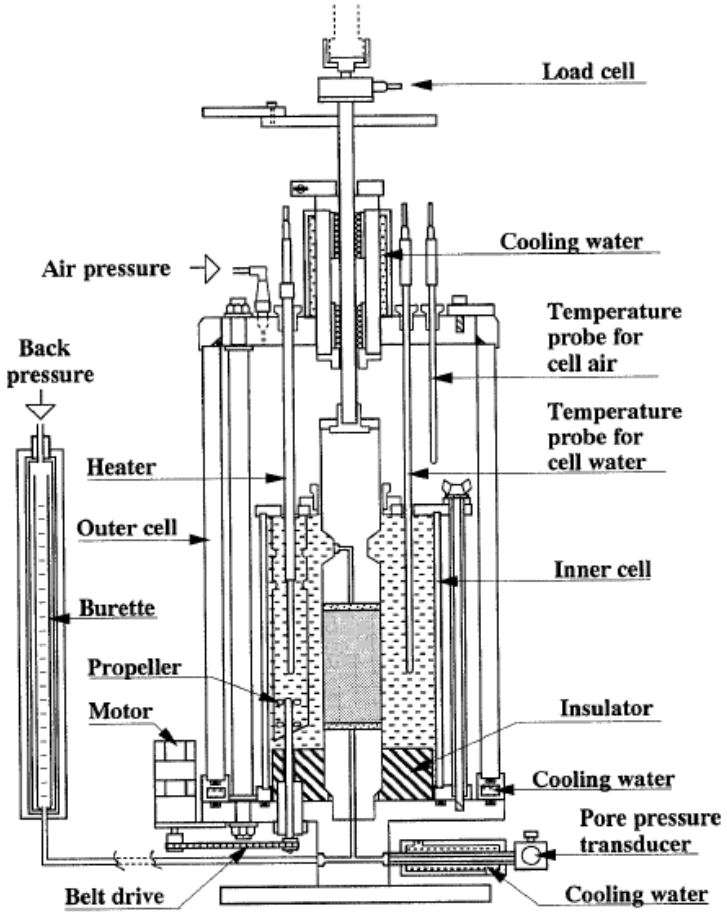

Figure 2-14: Schematic view of a temperature-controlled triaxial apparatus (Kuntiwattanakul et al. 1995)

A similar heating system to that presented by Kuntiwattanakul et al. (1995) was employed by Moritz (1995) (Figure 2-15) at the Sweden Geotechnical Institute. Three sheets of heat foil were placed inside the cell, allowing heating of the specimen from 20 °C to 70 °C, with an accuracy of ±0.1°C. The heat foil was mounted on a holder to avoid direct contact with the specimen and the cell wall. The author suggested that a heating rate of 20°C /h was appropriate to avoid temperature gradients in the specimen. The confining fluid in the cell consisted of water with a 20 mm layer of oil on top. Two thermometers were placed inside the cell water. One of them was used for recording the cell temperature and the other was used to provide feedback for heat servo controller. The cell was taller than standard triaxial apparatus to provide space for cables for the heater and thermometers. No details of temperature-based calibration were presented by Moritz (1995).

Specimens were taken from an area just outside the Swedish Geotechnical Institute's experimental field, at depths of 6 and 9 metres for heat storage in clay near the marina in Linköping.

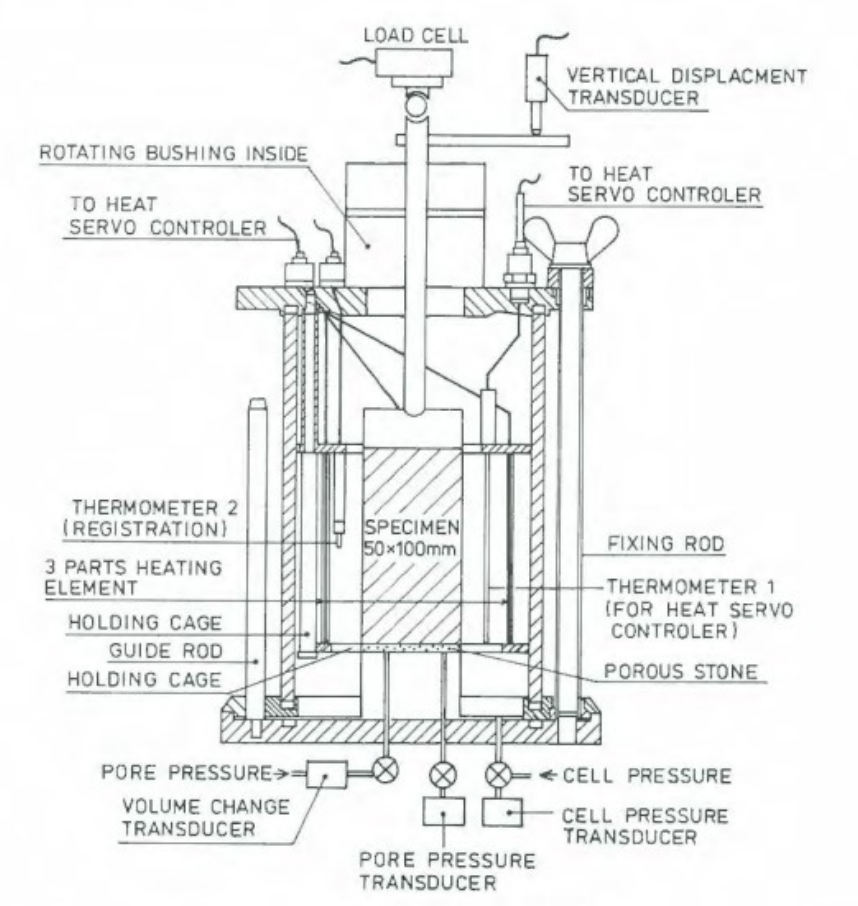

(a) Triaxial cell

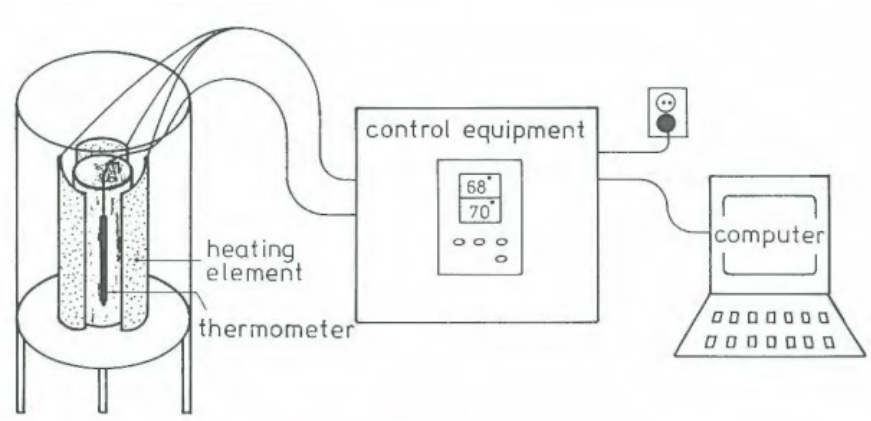

(b) Heating device

Figure 2-15: Schematic view of a temperature-controlled triaxial cell at the Sweden Geotechnical Institute (Moritz 1995)

De Bruyn and Thimus (1996) at the University of Leuven (Belgium) described a high temperature triaxial cell, as shown in Figure 2-16. Heating was achieved through a copper spiral in the fluid-filled cell. The highest temperature was 80 °C if water was used as the confining fluid and could be further increased to 120 °C if silicon oil was used. Two temperature sensors were placed in the cell water, as shown in Figure 2-16 (c) and (d) and another two in pressure transducers. The axial load was measured by an external load transducer, which was not sensitive to temperature and confining pressure changes in the cell. No details of temperature-based calibration were presented by the authors. Boom clay samples were tested in this research.

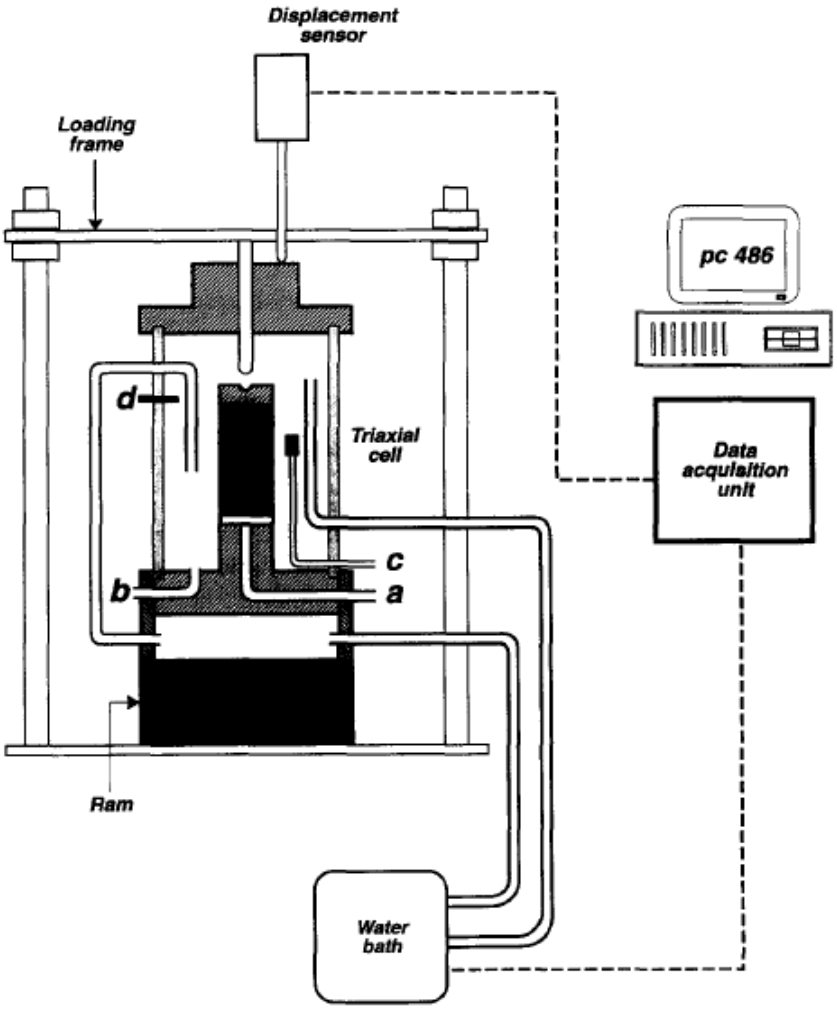

Figure 2-16: Schematic view of a high temperature triaxial cell at the University of Leuven. a) pore water pressure measurements, b) confining pressure measurements, c) temperature sensor (close to specimen, cable coming through cell base), d) temperature sensor (in confining fluid, cable coming through cell body) (De Bruyn and Thimus 1996)

A heating system that is similar to the one presented by De Bruyn and Thimus (1996) was described by Cekerevac et al. (2005) at the Ecole Polytechnique Fédérale de Lausanne (Switzerland), as shown in Figure 2-17. The heating system consisted of the heater in the water bath, the circulating pump, the insulation and the temperature-controlling unit. Water was heated by an electric heater in the bath and then circulated inside a spiral metal tube around the specimen. The maximum pressure that could be reached was 2 MPa and the maximum temperature was 90 °C, with an accuracy of ±0.25°C. Five thermocouples (T1 to T5 in Figure 2-17) were used to measure the temperature at different locations. T1 and T2 were located close to the specimen to give feedback signal to the heater and to record data. T3 to T5 were used for measuring water bath temperature, room temperature and cooling container temperature, respectively. Calibration tests were performed among the measured temperature close to the

specimen, in the heating bath and the temperature inside the specimen. A relationship was established among the three temperature values at different confining pressures. This relationship allowed the selection of the imposed thermostat temperature necessary to reach the desired sample temperature. Thermal corrections were applied to volume, load, axial strain and pore pressure measurement, by assessing the performance of instrumentation and drainage lines under elevated temperature and different levels.

Kaolin clay powder (LL=45%, PL=24%) was mixed with distilled water at a water content two times the liquid limit of the soil. Then the slurry was preconsolidated to a 'cake' under a confining pressure of 100 kPa. Specimens were trimmed from the reconstituted 'cake' for testing.

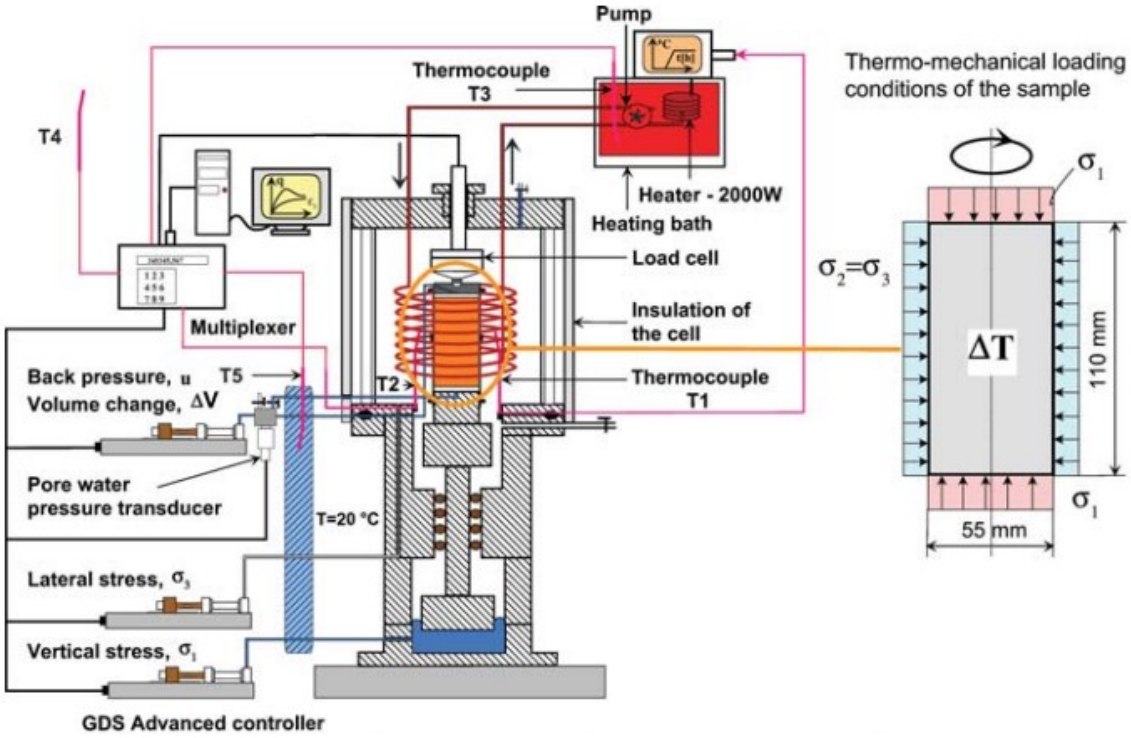

Figure 2-17: Schematic view of a temperature-controlled triaxial cell (Cekerevac et al., 2005)

Ng. et al (2016) at the Hong Kong University of Science and Technology developed a temperature-controlled triaxial cell, based on a computer-controlled global digital systems (GDS) triaxial apparatus. Schematic view of the apparatus is shown in Figure 2-18. Temperature was controlled by circulating heated/cooled water from the water bath to the spiral metal tube around the specimen, with the help of a circulating pump. Thermocouples T1 and T2 were used to measure the temperature of the soil at the top and bottom, to check the uniformity of soil temperature. Thermocouple T3 was placed at a distance of around 5 mm from the specimen, to give feedback to the thermostat, which in turn adjusted the power of the

heating/ cooling unit until thermal equilibrium was reached. It was reported that the temperature difference between measurements from T1 and T2 was less than 0.4 °C and temperature fluctuation was below 0.2 °C, indicating a stable and uniform temperature profile along the height of the specimen. To account for the effect of thermal expansion/ contraction of the water drainage system, including drainage tube, porous stone and water filling them, the calibration procedures presented by Cekerevac et al. (2005) were adopted. The relationship between applied temperature and measured volume change of the drainage system was used to correct the measured soil volume changes under elevated temperature.

Saturated Toyoura sand with different relative densities (from 21 to 90%) was tested, in a temperature range of 23 °C to 50 °C.

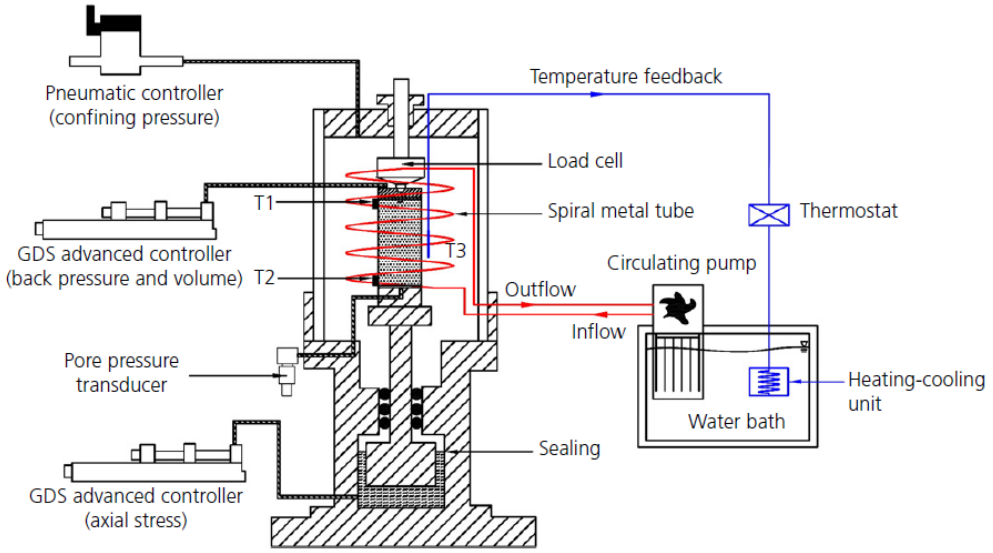

Figure 2-18: Schematic diagram of the temperature-controlled triaxial apparatus (Ng et al., 2016)

2.3 Thermo-hydro-mechanical behaviour of soils

This section introduces some experimental studies and their interpretation of the thermo-hydro-mechanical behaviour of soils. The first part presents one-dimensional compression tests on soils, using oedometer apparatus that were reviewed in Section 2.2.1. The second part presents results from temperature-controlled triaxial and isotropic apparatus reviewed in Section 2.2.2.

2.3.1 One-dimensional compression tests on soils

In this section, effect of temperature on soils tested in temperature-controlled oedometer apparatus is presented. Soil behaviour discussed includes pre-consolidation pressure, compression and swelling indices. There are other aspects of soil behaviour that can be

investigated using oedometer apparatus, including permeability, water retention and swelling capacity. These are not the main focus of this research and will not be discussed in this section.

Finn (1995) performed nine isothermal loading tests on a soil described as 'slightly organic silt or clay with high compressibility. Two tests were performed at 4.4 °C (40 °F), 10 °C (50 °F) and 26.7 °C (80 °F), and three tests at 21.1 °C (70 °F). The specimens were heated or cooled to the desired temperature, then consolidated incrementally, by adding dead weights to the hanger of the apparatus every 24 h. The normally compression lines at four different temperature levels were parallel to each other, indicating that the gradient of the normal compression lines did not change with temperature (Figure 2-19).

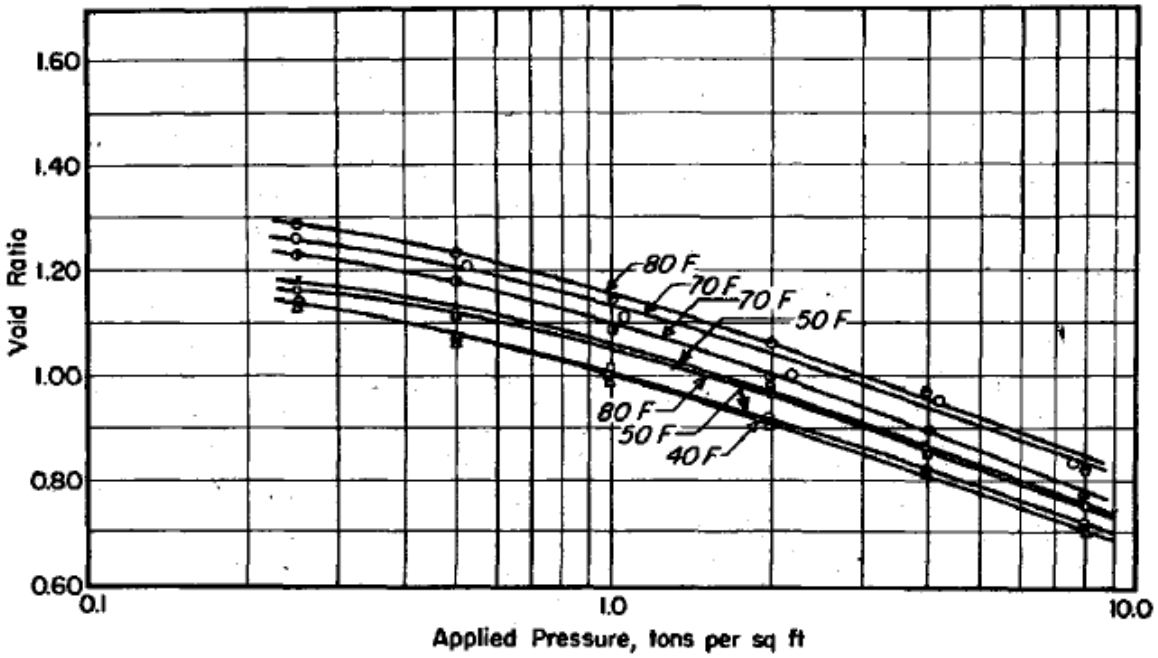

Figure 2-19: Effect of temperature on the compression curve (Finn, 1995)

Towhata et al. (1993) consolidated MC clay specimens at room temperature to 160 kPa, then heated it to 90 °C. Temperature and pressure were hold at 90 °C, 160 kPa for 2 months, 2 weeks or 1 day, before the specimen were further consolidated, as shown in Figure 2-20 (a). After heating, the soil behaved as if it was overconsolidated and its behaviour plotted below the normal compression line at ambient temperature (dashed line in Figure 2-20). When the specimens were consolidated to higher temperature, soil behaviour at 90 °C approached that at ambient temperature. Another test was performed on the same soil, as shown in Figure 2-20 (b). The specimens were heated to 90 °C at 160 kPa, then hold for 2 months, 2 weeks or 1 day, before they were cooled to ambient temperature and consolidated further. The soil behaved as if it was overconsolidated, when it was heated to 90 °C, but rejoined the normal compression

line at a lower pressure compared to the case shown in Figure 2-20 (a). The authors suggested that the gradient of NCL was independent of temperature, similar to the finding by Finn (1995)

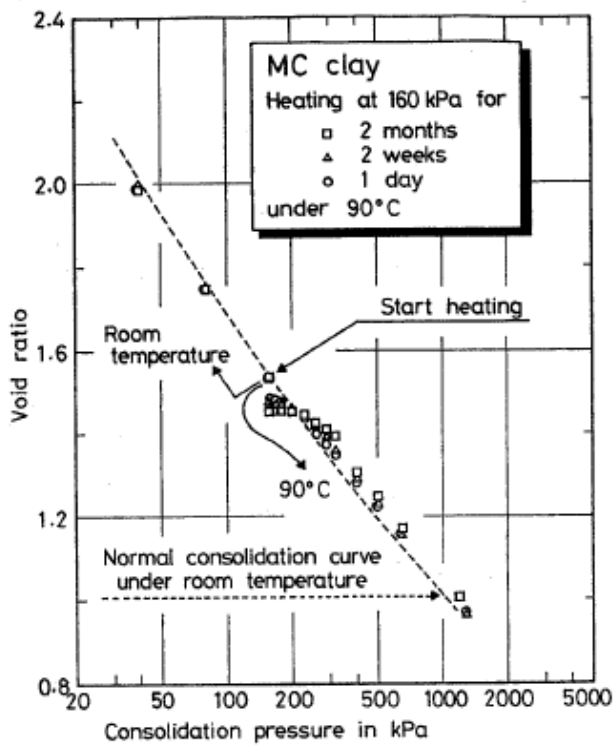

(a) for heated MC clay

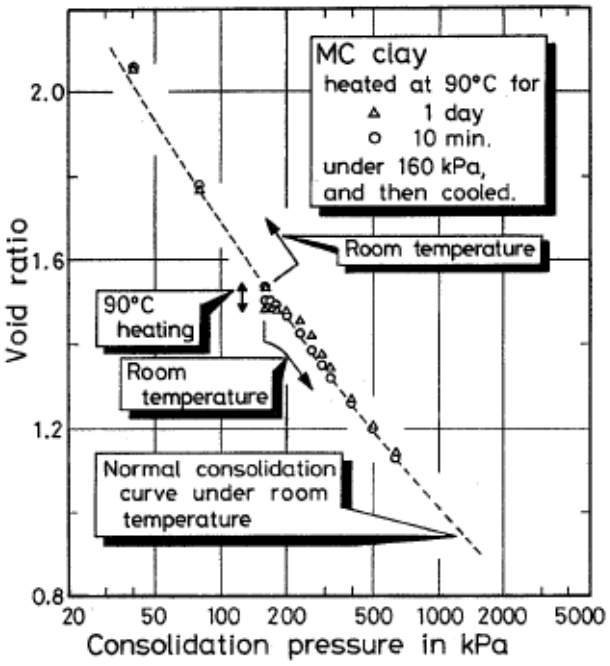

(b) for heated and cooled MC clay

Figure 2-20: Effect of temperature on NCL of MC clay (Towhata et al., 1993)

Abuel-Naga et al. (2005) found that the preconsolidation pressure reduced with the increase in temperature (Figure 2-21). They performed two isothermal loading tests on soft Bangkok clay specimens, at two vertical effective stress levels, 100 kPa and 200 kPa. The results also showed that the percentage of the change in preconsolidation pressure was stress level independent. At a vertical effective stress of 100 kPa, the preconsolidation pressure reduced by 24% at 90 °C, compared to that at ambient temperature. At a vertical effective stress of 200 kPa, the preconsolidation pressure reduced by 22% at 90 °C. The difference between the reduction of preconsolidation pressure at these two stress levels was negligible.

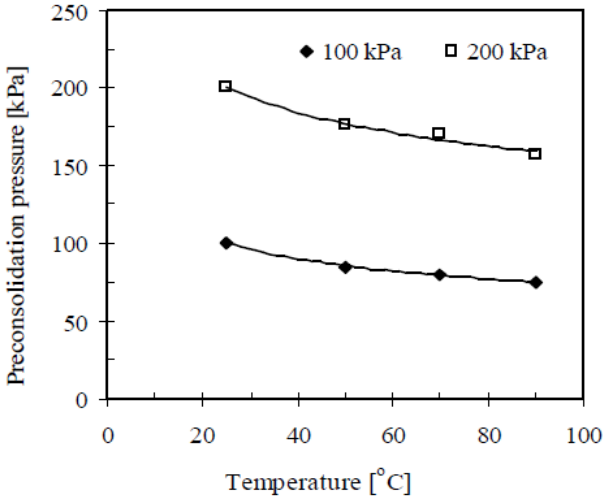

Figure 2-21: Thermal evolution of soft Bangkok clay preconsolidation pressure (Abuel-Naga et al., 2005)

Abuel-Naga et al. (2005) also performed one-dimensional compression tests on normally consolidated soft Bangkok clay with a heating/ cooling cycle. Specimens were heated to 50 °C, 70 °C and 90 °C, with a vertical effective stress of 100 kPa, 200 kPa or 300 kPa before heating. After heating, the specimens were further consolidated at ambient temperature. The results are shown in Figure 2-22. Preconsolidation pressure increased with an increase in the maximum cyclic temperature. The change in preconsolidation also increased with the stress level, provided that the maximum cyclic temperature was the same. They also plotted the maximum cyclic temperature against OCR value of each test after a temperature cycle was applied, in Figure 2-23. The increase in OCR due to thermal cycling was referred to as 'thermally-induced OCR'. From results presented in Figure 2-23, thermally-induced OCR was independent of stress level.

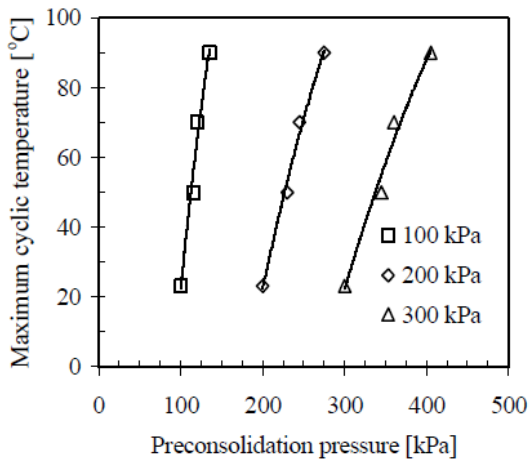

Figure 2-22: The change in the preconsolidation pressure after heating/cooling cycle at different temperature level (Abuel-Naga et al., 2005)

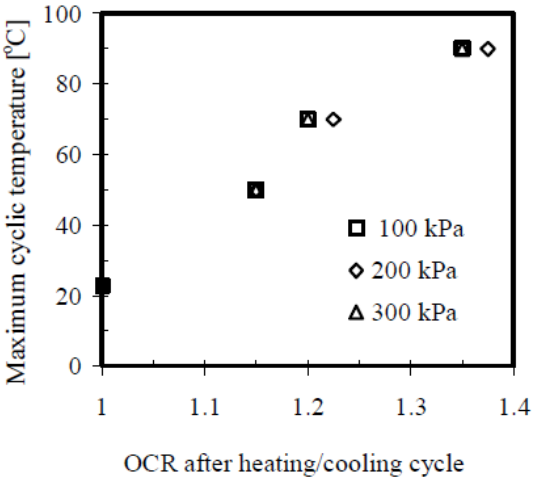

Figure 2-23: Change in OCR value after heating/ cooling cycle at different temperature level (Abuel-Naga et al., 2005)

Di Donna and Laloui (2015) performed thermal cyclic tests on four undisturbed natural samples of Geneva clay. Each sample was taken at different depth with a different initial void ratio. Results from thermal cyclic loading tests are shown in Figure 2-24. Normally consolidated (NC) samples contracted in the first thermal cycle, while overconsolidated (OC) samples either dilated or with negligible volume change during the first thermal cycle, regardless of their initial void ratio. In the subsequent thermal cycles, NC samples continued to contract with smaller volumetric deformation compared to that in the first thermal cycle, while OC samples did not show much change in volumetric deformation.

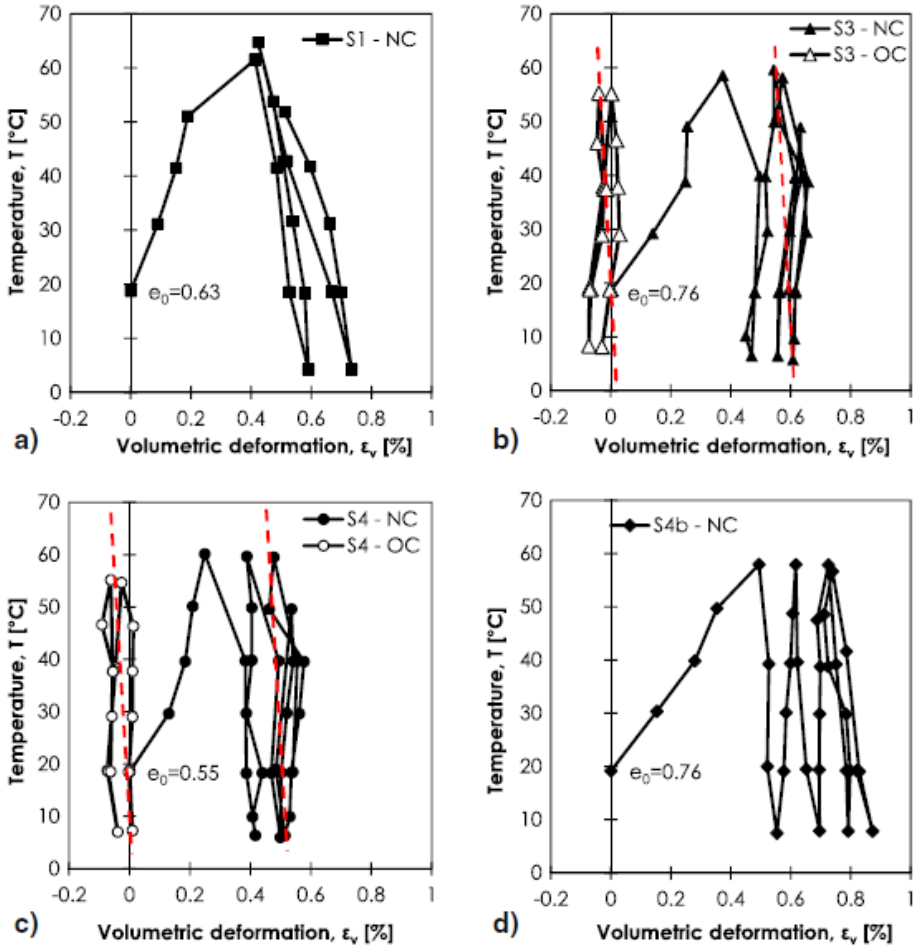

Figure 2-24: Volumetric deformation of Geneva clay during thermal cycles (Di Donna and Laloui, 2015)

Vega and McCartney (2015) carried out thermal cyclic tests on compacted, saturated Bonny silt. Four heating and cooling cycles (18 °C -91 °C-18 °C) were applied to specimens with different OCRs. Results are shown in Figure 2-25. NC specimens contracted in the first heating-cooling cycle. They continued to contract in the subsequent thermal cycles, but the amount of contraction was smaller compared to that in the first cycle. OC specimens dilated in the first thermal cycle, while in the subsequent cycles, the change in the thermal axial strain was minimal.

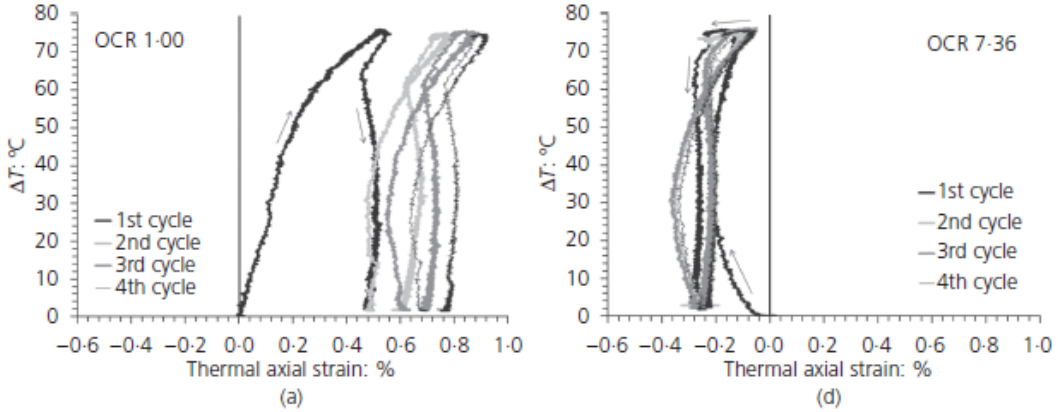

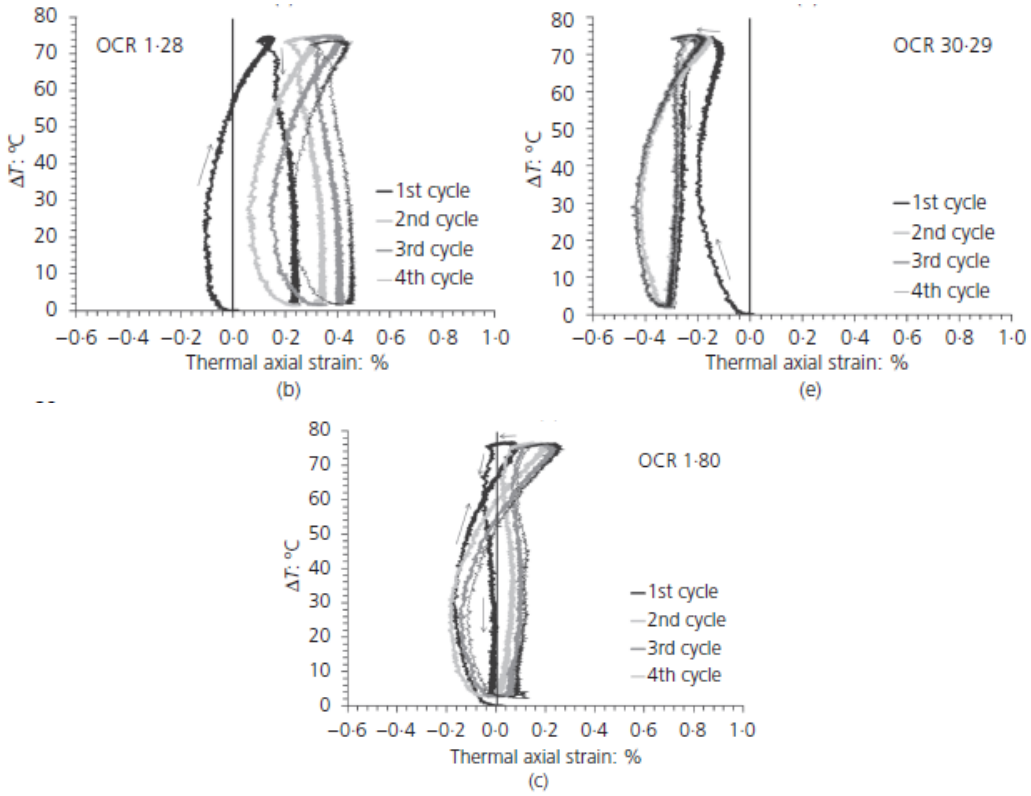

Figure 2-25: Thermal axial strain for saturated Bonny silt (Vega and McCartney, 2015)

Favero et al. (2016) performed tests on Opalinus clay, under three test paths (Figure 2-26). In test 1, the reloading path at 23 °C plotted above the expected normal compression line at 80 °C, showing an increase in pre-consolidation pressure with decreasing temperature. In test 2, the reloading path at 80 °C plotted below the expected compression line at 23 °C, indicating a decrease in pre-consolidation pressure with increasing temperature. Test 3 confirmed the finding in test 2, with the reloading path at 80 °C plotted below the expected compression line at 23 °C.

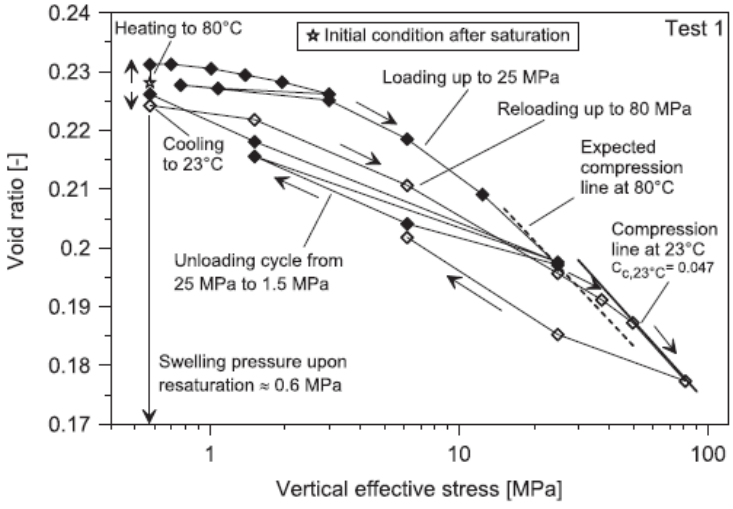

(a) test 1

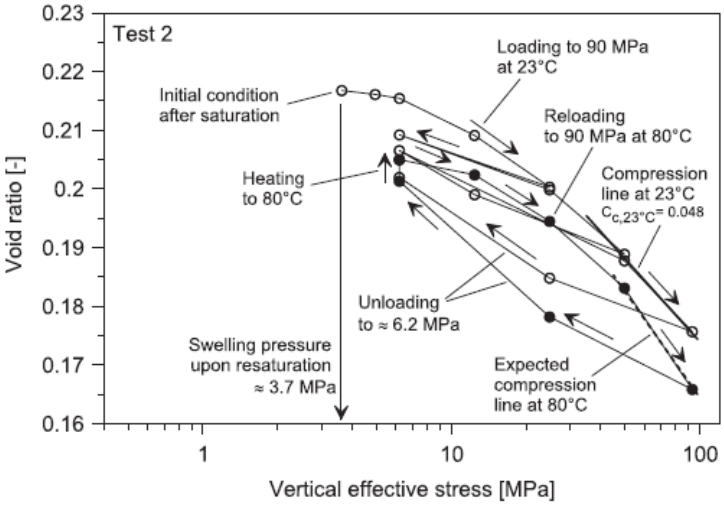

(b) test 2

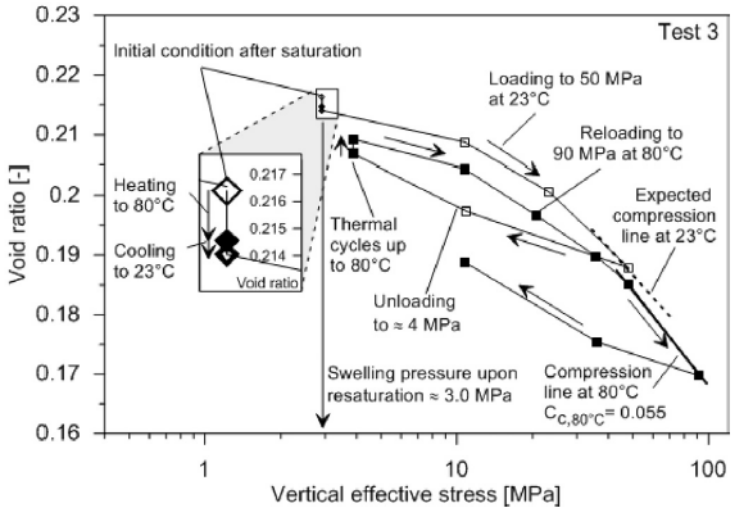

(c) test 3

Figure 2-26: Void ratio versus vertical effective stress for Opalinus clay (Favero et al., 2016)

Sittidumrong et al. (2019) carried out tests on Bangkok sand. Multiple heating and cooling cycles (28 °C-50 °C-28 °C) were applied to sand samples with relative density of 70% and 30%, under a constant vertical stress of 3.211 MPa. Figure 2-27 compares the thermal induced vertical strain for both samples, in the first five cycles. For both samples, the first thermal cycle induced the largest strain of about 0.06% while subsequent cycles induced a progressively lower strain. The initial density did not have significant effect on the thermal induced vertical strain in the first thermal cycle, but in the subsequent thermal cycles, the looser sample showed larger vertical strain.

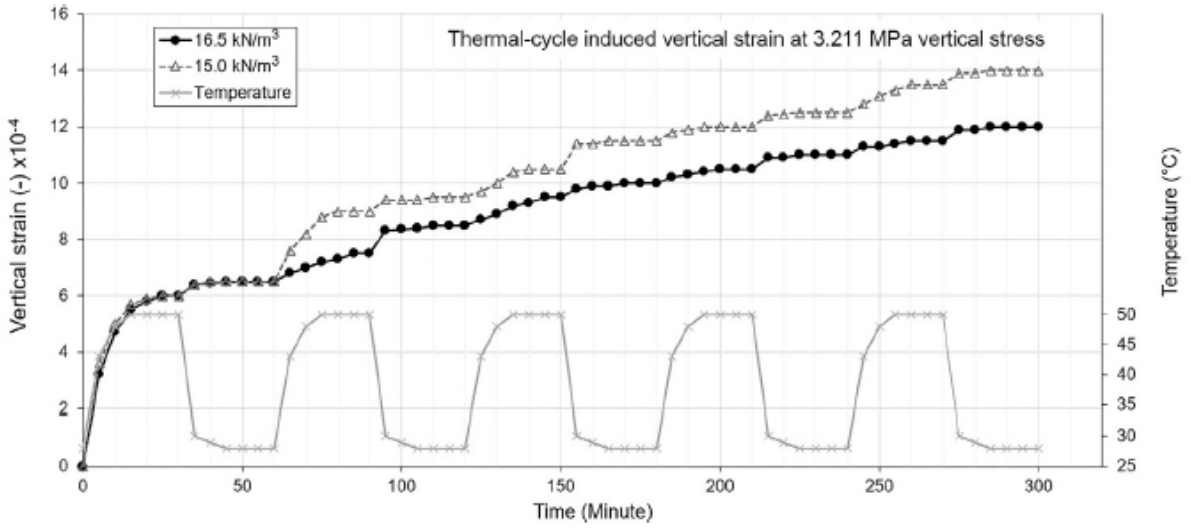

Figure 2-27: Thermal induced vertical strain for the first five thermal cycles (Sittidumrong et al., 2019)

2.3.2 Triaxial or isotropic consolidation tests on soils

This section provides a bibliography review of previous research works on the laboratory work that aims at understanding the soil behaviour at different temperatures, including thermally induced pore water pressure and changes in volumes.

An early laboratory work was described by Campanella and Mitchell (1968) on the influence of temperature variations on soil behaviour. Pore pressure increased during undrained heating due to different thermal expansion coefficients of water (α_w) and soil (α_s). Thermal failure could be induced by undrained heating of the soil as the effective stresses decrease and so does the strength. An equation to calculate the change in pore water pressure was proposed.

$$\Delta u = \frac{n\Delta T(\alpha_s - \alpha_w) + \alpha_{st}\Delta T}{m_v} \qquad 2\text{-}1$$

where n refers to the porosity of soil, α_{st} is the physico-chemical coefficient of structural volume change induced by temperature variations and m_v is the volumetric compressibility.

Saturated illite was tested under different temperatures. The temperature variations led to volume change under drained conditions and changes in effective stress under undrained conditions as shown in Figure 2-28 and 2-29, respectively. Volume of the specimen decreased as the temperature increased from 4.4 °C to 60 °C (40°F to 140°F), then the volume increased as cooling was initiated but the volume change path did not follow the one in heating. Instead, the specimen reached a smaller volume compared to the initial condition. Similar results were observed in temperature induced effective stress changes. Effective stress decreased with the increase in the temperature, then the effective stress increased upon cooling but it not fully recoverable when the specimen was cooled to the initial temperature.

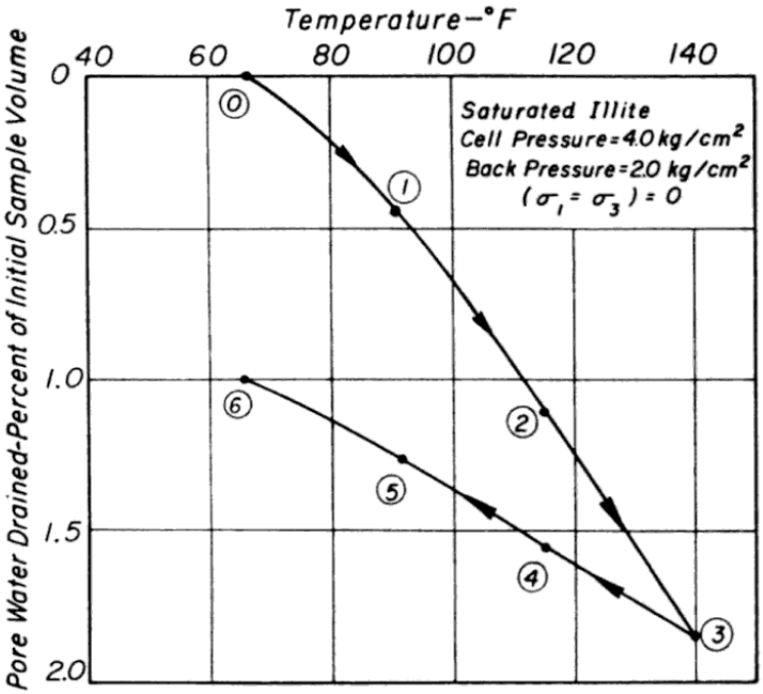

Figure 2-28: Effect of temperature variations on volume under drained conditions (Campanella and Mitchell, 1968)

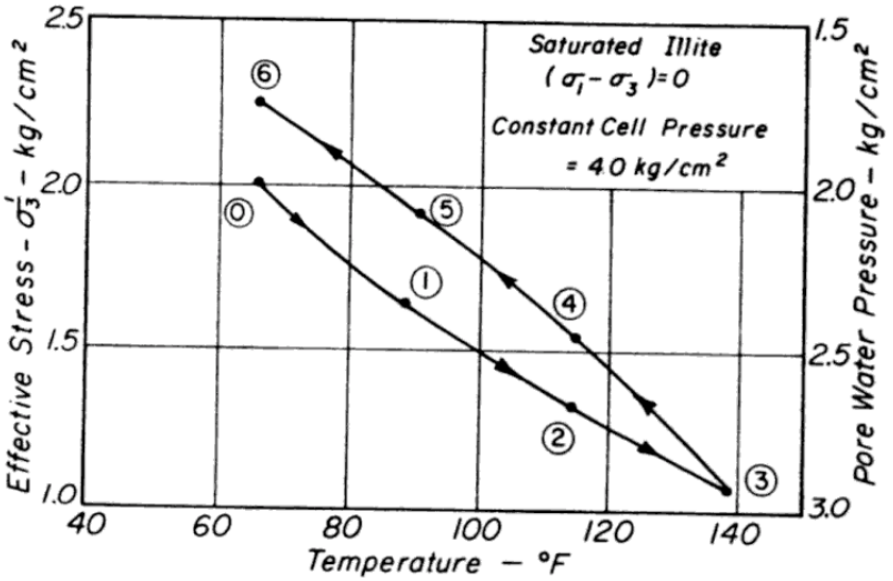

Figure 2-29: Effect of temperature variations on effective stress under undrained conditions (Campanella and Mitchell, 1968)

Figure 2-30 shows the effect of temperature on isotropic behaviour of the soil. The specimen contracted with elevated temperature but compressibility, which was represented by the slope of the lines, was not sensitive to the changes in temperature.

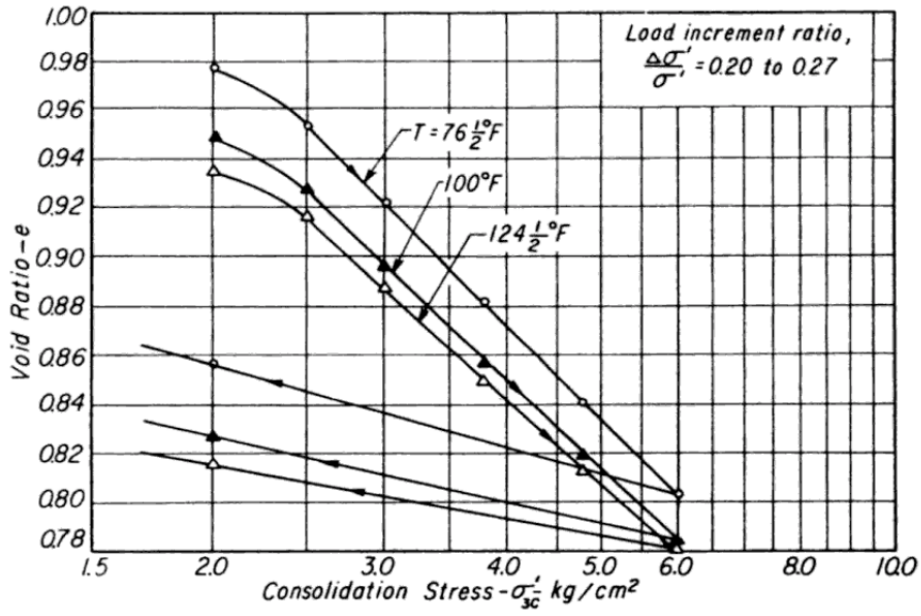

Figure 2-30: Effect of temperature on isotropic consolidation behaviour of saturated illite (Campanella and Mitchell 1968)

Hueckel and Baldi (1990) performed thermomechanical tests on three clays under different temperatures and drainage conditions, using the high pressure, high temperature triaxial cell presented by Baldi et al. (1985) and described in Section 2.2.2. Results of drained heating tests on Pontida clay showed that normally consolidated clays contracted while overconsolidated clays dilated when temperature increased, as in Figure 2-31. Similar results have been observed on Pasquasia clay as in Figure 2-32. This provided a possible soil improvement method for overconsolidated soil, as larger shear stress would be generated between soil and pile when heated thus increasing the bearing capacity.

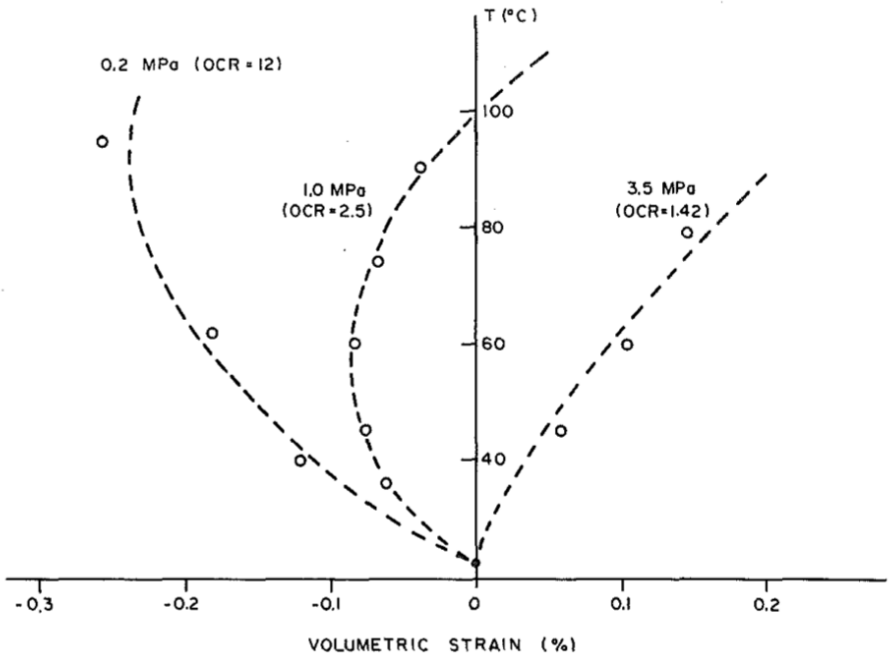

Figure 2-31: Drained heating tests at constant effective stress at various OCR on remoulded Pontida clay (Hueckel and Baldi, 1990)

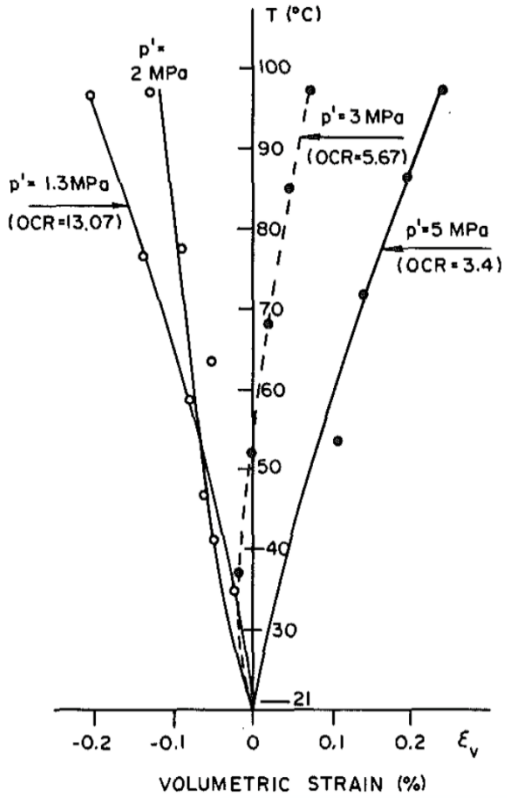

Figure 2-32: Drained heating tests at constant effective stress at various OCR on natural Pasquasia clay (Hueckel and Baldi, 1990)

Ductility increased and dilation decreased with an increase in temperature as in Figure 2-33. At high temperature, the specimen only exhibited dilation, while at low temperature, the specimen contracted and then dilated.

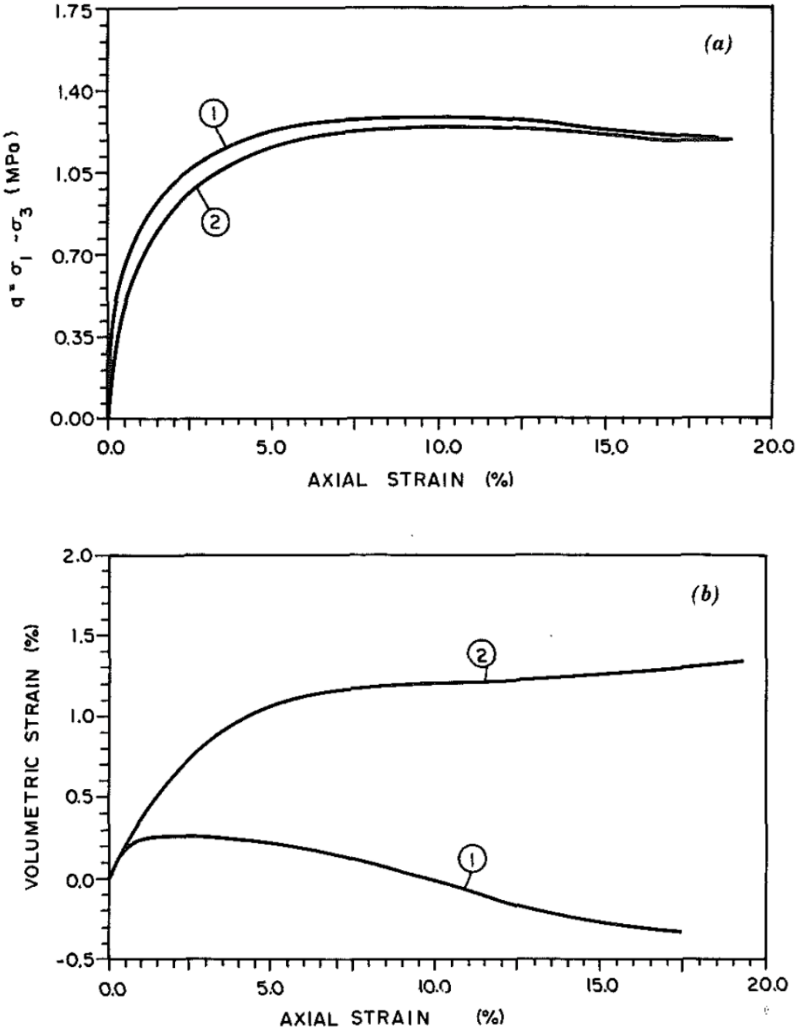

Figure 2-33: Drained triaxial compression tests on Pontida clay at room and high temperature at confining stress of 0.5 MPa (OCR = 5.0); 1 at 23° C, 2 at 98° C (a) stress-strain behaviour; (b) volumetric behaviour (Hueckel and Baldi, 1990)

Figure 2-34 shows two predicted theoretical stress paths under different temperatures. Yield surface shrank with increasing temperature and the specimen was expected to fail at lower deviatoric stress. The direction of the plastic strain rate vector would also change with temperature. These predictions have been verified by experiments.

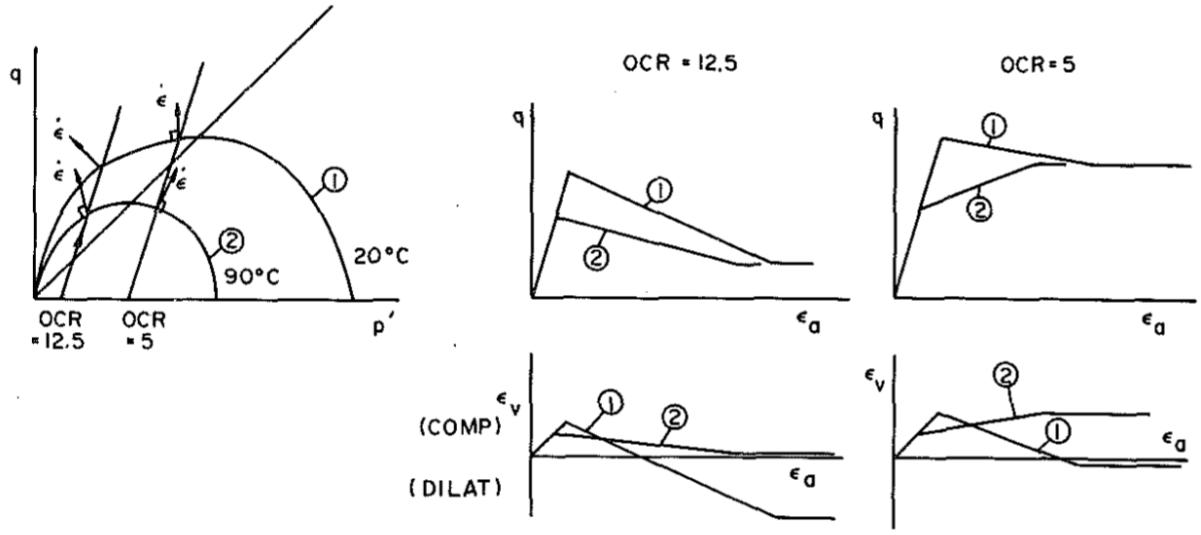

Figure 2-34: Two stress paths and theoretical response at two temperatures based on associated flow rule (Hueckel and Baldi, 1990)

De Bruyn and Thimus (1996) investigated the mechanical properties of Boom clay under undrained heating on triaxial apparatus and found that the strength decreased with increasing temperature, which could be explained by the built-up of excess pore pressure and decrease in effective stress.

Lingnau et al. (1996) investigated the effect of temperature on the shear strength and compressibility of a sand-bentonite buffer material in a high pressure temperature cell as in Section 2.2.2. The buffer was produced by mixing equal weight of silica sand and sodium bentonite and it behaved like a stiff, normally consolidated plastic clay. Figure 2-35 shows the specific volume of clay when consolidated under different temperatures. As the temperature increased from 26℃ to 100℃, volume decreased by about 15%. The normal consolidation lines remained parallel to each other, which agreed with the previous finding that the compressibility was almost unaffected by changes in temperature. The effects of elevated temperature on the increase of pore water pressured and stiffness were relatively small.

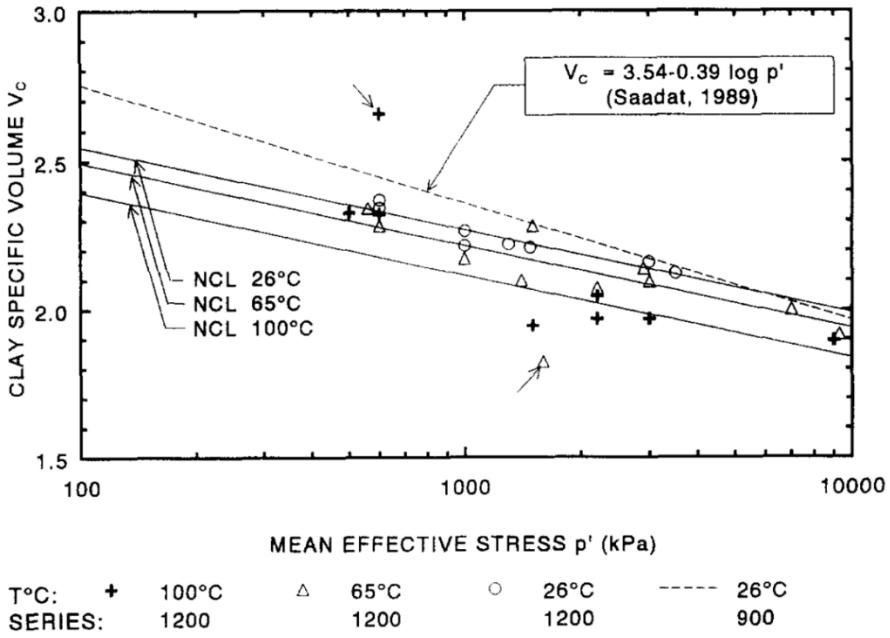

Figure 2-35: Soil response when consolidated at different temperatures (Lingnau et al., 1996)

Figure 2-36 shows the undrained shear tests with specimens consolidated under 0.6MPa pressure. The specimens had slight strain softening after peak with ductile failure mode. Maximum deviator stress was mobilised when the axial strain was approximately 5%. At higher temperatures, the specimens exhibited lower strengths and larger changes in pore water pressure. It can be indicated from Figure 2-36 (c) that the specimens might not reach equilibrium when the axial strain was around 12%.

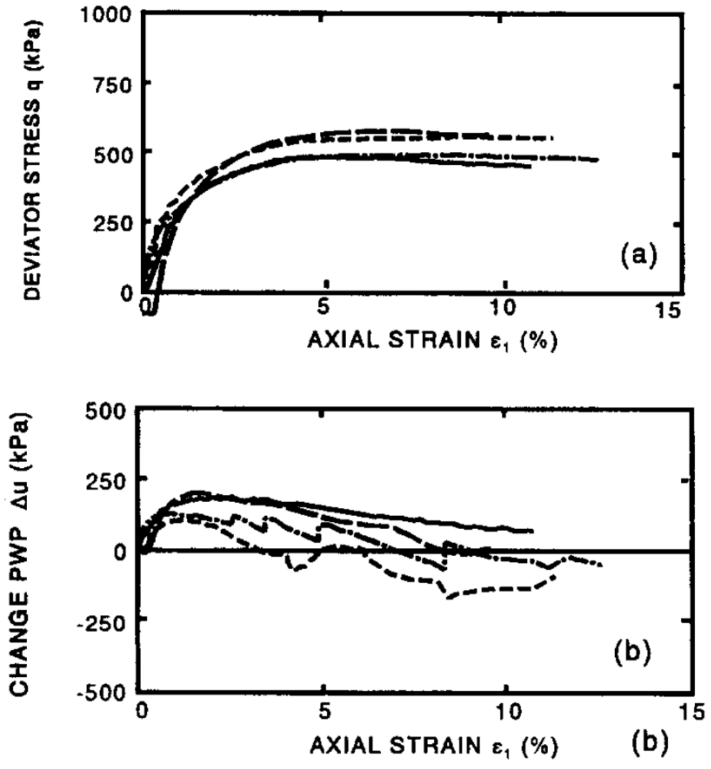

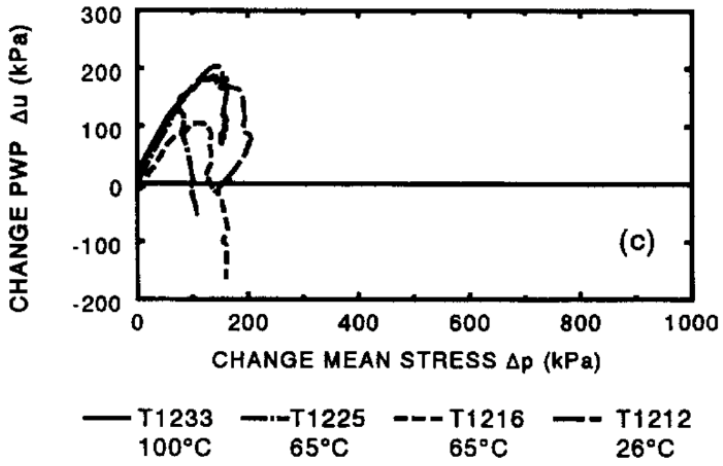

Figure 2-36: Undrained triaxial compression tests results consolidated under 0.6MPa pressure (Lingnau et al., 1996)

Cekerevac and Laloui (2004) tested Kaolin clay under drained conditions at 22 and 90 ℃ using triaxial apparatus. Specimens sheared under high temperature exhibited higher peak strength. At large strains, the strength at critical state tends to be insensitive to changes in temperature.

Abuel-Naga (2007c) concluded that the drained strength of clay at large strains was independent of temperature (i.e. critical state line would not change with temperature). Therefore, the internal angle of shear resistance of clay at room temperature could be a representative value for friction angles at critical state under different temperatures.

Ng et al. (2016) studied the volume changes of saturated Toyura sand under heating and cooling cycles through temperature-controlled triaxial tests. Details of the experimental programme are shown in Table 2-1. Thermo-mechanical path of each specimen is presented in Figure 2-37. Soil specimens were isotropically consolidated to a mean effective stress of 200 kPa, and in some of the cases, they were isotropically unloaded to 50 kPa. After consolidation, specimens in the first two series were heated from 23 to 50 ℃ in steps under drained condition. Specimens in the third series went through two heating/cooling cycles of 23-50-23 ℃. Soil specimens had different relative densities before heating, ranging from 21% to 90%. Heating-induced volume changes are shown in Figure 2-38. In the first heating cycle, specimens that were not too dense (Dr20P200TC, Dr20S200H, Dr70S200TC, Dr70S200H) showed contractive strains with an increase in temperature from 23 to 35℃. As the temperature increased further to 50℃, the specimens started to exhibited dilation, with overall volumetric strain still being contracting. On the other hand, densest specimens (Dr90S200H) exhibited only dilation with an increase in temperature due to the more stable structure they had.

Table 2-1: Details of the experimental programme on saturated Toyura sand (Ng et al., 2016)

Series number	Specimen identity	Relative density, D_r*: %	Void ratio, e*	Mean effective stress, p': kPa	State parameter, Ψ*	Stress path
1	D20S200H	21	0·89	200	−0·012	C → F → F_1
	D70S200H	70	0·71	200	−0·192	B → E → E_1
	D90S200H	90	0·62	200	−0·282	A → D → D_1
2	D20S50H	21	0·90	50	−0·021	C → G → G_1
3	D20S200TC	26	0·87	200	−0·062	C → F → F_1 → F → F_1 → F
	D70S200TC	70	0·71	200	−0·212	B → E → E_1 → E → E_1 → E

*D_r, e, Ψ are the values prior to the thermal cycle.

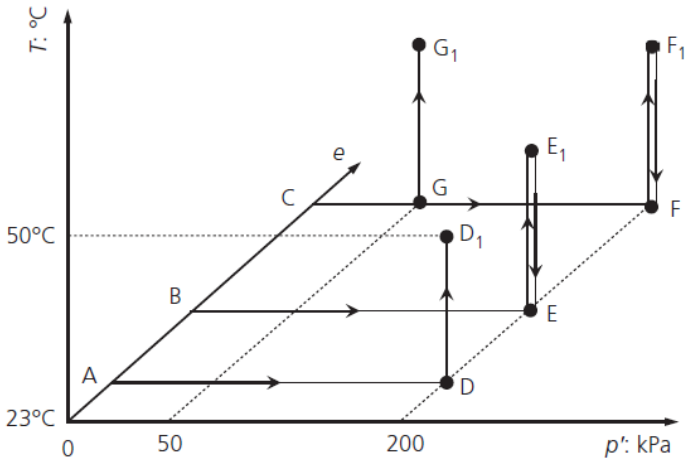

Note:
[1] p', e and T are the mean effective stress, void ratio and soil temperature, respectively.
[2] For simplicity, any change in e under thermo-mechanical loads is not taken into account in this figure.
[3] Specimens with an initial state of A, B and C are classified as dense, medium dense and loose specimens respectively based on their relative densities (Budhu, 2015).

Figure 2-37: thermo-mechanical path of each specimen (Ng et al., 2016)

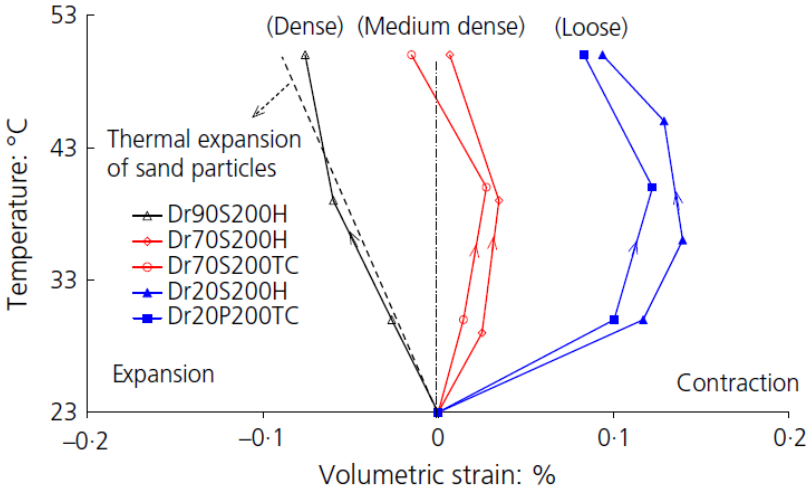

Figure 2-38: Heating-induced volume changes of Toyura sand (Ng et al. 2015)

2.4 Summary

In this chapter, the published literature on testing equipment for characterising the thermo-hydro-mechanical behaviour of soils, as well as the testing results using the equipment, is reviewed.

The main findings from the literature are summarised in the following points:

- Temperature-controlled oedometer apparatus were developed during the early stage of characterising the thermo-hydro-mechanical behaviour of soils (Gray, 1936; Finn, 1951; Paaswell, 1967; Plum and Esrig 1969). Effect of temperature on pre-consolidation pressure and compression behaviour can be investigated using thermal oedometer apparatus (Finn, 1995; Towhata et al., 1993; Abuel-Naga et al., 2005)
- Due to thermal expansion and contraction of the apparatus and the confining ring, temperature-based calibrations were performed, and corrections were applied to the data (Finn, 1952; Towhata et al. 1993; Romero, 1999; Abuel-Naga et al., 2005; Frąncois and Laloui, 2010; Shariatmadari and Saeidijam, 2011; Ye et al., 2012; Vega and McCartney, 2015; Favero et al., 2016).
- Temperature-controlled triaxial or isotropic apparatus were developed at a slightly later stage of characterising the thermo-hydro-mechanical behaviour of soils (Campanella and Mitchell, 1963; Savvidou and Britto, 1995; Baldi et al., 1985).
- Based on the way the heat is applied to the specimen, Cekerevac et al. (2005) distinguished the temperature-controlled triaxial and isotropic cells into three categories, including circulating the confining fluid (Campanella and Mitchell, 1963; Savvidou and Britto, 1995), lateral and/or external heaters (Baldi et al., 1985; Lingnau et al., 1996; Delage et al., 2000) and internal heaters (Demars and Charles, 1982; Kuntiwattanakul et al., 1995; Moritz, 1995).
- Effect of temperature on strength, stiffness, volume change and pore pressure of soils can be investigated using thermal triaxial or isotropic apparatus.

Chapter 3: Methodology

3.1 Introduction

This chapter presents the testing equipment, materials tested in this research, sample preparation process and experimental procedures. Firstly, three pieces of temperature-controlled equipment are presented. They were developed at the Imperial College Geotechnics Laboratory (ICGL) for the experimental research on the thermo-hydro-mechanical behaviour of soils and comprised: i) The isotropic apparatus developed by Martinez-Calonge (2017) was enhanced with the installation of a mid-height pore pressure probe, in addition to conventional pore water pressure measurement at the base of the specimen, to enable accurate monitoring of pore water pressure changes at different locations of the soil specimen during multiple cycles of heating and cooling; ii) a new thermal triaxial apparatus with a double load-cell measuring system (to compensate for temperature effects) was developed to enable the shearing of London clay specimens at both ambient and elevated temperatures; iii) a new oedometer apparatus with a thermal bath was developed for the measurement of compression properties of London clay under different temperature levels. Secondly, material tested in this research is described, including its source, geological history, minerology, and some of its mechanical properties. Thirdly, sample preparation process is presented. This includes the preparation of slurry-consolidated London clay and the reconstituted London clay cake. Finally, experimental procedures for tests using each of the equipment are described.

3.2 Isotropic apparatus with mid-height pore pressure probe

The temperature-controlled isotropic apparatus used in this research was developed based on the existing thermal isotropic apparatus at the ICGL (Martinez-Calonge, 2017). The main improvement of the current apparatus was that a mid-height pore pressure probe was installed to enable the measurement of pore water pressure at the mid-height of the specimen inside the cell, apart from the pore water pressure measurement from the pressure transducer connected to the base pedestal.

3.2.1 Description

Undrained heating tests on specimens of reconstituted London clay were performed in a temperature-controlled isotropic apparatus (Figure 3-1). Distilled water inside the stainless-steel cell (Figure 3-1 (a)) supplied a confining pressure of up to 800 kPa. Three 150 W cartridge heaters (Figure 3-1(b)) were installed in the bottom plate and another three heaters were placed in the top plate, capable of raising the temperature of water surrounding the specimen up to 85 °C. Temperature sensors (Figure 3-1 (c)) were installed next to each heater and also inside

the confining fluid at the mid-height level of the specimen to monitor the temperature throughout each test. Temperature of the soil specimen at the bottom, mid-height and top was monitored in trial tests by Martinez-Calonge (2017), to assess the rate of the sample's heating compared to cell water as well as the temperature difference along the sample height. The maximum difference in temperature at the monitoring points of the cell water and at the three locations of the soil specimen was shown to be only 0.15 °C. Therefore, the temperature of the soil specimen can be represented by the temperature measured by the sensor inside the confining fluid. The isotropic cell was insulated by a cylindrical chamber with several layers of bubble wrap placed around the cell in a controlled pattern, to ensure uniformity of insulation between different tests. Specimens (Figure 3-1 (f)) with 50 mm diameter and 100 mm in height could be tested in this apparatus. Water flowing in and out of the cell was monitored using cell pressure air/water interface. Pore water pressure was monitored from a transducer located in the back pressure line at the base of the cell and also using a mid-height pore pressure probe (Figure 3-1 (g)) that was located at the mid-height of the soil specimen. The TRIAX software (Toll, 1999) was used to digitally control, monitor and record pressures, axial load and displacements.

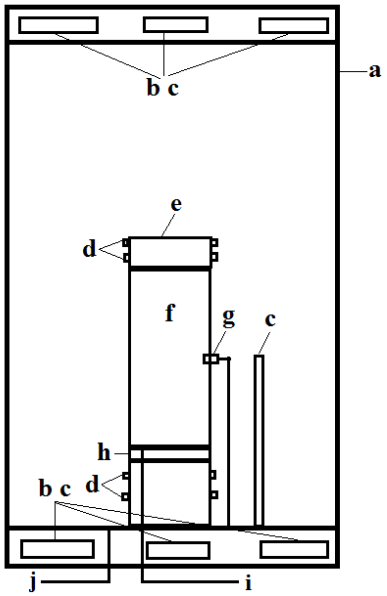

Figure 3-1: Schematic view of temperature-controlled isotropic apparatus. (a) stainless steel chamber; (b) heater; (c) temperature sensor; (d) O-ring; (e) topcap; (f) soil specimen; (g) mid-height pore pressure probe; (h) porous disc; (i) to back pressure volume gauge; (j) to cell pressure volume gauge

3.2.2 Calibrations of instrumentation

In the thermal testing of soils, several issues must be taken into consideration to ensure the quality of the tests. Firstly, changes in physical quantities due to temperature may be very small, close to the resolution and accuracy of the instrumentation. Secondly, the instrumentation output may be temperature sensitive. It is important to distinguish the soil response and the response of the instrumentation due to temperature variations. Lastly, tests last for a long time and a small leakage in the system can lead to considerable errors. To address these issues, long-term monitoring and temperature-based calibrations need to be performed.

Calibration is defined as the 'determination of the relationship between the transmitted electrical signal and the physical quantity being measured' (Head, 1998). In some of the cases, it also involves quantifying the effects dependent on the laboratory environment, for example, temperature as in this research. It helps to ensure the reliability of the data and allows assessing errors in measurement. Temperature-based calibrations for testing equipment were not well-developed to a protocol in the literature. Calibrations of the instrumentation were performed at ambient and elevated temperature. Recalibrations were performed on instrumentation at regular intervals. During the calibration process, unloading/ reloading loop was repeated for three cycles, to assess the possible hysteresis in the performance of the instrumentation.

Back pressure volume gauge

The volume gauge was calibrated by flushing water from the gauge to a container placed on a scale. Changes in the mass of water were converted to volume, by dividing it by the density of water at the temperature level that the calibration was performed at ($V_w = W_w/\gamma_w$). Effect of temperature was assessed by flushing heated water at 30 and 40 °C and repeating the calibration process in the same manner as at ambient temperature. Calibration factors for the back pressure volume gauge did not change with temperature. This is because the volume gauge is located at a distance (>1 m) from the cell and the heated water would have cooled down to ambient temperature before reaching the volume gauge.

Back and cell pressure transducers

Measurements from the back and cell pressure transducers are one of the few direct measurements in tests performed in the isotropic cell. They are also used as feedback to the system to control the back and cell pressures. Therefore, it is important to perform calibrations at both ambient and elevated temperature to ensure these measurements are accurate. The pressure transducers (manufactured by RS components, models 461-301) have a capacity of 0

to 1 MPa, with a resolution of 0.05 kPa. In the tests performed in this research, pressures ranged from 0 to 700 kPa, which is within the working range of the transducers.

Some actions were taken to reduce the thermal effect on pressure transducers. Back pressure and cell pressure transducers were connected to the cell via steel tubing and located at a distance (>1 m) from the cell to minimise the amount of heat transferred to the instrumentation. Heated water from the cell would have cooled down before it entered the pressure transducers. In addition, the outer shell of the transducers was made of stainless steel and had good thermal conductivity. This would allow heat to dissipate to the environment in a short period of time. In order to confirm this, a lamp that produced heat up to 60 °C was placed at a distance of 30 cm to the transducers. It was observed that the output voltage of the transducers at elevated temperature did not change compared to that at ambient temperature. During testing, it was possible that the heated water would enter the pressure transducer and influence the pressure readings. In order to obtain calibration factors of the instrumentation under different temperature levels, the back pressure transducer was connected to the triaxial cell and the Budenburg dead weight calibrator at the same time, using a T-shape valve. Water in the triaxial cell was heated and allowed to reach the pressure transducer as in the case of real tests. Back pressure transducer was then loaded from 0 kPa to 600 kPa using the Budenburg dead weight calibrator for three loading and unloading cycles, with 72 data points obtained for plotting calibration curves at each temperature level. The calibration curves with the back pressure plotted against output voltage are presented in Figure 3-2. The range of calibration was from a back pressure of 41 to 772 kPa. Calibration factors were estimated up to four decimal places based on the analysis of the calibration data. The same calibration procedure was applied to the cell pressure transducer. For back pressure transducer, if a single calibration factor was used for temperature ranging from 20 to 60 °C, the maximum error for the combined data was 0.4 %, which was close to the maximum error of the data at a single temperature level (Table 3-1). Therefore, changing the temperature from 20 to 60 °C did not affect the performance of back pressure transducer. A single calibration factor can be used for back pressure transducer despite the temperature change in the isotropic cell during tests. The same applied to the cell pressure transducer.

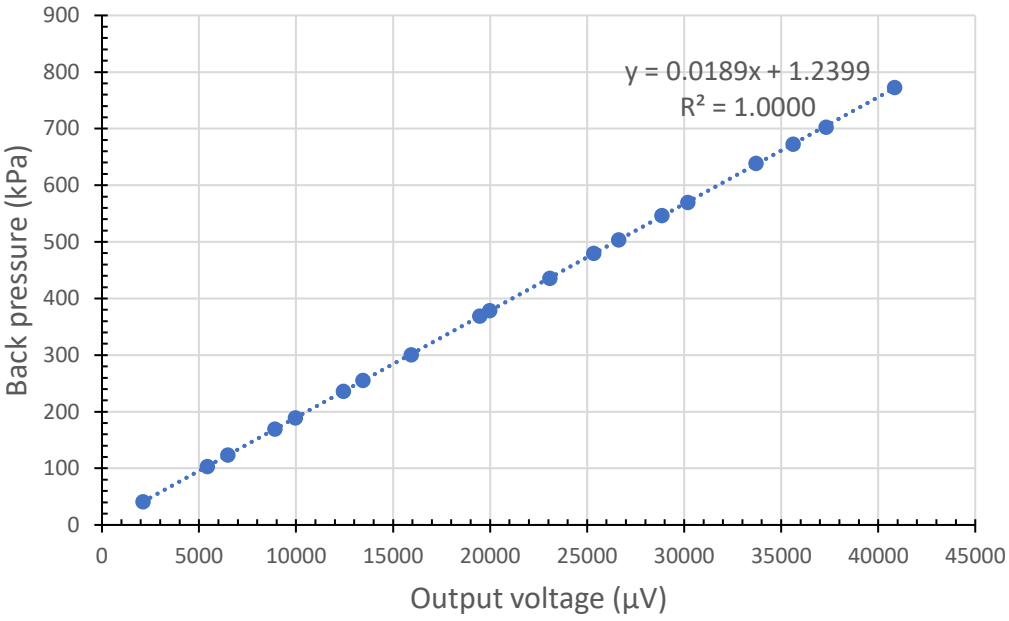
y = 0.0189x + 1.2399
R² = 1.0000
Back pressure (kPa)
Output voltage (μV)
0
100
200
300
400
500
600
700
800
900
0
5000
10000
15000
20000
25000
30000
35000
40000
45000

(a) 20°C

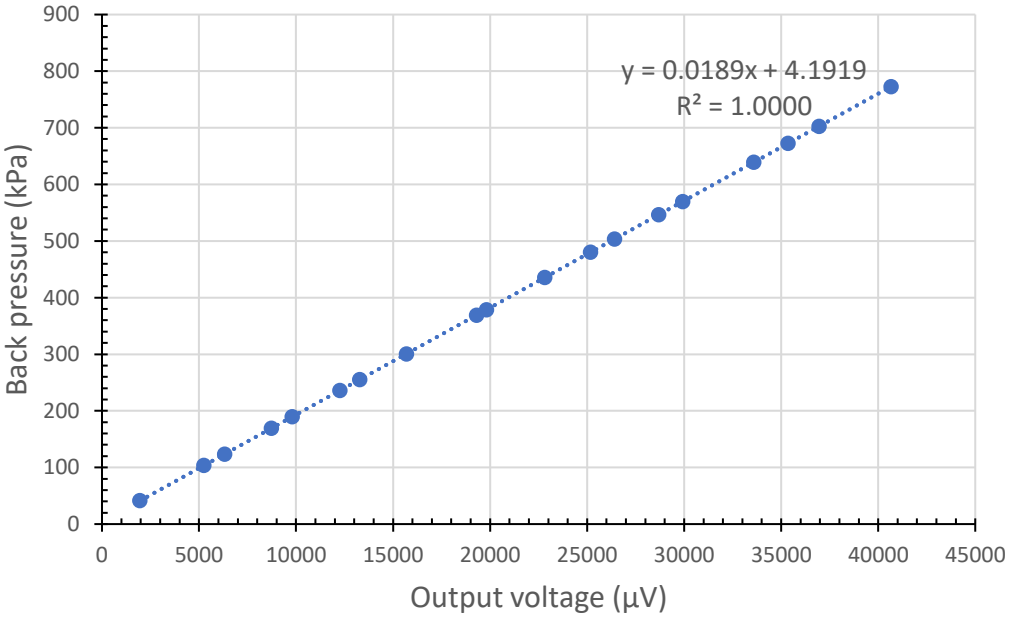
y = 0.0189x + 4.1919
R² = 1.0000
Back pressure (kPa)
Output voltage (μV)
0
100
200
300
400
500
600
700
800
900
0
5000
10000
15000
20000
25000
30000
35000
40000
45000

(b) 40°C

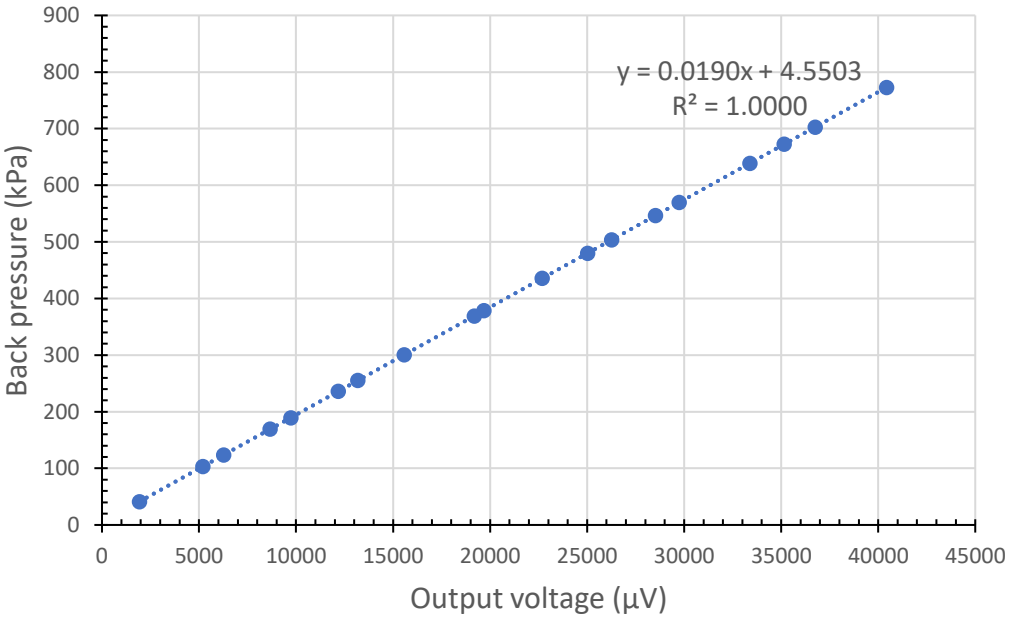

(c) 60°C

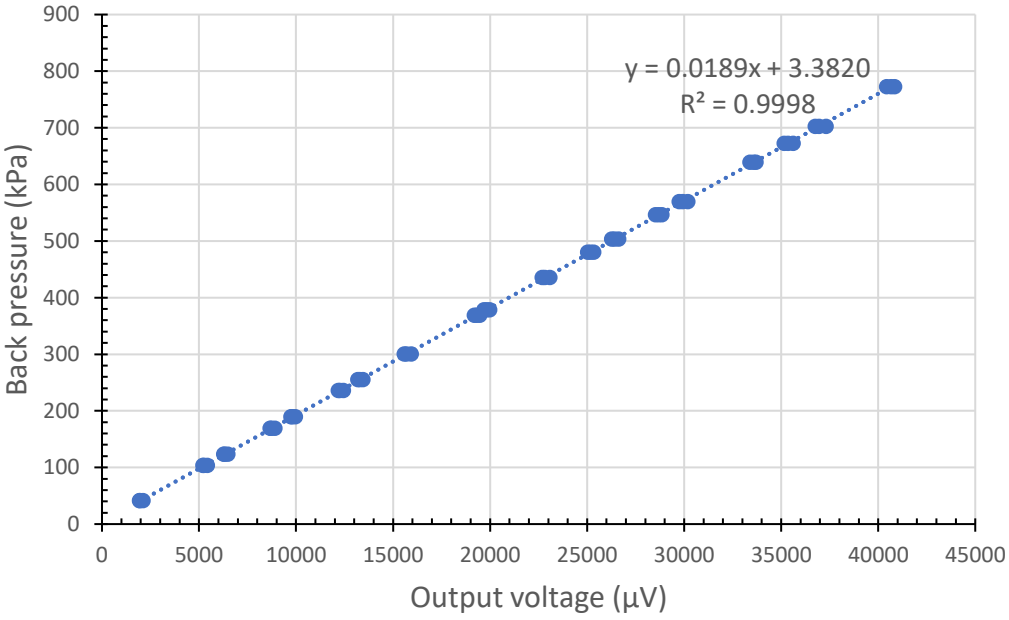

(d) 20-60°C

Figure 3-2: Calibration curves of back pressure transducer under different temperature levels a) 20°C; b) 40°C; c) 60°C; d) 20-60°C

Table 3-2: Calibration factors of back and cell pressure transducers under different temperature levels

	Temperature (°C)	Calibration curve	Max. error (kPa; %)
Back pressure transducer	20	$y = 0.0189x + 1.24$ *	3.9; 0.8
	40	$y = 0.0189x + 4.19$	1.4; 0.3
	60	$y = 0.0190x + 4.55$	1.6; 0.4
	20-60	$y = 0.0189x + 3.38$	4.2; 0.8
Cell pressure transducer	20	$y = -0.0188x + 4.24$	2.0; 0.4
	40	$y = -0.0188x + 8.28$	1.1; 0.2
	60	$y = -0.0189x + 8.20$	1.6; 0.3
	20-60	$y = -0.0189x + 7.86$	2.3; 0.4

* x and y represent the output electrical signal of instrumentation in uV and pressure in kPa, respectively.

Mid-height pore pressure probe

During the test, mid-height pore pressure probe was placed inside the isotropic cell, and it may also be affected by the heated soil specimen around it. Having proved that calibration factors of back and cell pressure transducers were insensitive to changes in temperature, calibration curves of mid-height pore pressure probe were obtained by using pressure readings from back pressure transducer at different temperature levels as a reference (Table 3-2). When the temperature was increased from 20 to 60 ℃, calibration factors changed from -0.0163 to -0.0178. At the same temperature level, the maximum error was 0.4%. When the calibration data at different temperature levels were plotted together, the maximum error that was induced by using a single calibration factor increased to 8.0%, equivalent to 63 kPa when the pressure is 700 kPa. In other words, using a single calibration factor to represent the response of mid-height pore pressure probe could lead to considerable errors in measurement. Therefore, changing of temperature in the range of 20 to 60 ℃ affects the performance of mid-height pore pressure probe. Temperature-based calibration factors should be applied to obtain reliable readings.

Table 3-3: Calibration curves of mid-height pore pressure probe under different temperature levels

Temperature (℃)	Calibration curve	Max error (kPa; %)
20	$y = -0.0163x + 25.87$ *	1.5; 0.3
37.5	$y = -0.0169x + 27.08$	1.7; 0.3
40	$y = -0.0170x + 29.01$	0.8; 0.2
60	$y = -0.0178x + 28.98$	2.1; 0.4
20-60	$y = -0.0168x + 32.74$	38.6; 8.0

* x and y represent the output electrical signal of mid-height pore pressure probe in uV and pressure in kPa, respectively.

By plotting slopes of calibration curves at 20, 37.5, 40 and 60 ℃ against corresponding temperature levels (Figure 3-3), calibration factors under temperature levels from 20 to 60 ℃ can be estimated using linear interpolation. In this way, pore water pressure at the mid-height of the specimen can be accurately measured and then compared with that measured from the base pedestal. A comparison of the pore water pressure measured at the two locations of the specimen is shown in Figure 3-4. Test ISO-150-2 is chosen as a representative of all the tests to show the general trend. After temperature-based calibration factors were applied to correct the measurements from mid-height pore pressure probe, pore water pressure measured from two locations of the specimen was consistent with each other. The maximum error between the two measurements was 2.9 kPa, equivalent to 5.8% in the test considered. It occurred at the first heating-cooling cycle, when the specimen was heated to 40 ℃. At lower pressure levels, measurements from the two sources agreed well with each other.

Radial LVDTs were calibrated at ambient and elevated temperatures at the initial stage of this research. It was found that the changes in readings due to temperature were larger than the order of magnitude of changes in dimensions of the specimen, and that the calibration factors at different temperature levels did not follow a trend. Therefore, radial LVDTs were not used in this apparatus.

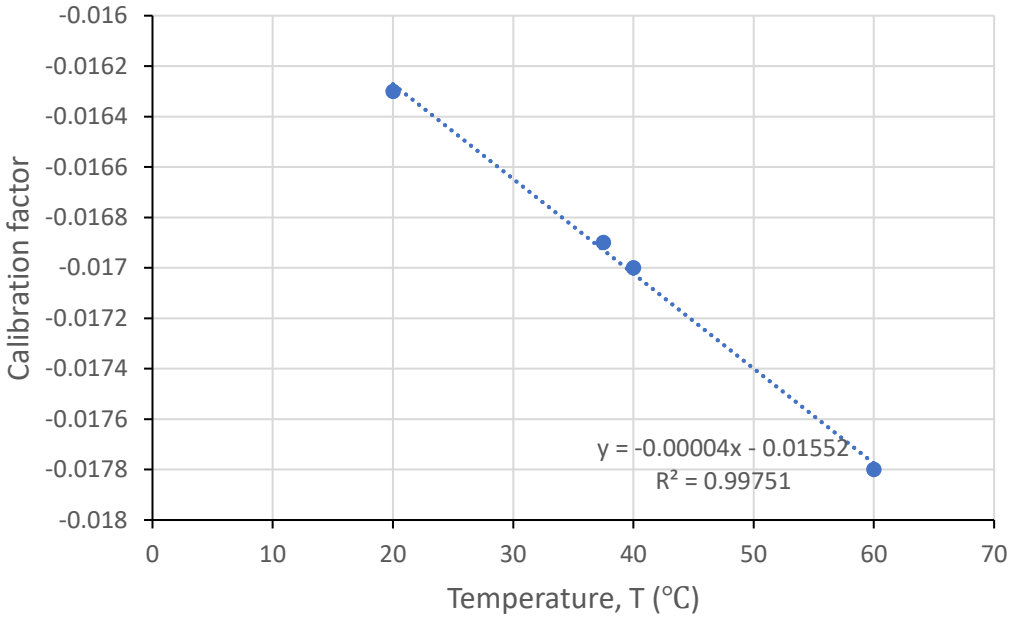

Figure 3-3: Regression curve of calibration factors of mid-height pore pressure probe under different temperature levels

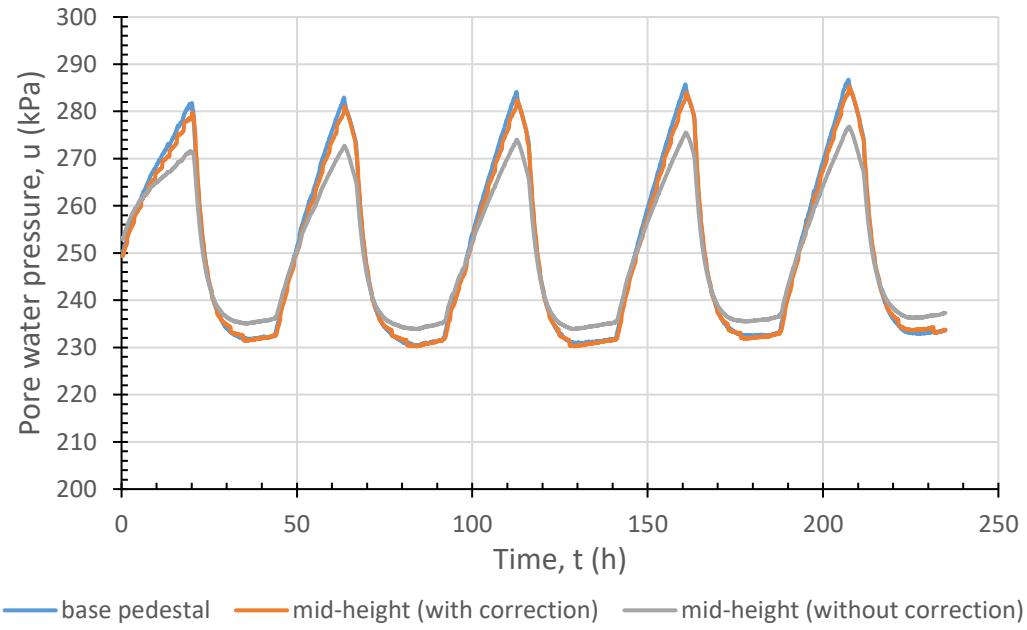

Figure 3-4: Comparison of pore water pressure measured at different locations in the test ISO-150-2

Summary of instrumentation calibrations in the isotropic thermal cell

Calibrations of instrumentation of the isotropic apparatus are summarised in Table 3-3. These calibrations were incorporated into the TRIAX software to convert the electric signals of the instrumentation to physical quantities that can be used to control the tests and recorded for data analysing purpose.

Table 3-4: Summary of calibration of instrumentation of the isotropic apparatus

Instrumentation	Temperature (°C)	Calibrated against	Calibration range	R square	Max. error	Resolution	Capacity
Back pressure volume gauge	20	Weight scale	3-44 cc	1.0000	0.035 cc (0.1%)	0.01 cc	0-50 cc
Mid-height pore pressure probe	20	Budenberg dead-weight calibrator	35.5 – 725.0 kPa	1.0000	0.7 kPa (0.2%)	0.05 kPa	-
	40	Back pressure transducer	103.5 – 620.6 kPa	1.0000	0.8 kPa (0.2%)		
	60	Back pressure transducer	103.5 – 620.6 kPa	1.0000	2.1 kPa (0.4%)		
Cell pressure transducer	20	Budenberg dead-weight calibrator	103.5 – 862.0 kPa	1.0000	2.0 kPa (0.3%)	0.05 kPa	0-1 MPa
	40		103.5 – 620.6 kPa	1.0000	1.1 kPa (0.3%)		
	60		103.5 – 620.6 kPa	1.0000	1.6 kPa (0.4%)		
Back pressure transducer	20	Budenberg dead-weight calibrator	41.0 – 772.5 kPa	1.0000	2.4 kPa (0.3%)	0.05 kPa	0-1 MPa
	40		41.0 – 772.5 kPa	1.0000	1.4 kPa (0.2%)		
	60		41.0 – 772.5 kPa	1.0000	1.6 kPa (0.2%)		

3.3 Double load cell triaxial apparatus

3.3.1 Description

A typical triaxial cell enables the confining fluid around a cylindrical soil specimen in a pressurised cell to apply an initial stress condition and then shearing to failure, in order to determine the shear strength and stiffness of the specimen. In this research, particular emphasis is placed on studying the temperature effect on the shear strength and stiffness of reconstituted London clay. To enable thermal testing on geomaterials, a new temperature-controlled triaxial apparatus was developed at the ICGL. The main components of the apparatus are shown in the schematic view in Figure 3-5.

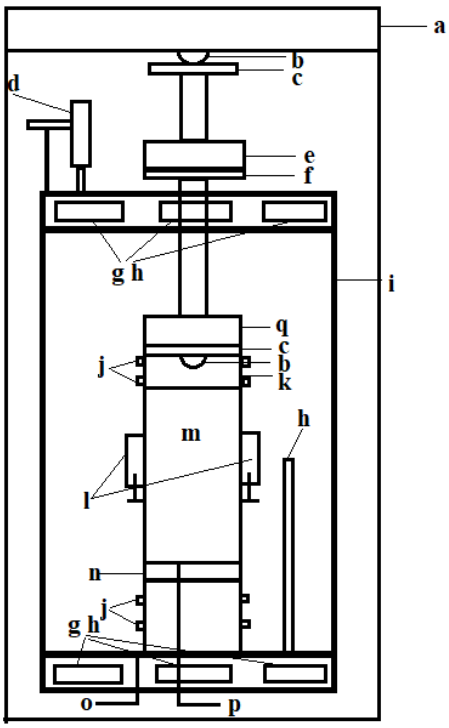

Figure 3-5: Schematic view of temperature-controlled triaxial apparatus (a) loading frame; (b) half ball bearing; (c) friction reduction end; (d) linear variable differential transformer; (e) external load cell; (f) insulation plate; (g) heater; (h) temperature sensor; (i) stainless steel chamber; (j) O-ring; (k) topcap; (l) axial linear variable differential transformer; (m) soil specimen; (n) porous disc; (o) to cell pressure volume gauge; (p) to back pressure volume gauge; (q) internal load cell

The triaxial cell consists of a stainless-steel chamber (Figure 3-5 (i)) that reduces the system compliance under temperature, compared to some conventional triaxial apparatus that use Perspex chambers. Inside the chamber, deaired water is used as the confining fluid. The confining pressure can be raised up to 800 kPa. This is achieved through an air compressor system that supplies 800 kPa air pressure and then controlled using digitally controlled stepper motors. Cell and back pressure are measured using pressure transducers with a capacity of 1 MPa and resolution of 0.05 kPa, similar to the isotropic cell pressure transducers. Water that flows in and out of the cell is measured using the Imperial College type volume gauges (Figure 3-5 (o) (p)) with a capacity of 50 cm^3 and a resolution of 0.001 cm^3. This measurement is achieved by the movement of the air-water interface in the volume gauges. Both the cell and back pressure volume gauges are connected to the cell using metal tubing and they are located at a distance that is over 1 m from the cell, in order to minimise the effect of temperature on their performances. Two axial linear variable differential transformers (LVDTs) (Figure 3-5 (l)), as described by Cuccovillo and Coop (1997), are used to measure the local deformation of the specimen during the test. The two axial LVDTs are glued to the specimen using two mounts. The upper mounts contain the main body of the LVDTs and the lower mounts hold the armature. In conventional 50 mm diameter triaxial tests at ICGL, there are usually three local LVDTs

inside the cell distributed evenly around the cylindrical specimen, to measure the local displacement of the specimen. Due to the limited space in this apparatus, two local LVDTs are placed on opposite sides of the specimen. An external LVDT (Figure 3-5 (d)) is located at the top of the apparatus and outside the cell. Readings from this external LVDT is used to regulate and control the shearing rate of the test, as it is not affected by the formation of local shear plane, and is also not affected by the temperature effect, as presented in Section 3.3.2. Cylindrical shape specimens (Figure 3-5 (m)) with a diameter of 50 mm and height of 100 mm can be tested in this apparatus.

A special design of this apparatus that is worth noting is the double load cell system. An internal load cell (Figure 3-5 (q)) with a capacity of 5 kN and resolution of 0.1 N locates at the top of the specimen to measure the force during the shearing stage of the test. Another external load cell (Figure 3-5 (e)) that connects to the internal load cell but is located outside the triaxial cell has a capacity of 10 kN and a resolution of 0.2 N. In between the two load cells, there is a circular plate (Figure 3-5 (f)) that reduces heat flux from the triaxial cell to directly going to the external load cell, by radiating part of the heat flux to the environment. This double load cell system has the following advantages. Firstly, it enables the temperature-based calibration of the internal load cell, considering that the internal load cell locates in the water bath and its calibration factor may be affected by temperature, while the external load cell remains at ambient temperature and can be used as a reference. Secondly, by comparing the readings from the two load cells, quantifying the system compliance at different pressure and temperature levels becomes possible. Thirdly, due to the nature of the test and the low permeability of the soil tested, test duration can be long, with some tests taking up to 55 days. During this timeframe, incidents may happen, including overheat of the heaters and failure of the load cell. Under these circumstances, the double load cell system provides a backup measurement of the axial force.

Another special design of the system is the connections between the internal load cell and the soil specimen, and between the external load cell and the loading frame (Figure 3-5 (c)). The new connections are made of two brass circular plates and a circular ring that is made of the same material in between them. Inside the ring, small ball bearings were placed (Figure 3-6), together with a thin layer of grease to reduce the friction. The topcap that locates between the specimen and the internal load cell is modified to accommodate a half-ball bearing. This design minimises the friction at the top of the sample and reduces the bending of the sample during shearing. In early stage of this research, some trial tests were performed which showed that during the undrained shearing stage, after the shear plane formed, clay specimens were so

distorted in the horizontal direction and no longer centred that the load cell lost contact with the specimens, or in some cases, the load cell became greatly tilted, leading to errors in the measurement of the shearing force (Figure 3-7 (a)). After the friction reduction end was implemented, the deformed shape of the specimen was less distorted (Figure 3-7 (b)). The load cell was still in contact with the specimen after the shear plane formed, in order to measure the shear force accurately. Suction cap was not used in this research as the load cell readings were always reset to zero before shearing, for temperature-based calibration purposes.

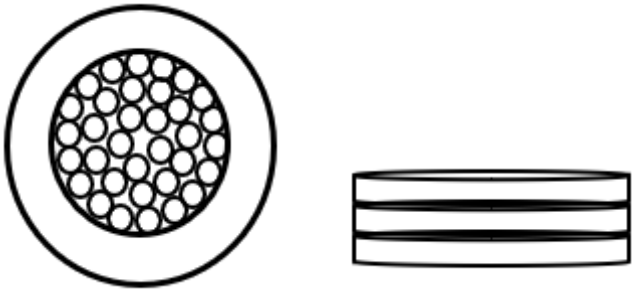

(a) top view (b) side view

Figure 3-6: friction reduction end (a) top view; (b) side view

(a) without friction reduction end (b) with friction reduction end

Figure 3-7: Photos of specimens after shearing

Heating of the specimen is achieved using six 150 W cartridge heaters. Three of the heaters are located in the top stainless-steel plate at 120° to each other. Another three of the heaters are distributed with a similar spacing in the bottom stainless steel plate. There are temperature sensors next to each heater to regulate and provide feedback to the computer system to control the temperature.

3.3.2 Calibrations of instrumentation

Calibration of instrumentation at ambient temperature follows procedures recommended by Head (1998). For most of the instrumentation, including back and cell pressure transducers, back and cell pressure volume gauges, load cells and linear variable displacement transformer, three cycles of loading-unloading loop are performed to assess the possible hysteresis in the instrumentation, similar to the process applied in the calibration of the isotropic cell presented in Section 3.2. Therefore, this section mainly presents temperature-based calibrations for axial LVDT and load cells.

External LVDT

The external LVDT (manufactured by RS components, model LDS-5) was calibrated using a micrometer. It has a resolution of 0.0001 mm and a capacity of 0-25 mm. The external LVDT was located on a mount on top of the cell, exposed to the atmosphere. The effect of temperature changes inside the cell on the performance of the external LVDT was assessed in two ways. Firstly, the external LVDT and the micrometer were placed in a water bath that was heated to 30 and 40 °C. Readings of the micrometer was reset to zero before it was used to calibrate the LVDT. Calibrations were performed following the same procedures as it was at ambient temperature. It was found that the calibration factors were not affected by an elevated temperature. Secondly, a thermometer was placed next to the external LVDT while the water inside the cell was heated. Temperature measured by the thermometer remained at the same value as the ambient temperature. Therefore, calibration factor at 20 °C can be used for the external LVDT, regardless of the heating and cooling process inside the cell.

Internal axial LVDT

The internal axial LVDTs were glued to specimens and might be affected by the temperature changes inside the cell. In order to assess the effect of temperature on the performance of the internal axial LVDTs, axial LVDTs were connected to a micrometre and then they were placed in a water bath. Calibrations were performed at 20, 40 and 60 °C. Calibrations were incorporated into the TRIAX programme as a function to represent the relationship between the physical quantity and electric signal. In the case of internal axial LVDT, a linear function was adopted as the calibration curve as shown in Equation 3-1, where y is the displacement (unit: mm), x is the output signal (unit: μV) and a is the calibration factor. b is the intercept of the calibration curve, but it is less important in the calibration as the displacement is always set to zero at the start of shearing.

$$y = ax + b \qquad 3\text{-}1$$

Calibration factors at 20, 40 and 60 °C are presented in Table 3-4. For both axial LVDTs, if a single calibration factor was used for temperature levels from 20 to 40 °C, the maximum error for calibration was 0.9%, which was comparable to the maximum error at a single temperature level. Therefore, a single calibration factor could be used for axial LVDTs at temperature levels between 20 and 40 °C, which covered all the tests performed in this cell for this research. In the case where the temperature is raised to 60 °C, the maximum error increases to 2.6% and 2.4% for the two axial LVDTs. Different calibration factors may be used to ensure the accuracy of displacement measurements at 60 °C, especially when the data is used to calculate small strain stiffness.

Table 3-5: Temperature-based calibrations for axial LVDTs

Instrumentation	Temperature (°C)	Calibration range	Calibration factor	Max. error
Axial LVDT 1	20	0-12 mm	-0.000781	0.0814 mm (0.7%)
	40		-0.000803	0.0917 mm (0.8%)
	60		-0.000816	0.0437 mm (0.4%)
	20-40		-0.000798	0.1156 mm (0.9%)
	20-60		-0.000804	0.3165 mm (2.6%)
Axial LVDT 2	20	0-12 mm	-0.001006	0.0729 mm (0.6%)
	40		-0.001024	0.0403 mm (0.3%)
	60		-0.001045	0.0258 mm (0.2%)
	20-40		-0.001014	0.1103 mm (0.9%)
	20-60		-0.001019	0.2823 mm (2.4%)

External and internal load cells

A double load cell system was composed of an internal load cell (model: STALC3-5KN-003-ICC01 s/n. 45615) and an external load cell (model: STALC3-10KN-003-ICC01 s/n. 34503). Both load cells were calibrated against Budenberg dead weight calibrator at ambient temperature before they were connected. A circular disk was placed between the external and internal load cell, to minimise the effect of heat flux on the external load cell. A thermometer was placed next to the external load cell to monitor the temperature in a trial test. It was found that the temperature remained at the same value as the ambient temperature. Therefore, readings from the external load cell could be used as a reference to calibrate the internal load cell at elevated temperature. Calibrations were performed under different cell pressure and temperature levels, to assess the performance of the double load cell system in different scenarios. In addition, piston friction was measured by initiating a small movement and observing changes in readings in both load cells. This was accounted for in the data analysing process.

Effect of temperature on load cells

Double load cells were tested at temperature levels ranging from 20 to 50 °C under a constant cell pressure of 600 kPa, with a dummy sample placed inside the cell. Readings from internal load cell against those from external load cell are plotted in Figure 3-8 (a). Slope of the lines represent sensitivity of load cells with respect to temperature levels. Lines at 20, 30 and 40 °C are similar to each other, with slopes changing between 1.037 and 1.045 as in Figure 3-8 (b). Data points from calibration at these three temperature levels plotted above a 1:1 line, indicating that there was a difference in readings from the external and internal load cell. A different calibration factor should be applied if tests are conducted at 50 °C, as there is a clear change in the pattern of the relationship between internal and external load cell. Readings from both the external and internal load cells are always reset to zero before shearing. Therefore, the intercept of the calibration curve was not important, but the slope played an important role. The maximum difference in the readings from internal and external load cell was 35 N, corresponding to an axial stress of 4.5 kPa. This difference is acceptable as it is in the order of magnitude of the calibration error of an individual load cell.

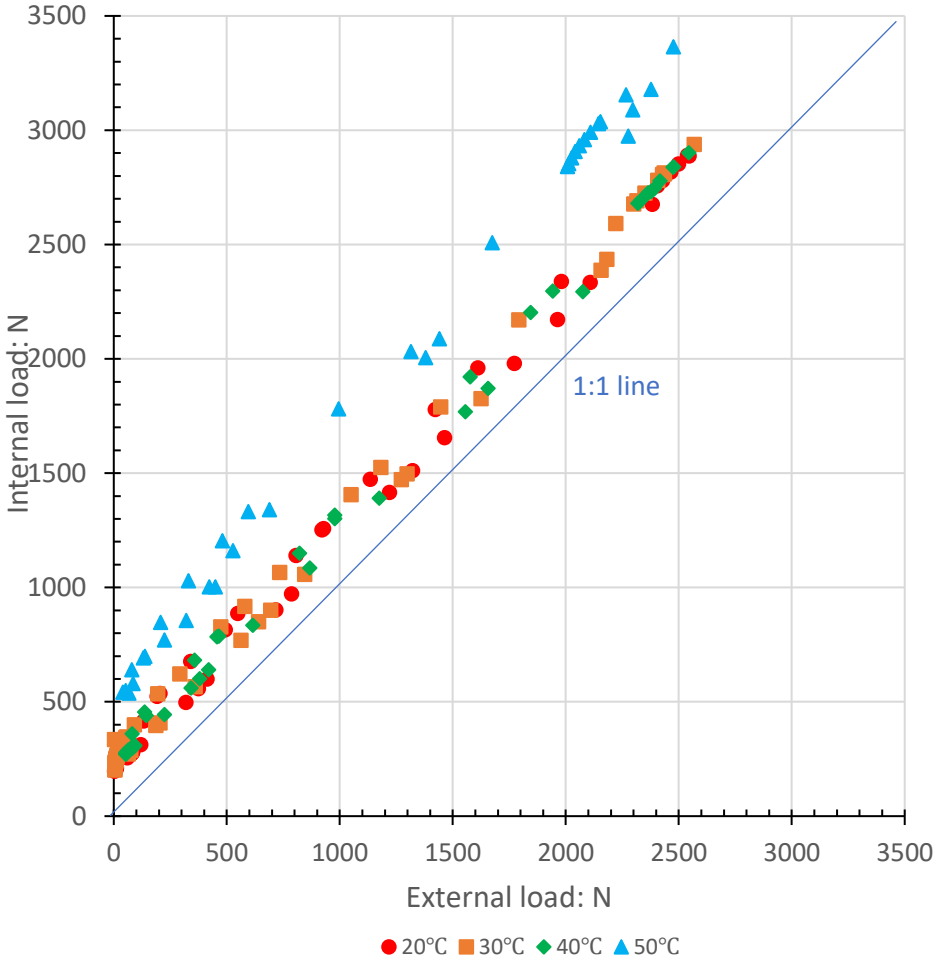

(a) internal load – external load

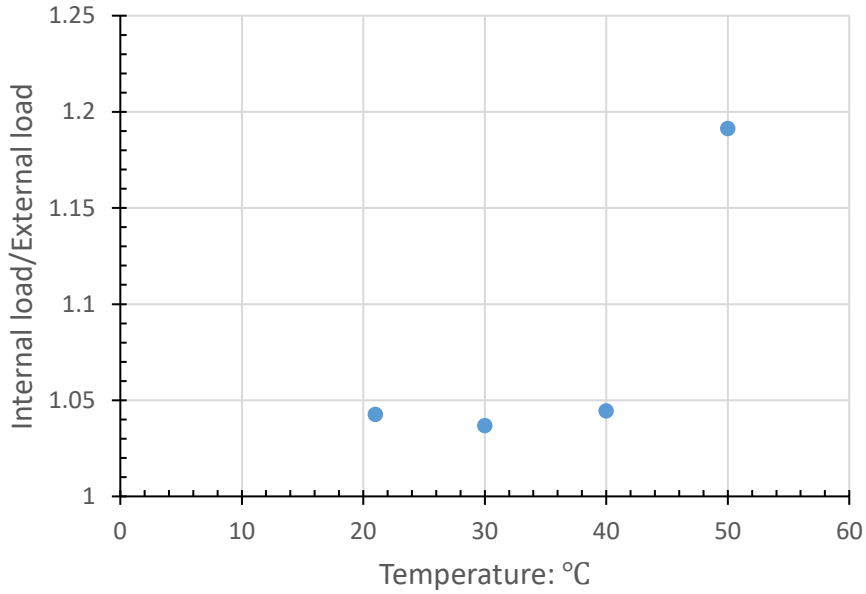

(b) internal load/external load- temperature

Figure 3-8: Effect of temperature on the performance of double load cell system

Effect of cell pressure on load cells

Double load cells were tested under cell pressure ranging from 0 to 600 kPa at 20°C. Measurements from internal and external load cell are plotted in Figure 3-9. No clear pattern of change in sensitivity was observed with changes in cell pressure. Slopes of the trend lines at different cell pressure levels varied between 1.025 and 1.057. Gradient of the trend lines increased with cell pressure, causing the curve to shift upwards when the cell pressure increased. The maximum difference in readings from internal and external load cell was 298 N, corresponding to a shear stress of 38 kPa. In testing programme, specimens were sheared in an undrained condition under a constant cell pressure. The internal load cell was submerged in the cell water, and the effect of cell pressure would be self-compensated. Therefore, difference in readings between the two load cells due to cell pressure can be minimised by resetting load value to zero before shearing. Effect of cell pressure was also quantified by multiplying the cell pressure by piston area and converting it to the reaction force of the piston. This was corrected in the data analysing process.

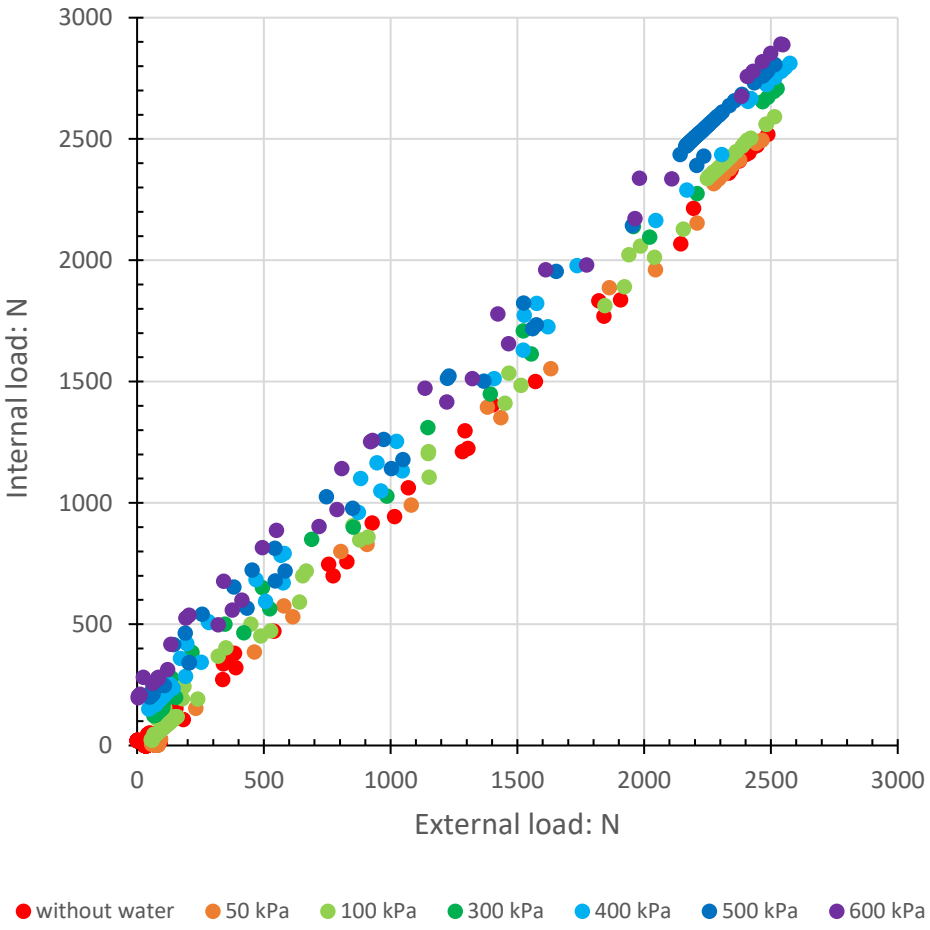

(a) internal load – external load

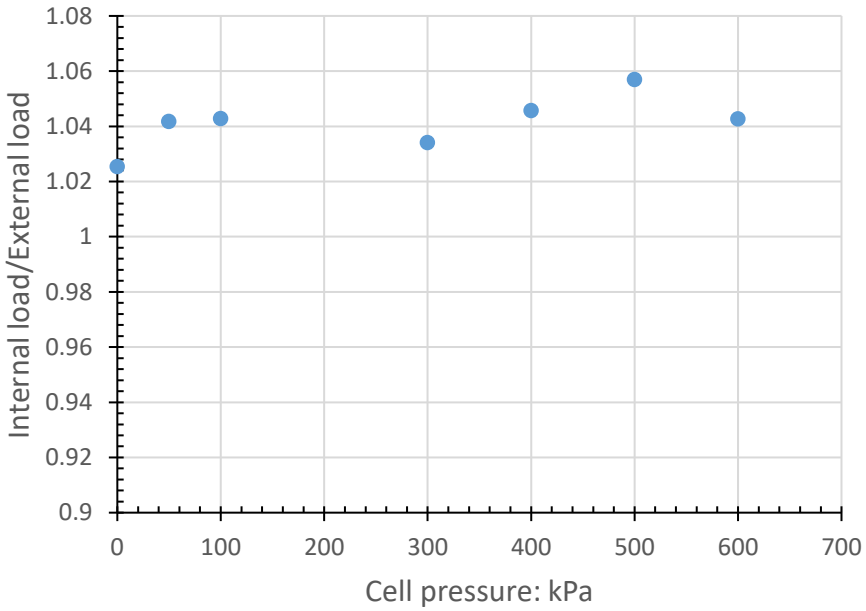

(b) internal load/external load – cell pressure

Figure 3-9: Effect of cell pressure on the performance of double load cell system

Summary of calibrations of instrumentation

Calibrations of instrumentation in the temperature-controlled triaxial cell are summarised in Table 3-5.

Table 3-6: Summary of calibration of instrumentation of the isotropic apparatus

Instrumentation	Temperature (°C)	Calibrated against	Calibration range	Max. error	Resolution	Capacity
External LVDT	20	micrometre	0-24 mm	0.058 mm (0.24%)	0.0001 mm	0-25 mm
Axial LVDT 1	20	micrometre	0-12 mm	0.0814 mm (0.7%)	0.0001 mm	0-12 mm
	40			0.0917 mm (0.8%)		
	60			0.0437 mm (0.4%)		
	20-40			0.1156 mm (0.9%)		
	20-60			0.3165 mm (2.6%)		
Axial LVDT 2	20	micrometre	0-12 mm	0.0729 mm (0.6%)	0.0001 mm	0-12 mm
	40			0.0403 mm (0.3%)		
	60			0.0258 mm (0.2%)		
	20-40			0.1103 mm (0.9%)		
	20-60			0.2823 mm (2.4%)		
Internal load cell	20	Budenberg dead-weight calibrator	227-4839 N	18.0 N (0.4%)	0.1 N	0-5 kN
	30	External load cell	0-4000 N	43.2 N (1.1%)		
	40	External load cell	0-4000 N	29.3 N (0.7%)		
External load cell	20	Budenberg dead-weight calibrator	235-4846 N	2.8 N (0.2%)	0.2 N	0-10 kN
Back pressure volume gauge	20	Weight scale	4-47 cc	0.05 cc (0.1%)	0.01 cc	0-50 cc
Cell pressure volume gauge	20	Weight scale	4-46 cc	0.04 cc (0.1%)	0.01 cc	0-50 cc
Back pressure transducer	20	Budenberg dead-weight calibrator	40-809 kPa	0.90 kPa (0.1%)	0.05 kPa	0-1 MPa
Cell pressure transducer	20	Budenberg dead-weight calibrator	68.95-689.5 kPa	1.02 kPa (0.2%)	0.05 kPa	0-1 MPa

3.4 Oedometer apparatus

3.4.1 Description

The temperature-controlled oedometer apparatus was developed based on the standard VJ Tech front loading oedometer apparatus (mode number: VJT0650) available at ICGL. It is used for the determination of the consolidation and compression characteristics of soils when subjected to changes in the applied vertical effective stress, under different temperature levels. In this research, clay specimens with a diameter of 50 mm are confined laterally and allowed to drain freely at the top and bottom surfaces. The apparatus conforms to BS 1377 and ASTM D2435, D4546. The maximum load on the hanger is 150 kg. Major components of the temperature-controlled oedometer apparatus are shown Figure 3-10. A linear variable differential transformer (LVDT) locates at the top of the loading spindle that sits on the oedometer cell, to measure the vertical displacement of the specimen. Loading and unloading are achieved by adding or removing dead weights on the hanger. On the lever arm, there are three possible beam ratios that can be used by adjusting the location of the hanger, which are shown as position 1, 2 and 3 in Figure 3-10. The corresponding lever arm ratios when the hanger is placed at different locations are shown in Table 3-6. In this research, position 1 is used and the soil specimens can be loaded to a maximum vertical stress of 7 MPa.

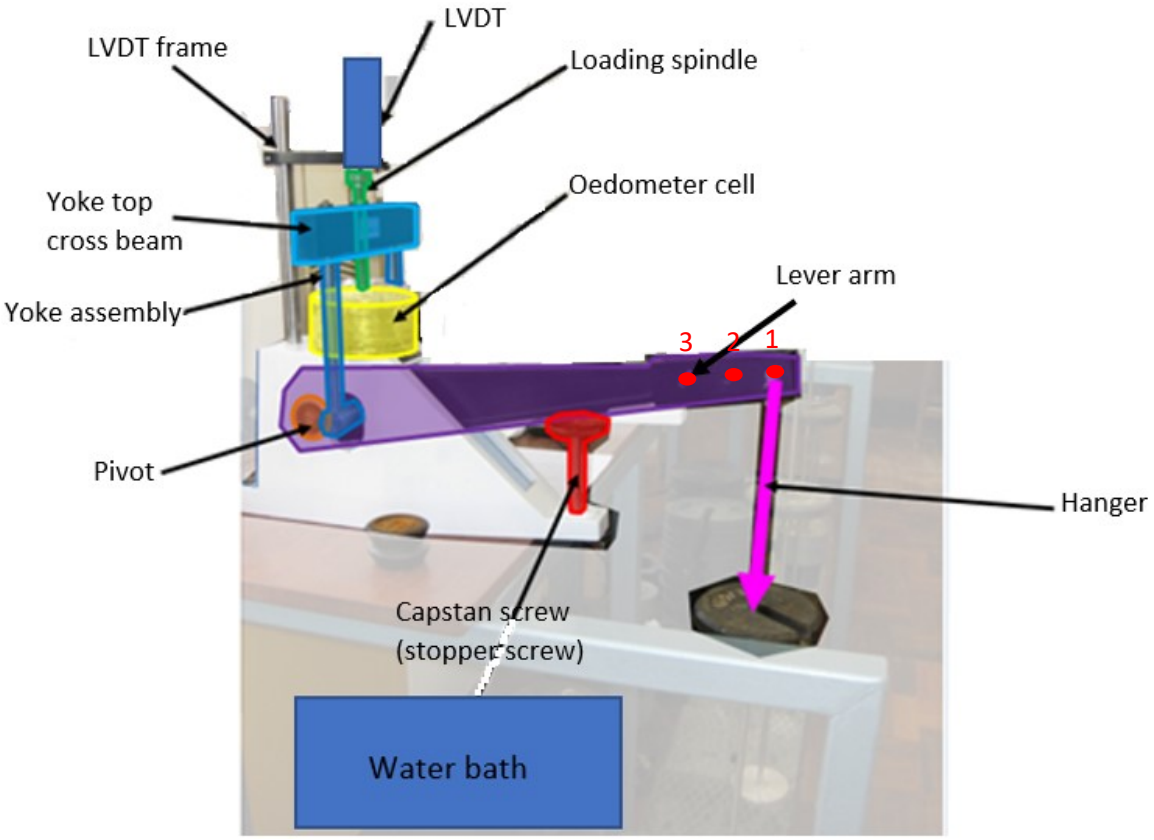

Figure 3-10: Major components of temperature-controlled oedometer apparatus

Table 3-7: Lever arm ratio when the hanger is at different location

Position of the hanger	1	2	3
Lever arm ratio	11.214:1	10.194:1	9.173:1

A schematic view of the oedometer cell is shown in Figure 3-11. The fixed ring cell is made from corrosion-resistant material. The soil specimen is placed on the lower porous disc with the cutter ring surrounding it. The cell ring then clamps down the cutter ring. The pressure pad (which has the upper porous disc attached to it) is placed over the specimen. The whole of this assembly is enclosed within a Perspex cylindrical-shape cell. The cell is filled with water, which is controlled at the desired temperature. A pump circulated the water from a temperature-controlled water bath to the cell. Water inlet and outlet are at the same level in the oedometer cell. The amount of water going in and out of the cell by pumping is the same. Water that is lost to the atmosphere by evaporation can be compensated by manually topping up the cell with water. The top of the oedometer cell is covered with a circular disk to minimise the evaporation of water to the atmosphere under elevated temperature. Temperature of the specimen can be controlled from 20 to 70°C with an accuracy of ± 0.5℃.

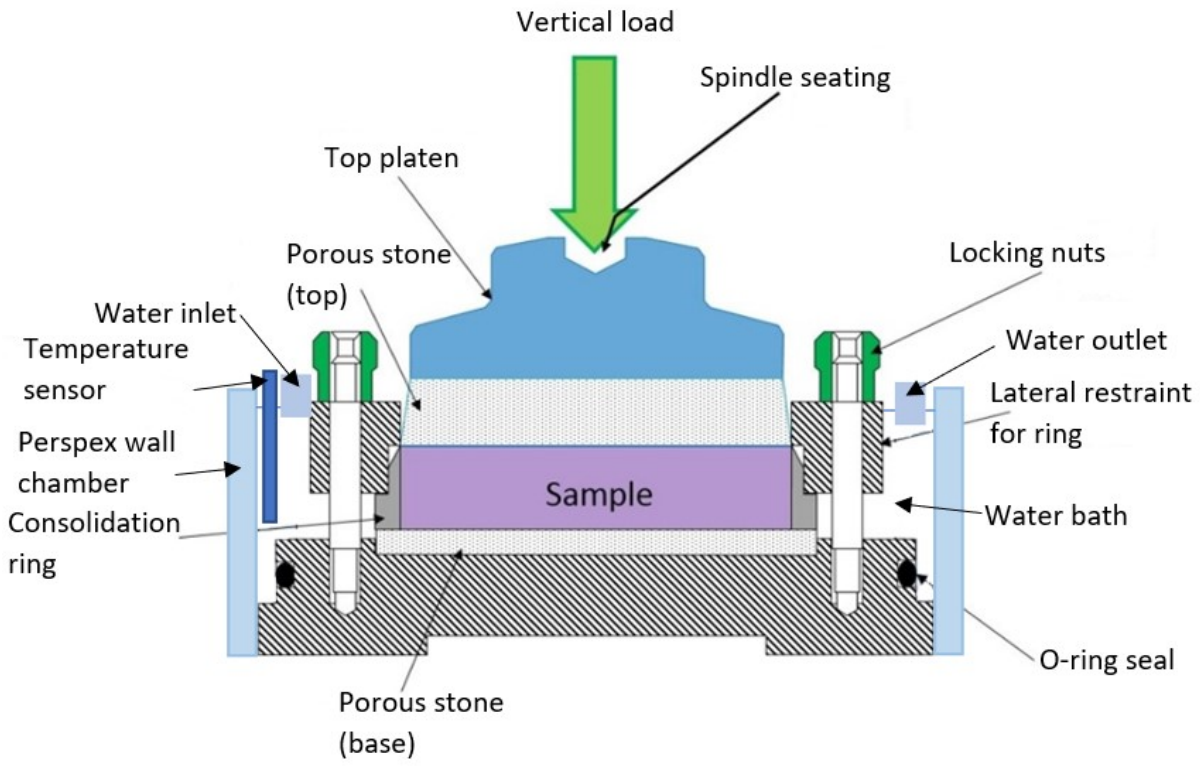

Figure 3-11: Schematic of temperature-controlled oedometer cell

3.4.2 Calibrations of instrumentation

Calibrations of instrumentation at ambient temperature were performed following the procedures for conventional oedometer apparatus described in BS1377 and Head (1998). Displacement measured by the LVDT and mass of the dead weights are the two direct measurements in the one-dimensional compression tests. The LVDT was calibrated against a micrometre with three cycles of compressing – releasing tests. In a trial test, a thermometer was placed next to the LVDT and the temperature remained at the same value as the ambient temperature, regardless of the temperature changes in the oedometer cell. Therefore, calibration factor for the LVDT at ambient temperature can be used throughout the tests. Dead weights were calibrated using a standard balance to an accuracy of 1 g.

During the test, both the specimen and the apparatus itself are compressed. System compliance was quantified by placing a stainless-steel dummy sample that had the same dimension as the real soil specimen into the oedometer cell. The dummy sample was loaded and unloaded following the same loading steps as in real tests. Changes in the dimension in the vertical direction were measured using the LVDT. This calibration process was repeated at 20, 30, 40 and 60 °C. In the horizontal direction, the major concern is the thermal expansion of the confining ring, as this may result in a gap between the soil specimen and the ring, and the one-dimensional compression assumption in conventional oedometer tests may not be valid anymore. Details of the correction applied to quantify the thermal expansion of the confining ring are presented in Section 3.8.4.

3.5 London clay as a testing material

3.5.1 Introduction

This section describes the material used for this research. Firstly, the London clay formation, including its geological history and stratigraphy, is introduced. Secondly, details of how and where the material was sourced are presented. Thirdly, the minerology of London clay is presented, followed by some of its mechanical properties.

3.5.2 The London Clay formation

Understanding the geological properties of London Clay Formation (LCF) is essential for the civil engineering construction in the London basin. The London Clay Formation is an assemblage of related sediments of similar age, rather than a single clay. According to the British Geological Survey, BGS (2016), the London Clay Formation mainly comprises ‘bioturbated or poorly laminated, blue-grey or grey-brown, slightly calcareous, silty to very silty clay, clayey silt and sometimes silt, with some layers of sandy clay. It usually contains

thin inclusions of carbonate concretions ('cementstone nodules') and disseminated pyrite. It also includes a few thin beds of shells and fine sand partings or pockets of sand, which commonly increase towards the base and towards the top of the formation. At the base, and at some other levels, thin beds of black rounded flint gravel occur in places. Glauconite is present in some of the sands and in some clay beds, and white mica occurs at some levels.' (BGS, 2016). The early Eocene LCF was deposited between 52 and 55 million years ago, when it was close to the western shoreline of a sedimentary basin that extended into the North Sea and beyond. This area covered the whole of Eastern Britain from East Anglia to Dorset and southwards over to the North of France, Belgium, Holland and North-west Germany (Martinez-Calonge, 2017).

The lower boundary of the London Clay Formation is taken as the bottom of the Walton Member (Division A2). It is usually marked by a thin bed of well-rounded flint gravel or a glauconitic horizon, or both, typically resting on a sharply defined planar surface, although locally uneven. It overlies the Harwich Formation or, where the Harwich Formation is absent, the Lambeth Group. The upper boundary of the London Clay Formation is taken as the top of the Claygate Member. It is over lied by the Bagshot Formation (BGS, 2016).

Depositional environment

The formation of the London Clay is a sequence of deposition-erosion events. For simplicity, it is assumed that the erosion and other processes occurred after the deposition process completed and therefore, the geological history of London Clay can be treated as a combination of depositional and post-depositional processes.

A comprehensive summary of the depositional process is presented by Gasparre (2005). In the Early Eocene (about 50 million years ago), London Clay started to deposit as a result of a sea level rise in the North Sea Basin. This area covers part of Southern England to the Welsh Massif, Northern France, Western and Northern Belgium and Northern Germany. Different geological zones formed subsequently due to regional geological events that were related to sea level changes. Among them, Hampshire Basin and the London Basin are in Southern England. The first material that was deposited into the embryonic sea is a glauconitic sand called the Harwich Formation. It lies above the Lambeth group which is composed of sands, silts and clays. The London Clay Formation lies in between the Harwich Formation and the Virginia Water Formation, which is a bioturbated glaucontic sand with clay lamines and lenses.

During the deposition process of the London Clay, the depositional environment changed due to the variation of the sea level, which further led to the non-uniformities within the London

Clay stratum (King, 1981). The Hampshire Basin soil was deposited in a shallow marine environment, a high energy environment with a varied stratigraphy. The London Basin soil was deposited in a deeper marine environment, a low energy environment that allowed for less time for the sediments to deposit completely and resulted in less obvious stratigraphy of the soil.

Post-depositional history

Some post-depositional processes and events occurred and influenced the behaviour of London Clay Formation. The preferential precipitation from calcium enriched pore water contributed to the formation of the claystone nodules, which formed as discontinuous bands at specific horizons (Hight et al., 2003).

The Alpine orogeny compressed the subsiding London Platform and its sediments producing the eastward plunging syncline, now referred to as the London Basin. This syncline is very gentle, with most of the dips of less than 3 °. There are some local folds and small faults, but major faults are rarely observed.

Erosion of substantial thickness of overlying sediments is probably the most significant post-depositional process that influenced the behaviour of London clay, which has led to mechanical overconsolidation. This process took place in late Tertiary and Pleistocene times and has removed most of the overlying deposits. The amount of erosion has been estimated to range from about 150m in Essex (Skempton, 1961) to 300m in the Wraysbury district (Bishop et al., 1965). Following the last part of this erosional process, the late Quaternary gravel sheets were deposited along the Thames Valley.

Weathering followed the erosion. The near surface clay has been affected by desiccation, which produces rough, sub-vertical discontinuities, by oxygenated groundwater, which converts ferrous iron to ferric iron, producing the colour change from blue to brown, and which removes pyrite and may dissolve calcium carbonate cement. Clay down to significant depths has been affected by ground freezing. Weathering leads to a loss of c', an apparent reduction in OCR, an increase in water content and to more intense fissuring (Chandler and Apted, 1988).

The formation of scour hollows also affected the London Clay (Berry, 1979).

Stratigraphy

The thickness of the London Clay Formation varies between 50m and 150m in the London Basin and between 50m and 130m in the Hampshire Basin, decreasing westwards in both basins. It has a maximum recorded vertical thickness of 150 m which is preserved in south Essex (King, 1981). The BGS proposed that the LCF could be put into five divisions based on

lithology as units A-D. King (1981) further refined this into a higher-resolution scheme based on the cycles of sea level rise and fall that could be correlated using biostratigraphic data (Figure 3-12). The units are more clearly defined in the Hampshire Basin due to their high-energy environment. While the full sequence of the units includes unit A to E (Figure 3-13), it is only observed in some areas of the London Basin, for example, in Southern Essex or Hampstead Heath (King, 1981). Only units C and below are preserved in most of the area in London.

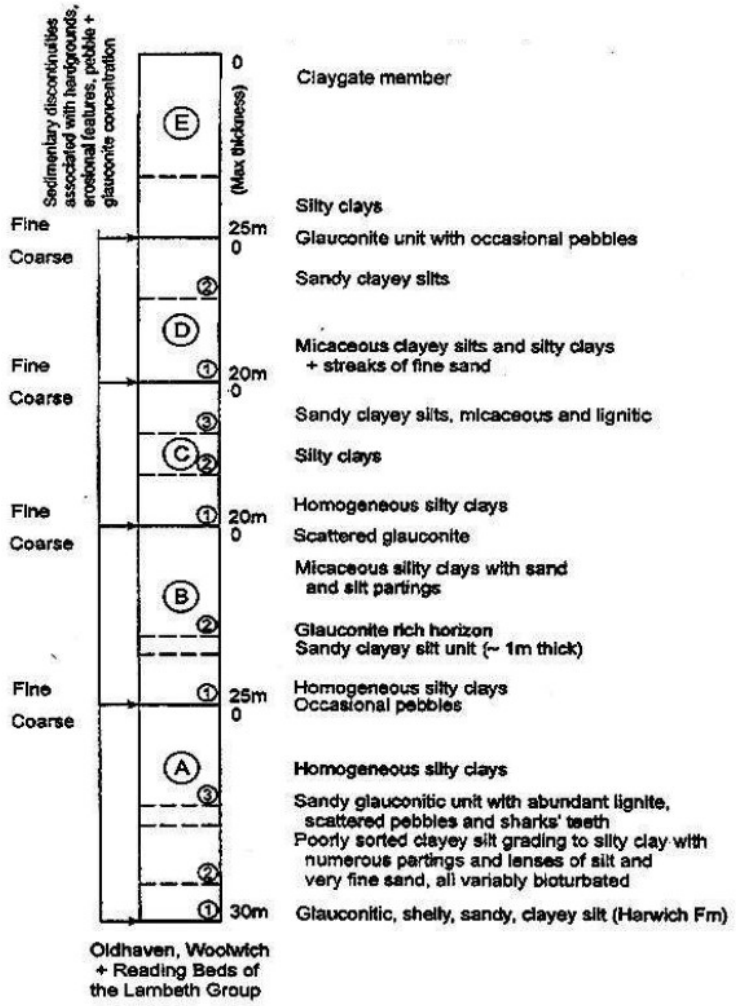

Figure 3-12: Main features of the lithological units in the London Clay (King, 1981)

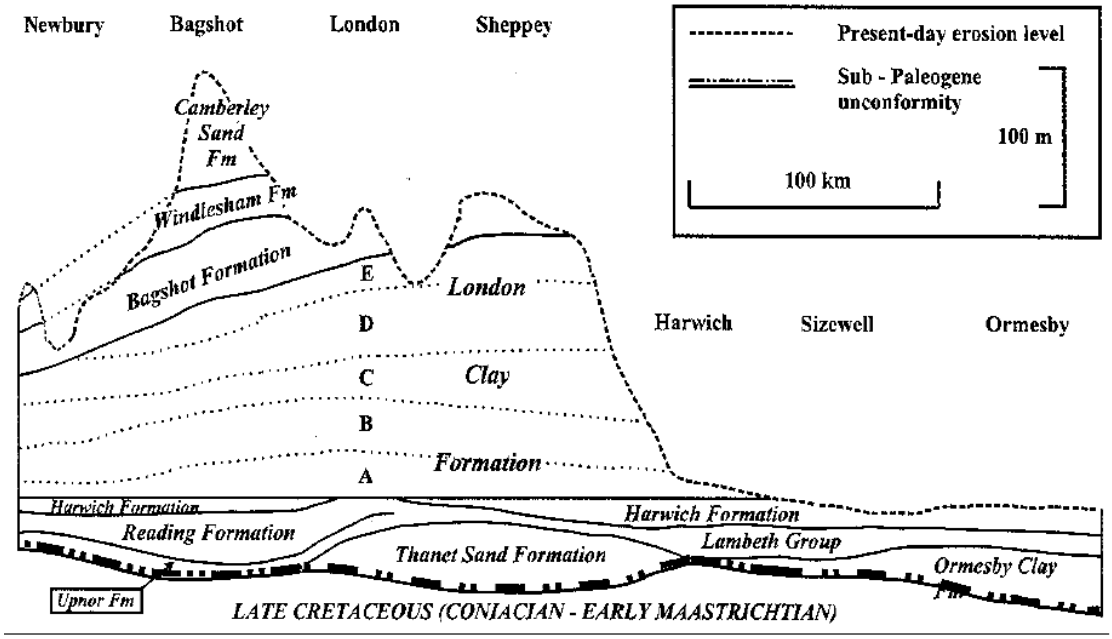

Figure 3-13: Palaeocene and Eocene sections of the London Clay Formation (King, 1981)

Unit A is the deepest among the five units, and it lies just above the Harwich Formation. The original unit A_1 is now included in the upper part of the Harwich Formation and neglected in the London Clay Formation. The lower unit A_2 has an overall thickness of about 12 m, consisting of a high percentage of poorly graded clayey silt, occasional wood fragments and pyrite nodules. It also contains numerous partings and lenses of silts and fine sands with no calcareous fauna present. The upper unit A_3 has an overall thickness of about 15 m and it is further divided into two sub-units, $A_{3\,(1)}$ and $A_{3\,(2)}$, corresponding to the base and top parts of the layer. The base part $A_{3\,(1)}$ contains a homogeneous silty clay and the top part $A_{3\,(2)}$ contains more clayey silts with fine sand partings.

Unit B has an overall thickness of about 25 m and it is further divided into unit B_1 and B_2. The base part B_1 lies between unit A and B_2, consisting of homogeneous sandy clays with some occasional pebbles. A glauconite rich layer lies in between unit B_1 and B_2. The upper part B_2 comprises silty clays with more silts and very fine sands.

Unit C has an overall thickness of about 20 m. It consists of a basal layer of homogeneous silty clay, and it is further divided into three subunits. The base units C_1 and mid unit C_2 both contains silty clays, and they are distinguished by changes in the amount and diversity of macro fauna. The upper part C_3 is sandier, micaceous and lignitic.

Units D and E are only occasionally observed in some parts of the London Basin but not in central London. Both units have an overall thickness between 20 and 25 m. Unit D is sandier compared to unit C. The base part D_1 consists of micaceous clayey silts and silty clays and the

upper part D_2 consists of sandy clayey silts. Unit E_1 contains more clayey soils compared to unit D, including silty clays and clayey silts. Unit E_2 is mainly composed of sandy silts. The top part E_3 is also known as Claygate member which contains laminated and interbedded clays and silty sands (King, 1981).

3.5.3 Source of the material

Specimens of London clay used in this research were sourced from piling works at the Victoria and Albert Museum (Spiral Project) on Exhibition Road in central London (Figure 3-14). The material was taken from a depth of 11-12 m below ground level. Based on the micropaleontological biostratigraphical analysis on two samples that were recovered, it was found that the material belongs to unit C_1 (Martinez-Calonge, 2017). At the site, the overall thickness of the London Clay Formation is about 59.25 m. From the borehole record shown in Figure 3-15, the London Clay layer is overlain by a 6.1 m thick terrace gravels layer and 0.5 m of made ground and it sits on top of the Lambeth Group (Lower Mottled Beds). The ground profile matches the typical features for sites in central London, as described in Section 3.5.2.

Figure 3-14: Location of the material sourced (Martinez-Calonge, 2017)

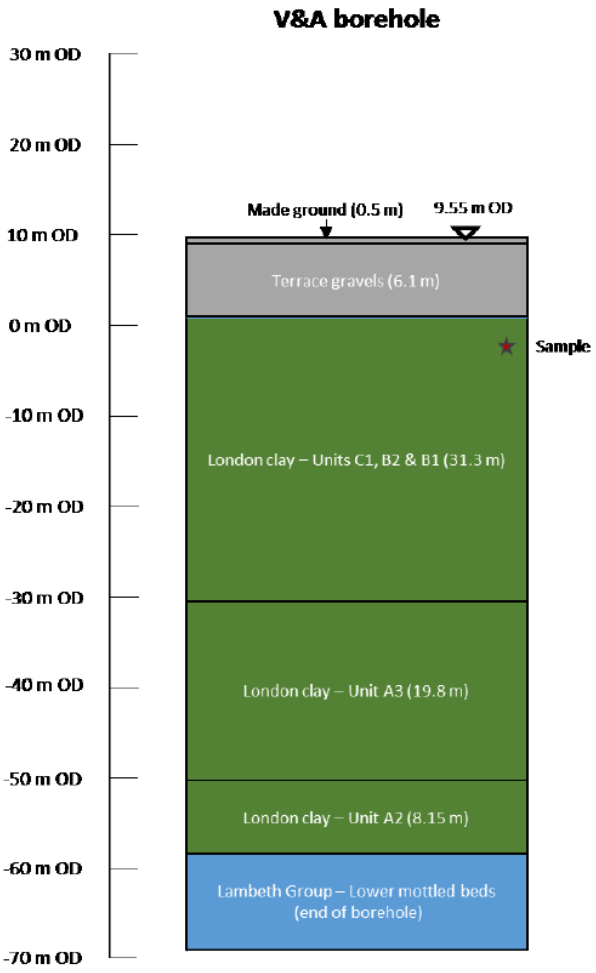

Figure 3-15: Ground profile at the V&A site (Martinez-Calonge, 2017)

3.5.4 Basic material classification

To characterise the soil, some basic classification tests were performed on the samples taken from V&A site, including the specific gravity, plastic and liquid limit. Results obtained are used in interpretating the thermo-mechanical tests on London clay.

Minerology

Martinez-Calonge (2017) carried out tests on the mineralogical composition of the London clay recovered from the V&A site, using the equipment at the Natural History Museum laboratory. The X-ray diffraction (XRD) technique was used to determine the crystallographic structure of the clay. X-rays are produced by the rapid deceleration of fast-moving electrons hitting on the matter and then they irradiate the sample. By measuring the intensities and scattering angles of the X-rays when they leave the material, the chemical composition of the material can be determined. Two different portions (batch 1 and batch 2) of the London clay sample from V&A site were tested in powder form. Results of the XRD analysis (Table 3-7) on these two batches are similar and this confirms the uniformity of samples recovered from the V&A site. An average value is taken for each mineral as a representative of the mineralogical composition of

the samples. The main components of the London clay samples taken from the V&A site are smectite (30.2%), followed by illite (26.3%) and quartz (22.6%). There is a small amount of other minerals, including chlorite (7.4%), k-feldspar (5.2%), kaolinite (4.8%), dolomite (2.8%), albite (0.9%). If these minerals are grouped together, the main components are clay (68.7%) and quartz (22.6%), followed by a small amount of feldspars (6.1%) and carbonates (2.8%).

Table 3-8: Mineral quantification of the bulk sample (modified from Martinez-Calonge, 2017)

Mineral	V&A batch 1	V&A batch 2	Average
Smectite	32.3%	28%	30.2%
Illite	26.1 %	26.5 %	26.3%
Kaolinite	4.4 %	5.2%	4.8%
Chlorite	7.3 %	7.5 %	7.4%
Quartz	21.5 %	23.6 %	22.6%
Albite	1.3 %	0.5 %	0.9%
K-Feldspar	4.7 %	5.6 %	5.2%
Dolomite	2.5 %	3 %	2.8%
Phyllosilicates/Clay	70.1 %	67.2 %	68.7%
Quartz	21.5 %	23.6 %	22.6%
Feldspars	6 %	6.1 %	6.1%
Carbonates	2.5 %	3 %	2.8%

Classification tests

Following the standard procedures recommended in the BS 1377-2: 1990, the classification tests were performed on the London clay samples recovered from V&A site (Martinez-Calonge, 2017). The specific gravity of the solids, G_s, was measured using the small pycnometer method. The plastic and liquid limits of the clay were measured using the thread rolling technique and cone penetrometer method. The particle size distribution chart (Figure 3-16) was established using the hydrometer test. The PSD curve for London clay taken from the V&A site was well bounded by the envelop of particle size distributions for London clay from different sites presented by King (1991). Over 90% of the mass of the soil particles belongs to the range of clay and silt. Results of these tests and the corresponding material properties measured are summarised in Table 3-9.

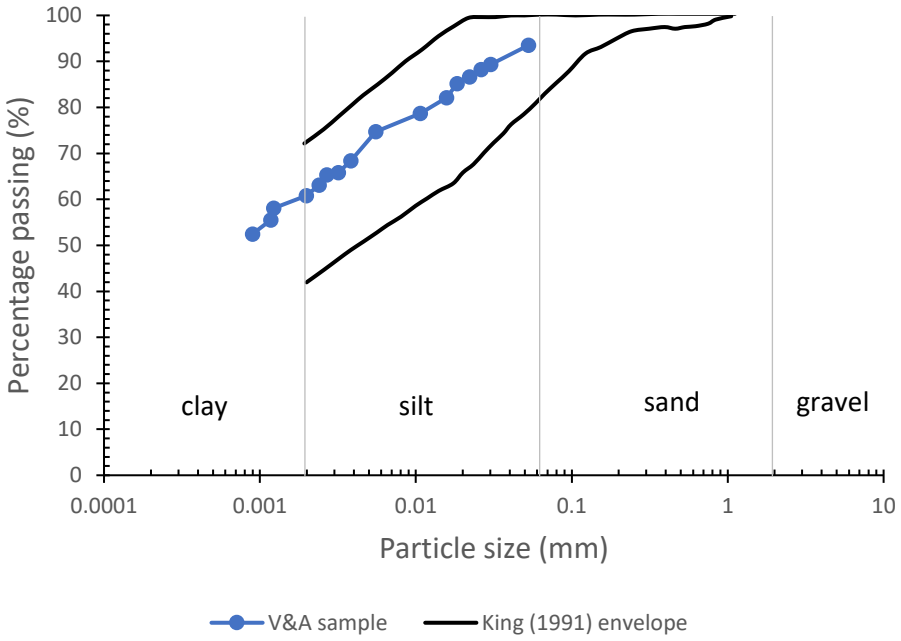

Figure 3-16: Particle size distribution (modified from Martinez-Calonge, 2017)

Table 3-9: Summary of the classification tests (modified from Martinez-Calonge, 2017)

Testing method	thread rolling technique	cone penetrometer method	-	small pycnometer method	hydrometer test
Material properties	Plastic limit, w_P (%)	Liquid limit, w_L (%)	Plastic index, PI (%)	Specific gravity, G_s	Clay content (%)
Results	29	74	45	2.774	61

3.6 Sample preparation

Specimens taken from reconstituted London clay cakes were used in the tests in this research. In this section, details of how the London clay cakes were prepared are presented.

Natural samples taken from the V&A site were broken into small pieces. They were then left in an air-conditioned room to allow to air-dry for seven days. Stones and roots of plants were removed from the material. These small pieces of natural samples were then grounded using an electronic grinding machine. The material obtained was passed through a set of sieves and the coarse material retained on the sieve was put into the grinding machine again, until all the material was in powder form. The London clay powder was mixed with distilled water to make a slurry that had a water content at 1.25 times the water content at liquid limit (Burland, 1990). The slurry was covered with cling film to preserve its water content and left for hydration for 24 hours. During this period, the slurry was stirred three times to make sure it was thoroughly

mixed. The well-mixed slurry was then consolidated under the effective vertical stress of 200 kPa for three weeks in a large consolidometer, leading to a London clay 'cake' with 225 mm in diameter, 130 mm in height and an average water content of 35%. The 'cake' was then covered with several layers of tin foil, cling film and wax to preserve its water content.

For tests performed in the temperature-controlled isotropic and triaxial apparatus, samples of clay were trimmed to a cylindrical shape with 50 mm in diameter and 100 mm in height, using a metal string saw, a trimming frame, a knife, and a two-piece metal hollow mould. For tests performed in the temperature-controlled oedometer apparatus, samples were trimmed to cylindrical shape with 50 mm in diameter and 20 mm in height, by pushing the oedometer ring through the London clay 'cake'. Water content of the trimmings for each trimmed specimen was measured and it varied between 33.7% and 35.5%, with lower water content for specimens taken at the edge of the cake, and higher water content in the middle part of the cake. This is most likely due to the fact that the cake was exposed to air when specimens were trimmed each time, and the parts that were closer to the edge were exposed more to the environment, leading to loss of water. Despite the small difference in the water content for specimens taken at different locations of the cake, the overall uniformity of the cake was deemed acceptable.

3.7 Experimental procedures

3.7.1 Undrained isotropic heating tests

Specimen setup

Distilled and deaired water was flushed through drainage lines of the thermal isotropic cell before testing, to get rid of air trapped in the tubes. Porous disks were saturated for at least 30 minutes, until no air bubbles appear floating to the surface of the water. The specimen of a London clay cake was installed with filter paper side drains and porous discs at the bottom. A topcap with a half ball bearing was placed at the top of the specimen. Latex membrane with thickness of 0.3 mm was used in this testing programme as no significant degradation of the membrane was observed in trial tests at elevated temperature ranging from 20 to 40℃. A mid-height pore pressure probe was installed at the mid height of the soil specimen, and it was properly sealed with liquid latex.

Initial mean effective stress

A cell pressure of 200 kPa was applied with valves to the drainage lines closed. This value was chosen as it was the maximum value that the specimen had experienced during the sample preparation process in the consolidometer. The increase in back pressure was monitored until

the back pressure became stable. The difference between the applied cell pressure (200 kPa) and the back pressure when it stabilised was recorded as the initial mean effective stress.

Saturation

Valves to the drainage lines were opened and the specimen was at drained condition. The cell pressure and back pressure were increased at a rate of 50 kPa/h, maintaining a constant initial mean effective stress, until a back pressure of 250 kPa was reached. This value was chosen as it ensured a satisfying degree of saturation was achieved and at the same time allowed enough change in cell pressure in the consolidation stage, for those tests that were performed on specimens with high stress levels and OCRs. Back and cell pressures were then held at constant values for 48 hours. A B-value test was performed by increasing or decreasing the cell pressure by 20 kPa and then monitor the change in back pressure in an undrained manner. B-value was calculated as the change in back pressure divided by the change in cell pressure. If the B-value was below 0.98 (Burland, 1990), cell pressure and back pressure would be further increased until the B-value reached at least 0.98. After B-value check, valves to back and cell pressure lines were open again.

Isotropic consolidation and swelling

The cell pressure was increased at a rate of 1 kPa/h until the mean effective stress reached the desired value. This rate was shown to be sufficient to maintain a constant pore pressure of 250 kPa in the specimen while the cell pressure increased. In some of the tests where the specimens were overconsolidated, isotropic swelling at a rate of 1 kPa/h was applied subsequent to compression to achieve the desired OCR value. At the end of the isotropic consolidation and swelling stage, the pressure values were maintained sufficiently long to allow for drained creep, until the rate of change of volumetric strain was less than 1/100 of the rate of axial strain during shearing. This was adopted as a general rule, although the tests in the isotropic cell did not involve shearing. The shearing rate in this research was taken as 5% of axial strain per day. Therefore, the acceptable creep rate in the volume gauge was 0.05% per day.

Undrained heating

Valves to back pressure volume gauge were closed. The isotropic cell was wrapped up with several layers of bubble wrap in a controlled manner, and it was properly insulated with a cylindrical chamber on the outside, to reduce heat loss to the atmosphere and to maintain a stable temperature. The specimen was heated in an undrained manner at a rate of 1°C/h, from 21 to 40°C. The total time for heating was 19 hours.

Natural cooling

After the temperature reached 40°C, heaters were turned off. The insulation chamber and bubble wrap were removed. Specimen was cooled to 20°C, which took around 14 hours after removing insulation. The heating-cooling cycle was repeated for at least five times, until the evolution of pore water pressure was comparable to that of the previous heating-cooling cycle.

Duration of tests

Due to the multiple stages involved in the undrained isotropic heating tests and the low permeability of London clay, it could take up to 53 days to perform one test. Duration of each test is shown in Table 3-9. It took longer to complete tests with higher OCR and higher initial stress level. This only accounts for the time from the moment that the specimen was installed in the cell, to the time when the specimen was taken out. It would take more time to perform one test if the time for sample preparation was considered.

Table 3-10: Duration of undrained triaxial heating tests

code	Isotropic loading, p'_{max} (kPa)	Isotropic swelling, p'_c (kPa)	OCR	Duration of test (days)
ISO-150-1	150	150	1	16
ISO-300-1	300	300	1	21
ISO-450-1	450	450	1	44
ISO-75-2	150	75	2	20
ISO-150-2	300	150	2	30
ISO-225-2	450	225	2	41
ISO-50-3	150	50	3	23
ISO-100-3	300	100	3	33
ISO-150-3	450	150	3	43
ISO-60-5	300	60	5	40
ISO-50-6	300	50	6	53
ISO-75-6	450	75	6	50

3.7.2 Drained isotropic heating tests

Specimen setup

Distilled and deaired water was flushed through drainage lines in the thermal triaxial cell before testing. Porous disks were saturated for at least 30 minutes, until no air bubbles appear floating to the surface of the water. A specimen of a London clay cake was installed with filter paper side drains and porous discs at the bottom. Latex membrane with thickness of 0.3 mm was used

in this test as no significant degradation of the membrane was observed in trial tests in the temperature range of 20 to 40 °C. Two axial linear variable differential transformers (LVDT) were placed at the mid one-third of the specimen, opposite to each other at 180°. A topcap with a half ball bearing was placed on top of the specimen. A friction reducting end was placed between the topcap and load cell. This was designed to reduce the effect of specimen bending that might be induced after the shear plane formed. At this stage, the load cell was held in the cell water and was not in contact with the specimen.

The assessment of the initial stress state in the specimen and the applied sample saturation process were the same as in the isotropic cell, described in Section 3.7.1.

Drained heating

For each stress path, specimens were subjected to three types of temperature paths: (i) specimens were kept at 20°C; (ii) specimens were heated in a drained manner at a rate of 1°C/h, from 20 to 40°C; the total time for heating was 20 hours; (iii) a temperature cycle (20°C-40°C-20°C) was applied to the specimen under drained condition; the heating stage was achieved by controlling the heating rate at 1°C/h, while the cooling stage started right after the specimen reached 40°C, by removing the bubble wrap and allowing the cell exposed to air. In both cases (ii) and (iii) where heating was involved, the triaxial cell was wrapped with several layers of bubble wrap in a controlled manner, to reduce heat loss to the atmosphere and to maintain a stable temperature. After the desired temperature was reached, the temperature was held at a constant value to allow sufficient time for thermal creep to occur. Based on the measurement from the back pressure volume gauge, change in volumetric strain should be less than 0.01%/day as an acceptable rate of thermal creep. After considering the intrinsic leakage that occurred in the back pressure volume gauge, the acceptable creep rate was 0.00136cc/h.

Undrained shearing

After applying one of the three isotropic drained temperature paths, the load cell was brought into contact with the specimen. Valves to the back pressure volume gauge were closed so that the specimen was in an undrained condition. Shearing rate was set to 0.2083 mm/h, which was equivalent to 5% shearing strain per day. This was achieved by controlling the displacement rate of the external axial LVDT. Temperature was held at a constant value that was achieved at the end of a drained heating stage. Undrained shearing stage stopped when the shearing strain reached 20% on average.

Duration of tests

Duration of each undrained shearing triaxial test, with a previous drained heating path, is summarised in Table 3-10. It took from 22 to 55 days to perform a one test in the temperature-controlled triaxial apparatus. The general trend is that the duration of the test increased with stress level, OCR and more complicated temperature path. The test TXC-200-1.5-20-40 took longer time to complete compared to other tests, due to the longer waiting time at the thermal creep stage for the change in back pressure volume gauge to reach the target creep criteria.

Table 3-10: Duration of drained triaxial heating tests

code	Isotropic loading, p'_{max} (kPa)	Isotropic swelling, p'_c (kPa)	OCR	Temperature path (°C)	Duration of test (days)
TXC-300-1-20	300	300	1	20	23
TXC-300-1-20-40	300	300	1	20-40	37
TXC-300-1-20-40-20	300	300	1	20-40-20	40
TXC-200-1.5-20	300	200	1.5	20	22
TXC-200-1.5-20-40	300	200	1.5	20-40	55
TXC-200-1.5-20-40-20	300	200	1.5	20-40-20	22
TXC-150-2-20	300	150	2	20	27
TXC-100-3-20	300	100	3	20	28
TXC-100-3-20-40	300	100	3	20-40	30
TXC-100-3-20-40-20	300	100	3	20-40-20	29
TXC-50-6-20	300	50	6	20	29
TXC-50-6-20-40	300	50	6	20-40	33
TXC-50-6-20-40-20	300	50	6	20-40-20	41

3.7.3 One-dimensional compression tests

Specimen setup

Porous stones placed in a container with distilled water were placed in a 20 mmHg vacuum for at least 30 minutes, until no air bubbles came out to the surface of water. The inner surface of the confining ring was lubricated with a thin layer of grease, to minimise the friction between the specimen and wall of the confining ring.

For specimens taken from reconstituted London clay cakes, confining ring was pushed through a small portion of the cake and excess soil from the top and bottom of the ring was removed. For specimens that came from London clay slurry, a teaspoon was used to place the clay slurry

into the confining ring in a careful and controlled manner. When the slurry approached the top of the confining ring, a small knife was used to level the surface and the excess clay slurry was carefully removed using tissue. Mass and dimensions of the specimen were measured and then the specimen was installed into the oedometer cell. Masses of the porous stone, topcap, confining ring were also measured and recorded. Filter paper was inundated with deaired and distilled water, and then placed in between the specimen and porous stones. The specimen and confining ring were placed into the oedometer cell. Topcap was gently placed on top of the porous stone.

The top cover of the oedometer cell, temperature sensor, water inlet and outlet, LVDT and hanger were put in place. Initial value of the LVDT was set so that it had sufficient travel in both directions. Test stages were set in the TRIAX programme to monitor and record the data. Water was heated in the water bath to desired temperature and then circulated to the oedometer cell by a pump. Changes in height of the specimen and in temperature were recorded for data analysing purpose.

Running the test

On the day of the specimen setup, a 100 g weight was placed on the hanger as the 'seating load' to ensure the hanger stayed in position. From the next day, specimen was loaded axially in increments of applied stress by adding or removing dead weights to the hanger, which further transmitted the stress to the specimen through a lever arm. The stress increment was held constant for 24 hours, before the next dead weight was added or removed. Distilled and deaired water was added to the oedometer cell at regular intervals, to ensure the specimen was always inundated in water throughout the test.

For tests that involved changes in temperature, temperature in the water bath was controlled to the desired value. In trial tests that were conducted to assess the performance under temperature, it was found that the temperature in the oedometer cell could reach the target value in 4 minutes, after the heated water started to circulate from the water bath to the oedometer cell. The temperature of the specimen could reach the target value in 12 minutes. This is considered a satisfying performance, considering the amount of water and soil in the oedometer cell was relatively small. Cooling was achieved by stopping the water bath and the pump. The oedometer cell was then exposed to the atmosphere and natural cooling started.

Finishing the test

To finish the test, the TRIAX programme was stopped and then the dead weights on the hanger were removed. The LVDT, lid of the oedometer cell and topcap were removed from the

specimen. Water in the cell was drained out. The specimen was then taken out and put in a moisture tin in the oven to measure its water content after the test. Components of the oedometer cell were cleaned and dried.

3.8 Calculations and corrections for data interpretation

In this section, methods of calculating some of the quantities are presented, including the equations and assumptions. These calculations are necessary to transfer what was measured in the tests to quantities that have physical meanings. Corrections to the data are also shown, where 'adjustment is applied to test data to make allowance for various physical factors inherent in the apparatus or in the test method' (Head, 1998).

3.8.1 Area corrections to triaxial shearing data

In shearing tests performed in the triaxial thermal apparatus, the mode of deformation affects strain measurements, leading to errors in calculating the sample cross-sectional area and affecting the accuracy of the calculation of deviatoric stress. Area corrections are applied to the test data, and they are determined by the form of the specimen after failure and by the changes in axial and volumetric strains. In this research, right cylinder area correction was applied in calculating the area before the shear plane formed, while single shear plane correction was applied afterwards. Details of these two methods of area corrections are presented below.

Right cylinder area correction

In this method of area correction, it is assumed that the strain measured at the mid third of the specimen represents the deformation of the whole specimen. During the shearing process, it is assumed that the specimen deforms as a right cylinder. The total volume of the specimen remains the same, while the height of the specimen decreases, leading to a larger cross-sectional area. The assumed shape of the deformed specimen is shown in Figure 3-17, where the taller cylinder is the shape of the specimen before shearing and the shorter one is the shape after shearing starts.

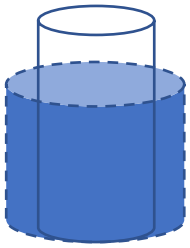

Figure 3-17: Shape of the specimen based on right cylinder assumption

The current area of the specimen can be calculated using Equation 3-2.

$$A = A_0(\frac{1-\varepsilon_v}{1-\varepsilon_a}) \quad 3\text{-}2$$

where compressive deformations are positive. In other words, ε_v is positive when water is expelled out from the sample and ε_a is positive when the sample shortens.

A_0 = initial area at zero strain

ε_v = volumetric strain

ε_a = axial strain

Single-plane slip

The area correction due to single-plane slip is presented by Head (1998). When a surface of shear forms in the specimen during shearing, the actual contact area between the two portions of the specimen decreases as the soil slips along the surface, as shown in Figure 3-18 (a). The overlapping area of the two portions of the specimen represents the actual area of contact. It can be projected vertically in plan to the shaded area as shown in Figure 3-18 (c). The area can be treated as two segments of a circle with a radius of $R = \frac{D}{2}$ and an angle of 2β. The area of contact projected on the plan can therefore be calculated by the equation

$$A_s = 2 \times \frac{1}{2}\left(\frac{D}{2}\right)^2 (2\beta - sin2\beta) = \frac{1}{2}D^2(\beta - sin\beta cos\beta) \quad 3\text{-}3$$

In practice, when correcting the area of the specimen of any diameter, the area ratio A_s/A is used, where A ($= \pi D^2/4$) is the initial area before the shear plane forms. It can be calculated using the following equation

$$\frac{A_s}{A} = \frac{2}{\pi}(\beta - sin\beta cos\beta) \quad 3\text{-}4$$

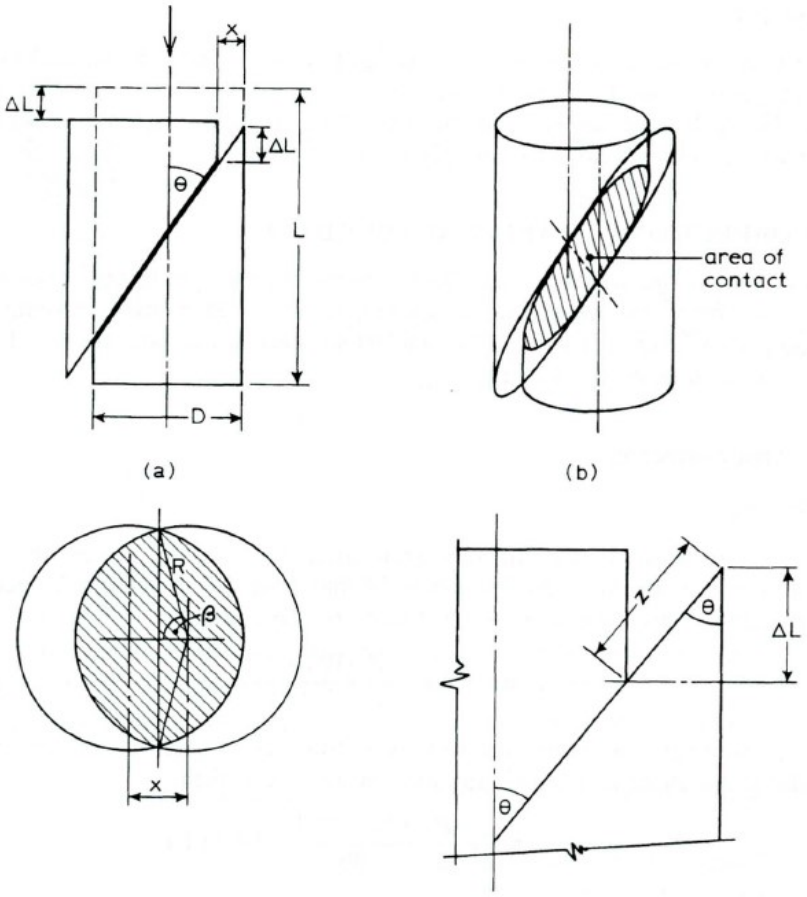

Figure 3-18: Area correction due to single-plane slip: (a) mechanism of slip; (b) area of contact between the two portions of the specimen; (c) projected area of contact; (d) displacement along slip surface related to vertical deformation (Head, 1998)

The deviatoric stress, q ($= F/A$), can be multiplied by the slip area factor, f_s, to obtain the corrected deviatoric stress. It is the reciprocal of the area ratio and can be calculated by the equation

$$f_s = \frac{\pi}{2(\beta - sin\beta cos\beta)} \qquad 3\text{-}5$$

3.8.2 Membrane corrections

Membrane corrections on the triaxial test data were proposed by some researchers. These corrections consider barrelling (Bishop and Wesley, 1975; Sandroni, 1977; Gens, 1982), slip plane (Chandler, 1966; Blight, 1967; La Rochelle, 1988), membrane penetration effect on volume change (Roscoe et al., 1963), membrane penetration effect on pore pressure (Lade and Hernandez, 1977), membrane stretching in shear plane failure (Chandler, 1968) and trapped air (Bishop and Henkel, 1962). By assessing and quantifying each of these factors on the test, it was found that these factors had negligible effect on the test result, considering the testing

condition and type of soil. Therefore, membrane corrections were not applied to test data in this research.

3.8.3 Calculation of thermal strains

Thermal strains refer to the volumetric strains that are induced due to temperature change in the soil. In conventional drained triaxial tests on saturated specimens, volumetric strains are calculated based on the measurements of water coming in and out of the specimen under the applied stress changes, as monitored by the volume gauges or local instrumentation. This is a mechanical volumetric strain. In drained tests that involve only changes in temperature under constant effective stress, water and solids in the specimen expand or contract with temperature, leading to additional, thermally-induced, volume changes. Direct measurements are rarely available due to the reasons stated in Section 3.2 and 3.3. Two interpretative methods, free water approach (Campanella and Mitchell, 1968) and adsorbed water approach (Baldi et al., 1988), were proposed in the literature for the estimation of thermal strains.

Free water approach (Campanella and Mitchell, 1968)

Under drained conditions, volume change of soil due to temperature variations under constant effective stress can be considered in terms of the temperature-dependent properties of a given saturated soil. In the free water approach, Campanella and Mitchell (1968) assumed that all the water in the specimen was in its free form and that the expansion or contraction of solid and water behaved independently. The volumetric strain of a soil during drained heating is calculated by subtracting from the net volume of the expelled water, V_{dr}, the expansion or contraction of water and solid due to changes in temperature, ΔT, as shown in Equation 3-6.

$$\varepsilon_{v,T} = \frac{V_{dr} - (\alpha_s V_s + \alpha_w V_w)\Delta T}{V_0} \qquad 3\text{-}6$$

where $\varepsilon_{v,T}$ is the thermal volumetric strain, α_s and α_w are the thermal expansion coefficients of solid and water, respectively; V_s and V_w are the volumes of solid and water in the specimen and V_0 is the volume of the specimen at the beginning of heating or cooling. Volume of drained water, V_{dr}, is negative when water goes into the specimen and positive when water goes out. Strains which result in a reduction in volume (contraction) are positive.

Change in void ratio (Δe) due to change in temperature in drained heating test can be calculated as

$$\Delta e = e_0[\frac{(\alpha_w - \alpha_s)\Delta T - \frac{\Delta V_{dr}}{V_w}}{1 + \alpha_s \Delta T}] \quad 3\text{-}7$$

where e_0 is the void ratio of the specimen before drained heating or cooling. When the volume of the specimen expands by $\alpha_s \Delta T$, there is no change in void ratio. Parameters in this equation are relatively straightforward to quantify. Therefore, the free water approach is chosen to calculate the thermal volumetric strains in drained heating tests in this research.

Adsorbed water approach (Baldi et al., 1988)

Baldi et al. (1988) believed that the free water approach did not work for low-porosity clays with a high adsorption potential. In this case, water is mainly in the form of adsorbed water. They assumed that the effective thermal expansion of water in fine clay pores depends only on the pressure bonding water molecules to the mineral and on temperature. Based on double layer theory, this pressure decreases exponentially with distance from the clay particles, which are simplified as particles that are uniform, long and parallelly arranged with a constant thickness. They proposed an expression to calculate the thermal volumetric strain as shown in Equation 3-8.

$$\varepsilon_{v,T} = \frac{V_{dr}}{V_0} - [\Delta v_a S_s \rho_d - \alpha_s (1 - n)]\Delta T \quad 3\text{-}8$$

where Δv_a is the volume of expanded adsorbed water per unit surface of clay mineral and per ºC, S_s is the specific surface of the clay mineral, ρ_d is the dry density of the soil and n is the porosity. Thickness of clay particles and the specific surface of the clay mineral are difficult to measure and can vary in some cases.

Coefficient of thermal expansion of water

In evaluating the thermal volumetric strains, a key parameter is the coefficient of thermal expansion of water, α_w. International Association for the Properties of Water and Steam (IAPWS) published formulations in 1997, known as 'The IAPWS Formulation 1997 for the Thermodynamic Properties of Ordinary Water Substance for General and Scientific Use' (IAPWS-IF97), as the international standard of several thermophysical properties of water (IAPWS, 2007). The IAPWS-IF97 consists of a set of equations for five different regions of temperature and pressure. Region 1 is of interest for soil mechanics as it covers the following range of temperature and pressure: 273.15 K $\leqslant T \leqslant$ 623.15 K and $p_s(T) \leqslant p \leqslant$ 100 MPa, where p_s is the saturation pressure. Based on the IAPWS-IF97 equations and the definition of the thermal expansion coefficient of water, Martinez-Calonge (2017) subdivided the

temperature range from 1 to 99 °C and pressures from 0 to 10 MPa (relative to atmospheric pressure) using 2250,000 points and then fitted a polynomial function, as shown in Equation 3-9.

$$\alpha_w(T,p) = \alpha_0 + \alpha_1 T + \alpha_2 p + \alpha_3 T^2 + \alpha_4 Tp + \alpha_5 T^3 + \alpha_6 T^2 p \qquad 3\text{-}9$$

The constants were calculated as

$$\alpha_0 = -(4.392 \times 10^{-5})°C^{-1}$$

$$\alpha_1 = (1.444 \times 10^{-5})°C^{-2}$$

$$\alpha_2 = (3.043 \times 10^{-6})°C^{-1}MPa^{-1}$$

$$\alpha_3 = -(1.113 \times 10^{-7})°C^{-3}$$

$$\alpha_4 = -(8.279 \times 10^{-8})°C^{-2}MPa^{-1}$$

$$\alpha_5 = (4.714 \times 10^{-10})°C^{-4}$$

$$\alpha_6 = (3.867 \times 10^{-10})°C^{-3}MPa^{-1}$$

In order to obtain the correct unit for α_w ($°C^{-1}$), temperature should be in °C and pressure should be in MPa and expressed in absolute value (i.e. atmospheric pressure is 0.101325 MPa). This expression suggests that α_w is nonlinear with temperature and that the influence of pressure is negligible in the range considered (0-10 MPa).

Coefficient of thermal expansion of solids

The coefficient of thermal expansion of solids is another important parameter in calculating thermal strains. It can be estimated from the weighted average of the thermal expansion coefficients of different minerals in the soil. Based on the mineralogy of the London clay specimens tested in this research, as presented in Section 3.5.4, the value for the coefficient of thermal expansion of solids, α_s, is taken as $2.99*10^{-5}$ $°C^{-1}$.

Volume change corrections

Volume change measured by volume gauges is the only direct measurement in the calculation of thermal strains using the free water approach (Campanella and Mitchell, 1968). The accuracy of volume change measurement directly influences the accuracy of thermal strain calculated. Due to the long period of time it took for each test, long-term performance of the drainage system was monitored. The natural drift in volume gauge is 0.00104 cc/h for the temperature-controlled isotropic cell, and it is 0.00115 cc/h for the temperature-controlled triaxial cell. This is accounted for and corrected in the calculation of thermal strains.

3.8.4 Thermal deformation of confining ring in oedometer apparatus

During the heating/cooling process in the temperature-controlled oedometer apparatus, both the soil and the confining ring had thermal deformation. In this research, thermally-induced lateral deformation of the confining ring was calculated based on the thermal expansion coefficient of stainless steel, instead of measured. Holes in materials expand and contract as if they were made from the surrounding material (Duffy, 2012). Therefore, the change in diameter of the confining ring can be calculated using Equation 3-10 (Kirkham, 2020).

$$\Delta d_{CR} = d_{CR,0} \cdot \alpha_{L,CR} \cdot \Delta T \qquad 3\text{-}10$$

where Δd_{CR} is the change in internal diameter of the confining ring; $d_{CR,0}$ is the initial internal diameter of the confining ring; $\alpha_{L,CR}$ is the linear thermal expansion coefficient of stainless steel; ΔT is the change in temperature.

Heating caused an increase in the internal diameter and height of the confining ring. It also led to expansion of the soil specimen. The thermal expansion coefficient of stainless steel was larger than that of the soil. When heated, changes in temperature for the two parts were the same, the confining ring would therefore expand more than the tested soil laterally. There was some interaction between the confining ring and the soil specimen. Theoretically, a gap could develop between the soil specimen and the confining ring. Therefore, the one-dimensional compression condition in conventional oedometer tests might not be valid anymore. In practice, however, the soil specimen expanded laterally and filled the gap, due to the vertical confinement on the specimen. The lateral expansion of the soil therefore led to a reduction in the height of the soil, in addition to the change in height due to vertical load. This reduction in height was a mechanical effect due to the differential thermal expansion of the confining ring and soil specimen (Kirkham, 2020). This differential thermal expansion was caused by the difference in thermal expansion coefficients between the two materials. If the two materials had the same thermal expansion coefficients, or the confining ring had a zero thermal expansion coefficient, no correction was needed. A correction was applied to quantify the change in height due to differential lateral expansion of the confining ring and soil specimen. It was assumed that the soil volume remained constant. In other words, lateral expansion of the soil resulting from the thermal lateral expansion of the confining ring results in a change in shape of the soil, but not its volume (Romero, 1999; Abuel-Naga et al., 2005).

The change in specimen height, ΔH, can be calculated as

$$\Delta H = H_1(\frac{d_1^2}{d_0^2} - 1) \quad 3\text{-}11$$

where d_0 is the initial diameter of the specimen, d_1 is the final diameter of the specimen and H_1 is the final specimen height.

Following the same concept as in Equation 3-10, the change in diameter of the soil specimen can be calculated as

$$\Delta d_{soil} = d_{soil,0} \cdot \alpha_{L,soil} \cdot \Delta T \quad 3\text{-}12$$

where Δd_{soil} is the change in diameter of the soil specimen; $d_{soil,0}$ is the initial diameter of the soil specimen; $\alpha_{L,soil}$ is the linear thermal expansion coefficient of soil; ΔT is the change in temperature. Positive Δd means there is an increase in the diameter.

The diameter of soil specimen and confining ring that resulted from thermal effect is

$$d_{soil,1} = d_{soil,0} + \Delta d_{soil} \quad 3\text{-}13$$

$$d_{CR,1} = d_{CR,0} + \Delta d_{CR} \quad 3\text{-}14$$

By substituting $d_{soil,1}$ and $d_{CR,1}$ into Equation 3-11, the change in height of soil can be calculated as

$$\Delta H = H_1(\frac{d_{CR,1}^2}{d_{soil,1}^2} - 1) \quad 3\text{-}15$$

The correction can then be applied to the measured height of the soil specimen:

$$H_{corrected} = H_{measured} + \Delta H \quad 3\text{-}16$$

Positive ΔH means a reduction in measured soil height. For heating, ΔT is positive, giving a positive ΔH.

3.9 Summary

In this chapter, methodology used in this research is presented, including descriptions and calibrations of three pieces of temperature-controlled equipment, London clay as a testing material, sample preparation, experimental procedures, calculations and corrections for data interpretation.

Temperature-controlled isotropic apparatus with mid-height pore pressure probe was developed mainly for undrained heating tests, to investigate the effect of temperature on thermally-induced pore water pressures. Double load cell triaxial apparatus was used for drained heating tests, followed by undrained shearing, to investigate the effect of temperature on the thermally-induced volumetric strains, strength and stiffness. Temperature-controlled oedometer apparatus was developed to investigate the effect of temperature on compression properties of the testing material. Instrumentation was calibrated at both ambient and elevated temperature. Temperature-based calibrations were incorporated to correct for errors due to the temperature effect on the readings of instrumentation.

London clay was used as a testing material in this research. Its geological history, stratigraphy, details of how and where it was sourced, minerology were presented. Some basic classification tests were performed to characterise the material.

Experimental procedures for tests performed in each of the three pieces of equipment were presented. There are no standard procedures in the literature, due to the uniqueness of the equipment. Experimental procedures presented in this research ensure the repeatability and quality of tests.

Methods of calculating some of the quantities and corrections to the data are presented, including the equations and assumptions. These are necessary in converting what was measured in the tests to quantities that have physical meanings, for date interpretation purpose.

Chapter 4: Thermally-induced pore pressures in undrained conditions

4.1 Introduction

This chapter presents the results of laboratory tests performed on specimens of isotropically consolidated reconstituted London clay, to investigate the thermally-induced pore water pressures under undrained conditions. The focus of experiments was to quantify the excess pore water pressures in a saturated clay, generated under the cycles of heating (from ambient temperature, $T_{am} = 20^{o}\text{C}$, to a maximum of $T_{max} = 40^{o}\text{C}$) and cooling (back to ambient temperature), for a range of values of the initial mean effective stress and overconsolidation ratio. The importance of understanding the evolution of excess pore water pressures under temperature changes in undrained conditions is the effect that this has on reducing the effective stresses in clay ground conditions in the short term.

4.2 Applied stress and temperature paths

Prior to applying temperature changes, specimens of reconstituted London clay were subjected to isothermal isotropic compression or swelling to a range of mean effective stress values (50 to 450 kPa) and overconsolidation ratios (1 to 6). Details of the experimental procedures were presented in Section 3.7.1. Applied stress paths of each test are summarised in Table 4-1. Tests are named based on their stress history. 'ISO' refers to tests in the isotropic apparatus. The first number refers to the mean effective stress at the end of isothermal isotropic compression or swelling stages. The second number refers to the overconsolidation ratio (OCR), defined as the ratio between the maximum vertical effective stress ($\sigma'_{v,max}$) and the current value of vertical effective stress ($\sigma'_{v,c}$). Because the consolidation path is isotropic, the overconsolidation ratio can also be calculated as the ratio between the maximum mean effective stress after isotropic loading (p'_{max}) and mean effective stress at the end of the isotropic consolidation / swelling path (p'_c).

For example, for the first test listed in Table 4-1, the name code is ISO-50-3. This means the test was performed in the isotropic apparatus, with the initial mean effective stress $p'_c = 50$ kPa and an $OCR = 3$ reached at the end of the applied consolidation path. Subsequent to this, specimens were subjected to undrained heating from 20°C to 40°C, at a rate of 1°C/h. When the temperature of clay specimens reached 40 °C, heaters were turned off and insulation chamber around the isotropic cell was removed, to allow for natural cooling under undrained conditions. The heating-cooling cycles were repeated for at least five times, until the change in pore water pressure was comparable to the previous heating-cooling cycle and the final pore pressure was stable at $T_{am} = 20^{o}\text{C}$.

Table 4-1: Applied stress paths for tests in temperature-controlled isotropic apparatus

code	Isotropic loading, p'_{max} (kPa)	Isotropic swelling, p'_c (kPa)	OCR	Void ratio at the start of test, e_0	Void ratio at the start of heating, e_c	Porosity at the start of heating, n
ISO-150-1	150	150	1	1.115	1.111	0.526
ISO-300-1	300	300	1	1.138	0.986	0.496
ISO-450-1	450	450	1	1.104	0.907	0.476
ISO-75-2	150	75	2	1.111	1.122	0.529
ISO-150-2	300	150	2	1.130	1.021	0.505
ISO-225-2	450	225	2	1.085	0.993	0.498
ISO-50-3	150	50	3	1.138	1.156	0.536
ISO-100-3	300	100	3	1.132	0.996	0.499
ISO-150-3	450	150	3	1.100	1.074	0.518
ISO-60-5	300	60	5	1.085	1.085	0.520
ISO-50-6	300	50	6	1.138	1.072	0.517
ISO-75-6	450	75	6	1.045	1.034	0.508

4.3 Effect of initial stress

This section discusses the effect of the initial mean effective stress value at the start of the heating-cooling cycle, p'_c, on the generated excess pore water pressure, or thermally induced pore water pressure. Results for tests with the same OCR but different initial stresses before undrained heating-cooling cycles are presented. All tests started from an initial pore water pressure $u_{init} = 250$ kPa.

4.3.1 Normally consolidated clay

Figure 4-1 (a) shows the temperature versus pore water pressure, $T - u$, plot for normally consolidated specimens ($OCR = 1$), when they were subjected to the first undrained heating-cooling cycle from $p'_c = 150, 300$ and 450 kPa. For all three specimens the pore water pressure increased upon heating, with the increase being higher for the higher initial p'_c magnitude. During the cooling phase of the first cycle the pore water pressure decreased, creating some hysteresis and mostly closing the loop by returning to around the initial value of $u_{init} = 250$ kPa.

Figure 4-1 (b) presents the plot of normalised excess pore water pressure against temperature during the first heating-cooling cycle. Excess pore water pressure, Δu, was calculated by deducting from the current pore water pressure, u_{curr}, the pore water pressure at the beginning

of the first heating-cooling cycle, u_{init}. The excess pore water pressure was then normalised by the mean effective stress at the beginning of undrained heating-cooling stage (i.e.$\Delta u/p'_c$). For example, for the test ISO-150-1 shown in the plot, normalised excess pore water pressure was calculated by dividing the excess pore water pressure by 150 kPa.

At the same temperature level, the normalised excess pore water pressures for the first heating-cooling cycle for the three specimens were very similar. For the maximum change in temperature, $\Delta T = 20^{o}$ C, the maximum $\Delta u/p'_c \sim 0.27$ on average (varying from 0.25 to 0.29), implying that the increase in pore water pressure was around 27% of the initial mean effective stress at the end of first heating. The values of pore pressure, u, at the end heating and cooling paths, as well as the respective Δu and $\Delta u/p'_c$ for all tests presented in this section are summarised in Table 4-2.

Table 4-2: Thermally-induced pore water pressure in the first heating-cooling cycle

Temperature	**40 °C (end of heating)**			**20 °C (end of cooling)**		
Parameters	Pore pressure u (kPa)	Excess pore pressure Δu (kPa)	Normalised pore pressure $\Delta u/p'_c$	Pore pressure u (kPa)	Excess pore pressure Δu (kPa)	Normalised pore pressure $\Delta u/p'_c$
ISO-150-1	294	44	0.29	249	-1	-0.01
ISO-300-1	332	82	0.27	262	12	0.04
ISO-450-1	362	112	0.25	268	18	0.04
ISO-75-2	269	19	0.25	237	-13	-0.17
ISO-150-2	282	32	0.21	232	-18	-0.12
ISO-225-2	287	37	0.16	216	-34	-0.15
ISO-50-3	263	13	0.26	239	-11	-0.22
ISO-100-3	267 (270*)	17 (20*)	0.17 (0.20*)	233	-17	-0.17
ISO-150-3	275	25	0.17	221	-29	-0.19
ISO-60-5	261	11	0.18	233	-17	-0.28
ISO-50-6	257	7	0.14	224	-26	-0.52
ISO-75-6	260	10	0.13	224	-26	-0.35

* Represents projected values for the full temperature change to 40^{o}C

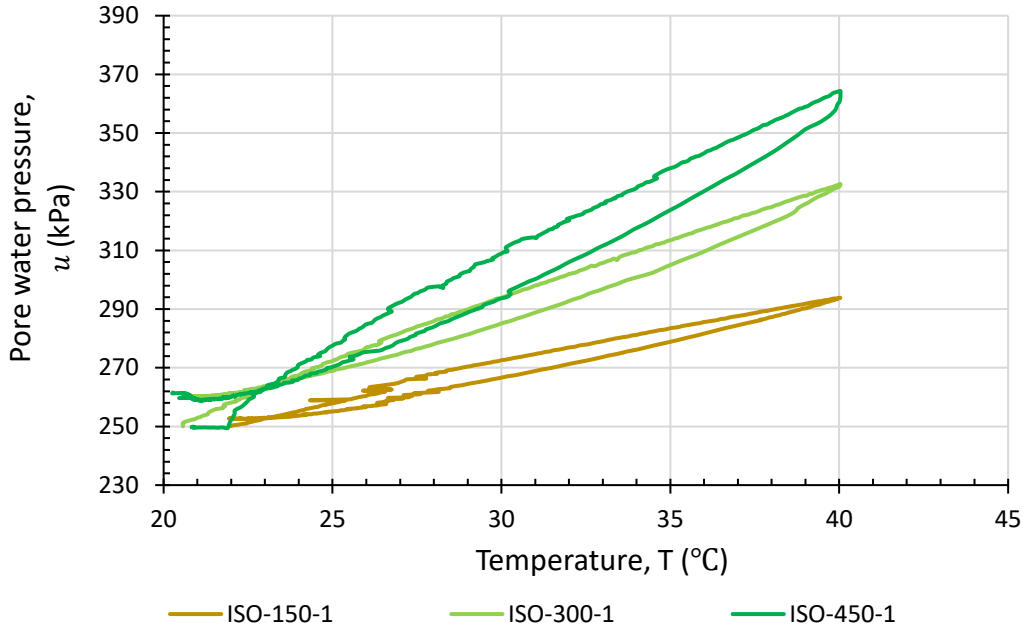

(a)

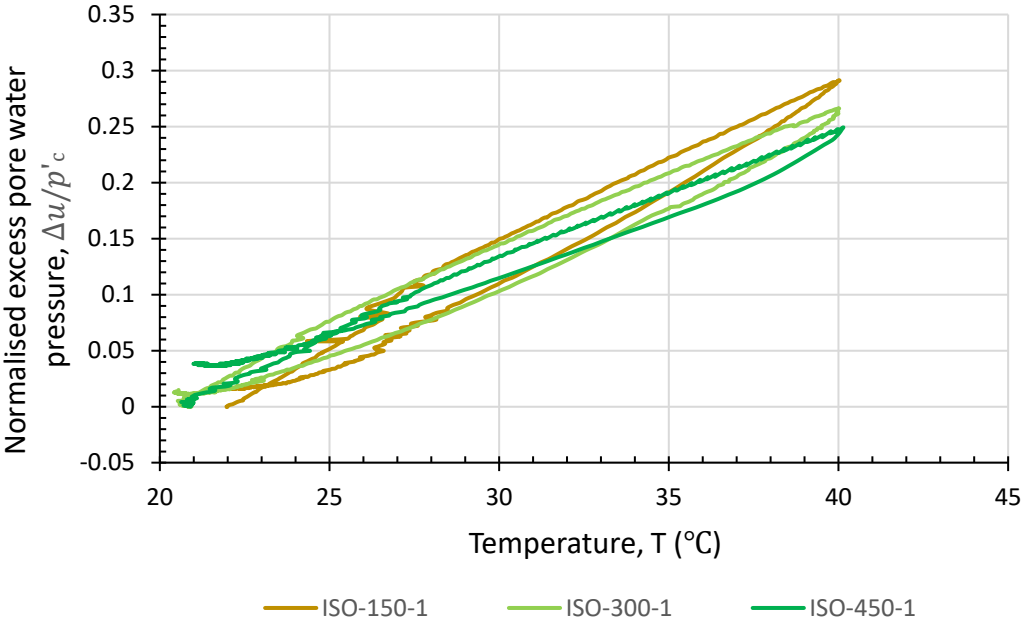

(b)

Figure 4-1: Effect of the initial stress, p'_c, for normally consolidated clay, OCR=1 (a) Pore water pressure-temperature; (b) Normalised pore water pressure-temperature

4.3.2 Overconsolidated clay

Figure 4-2 (a) shows the $T-u$ plot for lightly overconsolidated specimens ($OCR=2$) when subjected to the first undrained heating-cooling cycle from $p'_c = 75, 150$ and 225 kPa. Similar to $OCR=1$ specimens, the pore pressure increased upon first heating, with higher values generated as the magnitude of p'_c increased. Upon cooling, however, pore water pressure

decreased at a faster rate than the rate of increase during heating, leading to a hysteresis and to lower pore pressure magnitude than u_{init}, at the end of cooling to ambient temperature.

In Figure 4-2 (b), the normalised excess pore water pressures, $\Delta u/p_c'$, are plotted against temperature for the same set of tests. The normalised values at the end of heating, after $\Delta T = +20^{o}$C, varied from 0.16 to 0.25, indicating an average maximum increase of pore pressure by around 21% on average of the respective p_c' value. The normalised excess pore pressure values at the end of cooling back to ambient temperature, after $\Delta T = -20^{o}$C, varied from -0.12 to -0.17, indicating an average 15% pore pressure reduction of u_{init}, with respect to the initial p_c'.

Similar behaviour could be observed in Figure 4-3(a) for the three specimens at $OCR = 3$, subjected to an undrained heating-cooling cycle from the initial $p_c' = 50$, 100 and 150 kPa. For the test ISO-100-3, temperature of the clay specimen only reached 37.5°C instead of 40°C, due to an error in controlling the test. Based on the pore water pressure trend in the heating cycle of this test, it could be foreseen that the value measured at 40°C would have been around 270 kPa. The three heating paths show an increase in pore pressure as the initial p_c' increases and the average normalised excess pore water pressure at the end of heating was around 0.21 (see Figure 4.3(b)). At the end of first cooling, the pore water pressure was smaller than u_{init}, with $\Delta u/p_c'$ being around -0.2 on average.

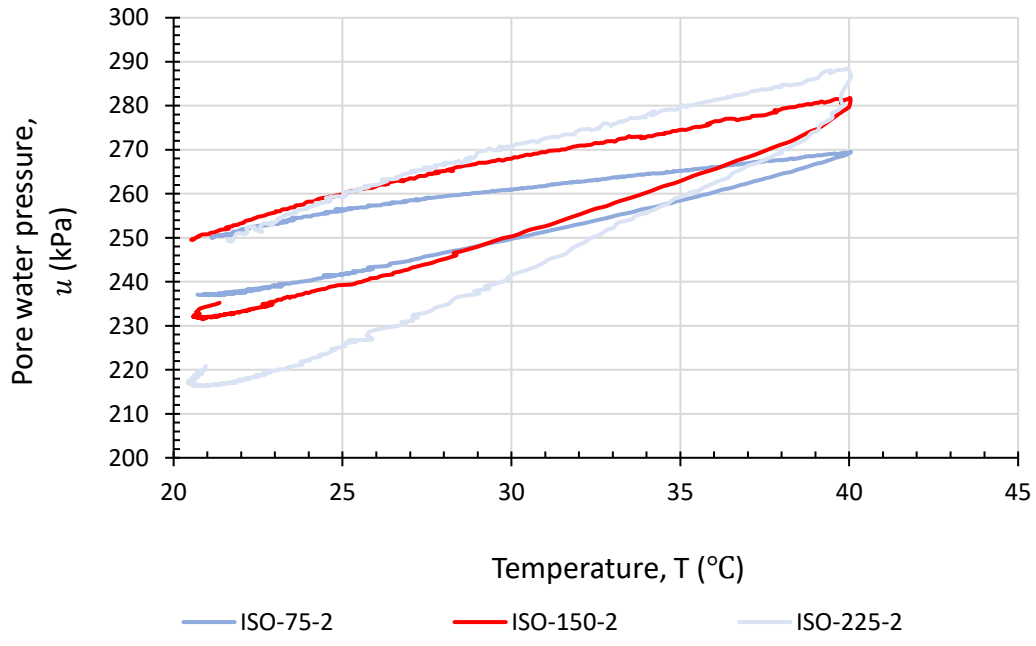

(a)

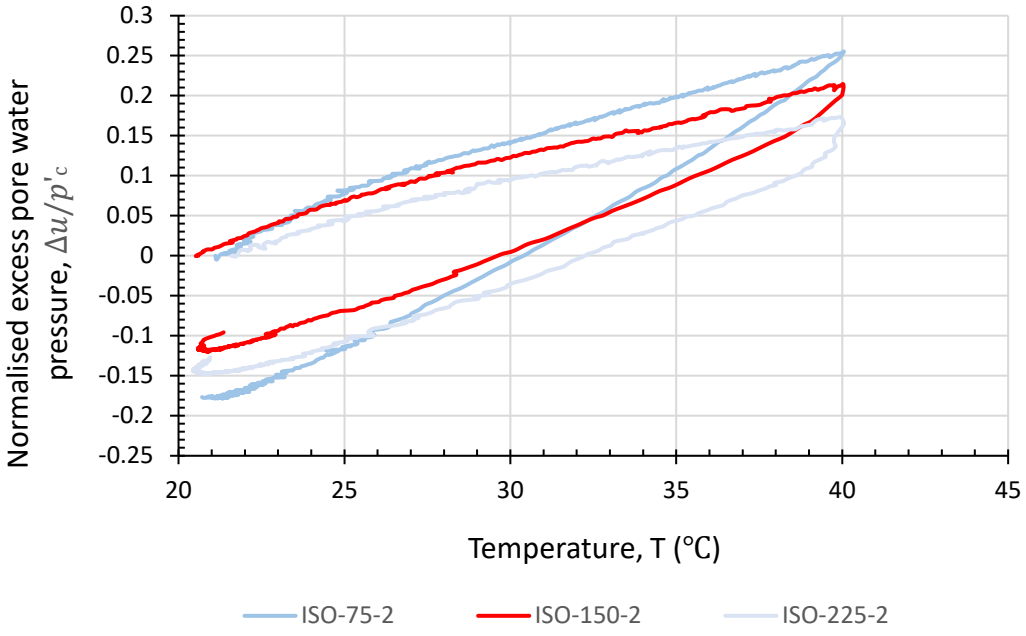

(b)

Figure 4-2: Effect of the initial stress, p'_c, for overconsolidated clay at OCR=2 (a) Pore water pressure-temperature; (b) Normalised excess pore water pressure-temperature

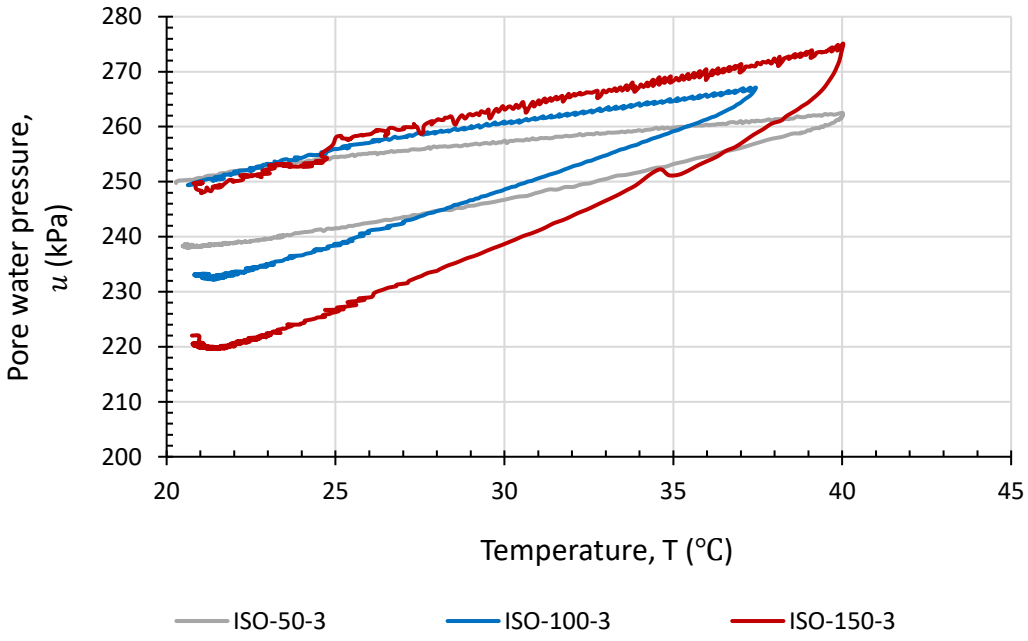

(a)

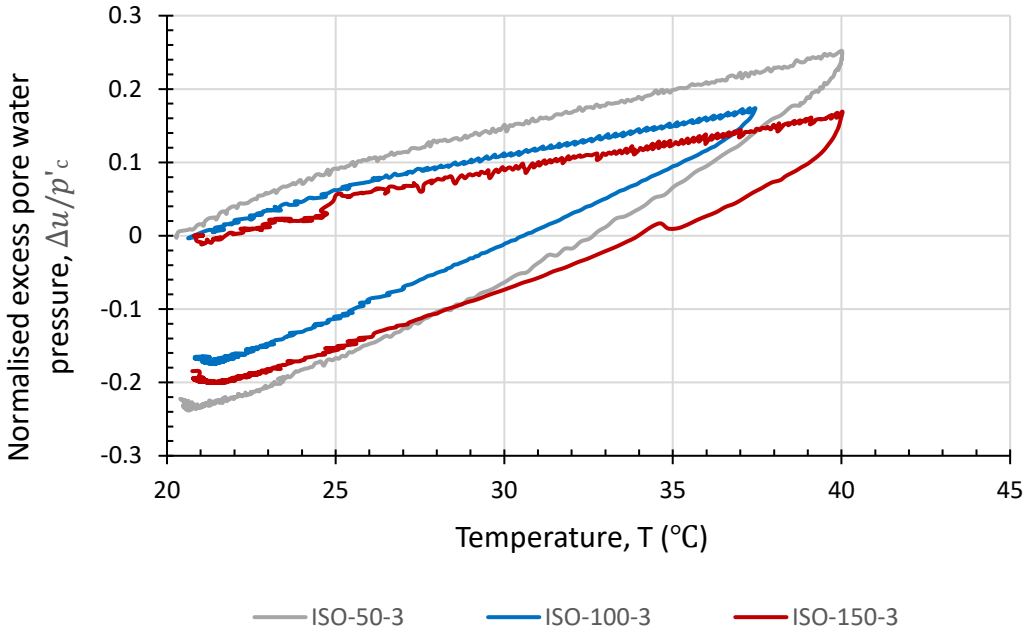

(b)

Figure 4-3: Effect of initial stress state for overconsolidated clay at OCR=3 (a) Pore water pressure-temperature; (b) Normalised excess pore water pressure-temperature

Figure 4-4 shows the same set of plots for a more heavily overconsolidated clay specimens, at $OCR = 6$ and 5, subjected to the same $\Delta T = \pm 20^{o}\text{C}$ undrained heating-cooling cycle. The three tests, two at $OCR = 6$ and one at $OCR = 5$, were grouped together due to a narrow range of the initial mean effective stress, $p'_c = 50\,, 60$ and 75 kPa, compared to tests performed at lower OCR values. All three tests showed an increase in pore pressure upon heating (Figure 4-4(a)) and a reduction of pore pressure below u_{init} at ambient temperature at the end of cooling. The three tests showed similar responses, averaging around 0.15 for the normalised excess pore pressure, Figure 4-4(b). The normalised excess pore pressure at the end of cooling was around -0.38 on average. It was evident from Figure 4-4 that there was little distinction between the specimen responses at higher OCR values, possibly due to the narrow range of the initial mean effective stress, p'_c, at the start of the thermal cycle. The high overconsolidation ratio range would benefit from testing specimens at a larger range of initial mean effective stress values, p'_c, at the end of swelling, which was not possible to achieve in a standard triaxial cell that was used in this research.

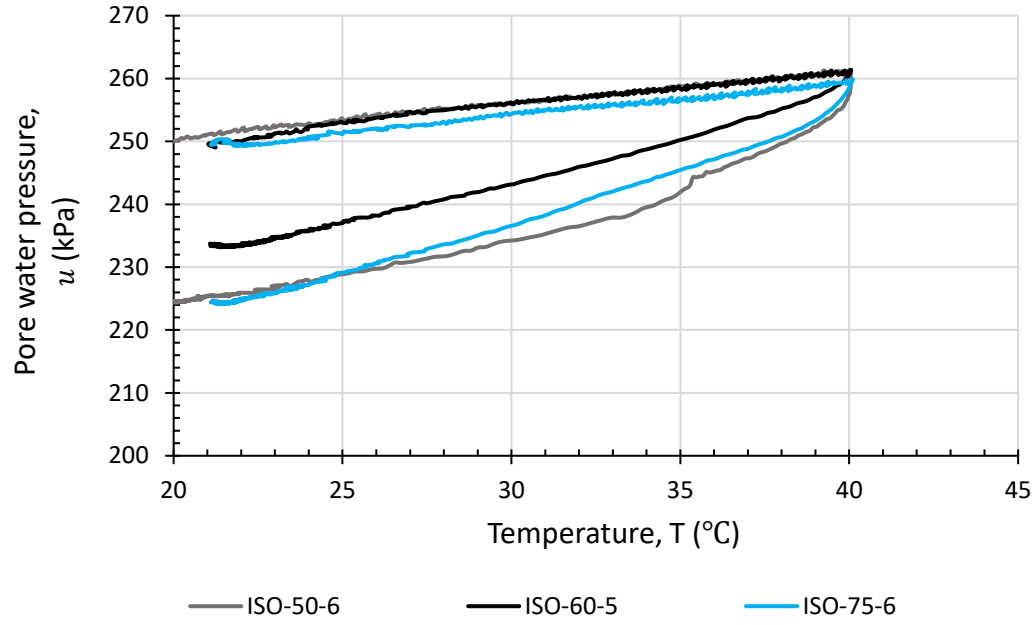

(a)

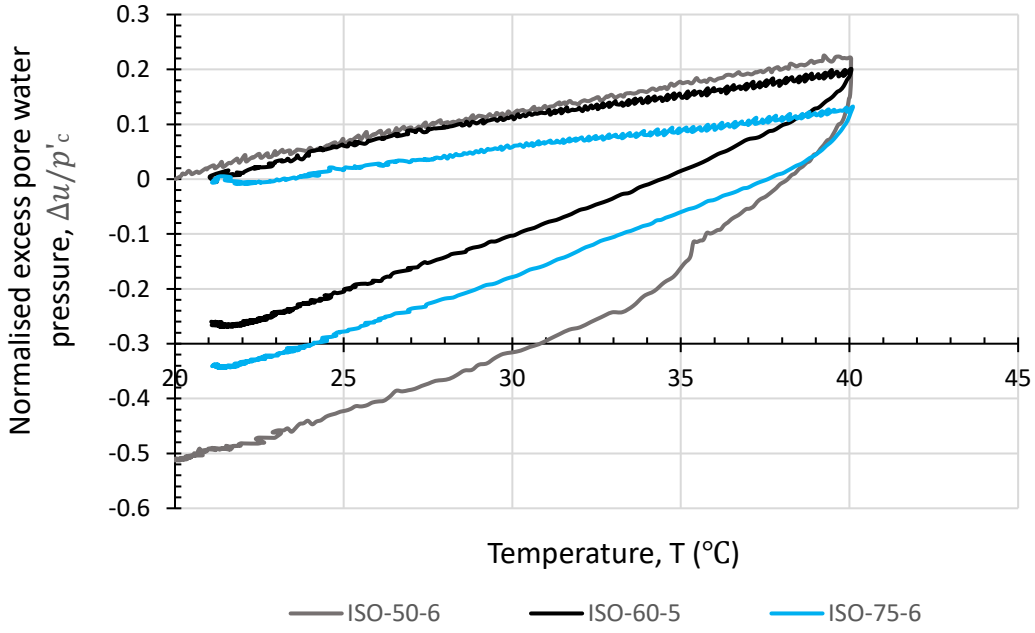

(b)

Figure 4-4: Effect of initial stress state for heavily overconsolidated clays at OCR=5 or 6: (a) Pore water pressure-temperature; (b) Normalised excess pore water pressure-temperature

4.4 Effect of overconsolidation ratio

The effect of the overconsolidation ratio, OCR, on the thermally-induced pore water pressure, from tests summarised in Table 4-2, is presented in Figure 4-5, by comparing tests with the same value of p'_c but with different OCR. Comparisons were possible for the values of $p'_c = 50, 75$ and 150 kPa.

With the exception of tests at $p'_c = 50$ kPa in Figure 4.5(a), the comparisons in Figure 4-5(b) and Figure 4-5(c) showed that the effect of OCR, for the same p'_c (75 and 150 kPa, respectively) at the start of the first thermal cycle, was to reduce the magnitude of pore pressure upon heating as the value of OCR increased. The rate of pore pressure reduction upon cooling back to ambient temperature appeared independent of OCR for the same p'_c. Test ISO-50-6 at $OCR = 6$ in Figure 4.5(a) seemed slightly anomalous, as it would be expected to generate lower pore pressure upon heating compared to test ISO-50-3 at $OCR = 3$.

In general, the analysis of the first cycle of normalised thermally-induced pore pressures in Section 4.3 showed that, regardless of the p'_c value, the specimens at $OCR = 1$ generated the largest thermally-induced pore pressure upon heating, on average 27% of the p'_c value. This percentage reduced with the increase of OCR, to 21%, 21% and 15% for OCR of 2, 3 and 6, respectively. On the other hand, while thermally-induced pore pressures upon cooling of $OCR = 1$ samples closed the loop when ambient temperature was reached (i.e. reaching the initial pore pressure of 250 kPa), the thermally-induced pore pressures generated an open loop at the end of cooling for higher OCR values, with and absolute value of $\Delta u/p'_c$ increasing to 15%, 19% and 38% for OCR of 2, 3 and 6, respectively.

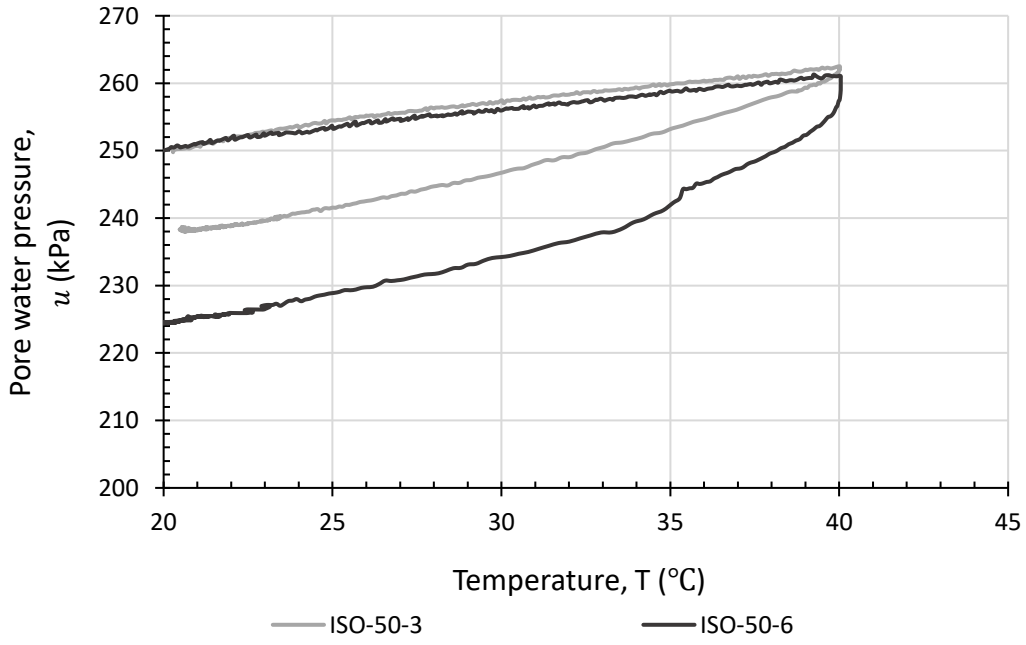

(a) $p'_c = 50\ kPa$

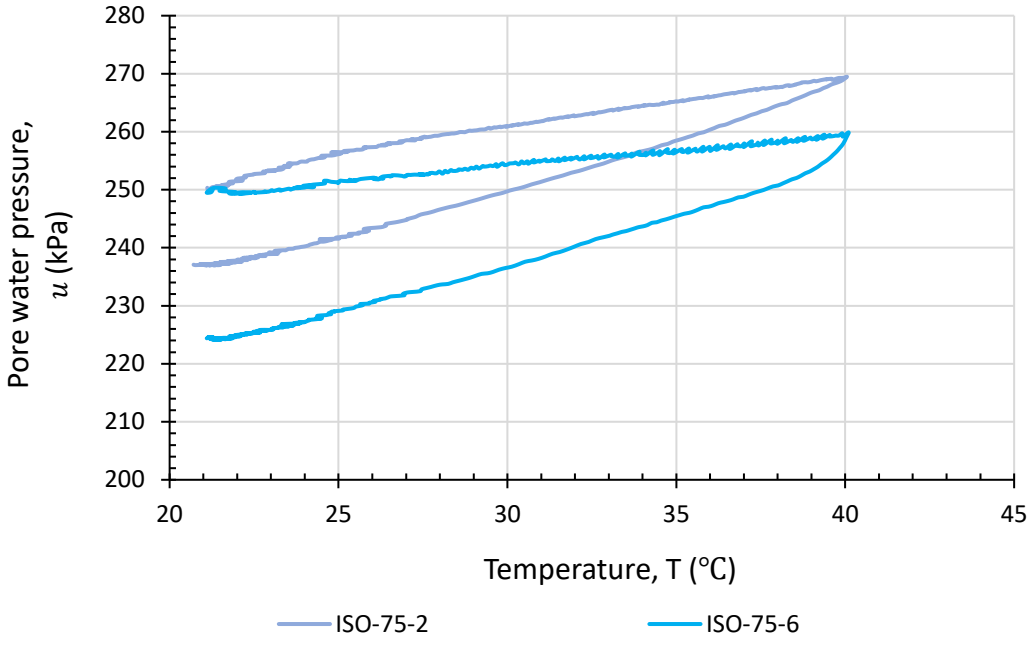

(b) $p_c' = 75\ kPa$

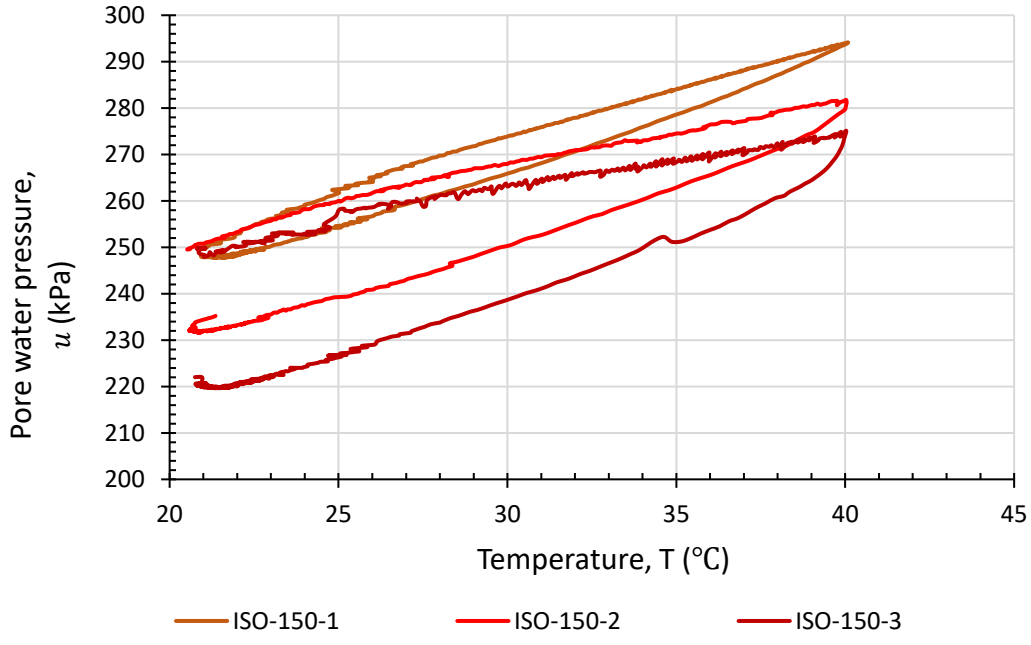

(c) $p_c' = 150\ kPa$

Figure 4-5: Effect of overconsolidation ratio at (a) p'$_c$=50 kPa; (b) p'$_c$=75 kPa; (c) p'$_c$=150 kPa

4.5 Effect of the magnitude of temperature change

Based on the graphs presented above, it could be observed that for all the tests, larger thermally-induced pore water pressure was generated when the magnitude of temperature change was larger, regardless of whether the clay specimens were in heating or cooling stage. Pore water pressure did not change linearly with the change of temperature. It increased at a higher rate at

the beginning of heating then slowed down towards the end of heating. The same applied to cooling stages, where pore water pressure changed more quickly with the change in temperature at the beginning of cooling, but then slowed down and tended to change linearly with temperature when the temperature was below 30°C. The overall non-linearity in the mobilisation of pore water pressure with temperature meant that there was hysteresis in this process.

4.6 Effect of the number of thermal cycles

This section discusses the effect of the number of undrained thermal cycles on the evolution of pore water pressure. Individual results are presented first, with some representative tests chosen from both normally consolidated and overconsolidated clay specimens. Then the combined results of all tests are presented.

4.6.1 Individual results

Test ISO-150-2 was chosen as a representative test to show how temperature and pore water pressure changed with time, as shown in Figure 4-6. Pore water pressure increased with the increase in temperature and decreased with the decrease in temperature. There was no observable time lag between the change in temperature and in pore water pressure. In other words, pore water pressure changed instantaneously with change in temperature.

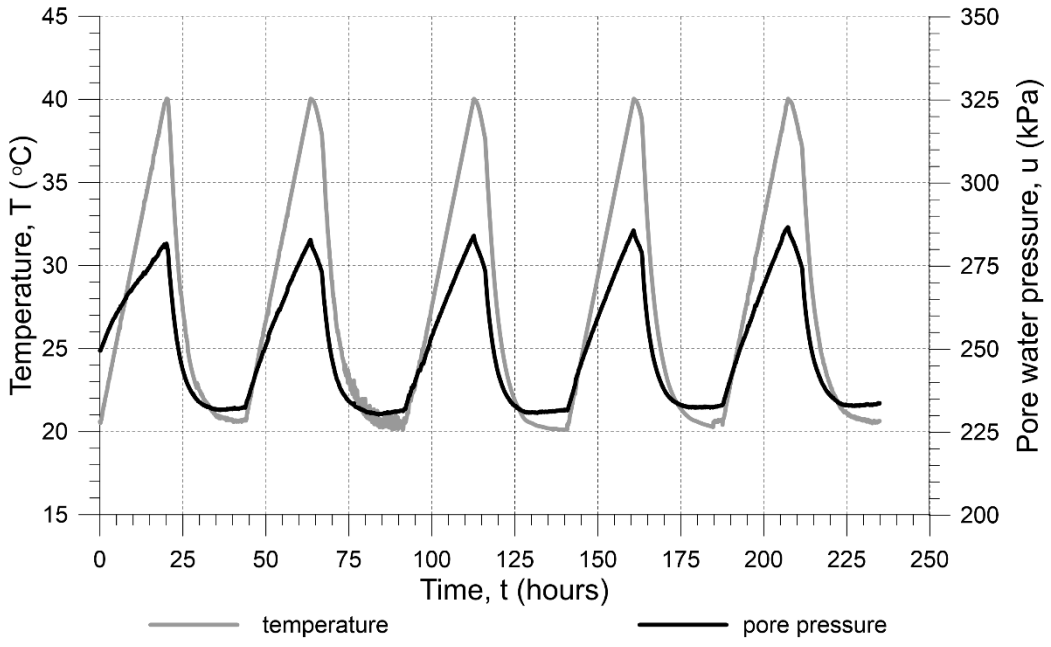

Figure 4-6: Change of temperature and pore water pressure with time (test ISO-150-2)

The test ISO-300-1 was selected as an example for normally consolidated clay specimens. The specimen in this test had a mean effective stress $p'_c = 300$ kPa and an $OCR = 1$ at the start of heating. As shown in Figure 4-7 (a), after the first heating cycle, positive excess pore water pressure of 10 kPa was induced. For the rest of the four thermal cycles, pore water pressure generated upon heating was recovered upon cooling, except at the end of the 3rd cycle where further 4 kPa of excess pore water pressure was generated. This was, however, recovered in the subsequent thermal cycles. Figure 4-7 (b) shows the pore water pressure cycles plotted against temperature. Apart from the first thermal cycle, the remaining four thermal cycles were similar to each other, with almost a closed hysteresis loop in pore water pressure. This indicated that with the increase in the number of thermal cycles, change in pore water pressure tended to stabilise and followed the same trend in the subsequent thermal cycles.

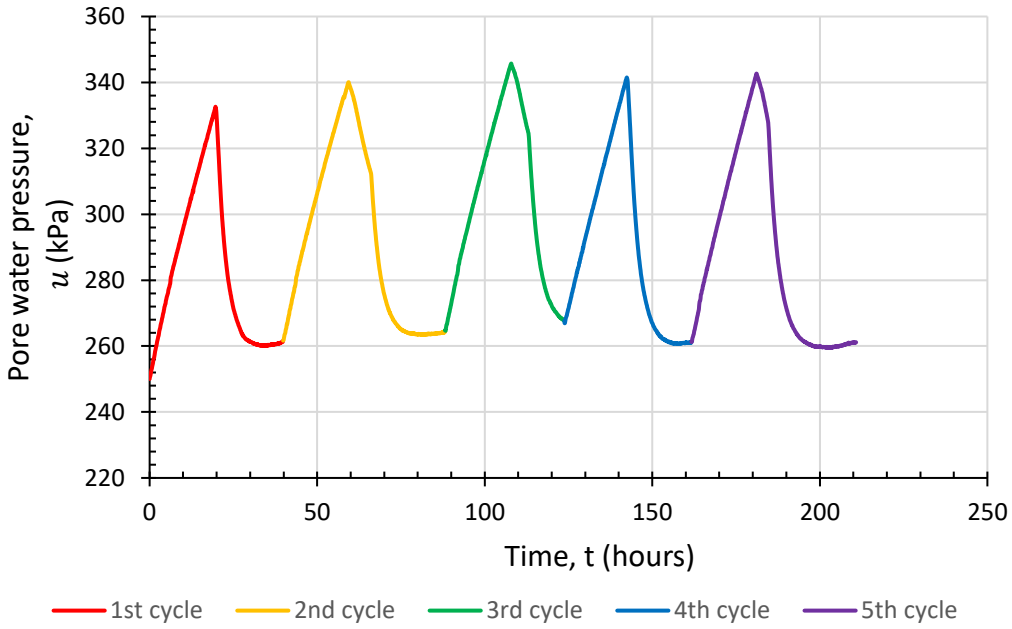

(a) pore water pressure evolution with time (test ISO-300-1)

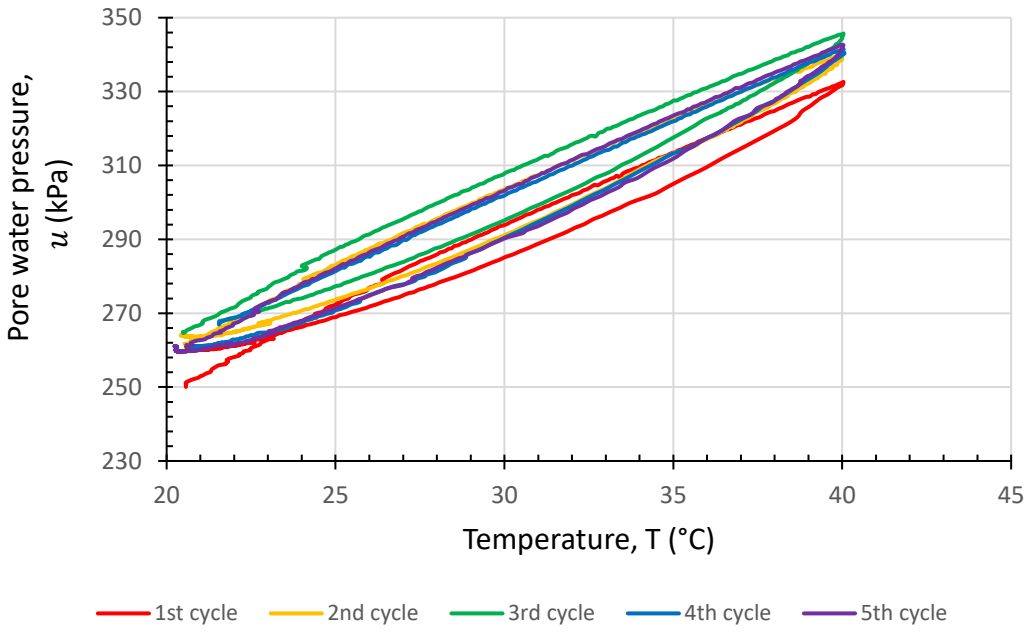

(b) pore water pressure evolution with temperature (test ISO-300-1)

Figure 4-7: Pore water pressure evolution with thermal cycles for normally consolidated clay (OCR=1)

Figure 4-8(a) shows the pore water pressure evolution with thermal cycles for test ISO-150-2, as an example of a lightly overconsolidated clay specimen. In the first thermal cycle, the pore pressure at the end of cooling was 18 kPa lower than $u_{init} = 250$ kPa at the start of the thermal cycle. For the remaining four thermal cycles, the evolution of pore water pressure with change in temperature reached similar maximum values upon heating and minimum values upon cooling. Apart from the first thermal cycle which generated an open loop, Figure 4-8(b), the remaining four cycles generated practically the same closed loop which in cooling coincided with the cooling path of the 1st cycle.

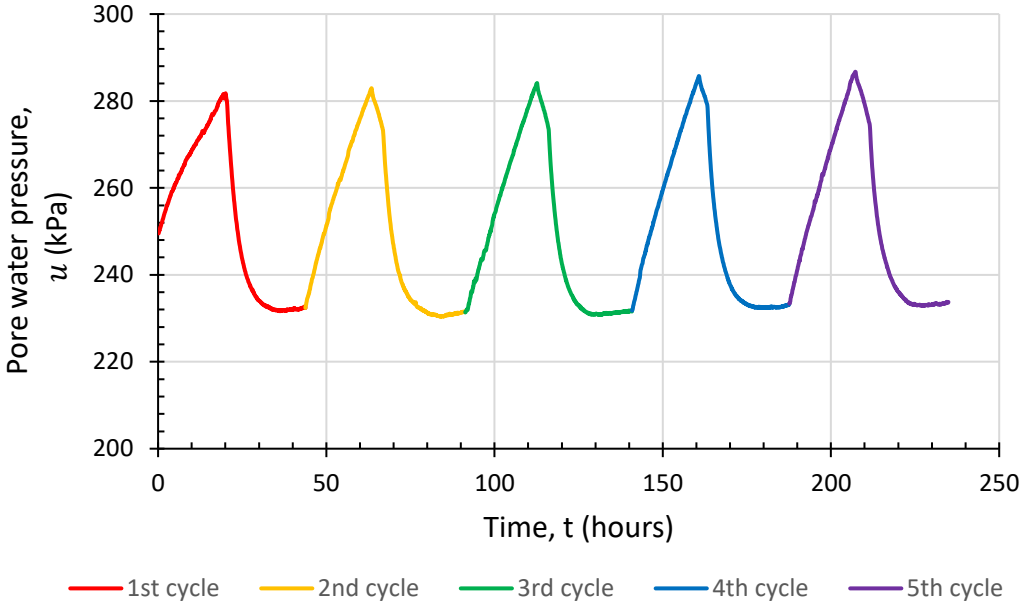

(a) pore water pressure evolution with time (test ISO-150-2)

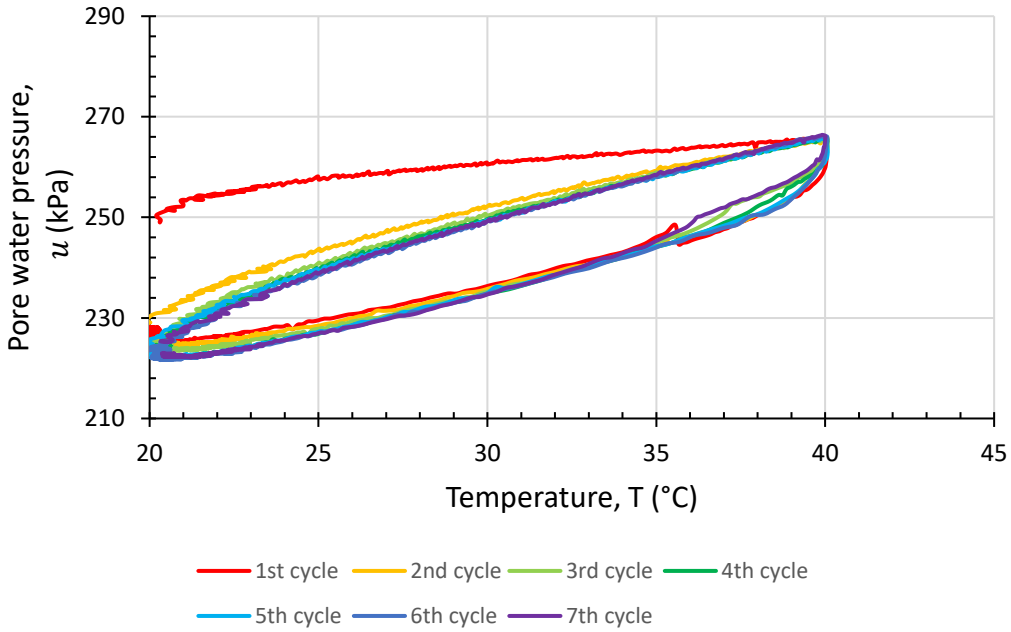

(b) pore water pressure evolution with temperature (test ISO-150-2)

Figure 4-8: Pore water pressure evolution with thermal cycles for OCR=2

Figure 4-9(a) shows the pore water pressure evolution with thermal cycles for test ISO-60-5, as an example of a heavily overconsolidated clay specimen. In the first thermal cycle, the pore pressure at the end of cooling was 23 kPa lower than $u_{init} = 250$ kPa. In the subsequent thermal cycles, the amount of excess pore water pressure induced upon heating was the same, while slightly more excess pore water pressure was induced in each of the cycles up to cycle 5 when the clay specimen was cooled to ambient temperature. Starting from the 6th cycle, thermally-induced pore pressure was fully stabilised. When plotted against temperature in

Figure 4-9(b), apart from the 1st cycle which generated an open loop, the remaining cycles were nearly coincidental as closed loops, following closely during cooling the cooling path of the first cycle. Such a behaviour under multiple loops was observed for all other tests summarised in Table 4-1.

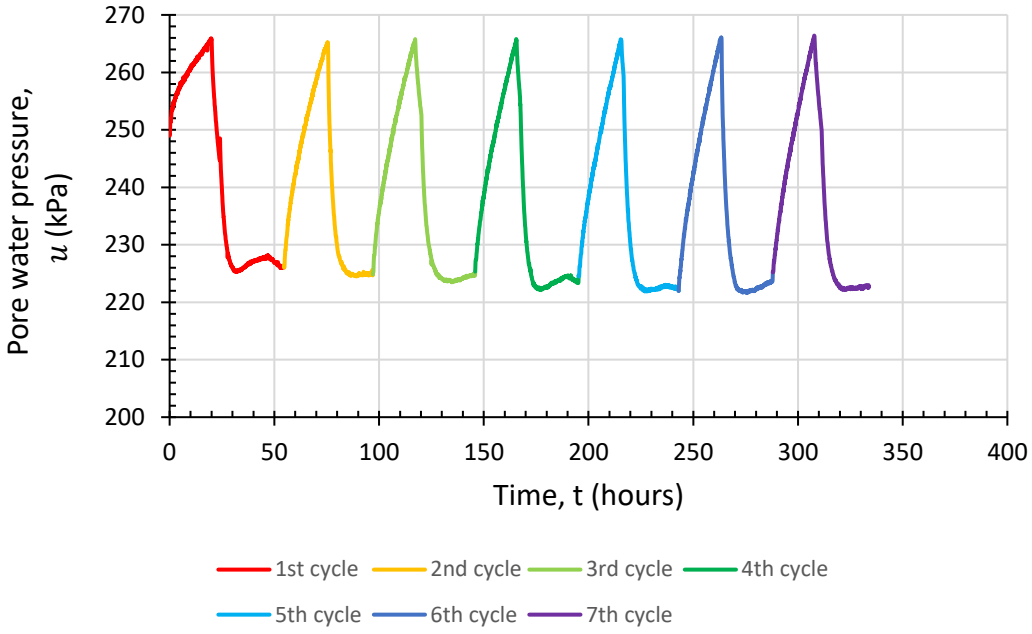

(a) pore water pressure evolution with time (test ISO-60-5)

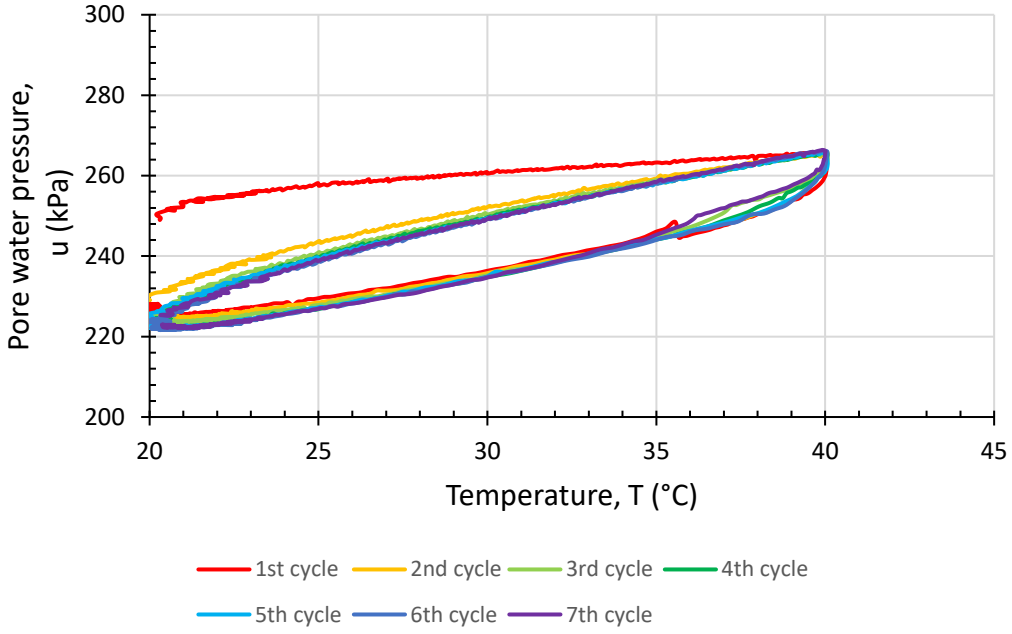

(b) pore water pressure evolution with temperature (test ISO-60-5)

Figure 4-9: Pore water pressure evolution with thermal cycles for OCR=5

4.6.2 Combined results

This section shows the combined results from all tests subjected to undrained thermal cycles, as discussed in the previous sections of this chapter. Since it was shown in Section 4.6.1 that the maximum increase, due to heating, and the maximum reduction, due to cooling, in pore pressure were established by the first thermal cycle in each test, Figure 4-10 shows test results for all first thermal cycles only. Upon heating, higher excess pore water pressures were distinctly induced in normally consolidated specimens (ISO-450-1, ISO-300-1 and ISO-150-1) and at higher p'_c values, while closing the loop back to u_{init} at the end of the cooling path. The maximum values of pore pressures induced by heating the overonsloidated samples were much smaller and also closer together for any value of p'_c and $OCR > 1$. The cooling path in overconsolidated specimens induced lower pore pressures than initial at ambient temperature, regardless of the stress level.

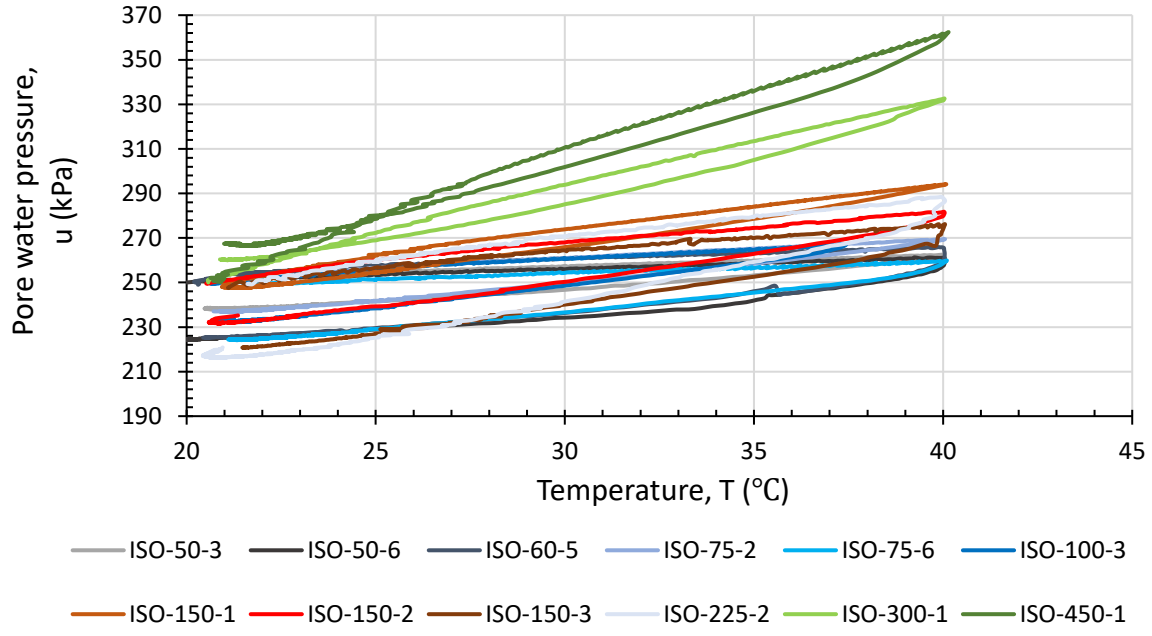

Figure 4-10: Thermally-induced pore pressures in the first undrained thermal cycle

Figure 4-11 shows the normalised excess pore water pressures, $\Delta u/u_{init}$, in the first thermal cycle plotted against temperature from all tests, where $u_{init} = 250$ kPa for all the tests. At 40°C, the normalised pore water pressure ranged from 0.04 to 0.45, therefore being 4% (for highly overconsolidated specimens with $OCR = 6$) to 45% (for normally consolidated specimens with OCR=1) higher than the initial pore water pressure. At the end of cooling stage back at ambient temperature, the normalised excess pore water pressure ranged from 0 to -0.1, therefore being up to 10% smaller than the initial pore water pressure for specimens with an increasing OCR from 2 to 6. In a similar manner Figure 4-12 shows the normalised excess pore

water pressures, $\Delta u/p'_c$, in the first cycle plotted against temperature. At 40 °C, following the temperature change of $\Delta T = +20^{o}$C, the normalised excess pore water pressures range from 0.13 to 0.29, with an average value of 0.21. In the cooling stage, the normalised excess pore water pressures show more diversity for clay specimens with different initial stress states, varying from 0 to -0.52 at ambient temperature.

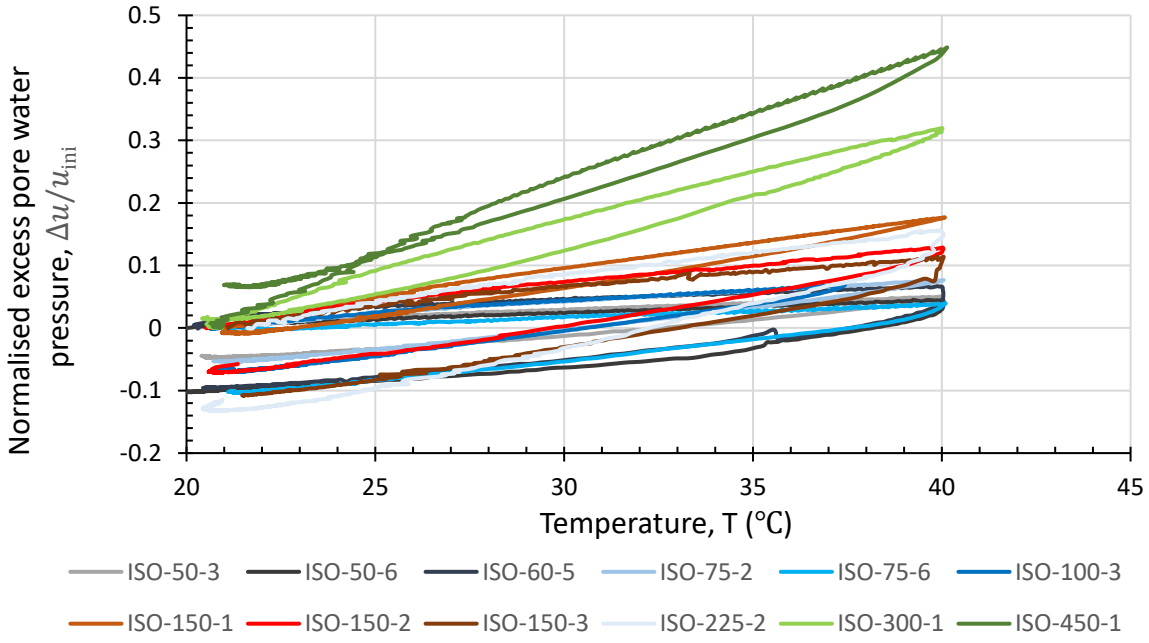

Figure 4-11: Thermally-induced pore water pressure normalised with respect to initial pore pressure, $\Delta u/u_{ini}$, in the first undrained thermal cycle

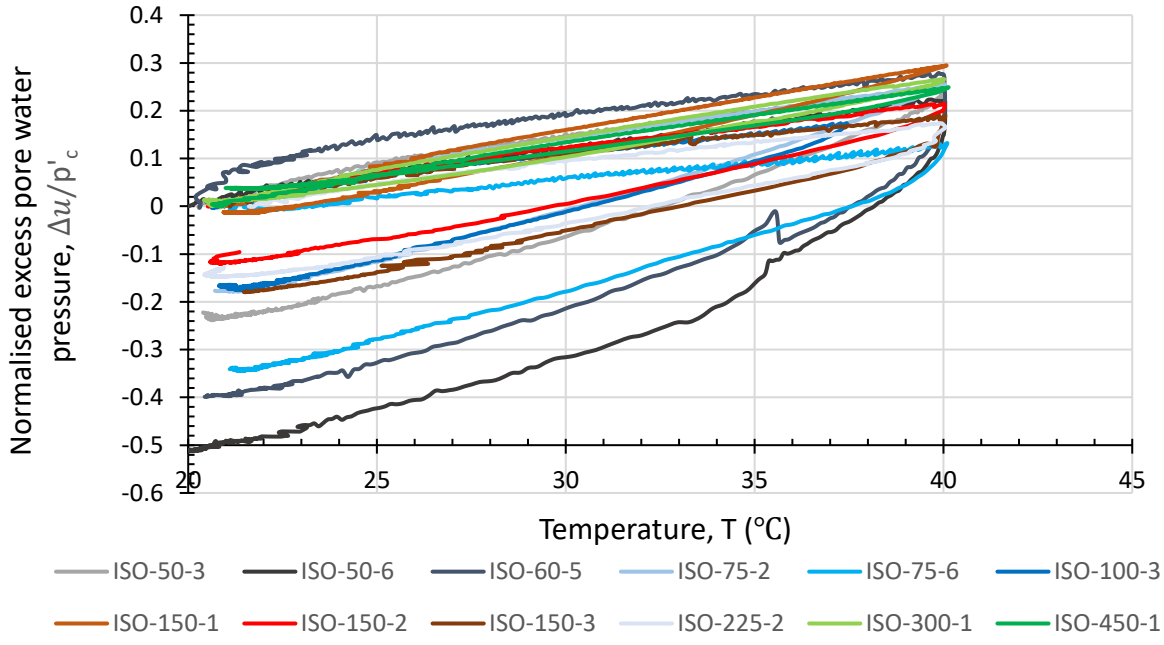

Figure 4-12: Thermally induced pore water pressure normalised with respect to mean effective stress at the start of heating, $\Delta u/p'_c$, in the first undrained thermal cycle

4.7 Comparison of measurements against numerical predictions

4.7.1 Numerical formulation

In this section experimental measurements of thermally-induced pore water pressures during the first heating, as elaborated above, are compared to those predicted numerically from simulations of the same experiments. The numerical simulations were performed with the finite element software ICFEP (Potts and Zdravkovic, 1999, 2001), which adopts a fully coupled thermo-hydro-mechanical (THM) formulation of the governing equations, as developed by Cui et al. (2018). The hydraulic governing equation for fully saturated soils is given by Equation 4-1:

$$\nabla \cdot v_w - \frac{n}{K_w}\frac{\partial u}{\partial t} + 3n(\alpha_s - \alpha_w)\frac{\partial T}{\partial t} - Q^f = -\frac{\partial(\varepsilon_v - \varepsilon_{vT})}{\partial T} \qquad 4\text{-}1$$

where K_w is the bulk modulus of the pore water; u is the pore water pressure; α_w and α_s are respectively the linear thermal expansion coefficients of the pore water and the soil skeleton; n is the porosity, determined from the void ratio, e, by Equation 4-2; t is time; T is temperature; ε_v is total volumetric strain and ε_{vT} is thermal volumetric strain.

$$n = \frac{e}{1+e} \qquad 4\text{-}2$$

In Equation 4-1 the first two terms on the left hand side represent the flow of pore water into and out of the soil element with a velocity v_w, and the changes in the volume of pore water due to its compressibility K_w, respectively. The third term denotes the change in volume of the pore water generated by the difference in thermal expansion coefficients between the soil particles and the pore water.

It is the difference in thermal expansion coefficients that dominates the mobilisation of thermally induced pore pressures during undrained temperature changes, as applied in the experiments presented in this chapter. This is because the value of α_w varies substantially with temperature change, as documented in the literature (Cengal and Ghajar, 2011), while a significantly smaller variation in α_s has been suggested by Campanella and Mitchell (1968), which can therefore be neglected. The variation of α_w with temperature adopted in ICFEP follows a third order polynomial function given in Equation 4-3 (Cengal and Ghajar, 2011), which has been shown to reproduce similar variation to that derived by Martinez-Calonge (2017) and introduced in Chapter 3.

$$\alpha_w(T) = 1.48 \cdot 10^{-10}T^3 - 3.64 \cdot 10^{-8}T^2 + 4.88 \cdot 10^{-6}T - 2.02 \cdot 10^{-5} \quad \text{4-3}$$

where temperature is input in ^{o}C.

4.7.2 Numerical model

An axi-symmetric finite element mesh was developed to discretise specimens with the 50mm diameter and 100mm sample height., adopting 10 quadrilateral elements across the specimen radius and 20 elements along its height. The simulated first heating paths reproduced the stress and temperature conditions of the four experiments selected to cover the spread of magnitudes of thermally induced pore pressures: ISO-300-1, ISO-150-2, ISO-50-3 and ISO-50-6. Each of the tests was initiated with an ambient temperature of $T_{amb} = 21^{o}$C; the pore pressure $u_{init} =$ 250 kPa; an isotropic mean effective stress p'_c =300, 150, 50 and 50 kPa, respectively; and with the void ratio at the start of first heating, as summarised in Table 4-1, e_c =0.986, 1.021, 1.156 and 1.072, respectively.

The mechanical behaviour of the reconstituted London clay was simulated with a modified Cam clay (MCC) model, adopting $\lambda = 0.171$, as interpreted in Chapter 5, $\kappa = 0.0171$, N = 3.026 and $\phi' = 20.7^{o}$, as interpreted in Chapter 5. The thermal properties of London clay were based on the work of Gawecka et al. (2021), adopting $\alpha_s = 1 \cdot 10^{-5}$ m/(mK); α_w varying according to Equation 4-3; specific heat capacity of pore water, $C_{pw} = 4.186$ kJ/(kg K); specific heat capacity of soil particles, $C_{ps} = 1.1$ kJ/(kg K); density of water, $\rho_w = 1000$ kg/m^3; density of soil particles, $\rho_s = 2.774$ kg/m^3; thermal conductivity, $k_T = 1.5 \cdot 10^{-3}$ kJ/(s m K); hydraulic conductivity, $k = 1.0 \cdot 10^{-9}$ m/s; bulk compressibility of the pore water, $K_w = 2.2 \cdot 10^6$ kPa.

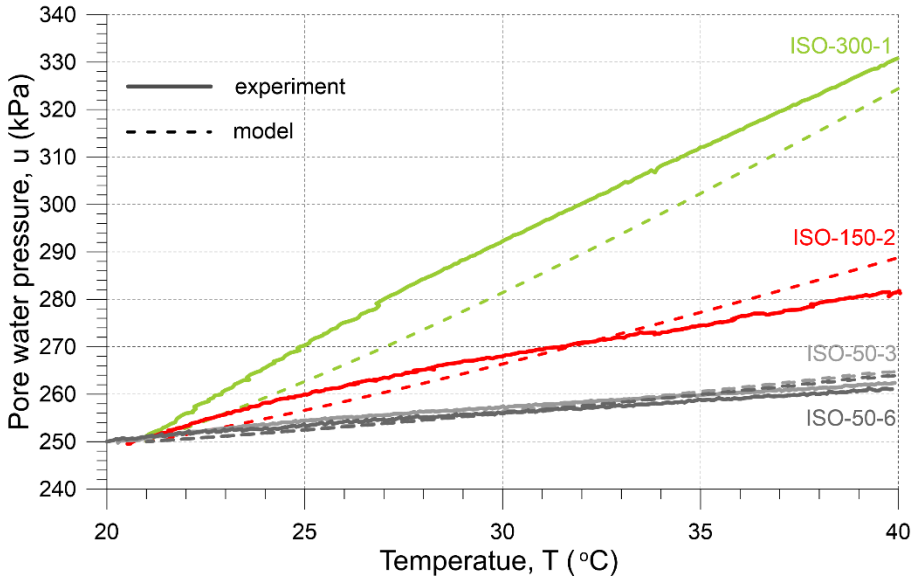

Figure 4-13: Measured and predicted values of thermally-induced pore water pressure: ISO-300-1; ISO-150-2; ISO-50-3; ISO-50-6

The analyses simulated the increase in temperature from 21°C to 40°, at a rate of 1° C/hour, as performed in the laboratory. The low hydraulic conductivity (permeability) contributed to the mobilisation of excess pore pressures due to temperature change, with the results shown in Figure 4-13, together with laboratory measurements. The model predictions are consistent with measurements, confirming theoretically the experimentally measured thermally induced pore pressures. The two tests with the same $p'_c = 50$ kPa but different OCR demonstrated very similar model outputs and in agreement with measurements, confirming that the thermal response is principally dependent on the stress level and initial void ratio, but not on the OCR.

4.8 Discussion

This section discusses the experimental results of thermally-induced pore pressures measured in the set of experiments interpreted in the above sections, with respect to similar published research. Possible mechanisms that led to the change of thermally-induced pore pressures with respect to different values of OCR and p'_c, as well as the hysteresis during heating-cooling cycles, are discussed.

One relevant study in the literature is that of Abuel-Naga et al. (2007a), who investigated the thermally-induced pore water pressures in an isotropically consolidated soft Bangkok clay using triaxial apparatus. Tests were performed on 50mm-diameter specimens at different mean effective stress values achieved at the end of a consolidation / swelling path ($p'_{cons} = 200, 300$ and 400 kPa) and at different overconsolidation ratios ($OCR = 1, 2$ and 4).

Specimens of this clay were subjected to heating and cooling in a 25^{o}C – 90^{o}C – 25^{o}C thermal loop, applying 10^{o}C increments under undrained condition.

4.8.1 Normally consolidated clay

Figure 4-14 (a) shows the thermally-induced pore water pressures in normally consolidated ($OCR = 1$) soft Bangkok clay specimens, at different initial mean effective stress p'_{cons}. It was evident that the rate of the thermally-induced pore water pressure increased with the increase in preconsolidation pressure, p'_{cons}, which was also observed in the case of the normally consolidated reconstituted London clay in Figure 4-1, which developed a visible hysteresis in thermally-induced pore pressures. A practically linear relationship between the normalised Δu and temperature increase in Figure 4-14(b) was also seen in the London clay study, with the maximum $\Delta u/p'_{cons}$ of around 0.2 at $T = 45^{o}$C ($\Delta T = 20^{o}$C) being slightly lower than that measured for London clay (around 0.27 on average for the same temperature change). The hysteresis in the thermally-induced pore pressure was negligible for the Bangkok clay case, with thermal loops being very narrow, compared to London clay. Nearly all of the excess pore water pressure generated upon heating was recoverable upon cooling.

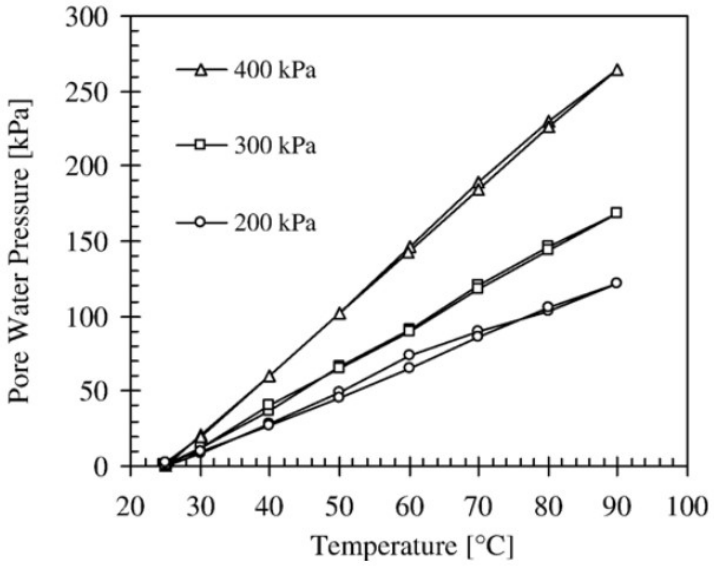

(a) Pore water pressure-temperature, OCR=1

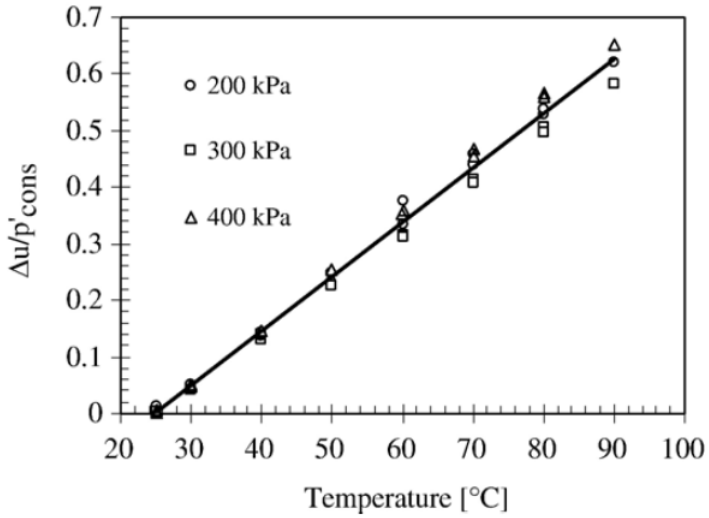

(b) Normalised pore water pressure-temperature, OCR=1

Figure 4-14: Effect of initial stress state for normally consolidated soft Bangkok clay (a) Pore water pressure-temperature, OCR=1; (b) Normalised pore water pressure-temperature, OCR=1 (Abuel-Naga et al. 2007)

4.8.2 Overconsolidated clay

Results for overconsolidated soft Bangkok clay specimens are shown in Figure 4-15. Specimens were isotropically consolidated to a mean effective stress of 200 kPa (OCR=1), or unloaded to different overconsolidation ratios (OCR=2 or 4). Upon heating, positive excess pore water pressure was induced, regardless of overconsolidation ratios. The rate of thermally-induced pore water pressure decreased with increase in OCR. Negative thermally-induced pore water pressure was generated when the overconsolidated soft Bangkok clay specimens were cooled to 25°C. The rates of thermally-induced pore water pressure on the cooling path for overconsolidated specimens were practically the same. Similar behaviour was observed in overconsolidated reconstituted London clay specimens, as presented in Section 4.4. Hueckel and Pellegrini (1992) reported similar observations in the study of bentonite-sand mixes subjected to temperature changes.

When the thermally-induced pore water pressures were normalised by the relevant preconsolidation pressure, as shown in Figure 4-15 (b), heating paths of clay specimens were practically the same, regardless of their overconsolidation ratios.

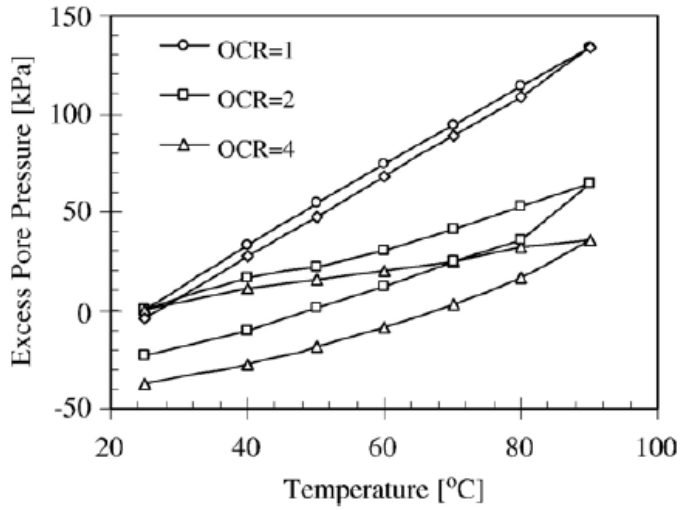

(a) Pore water pressure-temperature

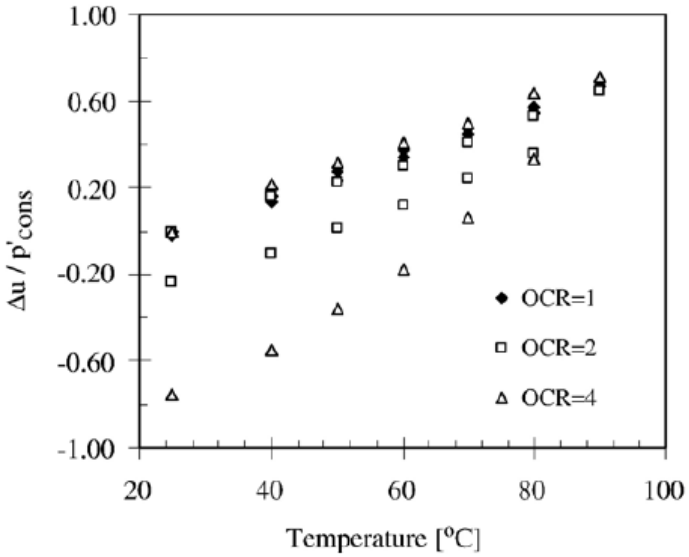

(b) Normalised pore water pressure-temperature

Figure 4-15: Effect of overconsolidation ratio for soft Bangkok clay specimens with preconsolidation pressure of 200 kPa (a) pore water pressure-temperature; (b) normalised pore water pressure-temperature (Abuel-Naga et al. 2007a)

4.8.3 Thermally-induced pore water pressure parameter

Based on the experimental results on reconstituted London clay and soft Bangkok clay, preconsolidation pressure was demonstrated to have great influence on the thermally-induced pore water pressures, as it restricted the expansion of clay skeleton upon heating. Consequently, thermally-induced pore water pressure increased with the increase in preconsolidation pressure upon heating. This was shown by normalising the thermally-induced pore water pressure with preconsolidation pressure. However, upon cooling, thermally-induced pore water pressure was insensitive to preconsolidation pressure, as the cooling paths were parallel to each other.

Campanella and Mitchell (1968) proposed the thermally-induced pore water pressure parameter, F, as the analogy between the heating-cooling paths in undrained heating tests and the compression or swelling index, C_c or C_s, in the loading or unloading-reloading paths in one-dimensional compression tests. They believed that the primary factors that controlled the magnitude of thermally-induced pore water pressure were the compressibility of the soil and the thermal expansion of water. The smaller the compressibility of the soil, the larger the thermally-induced pore water pressure. The parameter F could help to quantify and compare thermally-induced pore pressures for different soils with different stress history and under different testing conditions. It was defined as the change in pore pressure per unit change in temperature per unit effective stress, as in Equation 4-5:

$$F = \frac{\Delta u}{p_c'(\Delta T)} \qquad 4\text{-}5$$

Values of thermally-induced pore water pressure parameter found in the literature for several soils are summarised in Table 4-3. The average values of p_c' and Δu in the temperature range considered were used for calculating the parameter F. In these tests, a single value of F was identified for both the heating and cooling paths, without differentiating the effect of overconsolidation ratio. For clays that were investigated and presented in Table 4-3, the magnitudes of F were in a narrow range, from 0.0132 °C^{-1} to 0.0183 °C^{-1}, while this value was considerably higher for sandstone. This observation was consistent with Campanella and Mitchell (1968) statement that the magnitude of F increased when the soil was less compressible.

Table 4-3: Values of thermally-induced pore water pressure from literature

Soil type	Average p_c' (kPa)	Average Δu (kPa)	T (°C)	ΔT (°C)	F (°C^{-1})	Reference
Vicksburg Buckshot clay	98	27.5	20 to 36	16	0.0175	Ladd, 1961
	637.4	186.3			0.0183	
Weald clay	696.3	50	25 to 29	4	0.0180	Henkel and Sowa, 1963
Kaolinite	196	76.5	21 to 43	22	0.0177	Mitchell and Campanella, 1963

Illite	196	56.9	21 to 43	22	0.0132	Campanella and Mitchell 1968
San Francisco Bay mud	147.1	49	21 to 43	22	0.0151	Campanella and Mitchell 1968
Saturated porous stone (sandstone)	245.2	186.3	5.3 to 15	9.7	0.0783	Campanella and Mitchell 1968
	568.8	510			0.0924	

Abuel-Naga et al. (2007) reported the thermally-induced pore water pressure parameter of 0.01026 °C^{-1} for soft Bangkok clay, for the heating path, regardless of the overconsolidation ratios of the specimens. They also used averaged values of p_c' and Δu over the temperature range for calculating F. The F parameter for the cooling paths for soft Bangkok clay specimens of $OCR = 2$ and 4 were reported to be 0.01377 and 0.002263 °C^{-1}, respectively. In this case, the effect of OCR on the pore water pressure parameter was observed for the cooling path but not for the heating path.

The thermally-induced pore water pressure parameter F for tests on reconstituted London clay specimens is presented in Table 4-4. The parameter F was calculated from the first cycle of each test, by taking the gradient of the middle part of the heating or cooling path in the normalised pore water pressure versus temperature plots ($\Delta u/p_c' - T$, interpreted in Section 4.3), where the temperature ranged from 25 to 35 °C and the curve was observed to be more linear compared to lower (20-25 °C) or higher (35-40 °C) temperature range. On the heating path, F value varied from 0.0045 to 0.0145°C^{-1}, with an average value of 0.0104°C^{-1}. On the cooling path, thermally-induced pore water pressure parameters for London clay varied from 0.0005 to 0.0222°C^{-1}. The magnitude of F was shown to be more sensitive to the change in OCR than the change in initial stress level.

Table 4-4: Thermally-induced pore water pressure parameter for the first heating-cooling cycle on reconstituted London clay specimens

Test	Thermally-induced pore water pressure parameter F (°C^{-1})	
	Heating path (20 to 40°C)	Cooling path (40 to 20°C)
ISO-150-1	0.0145	0.0005
ISO-300-1	0.0135	0.0015
ISO-450-1	0.0125	0.0010

ISO-75-2	0.0135	0.0085
ISO-150-2	0.0105	0.0060
ISO-225-2	0.0085	0.0075
ISO-50-3	0.0120	0.0120
ISO-100-3	0.0100	0.0085
ISO-150-3	0.0085	0.0100
ISO-60-5	0.0065	0.0110
ISO-50-6	0.0099	0.0222
ISO-75-6	0.0045	0.0185

It could be observed that the thermally-induced pore water pressure parameters calculated based on the data from the first heating-cooling cycles differed significantly for different tests. No single value or an average value can be used as representative for all tests. This is because most of the irrecoverable excess pore water pressure was generated in the first heating-cooling cycle, as presented in Section 4.6. The subsequent cycles were shown to practically overlap, while retaining some hysteresis. In order to obtain the thermally-induced pore water pressure parameter that was more representative and consistent, normalised thermally-induced pore water pressure was plotted against temperature for all cycles, as shown for example tests in Figure 4-16. The parameter F was interpreted as a secant gradient, F_{sec}, of the normalised set of cycles except for the 1st cycle. Using this method, the thermally-induced pore water pressure parameter for both the heating and cooling paths was represented by a single value, thus avoiding the variations caused by the first heating-cooling cycle. Values of the secant gradient, F_{sec}, for all the tests were summarised in Table 4-5, ranging from 0.0131 to 0.0310°C^{-1}. For the test ISO-60-5, the thermally-induced pore water pressure parameter was abnormally high compared to other tests, probably due to experimental scatter. This test was excluded in the discussion. Thermally-induced pore water pressure parameters were plotted against the corresponding overconsolidation ratios in Figure 4-17. There was a clear difference between normally consolidated and overconsolidated clays. For normally consolidated London clay, an average value of 0.0147°C^{-1} can be used as a representative value of the thermally-induced pore water pressure parameter. For overconsolidated London clay, an average value of 0.0213°C^{-1} can be used. There was no clear difference between the F value for lightly and heavily overconsolidated soils though. Thermally-induced pore water pressure can be then calculated using Equation 4-6, provided that the value of F, p_c' and ΔT are known. When the soil was overconsolidated, it became less compressible and thermally-induced pore water pressure parameter would be expected to increase. This observation was different from what Abuel-

Naga et al. (2007a) reported for soft Bangkok clay, where they stated that the thermally-induced pore water pressure parameter of 0.01026 °C^{-1} for soft Bangkok clay, regardless of the overconsolidatoin ratios of the specimens. Soft Bangkok clay specimens with OCRs of 1, 2 and 4 were tested, but these did not include higher OCR values. In addition, the thermally-induced pore water pressure parameter reported by Abuel-Naga et al. (2007a) was calculated based on the pore water pressure evolution in the first heating-cooling cycle, but it did not reflect the behaviour in the subsequent temperature cycles.

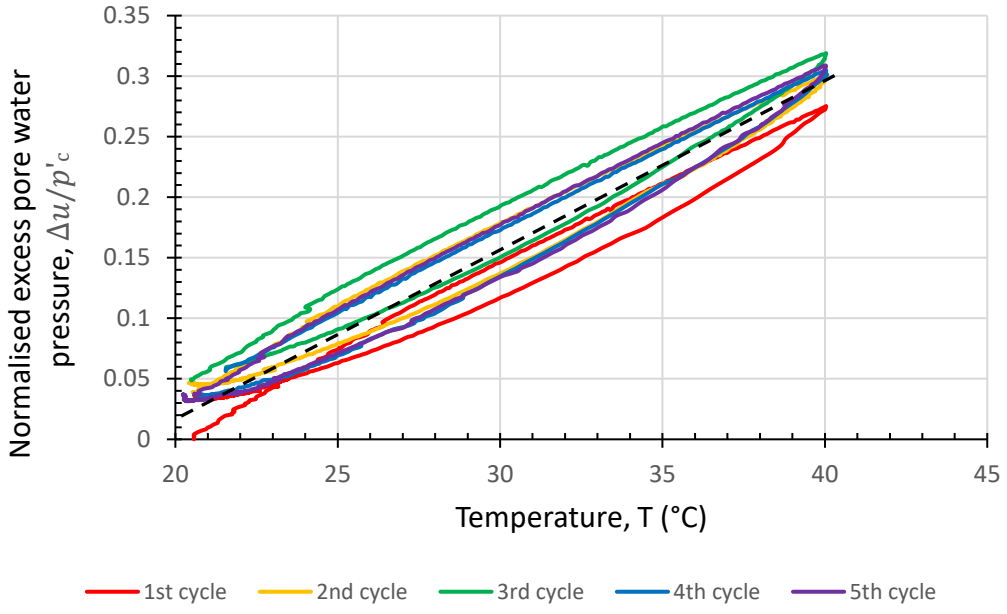

(a) OCR=1

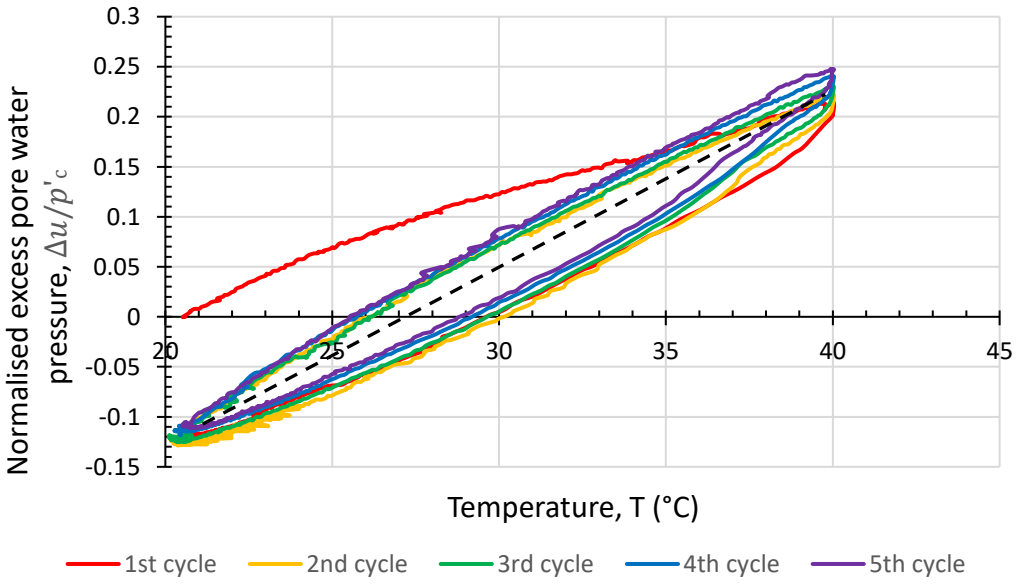

(b) OCR=2

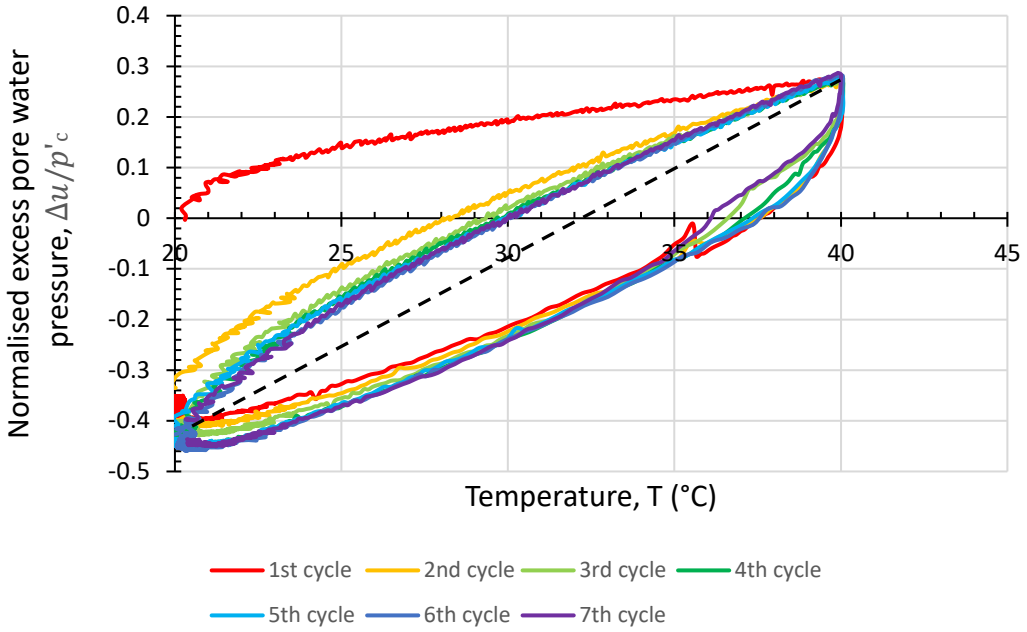

(c) OCR=5

Figure 4-16: Normalised thermally-induced pore water pressure evolution with temperature, for calculating thermally-induced pore water pressure parameter

Table 4-11: Gradient for normalised excess pore water pressure-temperature plots for subsequent heating-cooling cycles on reconstituted London clay specimens

Test	Gradient for normalised excess pore water pressure-temperature plots ($°C^{-1}$)
ISO-150-1	0.0171
ISO-300-1	0.0140
ISO-450-1	0.0131
ISO-75-2	0.0226
ISO-150-2	0.0177
ISO-225-2	0.0182
ISO-50-3	0.0242
ISO-100-3	0.0227
ISO-150-3	0.0202
ISO-60-5	0.0310
ISO-50-6	0.0220
ISO-75-6	0.0231

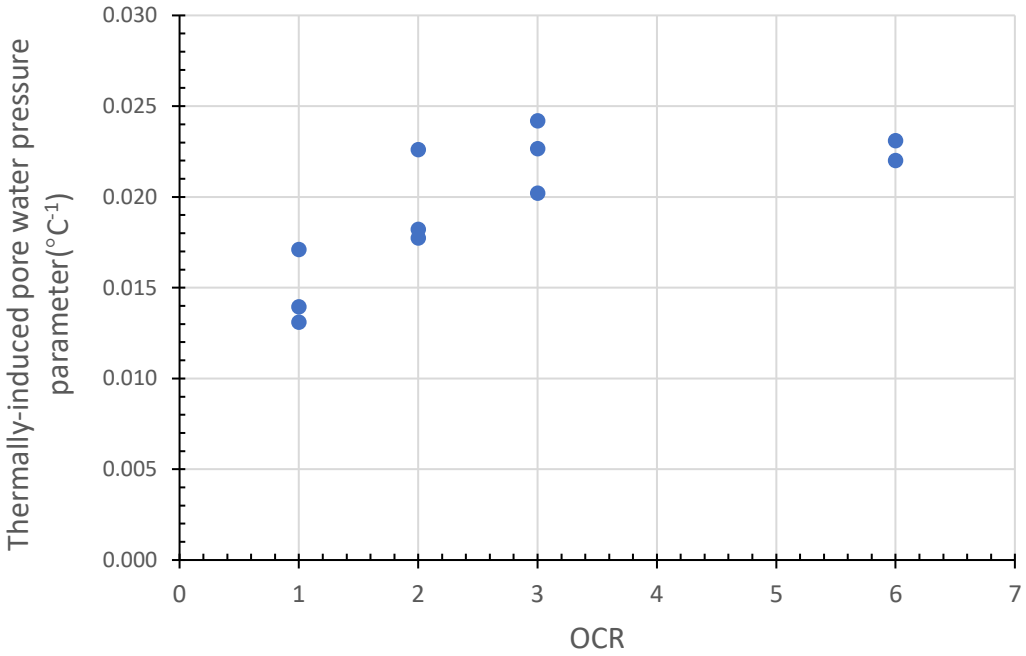

Figure 4-17: Change of thermally-induced pore water pressure parameter with OCR

$$\Delta u = F * p_c' * \Delta T \qquad 4\text{-}6$$

4.8.4 Hysteresis in thermally-induced pore water pressure during the heating-cooling cycle

The hysteresis in thermally-induced pore water pressure can be explained in a similar way as the hysteresis in the unloading-reloading curve in consolidation tests, as shown in Figure 4-18. The initial part of the heating path from point A to B had the same slope as the initial cooling path from point D to E. The slope of the heating path increased as the effective stress decreased with increasing temperature, while the slope of the cooling path increased as the effective stress increased with reducing temperature. This resulted in the irreversible change in pore water pressure in heating-cooling cycles. The difference in the slope of the heating-cooling path increased with the increase in overconsolidation ratio. Therefore, thermally-induced pore water pressure for normally consolidated clays was mostly reversible while it was irreversible for overconsolidated clays. When clay specimens were heated under undrained condition, due to the difference between the thermal coefficient of water and the thermal coefficient of solids, with the former being larger than the latter (Table 4-2), excess pore water pressure was induced in the clay and the effective stress decreased. The clay behaved as if it was unloaded in consolidation tests, and it followed the path from A to D. Upon cooling, pore water pressure decreased, and the effective stress increased. The clay behaved as if it was reloaded in consolidation tests, and it followed the path from D to A.

Another explanation to the hysteresis in the thermally-induced pore water pressure is the temperature effect on the change in fabric of the clay. Abuel-Naga et al. (2007a) speculated that when the clay was heated under undrained condition, interparticle physico-chemical forces increased and the interparticle viscous shear resistance of the adsorbed water decreased. This is reflected by the increase in pore water pressure and decrease in effective stress in macro scale. Pusch et al. (1991) speculated that the thermally-induced pore water pressure created unstable stress conditions for overconsolidated clay specimens, and this led to permanent disintegration of fabric. When the overconsolidation ratio of clay increased, this permanent change in fabric was more pronounced, compared to the situation when the clay was normally consolidated. Therefore, for normally consolidated clays, most of the thermally-induced pore water pressure induced upon heating was recoverable when the specimen was cooled to ambient temperature, while thermally-induced pore water pressure was irreversible for overconsolidated clays. The amount of irrecoverable pore water pressure increased with the increase of overconsolidation ratios.

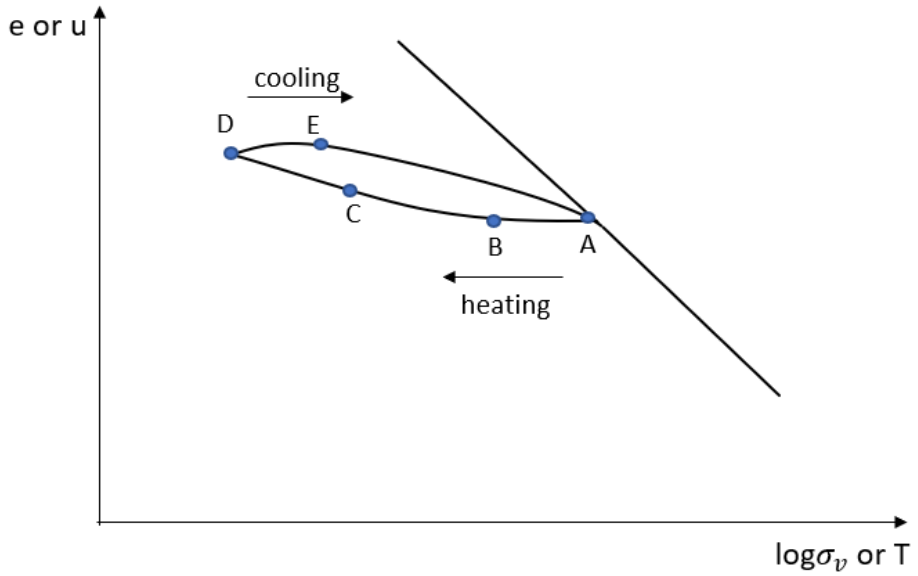

Figure 4-18: Mechanism of the thermally-induced pore water pressure in heating-cooling cycle

4.9 Summary points

This chapter presents the thermally-induced pore water pressure of reconstituted London clay. Specimens with different initial stresses and overconsolidation ratios were tested in the temperature-controlled triaxial apparatus, under undrained heating-cooling cycles of 20-40-20 °C. Results are summarised as follows.

For normally consolidated clays, thermally-induced pore water pressure increased with the increase of initial stresses. Excess pore water pressure generated upon heating was mostly reversible when the clay specimens were cooled to ambient temperature.

For lightly overconsolidated clays (OCR=2 or 3), thermally-induced pore water pressure was a function of both the initial stresses and overconsolidation ratios. On the heating path, thermally-induced pore water pressure increased with the increase of initial stresses but decreased with the increase of overconsolidation ratios. On the cooling path, however, rate of change in pore water pressure was insensitive to changes in initial stresses or overconsolidation ratios.

For heavily consolidated clays, the excess pore water pressure generated did not differ much with initial stresses. This may indicate that the thermally-induced pore water pressure was less sensitive to stress level at high overconsolidation ratios, or it may be caused by the similar stress states that the tests in this research were performed in. More laboratory evidence is necessary to confirm this observation.

Thermally-induced pore water pressure parameter, F, was calculated by taking the gradient of the normalised excess pore water pressure versus temperature plot of subsequent thermal cycles, without considering the first thermal cycle. Its magnitude varied from 0.0113 to 0.0310°C^{-1} and it increased with the increase in OCR.

Thermally-induced pore water pressure increased with the increase in the magnitude of temperature change but the relationship between the two was not linear. Pore water pressure changed at a higher rate at the beginning of both heating and cooling paths but then slowed down towards the end of heating and cooling. This hysteresis can be explained in a similar way as the hysteresis in the unloading-reloading curve in consolidation tests. It can also be explained by the thermally-induced fabric change of the clay. This permanent disintegration of fabric was more obvious in overconsolidated clays. Consequently, the amount of irreversible thermally-induced pore water pressure increased with the increase in overconsolidation ratios.

Most of the irrecoverable pore water pressure was generated in the first thermal cycle. For the remaining thermal cycles, most of the pore water pressure generated upon heating was recovered upon cooling. For tests with high OCR values, it took more thermal cycles for the change in pore water pressure to be repeatable compared to previous thermal cycles.

Chapter 5: Undrained shearing at elevated temperature

5.1 Introduction

This chapter presents the effect of temperature change on the volumetric strains, strength and stiffness of saturated reconstituted London clay. Laboratory tests were performed in the temperature-controlled triaxial apparatus on specimens trimmed from reconstituted London clay cakes. Details of the apparatus and experimental procedures are presented in Chapter 3.

5.2 Applied stress and temperature paths

Specimens of reconstituted London clay were isotropically consolidated / swelled at ambient temperature, $T_{amb} = 20^{o}$C, to a range of mean effective stresses and overconsolidation ratios, OCR. From the initial stress state, specimens were subjected to three types of stress and temperature paths: (i) after consolidation / swelling at ambient temperature, $T_{amb} = 20^{o}$C, specimens were sheared under undrained condition at $T_{amb} = 20^{o}$C. This group of tests serves as reference tests to be compared with tests with the same stress history but different temperature history; (ii) temperature of the specimen was elevated to $T_{elev} = 40^{o}$C under drained conditions, followed by undrained shearing at $T_{elev} = 40^{o}$C. This group of tests was designed to investigate the effect of elevated temperature on volumetric strains, strength and stiffness of the clay; (iii) a temperature cycle was applied under drained conditions (20^{o}C – 40^{o}C – 20^{o}C), followed by undrained shearing at $T_{amb} = 20^{o}$C. The applied temperature change of $\Delta T = 20^{o}$ C is compatible with temperature changes induced in the ground by thermo-active structures. This group of tests was designed to investigate the effect of a thermal cycle, referred to as thermal pre-conditioning, on the volumetric strains, strength and stiffness of the clay. Applied stress and temperature paths of each test are summarised in Table 5-1. Tests are named based on their stress and temperature history. For example, for the first test listed in the table, the name code is TXC-300-1-20. This means the test was performed in the triaxial apparatus, with a stress path that involved isotropic compression to a maximum mean effective stress $p'_{max} = 300$ kPa and $OCR = 1$, resulting in a $p'_c = 300$ kPa at the end of the consolidation / swelling path. The clay specimen then went through undrained shearing at $T = 20^{o}$C. For the last test listed in the table, the name code is TXC-50-6-20-40-20. This means that the test was performed in the triaxial apparatus, with an initial isotropic compression to $p'_{max} = 300$ kPa and swelling to $p'_c = 50$ kPa, with $OCR = 6$. The specimen then went through a thermal cycle of 20-40-20°C, before it was sheared in undrained condition at 20 °C. All the tests had the same mean effective stress $p'_{max} = 300$ kPa at the end of the isotropic consolidation stage but were unloaded isotropically to different p'_c and achieved different OCR

values before they went through thermal treatment and the undrained shearing stages. A double load cell triaxial apparatus was used for tests presented in this chapter.

Table 5-1: Applied stress and temperature paths for tests in the temperature-controlled triaxial apparatus

code	Isotropic loading / swelling			Temperature path (°C)
	p'_{max} (kPa)	p'_c (kPa)	OCR	
TXC-300-1-20	300	300	1	20
TXC-300-1-20-40	300	300	1	20-40
TXC-300-1-20-40-20	300	300	1	20-40-20
TXC-200-1.5-20	300	200	1.5	20
TXC-200-1.5-20-40	300	200	1.5	20-40
TXC-200-1.5-20-40-20	300	200	1.5	20-40-20
TXC-150-2-20	300	150	2	20
TXC-100-3-20	300	100	3	20
TXC-100-3-20-40	300	100	3	20-40
TXC-100-3-20-40-20	300	100	3	20-40-20
TXC-50-6-20	300	50	6	20
TXC-50-6-20-40	300	50	6	20-40
TXC-50-6-20-40-20	300	50	6	20-40-20

5.3 Effect of temperature on volumetric strains during drained heating/ cooling

Thermally induced volumetric strains of London clay specimens with different stress histories are shown in Figure 5-1. Positive volumetric strains represent contraction while negative volumetric strains represent expansion. For tests with the same stress history, volumetric strains generated during heating agreed with each other, indicating satisfactory repeatability and consistency of the tests. Normally consolidated clay specimens contracted upon heating and the thermally induced volumetric strains were irreversible upon cooling (test TXC-300-1). Lightly overconsolidated clays contracted upon heating and thermally induced volumetric strains were reversible when the specimens were cooled to ambient temperature (tests TXC-200-1.5 and TXC-100-3). Hysteresis was observed in the volumetric strains with heating/cooling cycle. The amount of contraction decreased with increasing OCR, until expansion was observed for heavily overconsolidated specimens upon heating (test TXC-50-6), and the expansion was reversible when the specimens were cooled to ambient temperature.

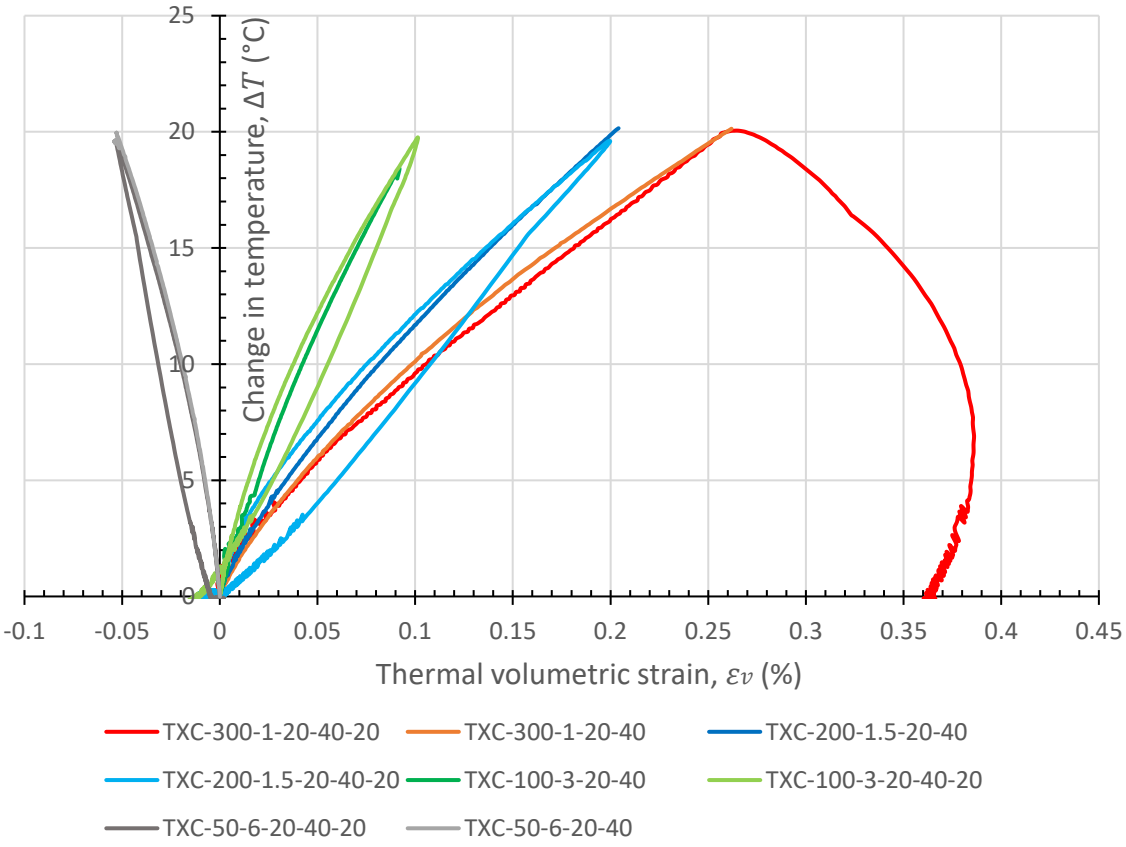

Figure 5-1: Thermally induced volumetric strains under drained heating/cooling

5.4 Effect of initial stress state on soil strength and stiffness

In this section, results of undrained shearing, following the drained heating / cooling described in Section 5.3, are presented. Effect of the initial stress state is discussed. This includes the initial mean effective stress, p'_c, and OCR.

5.4.1 Strength

Stress level mentioned in this section refers to the mean effective stress at the beginning of the undrained shearing stage. Stress paths in terms of the deviatoric stress, q, and mean effective stress, p', are presented in Figure 5-2. Five reference tests that were sheared at ambient temperature showed the effect of the initial stress state on soil strength and stiffness. The maximum mobilised deviatoric stress increased with the mean effective stress. The same was observed for specimens that were sheared at 40°C and with thermal preconditioning. Values of the deviatoric stress and the corresponding axial strains at different stages of tests are summarised in Table 5-2. Peak strength can be easily identified by choosing the maximum deviatoric stress in each test. The shear strength then dropped from peak to a reasonably constant value after relative displacement across the slip surface of only a few millimetres. This

value was termed as post-rupture strength (Burland, 1990; Burland et al., 1996). In this research, post-rupture strength was identified by taking the average value of the peak and the strength at large strains. Strength at large strains is taken as the mobilised deviatoric stress at an axial strain of 25%. In some of the tests where the specimens were not sheared to a 25% axial strain, it is taken as the deviatoric stress at the end of shearing. Strains at which the single shear plane formed were identified by analysing the data from internal displacement transducer. The general trend is that the peak strength increased with the increase in mean effective stress.

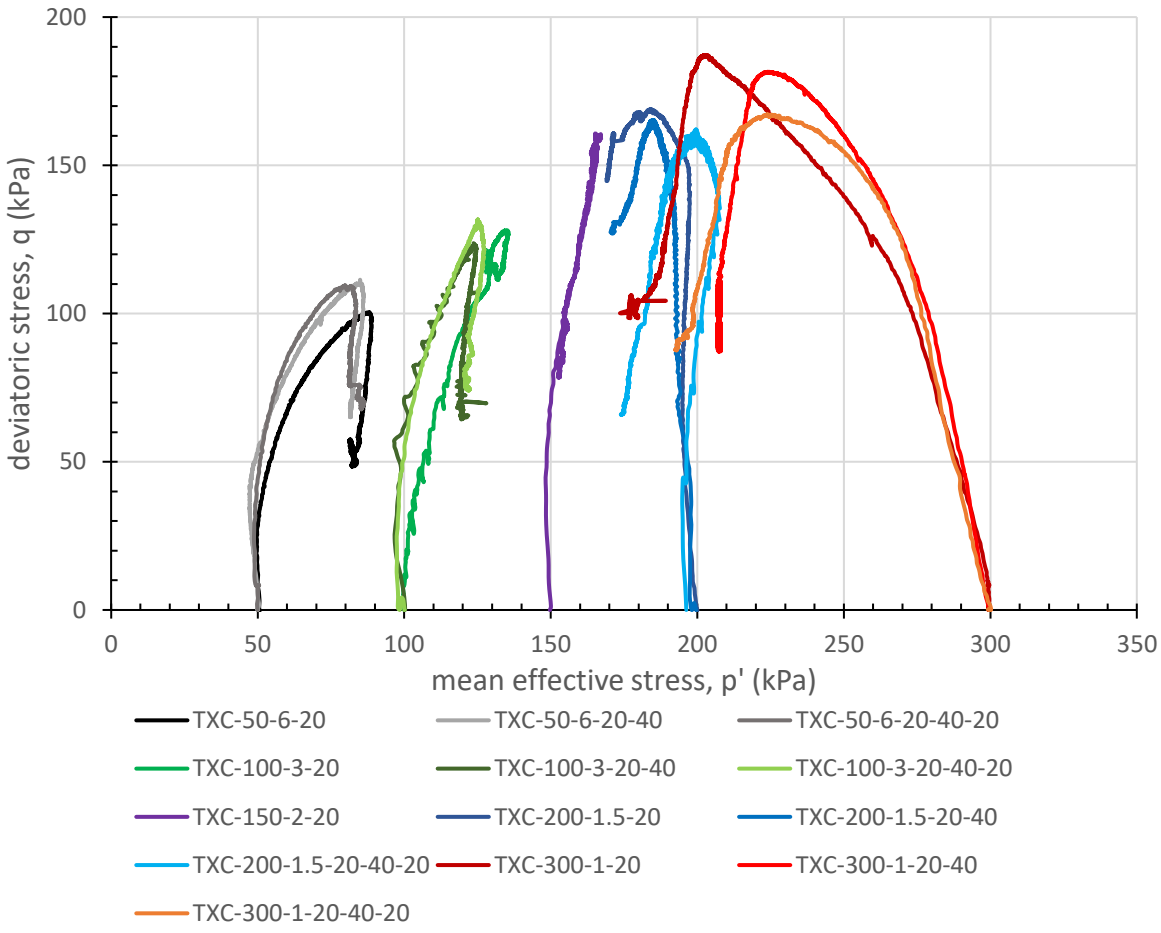

Figure 5-2: Undrained shearing effective stress paths on reconstituted London clay

Table 5-1: Deviatoric stress and the corresponding axial strains at different stages of tests

Test	peak		post rupture		large strains		single shear plane formed
	q	ε_a	q	ε_a	q	ε_a	ε_a
	kPa	%	kPa	%	kPa	%	%
TXC-300-1-20	187	10.9	147.5	13.9	100	25	14.2
TXC-300-1-20-40	181	5.7	152	10.2	88	25	11.6
TXC-300-1-20-40-20	166	6	136.5	12.2	88	19.2	13.8
TXC-200-1.5-20	165	4.6	164	6.8	145	21.2	12.7
TXC-200-1.5-20-40	162	8	140.5	12.2	127	21.5	13.9
TXC-200-1.5-20-40-20	160	5	114	13.2	68	21	12.7
TXC-150-2-20	160	5	123	13.6	86	25	15.6
TXC-100-3-20	130	11	122.5	18	115	25	17.4
TXC-100-3-20-40	123	5.4	98.8	8.4	74.6	24	12.9
TXC-100-3-20-40-20	129	5.2	104	9.2	74	17	11.2
TXC-50-6-20	98	6	76	7.6	43.5	25	8.7
TXC-50-6-20-40	110	5.1	85.5	7.6	65.9	25	6.5
TXC-50-6-20-40-20	109	4.1	85.3	10.1	68	25	7.9

The stress-strain curves with deviatoric stress, q, plotted against axial strain, ε_a, are shown in Figure 5-3 for all tests. Peak strength was usually observed when axial strain was around 5-7%. Shear plane formed when axial strain was around 11-13% for most of the tests. Strain softening was observed for most of the tests, except for TXC-100-3-20 and TXC-200-1.5-20, where the peak strength did not differ much from the strength at large strains.

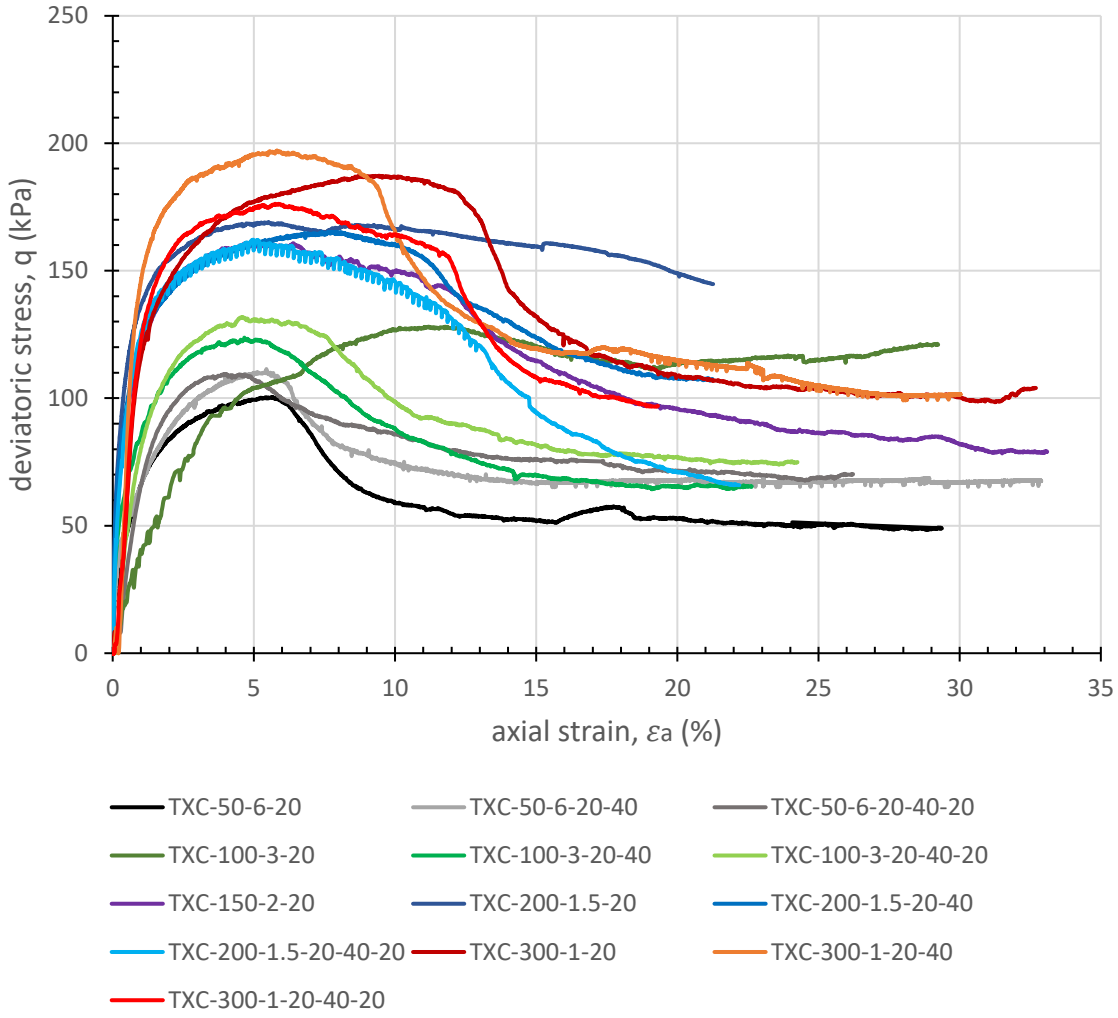

Figure 5-3: Stress-strain curves of reconstituted London clay

5.4.2 Excess pore water pressure

The excess pore water pressure generated during undrained shearing is shown in Figure 5-4. For an NC specimen, for example, TXC-300-1-20, positive excess pore water pressure was generated upon shearing. The value of Δu reached its peak when the axial strain was around 7%, which agreed with the axial strain where the peak strength was observed. Then it dropped slightly by 10 kPa and remained constant with further increase in axial strain. Similar behaviour was observed for lightly overconsolidated specimens with an overconsolidation ratio of 1.5 and 2. Specimens with $OCR = 3$ mobilised positive excess pore pressures throughout shearing, however, they were visibly reducing after the peak. Heavily overconsolidated clay specimens with an $OCR = 6$ behaved distinctly differently. For example, for test TXC-50-6-20, positive excess pore water pressure was generated initially upon shearing, and it reached its maximum value of 10 kPa when the axial strain was 0.8%. Then the excess pore water pressure dropped by 24 kPa. Negative excess pore water pressure was generated, and it reached its minimum

value when the axial strain was 8.2%. Then it kept at a constant value when the specimen was sheared to larger axial strain. Values of the excess pore water pressure generated for each test and the corresponding axial strains are summarised in Table 5-3. Ultimate excess pore water pressure in the table refers to the values of pore water pressure that stabilised at large axial strains. The amount of excess pore water pressure generated increased with the stress level.

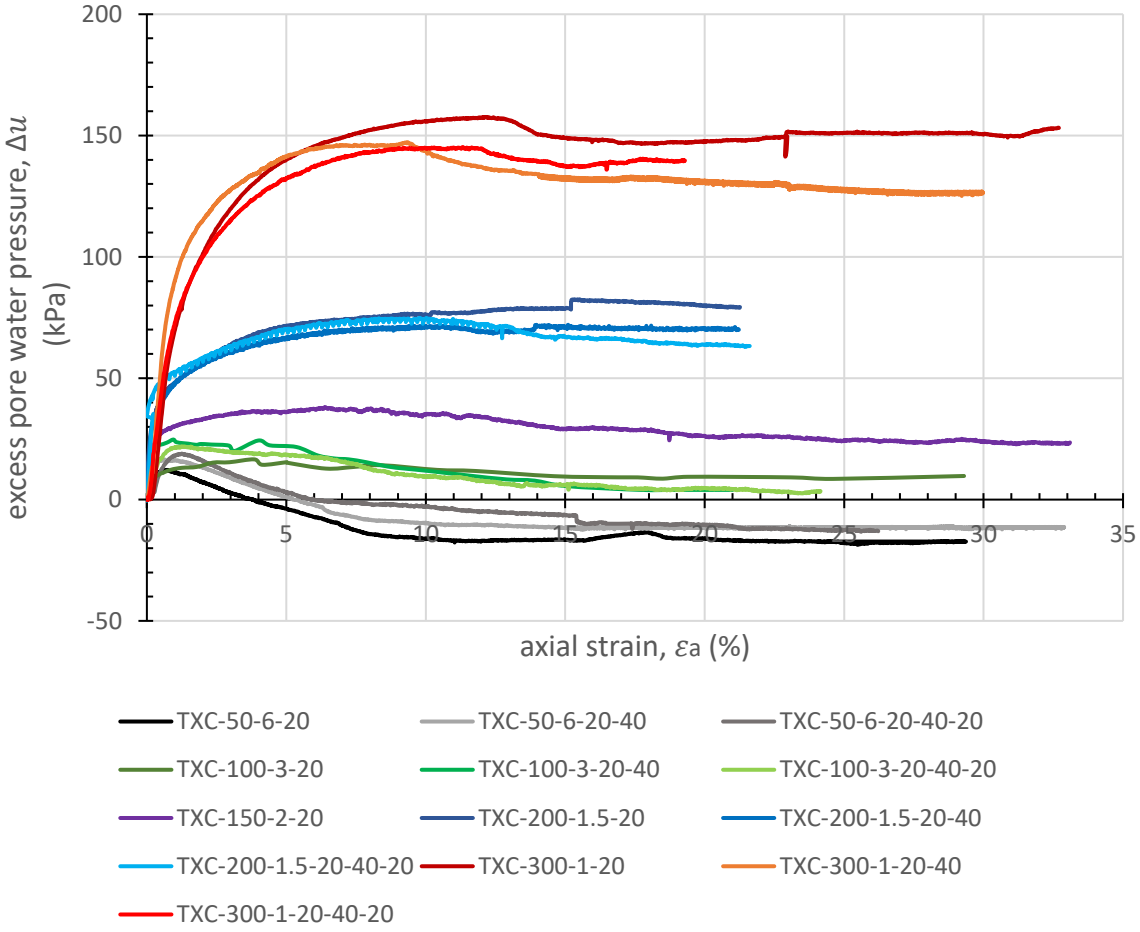

Figure 5-4: Excess pore water pressure generated in undrained shearing

Table 5-3: Excess pore water pressure generated in undrained shearing

Test	Peak excess pore water pressure		Ultimate excess pore water pressure	
	Δu	ε_a	Δu	ε_a
	kPa	%	kPa	%
TXC-300-1-20	156.7	11.0	146.8	17.1
TXC-300-1-20-40	141.2	7.1	131.3	15.7
TXC-300-1-20-40-20	144.5	10	137.2	14.9
TXC-200-1.5-20	74.3	10.3	78.9	15.1
TXC-200-1.5-20-40	73.2	9.8	68.3	13.8
TXC-200-1.5-20-40-20	72.9	8.9	66.8	15.1
TXC-150-2-20	36.0	5.0	26.2	19.9
TXC-100-3-20	18.6	4.7	6.1	15.1
TXC-100-3-20-40	24.3	4	4.2	15.1
TXC-100-3-20-40-20	21.8	0.4	5.9	14.5
TXC-50-6-20	10.5	0.8	-15	8.8
TXC-50-6-20-40	17.3	0.5	-9.3	9.2
TXC-50-6-20-40-20	20.4	0.8	-9.1	15.5

5.4.3 Stiffness

Stiffness is calculated as the secant gradient of the deviatoric stress q-axial strain ε_a curve, using Equation 5-1. Stiffness of London clay specimens is shown in Figure 5-5. In order to show the stiffness of individual test clearly, tests with the same stress history before heating and shearing were plotted in the same figure, using different types of lines to represent their temperature histories. Some of the experimental data showed scatter at strains that were smaller than 0.1%. At larger strains, the stiffness curves became smoother. The general trend is that the stiffness increased with stress level, in the small to medium strain range (0.01-0.1%), with a few exceptions (TXC-200-1.5-20, TXC-100-3-20, TXC-100-3-20-40-20). These discrepancies were probably caused by experimental scatter.

$$E_{sec} = \frac{q_{cur} - q_{ini}}{\varepsilon_{a,cur} - \varepsilon_{a,ini}} = \frac{q_{cur}}{\varepsilon_{a,cur}} \qquad 5\text{-}1$$

where q_{cur} and $\varepsilon_{a,cur}$ are the current deviatoric stress and axial strain, respectively; q_{ini} and $\varepsilon_{a,ini}$ are the initial deviatoric stress and axial strain, at the start of shearing. In this research,

readings of the load cell and displacement transducer were set to zero before shearing. Therefore, Equation 5-1 can be simplified as the latter form.

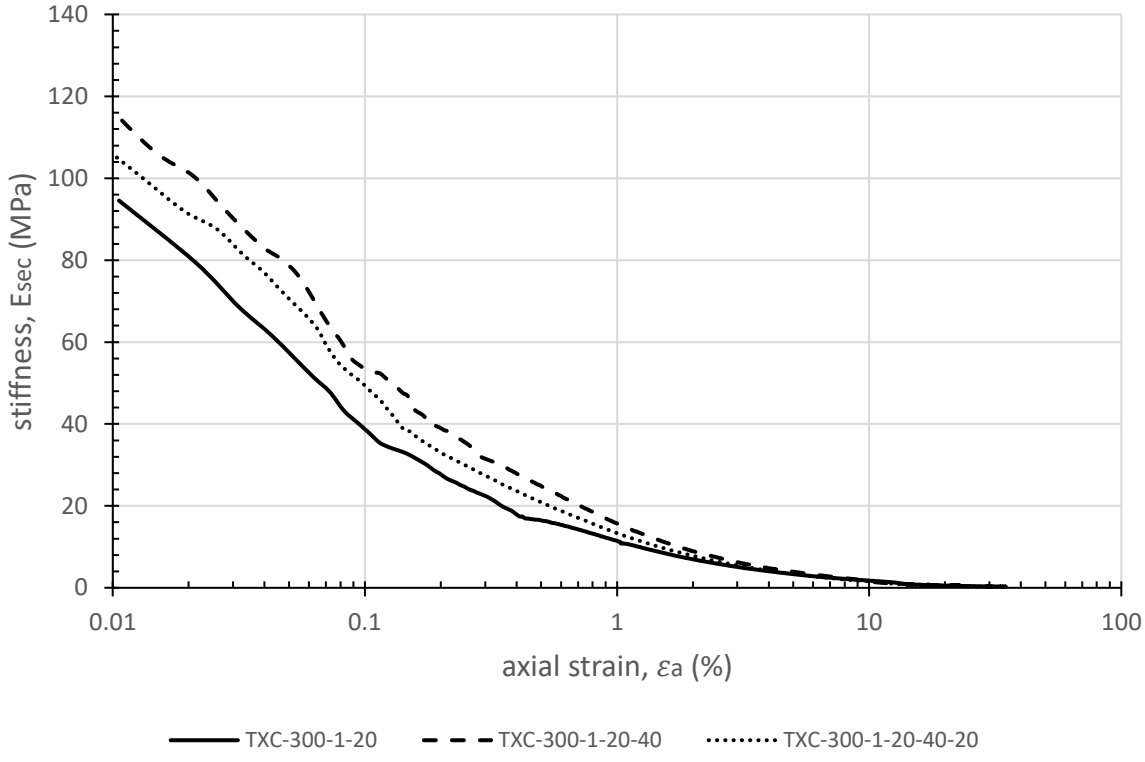

(a) OCR=1

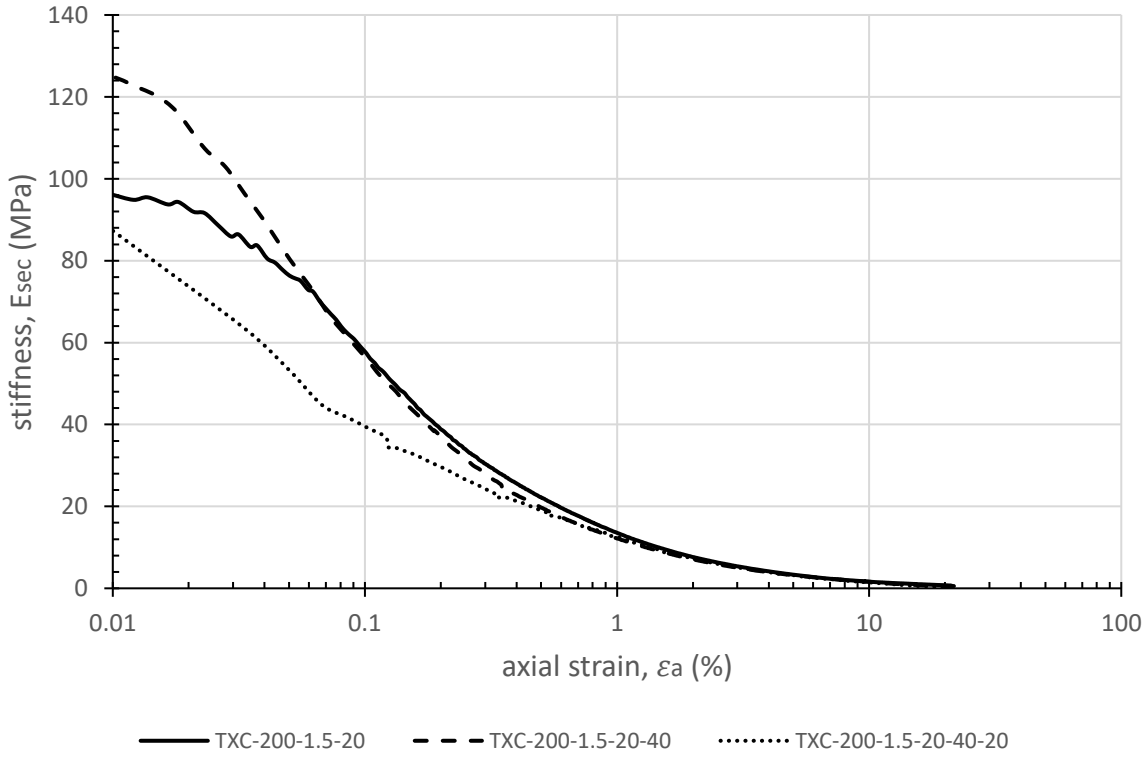

(b) OCR=1.5

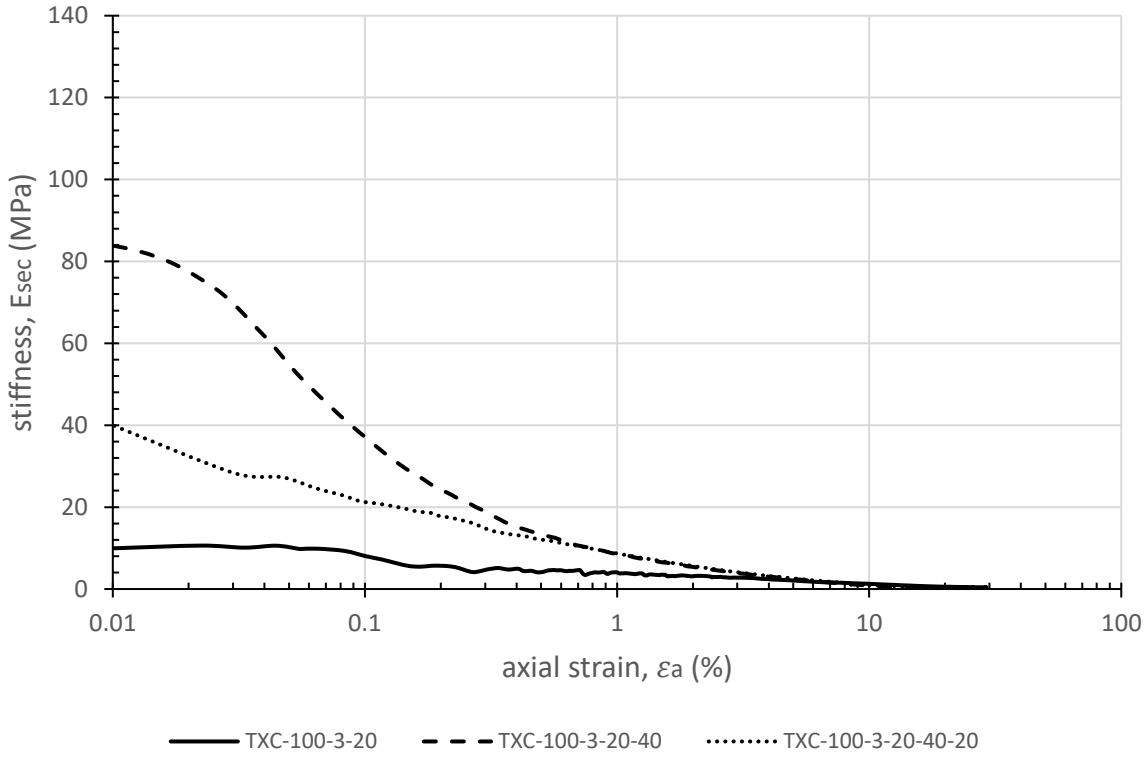
140
120
100
80
60
40
20
0
stiffness, Esec (MPa)
0.01
0.1
1
10
100
axial strain, εa (%)
TXC-100-3-20
TXC-100-3-20-40
TXC-100-3-20-40-20

(c) OCR=3

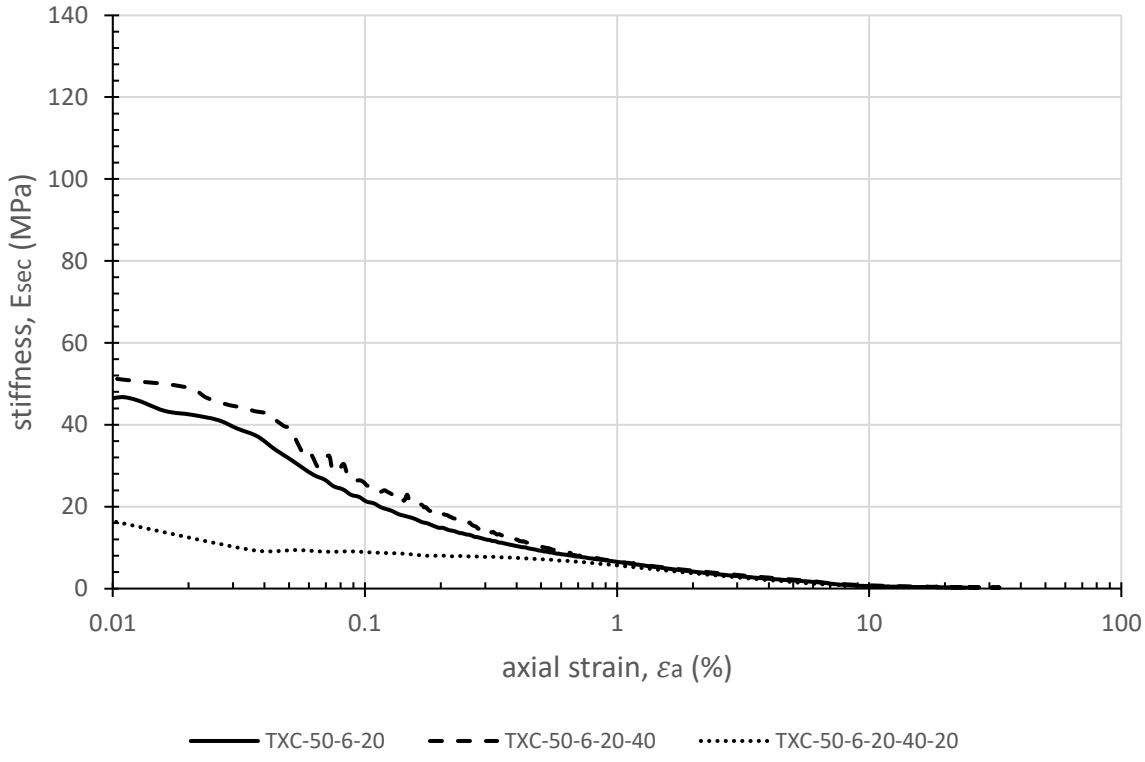
140
120
100
80
60
40
20
0
stiffness, Esec (MPa)
0.01
0.1
1
10
100
axial strain, εa (%)
TXC-50-6-20
TXC-50-6-20-40
TXC-50-6-20-40-20

(d) OCR=6

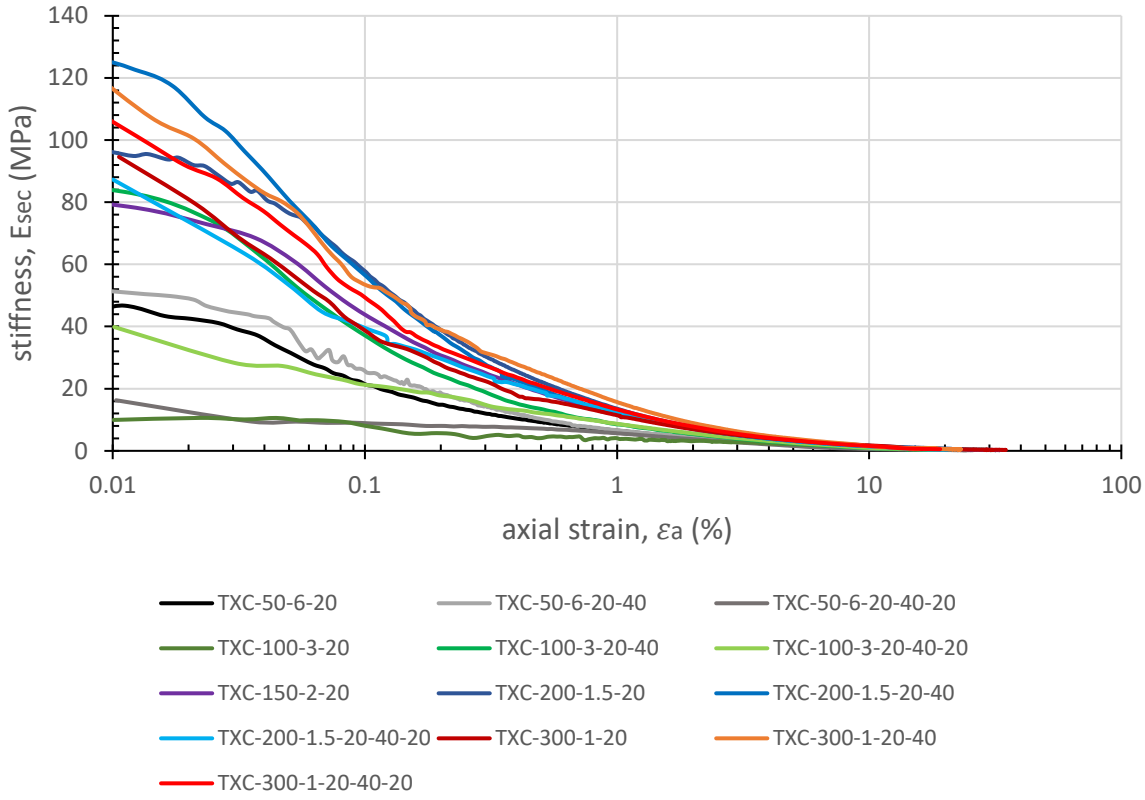

(e) for all OCRs

Figure 5-5: Stiffness of London clay specimens

5.5 Effect of the magnitude of temperature on strength and stiffness

This section presents the effect of the magnitude of temperature on strength, excess pore water pressure and stiffness, by comparing the results of tests performed on specimens that were sheared at 20 and 40°C.

5.5.1 Strength

Effective stress paths of reconstituted London clay specimens when they were sheared at 20 and 40 °C are shown in Figure 5-6. Deviatoric stresses at peak and void ratios of each test at the start of undrained shearing are summarised in Table 5-4. For normally consolidated specimens (e.g. TXC-300-1), the peak strength decreased by 3.3%, when the specimen was sheared at 40°C, compared to the peak strength when the specimen was sheared at ambient temperature, $T_{amb} = 20^{o}$C. For lightly overconsolidated specimens (TXC-200-1.5, TXC-100-3), the peak strength decreased by 1.9% and 11.9%, while it increased by 12.2% for highly overconsolidated specimens (TXC-50-6) when the magnitude of temperature increased from 20°C to 40°C. Similar trend of change in deviatoric stress was observed when specimens were sheared to large strains. For normally consolidated and lightly overconsolidated specimens, the

deviatoric stress at large strains decreased when the temperature increased from 20°C to 40°C, while it increased for highly overconsolidated specimens when the specimen was sheared at elevated temperature. Overall, there is no clear trend in the effect that the temperature change has on the magnitude of deviatoric stress at peak. The observed differences were small and are very likely the consequence of experimental scatter or sample differences.

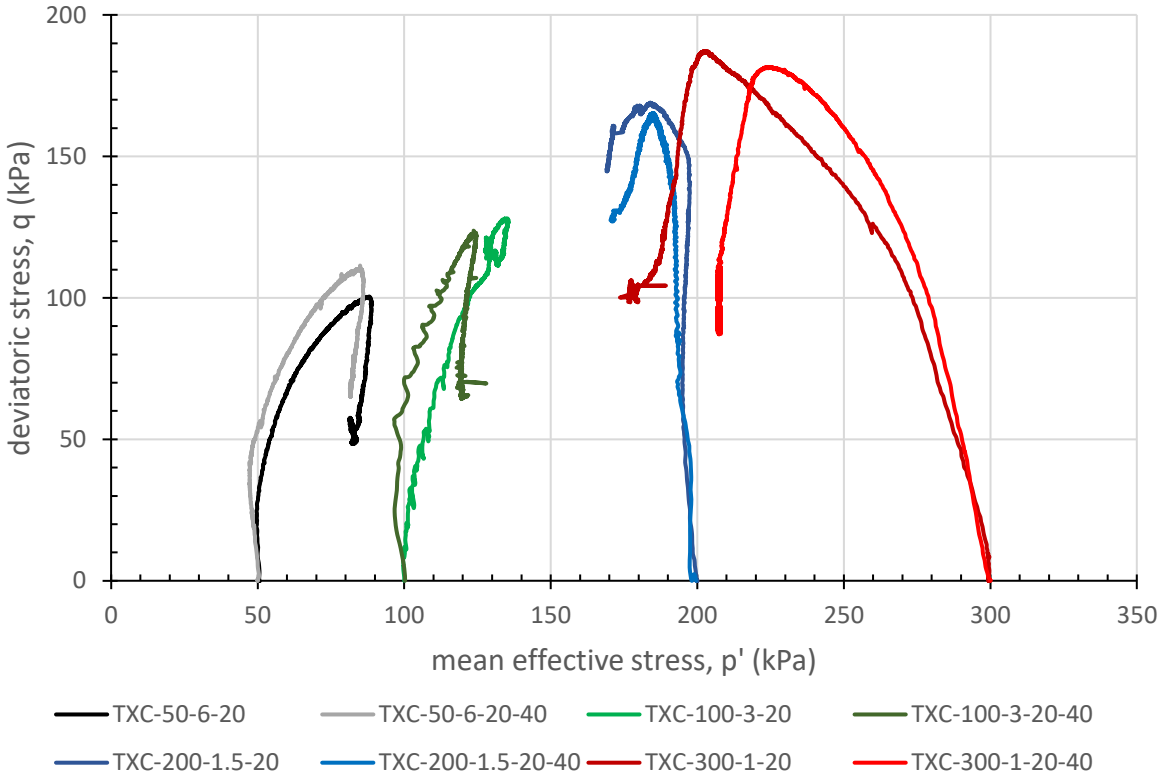

Figure 5-6: Undrained shearing effective stress path on reconstituted London clay at 20 and 40°C

Table 5-4: Change in deviatoric stress with elevated temperature

Test	peak		Void ratio at the start of shearing, e_s
	q (kPa)	change in q	
TXC-300-1-20	187		0.985
TXC-300-1-20-40	181	-6 kPa (-3.3%)	0.960
TXC-200-1.5-20	165		1.044
TXC-200-1.5-20-40	162	-3 kPa (-1.9%)	0.950
TXC-100-3-20	130		1.070
TXC-100-3-20-40	123	-7 kPa (-5.4%)	0.994
TXC-50-6-20	98		1.099
TXC-50-6-20-40	110	+12 kPa (+12.2%)	1.136

5.5.2 Excess pore water pressure

Excess pore water pressures generated during undrained shearing are summarised in Table 5-5. For normally consolidated and lightly overconsolidated specimens (TXC-300-1 and TXC-200-1.5), less excess pore water pressure was generated for specimens that were sheared under elevated temperature. For specimens that had slightly higher OCR (TXC-100-3), excess pore water pressure generated was similar for specimens sheared at ambient temperature and at 40 °C, while for heavily overconsolidated specimens (TXC-50-6), larger amount of excess pore water pressure was generated when the specimen was sheared at elevated temperature. The difference in excess pore water pressure generated for tests at ambient and elevated temperature is small. The overall trend is that excess pore water pressure generated was insensitive to the magnitude of temperature. This is probably because the specimens went through drained heating stage, where the excess pore water pressure dissipated before they were sheared in undrained condition.

Table 5-5: Change in excess pore water pressure with elevated temperature

Test	peak		ultimate	
	Δu (kPa)	change in Δu	Δu (kPa)	change in Δu
TXC-300-1-20	156.7		146.8	
TXC-300-1-20-40	141.2	-15.5 kPa (-11.0%)	131.3	-15.5 kPa (-11.8%)
TXC-200-1.5-20	74.3		78.9	
TXC-200-1.5-20-40	73.2	-1.1 kPa (-1.5%)	68.3	-10.6 kPa (-15.5%)
TXC-100-3-20	18.6		6.1	
TXC-100-3-20-40	24.3	+5.7 kPa (+30.6%)	4.2	-1.9 kPa (-45.2%)
TXC-50-6-20	10.5		-15	
TXC-50-6-20-40	17.3	+6.8 kPa (+64.8%)	-9.3	+5.7 kPa (+61.3%)

5.5.3 Stiffness

With reference to Figure 5-5 and Figure 5-6, the effective stress paths of specimens sheared at elevated temperature $T_{elev} = 40°C$ are generally stiffer in the medium strain range, compared to the specimens that were sheared at ambient temperature.

5.6 Effect of thermal pre-conditioning on strength and stiffness

In this section, effect of thermal pre-conditioning is presented. After the isotropic consolidation and swelling stage, a temperature cycle of 20-40-20°C was applied to specimens, before they were sheared in undrained condition at 20°C. This group of tests were compared with the

reference tests where the specimens were tested only at ambient temperature of 20°C, without any thermal intervention.

5.6.1 Strength

Effective stress paths for tests with and without thermal pre-conditioning are presented in Figure 5-7. Changes in deviatoric stress at peak and void ratios before shearing are summarised in Table 5-6. For tests TXC-300-1 and TXC-200-1.5, the specimen with a temperature cycle exhibited smaller strength at peak. For tests TXC-100-3 and TXC-50-6, specimens exhibited slightly larger strength at peak after thermal preconditioning. Deviatoric stress changed by a maximum of 21 kPa when specimens went through a temperature cycle before shearing (TXC-300-1). The overall trend is that peak strength was not sensitive to thermal conditioning. The observed change in peak strength was likely due to experimental scatter.

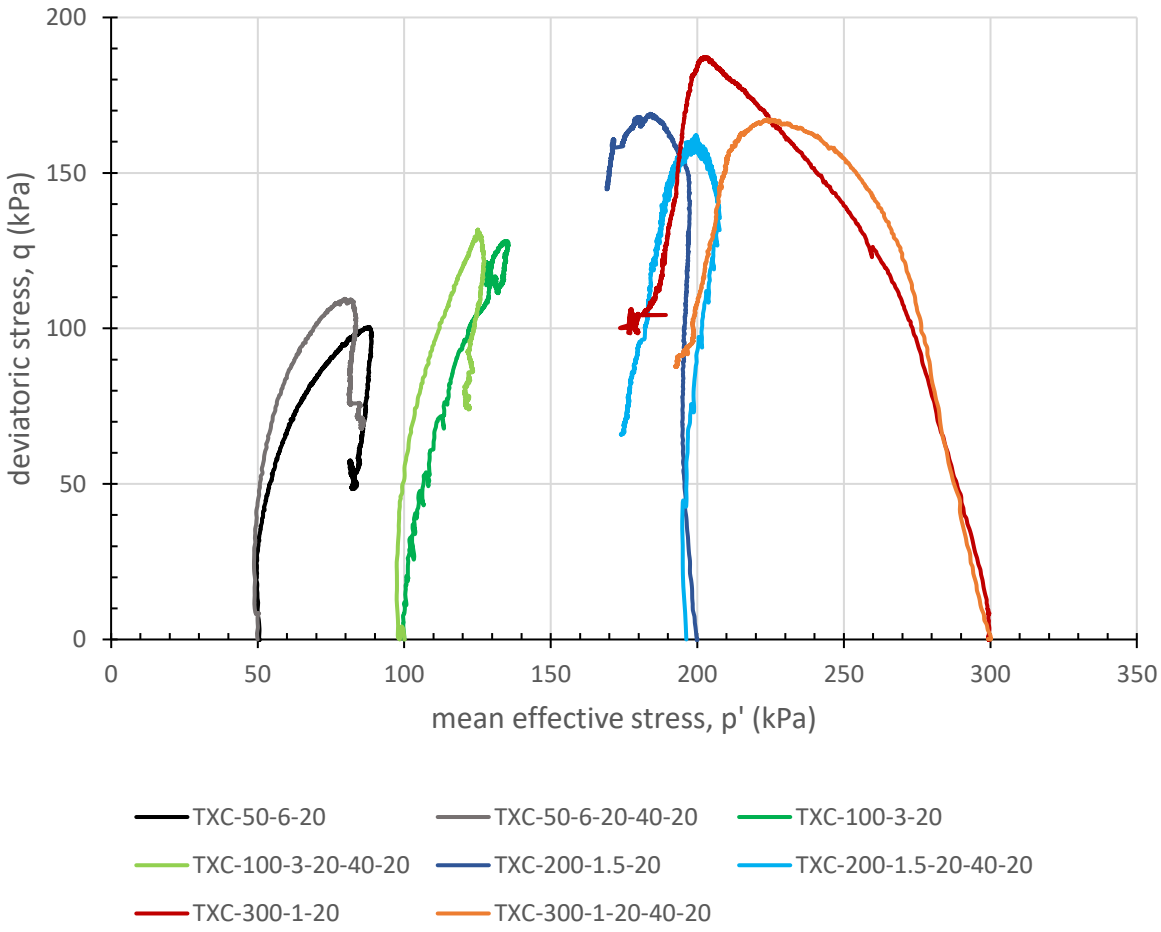

Figure 5-7: Undrained shearing stress path on reconstituted London clay with temperature cycle

Table 5-6: Change in deviatoric stress with temperature cycle

Test	peak		void ratio at the start of shearing, e_s
	q (kPa)	change in q	
TXC-300-1-20	187		0.985
TXC-300-1-20-40-20	166	-21 kPa (-12.7%)	0.968
TXC-200-1.5-20	168		1.044
TXC-200-1.5-20-40-20	159	-9 kPa (-5.4%)	1.096
TXC-100-3-20	130		1.070
TXC-100-3-20-40-20	126	-4 kPa (-3.1%)	0.989
TXC-50-6-20	98		1.099
TXC-50-6-20-40-20	109	+11 kPa (+11.2%)	1.114

5.6.2 Excess pore water pressure

Excess pore water pressure generated during undrained shearing is summarised in Table 5-7. For normally consolidated and lightly overconsolidated specimens (TXC-300-1 and TXC-200-1.5), excess pore water pressure generated decreased slightly for specimens that were sheared after a temperature cycle, compared to specimens without temperature cycle. For specimens that had a slightly higher OCR (TXC-100-3), excess pore water pressure generated was not sensitive to temperature cycle. For heavily overconsolidated specimen (TXC-50-6), larger excess pore water pressure was generated for specimen with a temperature cycle. Differences in excess pore water pressure between tests at ambient temperature and with a temperature cycle were negligible. This observation agrees with those from tests with elevated temperature, as described in the previous section.

Table 5-7: Change in excess pore water pressure with temperature cycle

Test	peak		void ratio at the start of shearing, e_s
	Δu (kPa)	change in Δu	
TXC-300-1-20	156.7		0.985
TXC-300-1-20-40-20	144.5	-12.2 kPa (-8.4%)	0.968
TXC-200-1.5-20	74.3		1.044
TXC-200-1.5-20-40-20	72.9	-1.4 kPa (-1.9%)	1.096
TXC-100-3-20	18.6		1.070
TXC-100-3-20-40-20	21.8	+3.2 kPa (+17.2%)	0.989
TXC-50-6-20	10.5		1.099
TXC-50-6-20-40-20	20.4	+9.9 kPa (+94.3%)	1.114

5.6.3 Stiffness

With reference to Figure 5-5 and Figure 5-7, there is a clear trend of increase in stiffness with temperature cycle for all tests. For tests TXC-300-1, TXC-200-1.5 and TXC-50-6, the initial stiffness of tests with and without temperature cycle was similar, while at medium strains, stiffness for specimens with temperature cycle was larger than those of specimens without temperature cycle. For test TXC-100-3, specimen with a temperature cycle started to show larger stiffness at small strains, compared to the one without temperature cycle.

5.7 Discussion

This section discusses the effect of temperature on thermally induced volumetric strains, strength and stiffness of reconstituted London clay. In drained heating tests followed by undrained shearing, the effect of temperature on thermally induced excess pore water pressure is negligible, as shown in Section 5.4.2, 5.5.2 and 5.6.2. The effect of temperature on thermally induced pore water pressure in undrained heating is presented in Chapter 4 and will not be discussed here.

5.7.1 Thermally induced volumetric strains

With reference to Section 5.3, normally consolidated London clay specimens exhibited contraction upon heating and thermally induced volumetric strains were irreversible upon cooling. Lightly overconsolidated (OCR=1.5 or 3) specimens contracted upon heating and the volumetric strains were reversible when specimens were cooled to ambient temperature. Heavily overconsolidated (OCR=6) specimens dilated upon heating and the volumetric strains were reversible upon cooling. With increase in the OCR, the magnitude of contraction upon heating gradually decreased, until it turned to dilation at high OCR. Hysteresis was observed in thermally induced volumetric strains when specimens went through a heating/ cooling cycle, regardless of the OCR. A similar trend of change of volumetric strains with OCR was reported by Abuel-Naga et al. (2007a, 2007b) on soft Bangkok clay, and Del. Olmo et al. (1996) for three deep clays, including Boom clay, Pasquasia clay, and Spanish clay.

Change of thermally induced volumetric strains with OCR can be explained by microstructure mechanism. For saturated fine-grained soils, their mechanical behaviour is controlled by the physico-chemical forces (Campanella and Mitchell, 1968; Abuel-Naga et. al, 2007). Changes in temperature have significant effect on such forces (Mitchell, 1993). The thermally induced volumetric strains, ε_v^T, can be decomposed into reversible expansion component of strain, ε_v^{Te}, and irreversible contraction component of strain, ε_v^{Tp} (Hueckel and Baldi, 1990; Cui et al., 2000; Graham et al., 2001; Laloui and Cekerevac, 2003). An idealization case is shown in

Figure 5-8. For normally consolidated clay, under heating process, ε_v^{Tp} predominates. As overconsolidation ratio (OCR) increases, the amount of ε_v^{Tp} decreases and the reversible component of strain, ε_v^{Te}, starts to predominate.

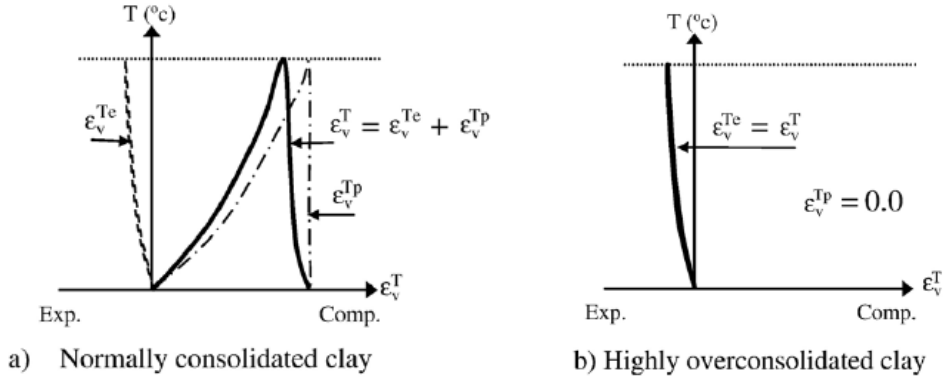

Figure 5-8: Idealization of thermally induced volume change components

The reversible expansion component of strain, ε_v^{Te}, is composed of two parts. The first part is generated due to thermal expansion of clay minerals (Campanella and Mitchell, 1968) and the second part is generated due to the temperature effect on the interparticle physico-chemical forces. Drained heating will increase the interparticle physico-chemical forces because of increasing repulsive forces. As $\Delta\sigma - \Delta u = \Delta\sigma' = 0$ during drained heating process, the interparticle spacing will increase to cancel out the expected increase in repulsive forces. Therefore, the reversible volumetric change can be observed for overconsolidated clays.

For normally consolidated London clay, 0.26% of contractive volumetric strain was induced when it was heated from 20 to 40 °C. This is consistent with results presented by Martinez-Calonge (2017) on similar samples from a reconstituted London clay cake, where they reported 0.24% contractive volumetric strain for normally consolidated specimen for the same change in temperature. Sultan et al. (2002) plotted thermally induced volumetric strains for several types of clays with different plasticity (Illite, PI=9%; MC clay, PI=29%; Boom clay, PI=36% or 46%; soft Bangkok clay, PI=60%) and for normally consolidated conditions when temperature changed by 65 to 70°C, as shown in Figure 5-9. They found that thermally induced volumetric strains increased with plasticity index.

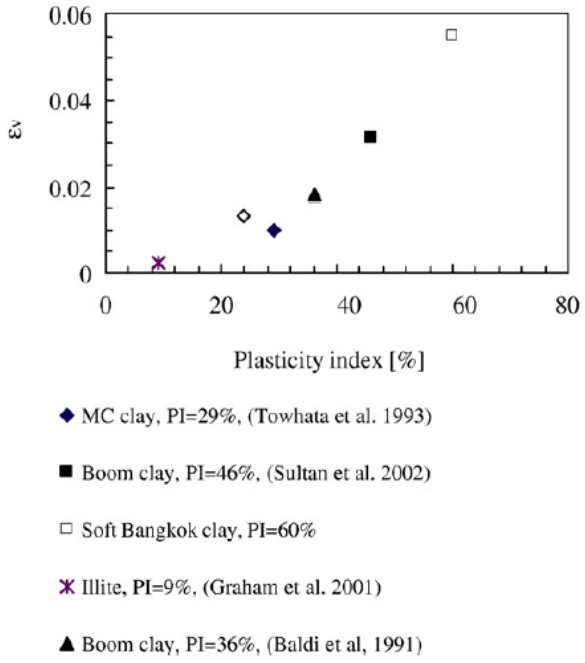

Figure 5-9: plasticity index of soil and temperature induced volumetric strain of different normally consolidated clays (⊿T ≈65–70 ℃, T_0 ≈20–25 ℃) reported in literature (Sultan et al., 2002)

5.7.2 Strength

In this section, shear strength of reconstituted London clay is discussed. Stresses are resolved and interpreted into $q - p'$, $\sigma' - \tau$ and $t - s$ planes. Results are compared with tests collated from the literature, performed on the same soil.

Calculation of deviatoric stress

The axial force applied to the specimens of London clay was measured using both the internal and external load cells. Single shear plane was observed in all the undrained shearing tests in this research. Photos of the specimen for test TXC-300-1-20 were presented as an example in Figure 5-10. Since the triaxial chamber was made of stainless steel instead of transparent Perspex, it was not possible to identify the onset of formation of shear plane by observation. After analysing the data from internal and external load cells, internal and external displacement transducers, the axial strain at which shear plane formed for each of the tests was established. This is where there was a sudden change in the readings in at least one of the internal displacement transducers, sometimes in both internal displacement transducers, depending on where they were located with respect to the location of the shear plane, while the external displacement transducer still exhibited stable and continues readings. Comparison of deviatoric stresses calculated using different methods and adopting different assumptions is shown in Figure 5-11. In this plot, readings from the internal load cell were corrected for temperature effect but not corrected for piston friction or the effect of cell pressure, to show

the effect of the latter two factors. After all these corrections were applied, the maximum difference in readings from the external and internal load cell was 35 N, corresponding to an axial stress of 4.5 kPa on a 50 mm diameter specimen. Details of these calibrations and corrections were presented in Chapter 3. In Chapter 5, deviatoric stress was calculated based on the readings from the external load cell. The black line shows the case where right cylinder assumption was adopted before shear plane was formed, while single shear plane assumption (Head, 1998) was adopted for calculation afterwards. Using this method resulted in larger deviatoric stress after peak, compared to the other two methods that only adopted right cylinder assumption and either the readings from the internal or external load cell. This also led to smaller strain softening behaviour, which agreed with the soil behaviour after shear plane was formed.

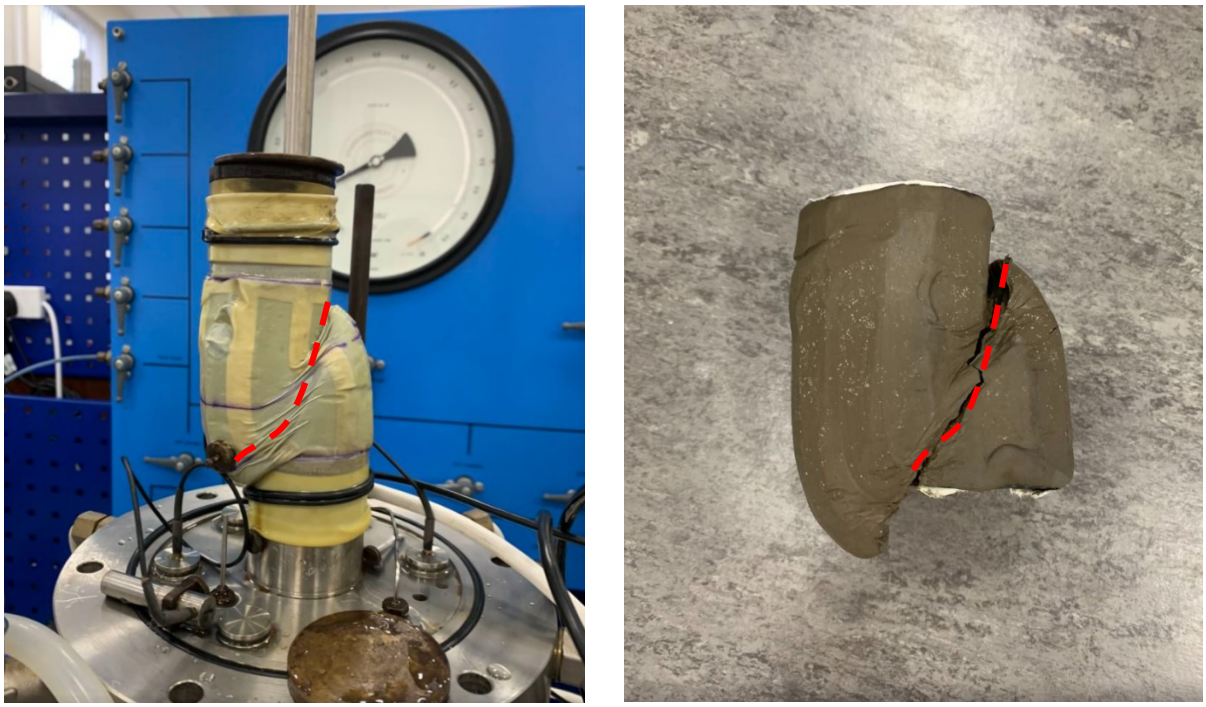

(a) with membrane (b) without membrane

Figure 5-10: Specimen with single shear plane after test for TXC-300-1-20

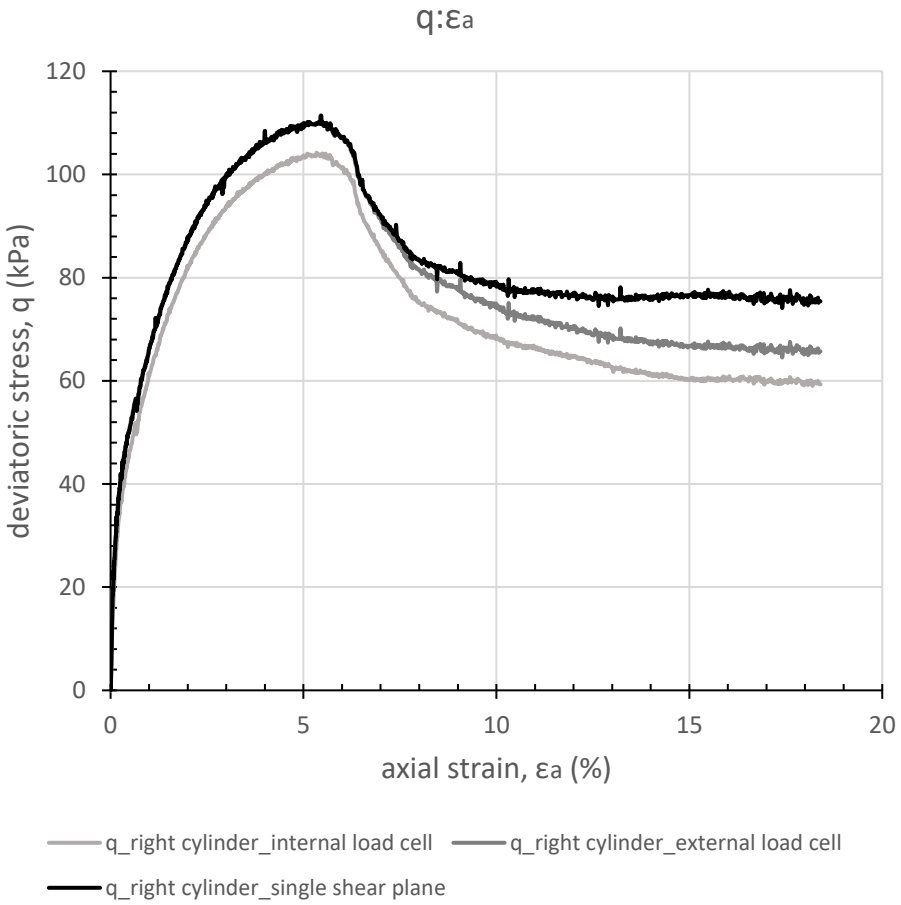

Figure 5-11: Comparison of deviatoric stresses calculated using different methods

Normalised stress-strain curves

Normalised stress-stain curve for undrained shearing tests on reconstituted London clay is presented in Figure 5-12. When the axial strain was at 20%, the ratio between deviatoric stress, q, and mean effective stress, p', ranged between 0.55 and 0.96. The discrepancies in the normalised deviatoric stresses made it difficult to determine the critical state stress ratio from the normalised stress-strain curves.

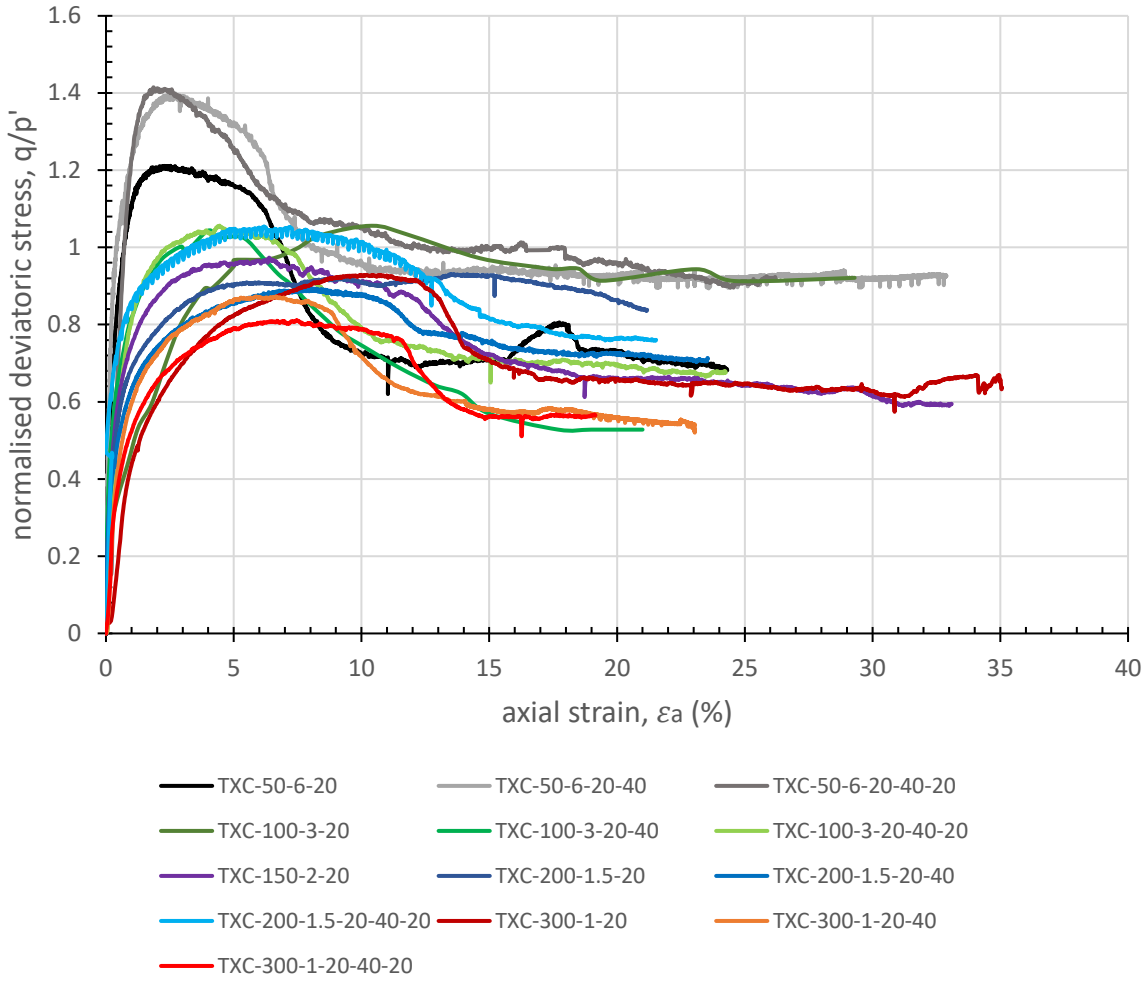

Figure 5-12: Normalised stress path of reconstituted London clay

$\sigma' - \tau$ plane

Due to the difficulty in determining the critical state stress ratio at large strains, from the normalised stress-strain curves, stresses applied on the specimen were resolved in the directions that were perpendicular and parallel to the shear plane, denoted as the effective normal stresses, σ_n', and shear stress, τ, using the inclination of shear planes measured at the end of each test. Graphs are shown in Figure 5-13, summarising the stress points on the shear plane. Critical state was identified where the deviatoric stress remained constant with further increase in axial strain. Stress state at large strains is taken at an axial strain of 25%. In some of the tests where the specimens were not sheared to a 25% axial strain, it is taken as the stress at the end of shearing. Linear regression was found to be the best fit for the data, as shown in Table 5-8. Coefficients of determination for both regressions were close to 1, indicating that the equation could well represent the dataset. Angle of shearing resistance at critical state derived from the linear regression was 20.5°. This is consistent with the value of $\varphi_{cs}' = 20.1°$ for London clay

at Ashford Common (Webb, 1964; Burland, 1990). It is slightly smaller than $\varphi'_{cs} = 21.3°$ for London clay sourced from several lithological units (Gasparre, 2005) and $\varphi'_{cs} = 22.1°$ for London clay recovered from piling works at the Victoria and Albert Museum (Martinez-Calonge, 2017).

The model parameter M in Modified Cam Clay (MCC) model (Roscoe and Burland, 1968) can be calculated as

$$\mathrm{M} = \frac{6 \cdot sin\varphi'_{cs}}{3 - sin\varphi'_{cs}} = \frac{6 \times sin20.5°}{3 - sin20.5°} = 0.8 \qquad 5\text{-}2$$

The model parameter M is the slope of the critical state line in $q - p'$ plane. This is slightly smaller than values of $M = 0.85$ reported by Gasparre (2005) and $M = 0.86$ found by Martinez-Calonge (2017) on reconstituted London clay.

Angle of shearing resistance dropped to 16.7° at large strains.

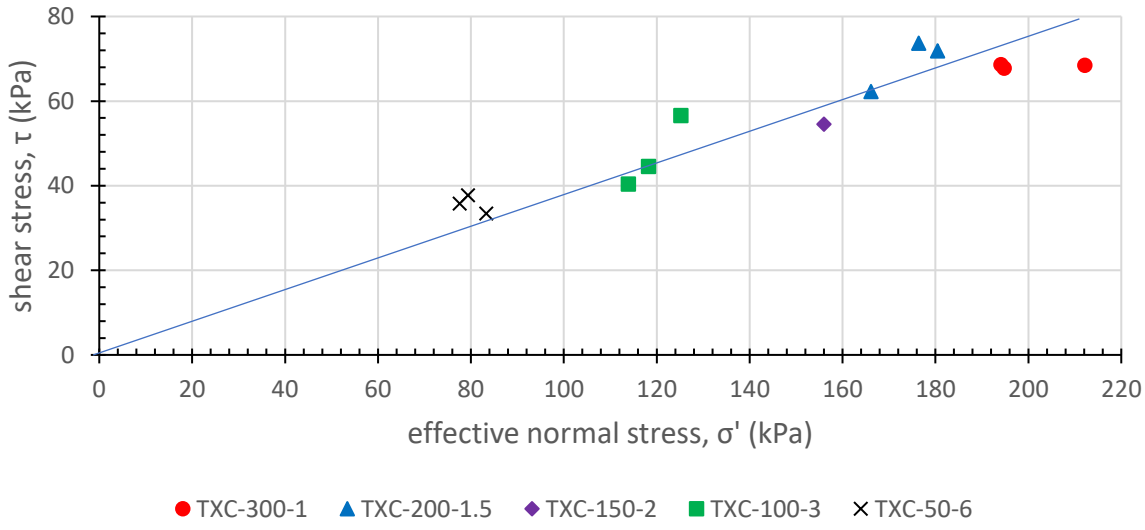

(a) critical state

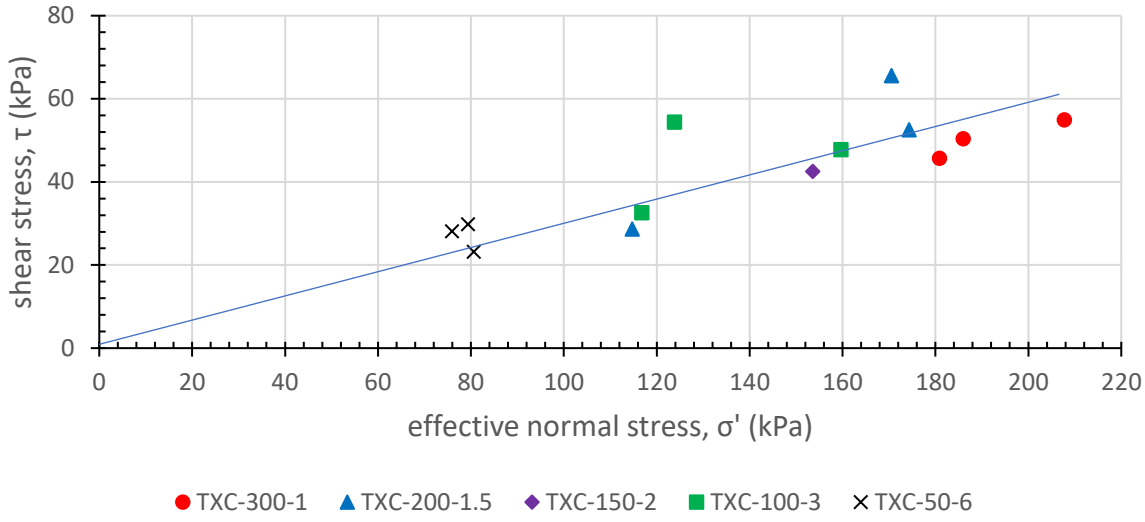

(b) at large strains

Figure 5-13: Stress states in τ- σ' plane a) critical state; b) at large strain

Table 5-8: Linear regression for stress states in τ- σ' plane

Stress states	Equation	R^2	φ'
Critical state	$\tau = 0.3734\sigma'$	0.9889	20.5°
At large strains	$\tau = 0.2995\sigma'$	0.9699	16.7°

$q/p'_e - p'/p'_e$ plane

For this interpretation, deviatoric stress and mean effective stress were normalised by the equivalent mean effective stress, p'_e, derived from the normal compression line of reconstituted London clay. The relationship between the specific volume and the mean effective stress can be described by Equation 5-3.

$$v = N - \lambda lnp' \qquad 5\text{-}3$$

Values of parameters in this equation can be derived from the one-dimensional compression tests on London clay presented in Chapter 6, where $C_c = 0.394$ was evaluated from the reconstituted cake specimens.

$$\lambda = \frac{C_c}{2.303} = \frac{0.394}{2.303} = 0.171 \qquad 5\text{-}4$$

In one-dimensional compression tests, the normal compression line is expressed as a relationship between the void ratio e and vertical effective stress σ'_v. These quantities can be converted to specific volume v and mean effective stress p', using the following equations.

$$v = e + 1 \qquad 5\text{-}5$$

$$p' = \frac{\sigma_v' + 2\sigma_h'}{3} = \frac{\sigma_v' + 2K_0\sigma_v'}{3} \quad 5\text{-}6$$

where K_0 is the coefficient of earth pressure at rest in terms of effective stress. For normally consolidated soils, the value of K_0 can be related approximately to the strength parameter φ' by the formula proposed by Jaky (1944)

$$K_0^{NC} = 1 - sin\varphi' \quad 5\text{-}7$$

where $\varphi' = 20.5°$ as presented in Table 5-8.

By converting data from one-dimensional compression tests on reconstituted London clay cake specimens in $e - log\sigma_v'$ to $v - lnp'$, value of parameter N is found to be 3.026. Equation 5-3 can be rewritten as

$$v = 3.026 - 0.171lnp' \quad 5\text{-}8$$

Void ratios of each test are summarised in Table 5-9. By substituting void ratio at the start of shearing into Equation 5-5 and Equation 5-8, mean effective stress for normalisation, p_e', can be determined.

Table 5-9: Void ratios of tests in the temperature-controlled triaxial apparatus

code	Void ratio		
	start of test, e_0	start of heating, e_c	start of shearing, e_s
TXC-300-1-20	1.105	-	0.985
TXC-300-1-20-40	1.101	0.983	0.960
TXC-300-1-20-40-20	1.084	0.984	0.968
TXC-200-1.5-20	1.089	-	1.044
TXC-200-1.5-20-40	1.089	0.962	0.950
TXC-200-1.5-20-40-20	1.090	1.094	1.096
TXC-150-2-20	1.084	-	1.056
TXC-100-3-20	1.089		1.070
TXC-100-3-20-40	1.089	1.002	0.994
TXC-100-3-20-40-20	1.089	0.986	0.989
TXC-50-6-20	1.093	-	1.099
TXC-50-6-20-40	1.074	1.138	1.136
TXC-50-6-20-40-20	1.103	1.110	1.114

Normalised effective stress paths of reconstituted London clay are presented in Figure 5-14. The behaviour of reconstituted London clay specimens, whether they were sheared at ambient temperature, elevated temperature, or went through a temperature cycle before shearing, was characterised by the same critical state line (CSL), as plotted in Figure 5-14 and Figure 5-15.

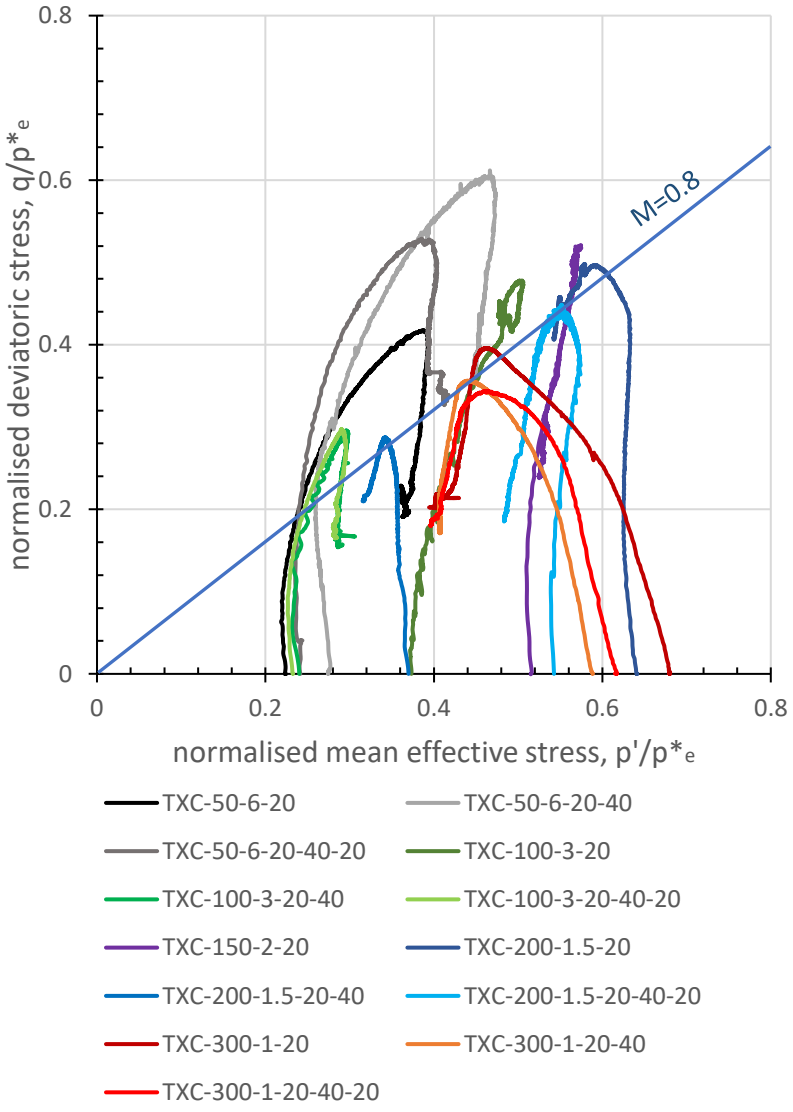

Figure 5-14: Normalised effective stress paths of reconstituted London clay

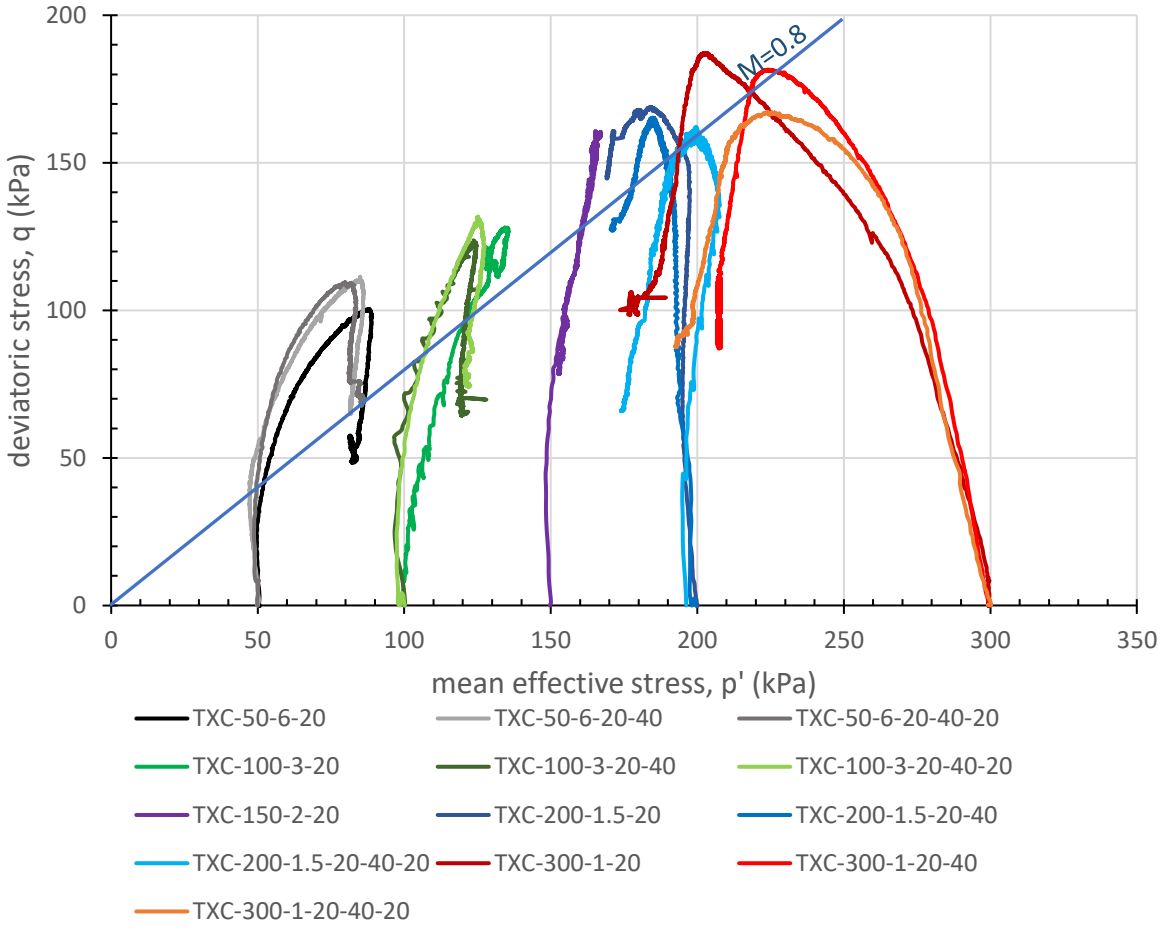

Figure 5-15: Stress paths of reconstituted London clay

$t - s$ plane

Stress states at peak, critical state and large strains were plotted in t-s' plane, as shown in Figure 5-16. Equations that represented the relationship between t and s' were found by linear regression, as shown in Table 5-10. Angle of shearing resistance at different state was calculated based on the slope of the regression line. Values were consistent with those calculated in $\tau - \sigma'$ plane. At critical state and large strains, it is assumed that there was no cohesion, as shear plane was formed when soil reached these two states. For peak strength, cases with and without cohesion were both considered. Angle of shearing resistance at peak with cohesion was close to that at large strains. If it is assumed that no cohesion existed when the soil reached peak strength, angle of shearing resistance was larger than that at critical state and at large strains.

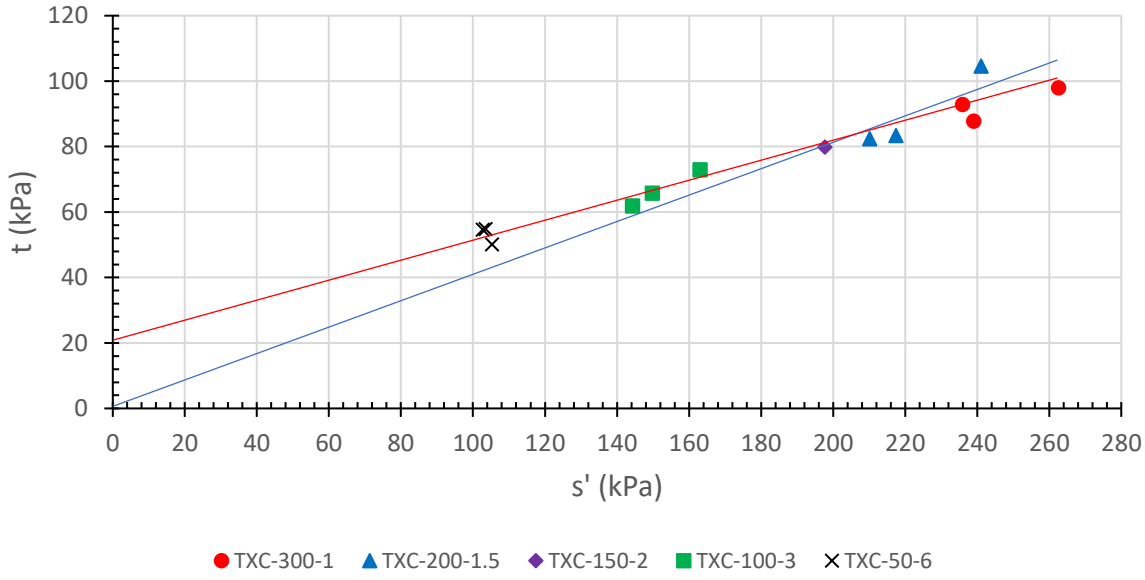

(a) peak

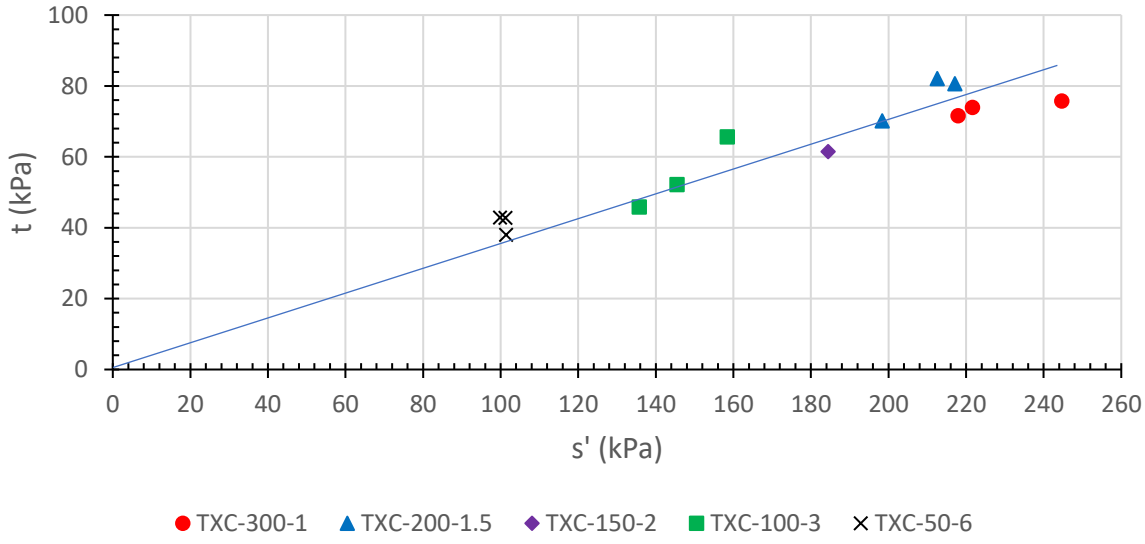

(b) critical state

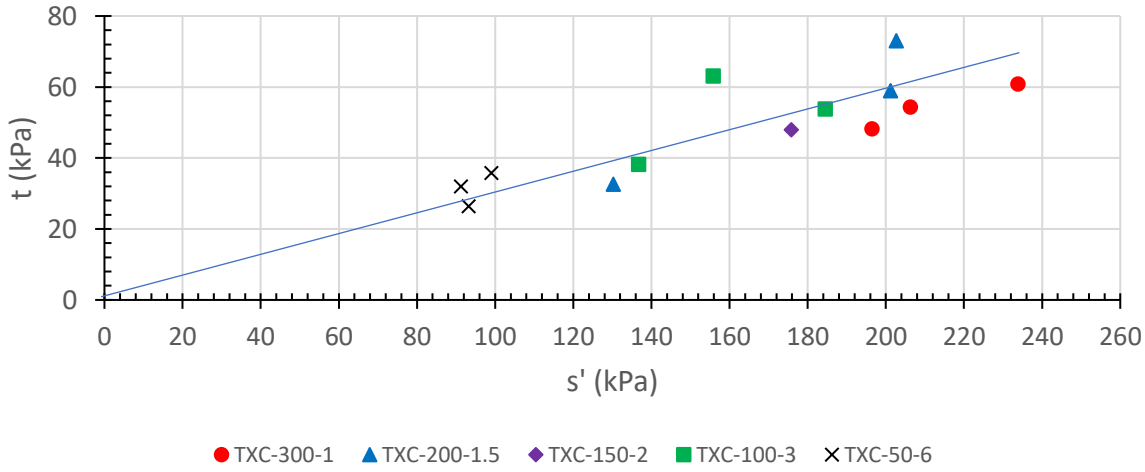

(c) large strains

Figure 5-16: Stress state in t-s' plane a) peak; b) critical state; c) large strains

Table 5-10: Linear regression for stress states in t-s' plane

Stress states	Equation	R^2	φ'
Peak (with cohesion)	$t = 0.2982s' + 21.637$	0.9456	17.3°
Peak (no cohesion)	$t = 0.4068s'$	0.9910	24.0°
Critical state	$t = 0.3532s'$	0.9914	20.7°
Large strains	$t = 0.2931s'$	0.9756	17.0°

Undrained shear strength profile

Undrained shear strength profile of reconstituted London clay is presented in Figure 5-17. This is calculated as the radius of the Mohr circles plotted based on the stress states at peak from the triaxial tests performed in this research. It showed how the undrained shear strength of the soil changed with vertical effective stress, which can be related to the depth below ground level. The undrained shear strength increased linearly with vertical effective stress, regardless of the temperature history that soil specimens had before shearing. This trend agreed with the observations from triaxial tests on reconstituted London clay at ambient temperature. The ratio $S_u/\sigma_v' = 0.27$ is determined from Figure 5-17, which is characteristic of an unstructured clay.

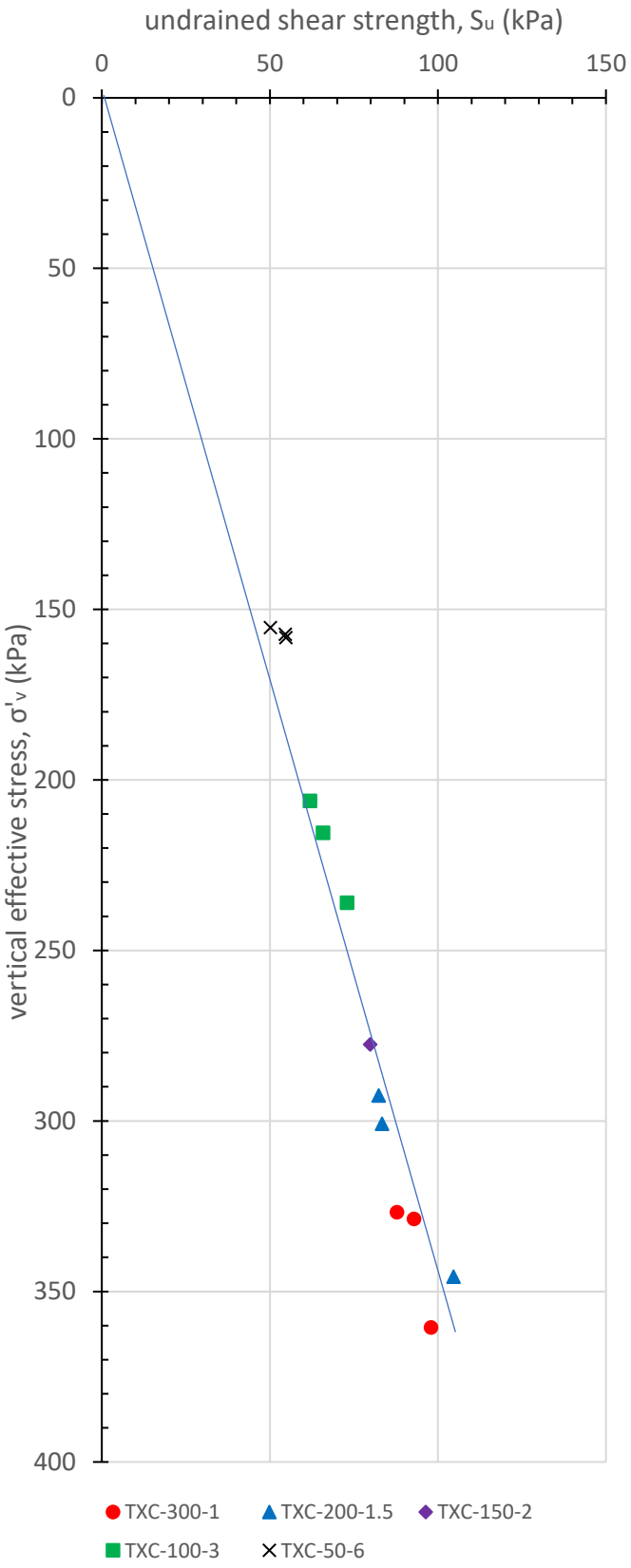

Figure 5-17: Undrained shear strength profile of reconstituted London clay

The effect of elevated temperature and temperature cycle on the peak strength of London clay seemed to be negligible, based on the results presented in this chapter. The applied temperature range (20 to 40 °C) and stress states (p'_c=50 to 300 kPa, OCR=1 to 6) in this research resulted in an average of 8% (and a maximum of 12%) change in void ratio between the start of test and the start of undrained shearing, which didn't seem large enough to cause conclusive differences in the mobilised peak shear strength. There are some contradicting results reported in the literature, where some researchers found peak strength decreased with increase in temperature (Pontida silty clay (Hueckel and Baldi, 1990); Boom clay (De Bruyn and Thimus, 1996)), while the opposite was reported where peak strength increased with increase in temperature (Kaolinitic clay (Cekerevac and Laloui, 2004); Soft Bangkok Clay (Abuel-Naga et al., 2007c)).

The critical state stress ratio is not affected by either the elevated temperature or thermal pre-conditioning with one temperature cycle. Similar observations were reported on other types of clays (Pontida Silty Clay (Hueckel and Baldi, 1990; Hueckel and Pellegrini, 1991, 1992); Boom Clay (De Bruyn and Thimus, 1996); Todi Clay (Burghignoli et al.,1992, 2000); Kaolinitic clay (Kuntiwattanakul et al., 1995; Ghahremannejad, 2003; Cekerevac and Laloui, 2004; Yavari et al., 2016); Illitic clay (Tanaka et al., 1997; Ghahremannejad, 2003); Soft Bangkok Clay (Abuel-Naga et al., 2006; Abuel-Naga et al., 2007c)).

5.7.3 Stiffness

Temperature was shown to have an effect on the stiffness of reconstituted London clay. This includes both the short-term temperature intervention (one temperature cycle) and the long-term effect (holding the elevated temperature at a constant value). The change in stiffness cannot be explained by the density of the specimen alone. For example, in test TXC-50-6-20 (e_s=1.099) and TXC-50-6-20-40 (e_s=1.136), specimen was denser before shearing for the test without thermal treatment, but it exhibited smaller stiffness. Therefore, the observed change in stiffness was caused by temperature history of the specimens. This finding is of particular importance when serviceability limit design is considered. The effect of elevated temperature and one temperature cycle seemed to have similar effect on the increase of stiffness. This may indicate that the short-term and long-term temperature intervention influenced the stiffness of clay in the same way, and that the increase in the stiffness of soil was irreversible, even if there was no net change in temperature in the clay. Similar trend has been observed for several types of clays (Kaolin clay (Cekerevac and Laloui, 2004); Boom clay (Kuntiwattanakul et al., 1995); soft Bangkok clay (Abuel-Naga et al., 2007)), while Pontida clay specimens tested by Hueckel and Baldi (1990) showed decrease in stiffness with increase in temperature.

5.8 Summary points

In this chapter, results from temperature-controlled triaxial tests on specimens taken from reconstituted London clay cakes are presented. Specimens went through drained heating or heating / cooling, followed by undrained shearing.

The following are the main observations:

- Normally consolidated London clay experienced irreversible volumetric change upon heating, while the thermally induced volumetric strains were reversible for overconsolidated London clay. The magnitude of contraction upon heating decreased with increase in OCR, until it turned to expansion for highly overconsolidated specimens.
- Peak strength was insensitive to elevated temperature or a temperature cycle, in the stress range and temperature range tested in this research. The critical state stress ratio was not affected by elevated temperature or a temperature cycle.
- Stiffness increased when the specimen was heated or went through a temperature cycle, compared to specimens that were tested at ambient temperature.

Chapter 6: One-dimensional compression at elevated temperature

6.1 Introduction

This chapter presents results from oedometer tests performed on slurry-deposited London clay and on specimens from a reconstituted London clay cake. Temperature, ranging from ambient to 60 °C, was applied during virgin consolidation, unloading / reloading cycles and creep periods. The temperature effect on the compression characteristics of the clay was interpreted from these experiments. The compression characteristics discussed in this chapter include compression and swelling indices (C_c and C_s) and pre-consolidation pressure (σ'_{vc}).

6.2 Applied stress and temperature paths

Applied vertical effective stress, σ'_v, and temperature, T, changes in the one-dimensional (1D) compression tests on slurry-deposited specimens of London clay and on specimens from a reconstituted London clay cake are summarised in Table 6-1. Details of the testing procedures were presented in Chapter 3. Tests were named based on types of specimens and on temperature history. They were categorised into five groups as follows.

(i) The first four tests listed in the table (OED-SL-20, OED-SL-30, OED-SL-40, OED-SL-60) were performed on slurry-deposited specimens, under the temperature of T = 20, 30, 40 and 60°C, respectively, to obtain intrinsic compression lines and swelling lines under the vertical effective stress, σ'_v, changes of up to 3 or 7 MPa, under isothermal loading condition. The purpose of this group of tests was to investigate the effect of temperature on the compression and swelling indices of slurry-deposited London clay.

(ii) Tests OED-SL-20-creep and OED-SL-40-creep were also performed on slurry-deposited specimens. One specimen was kept at T =20°C while the other was fist heated to 40°C, followed by loading both specimens to a vertical effective stress of 100 kPa, which corresponds to a depth where energy piles may be installed. Specimens were then left for creep for three months at constant temperature and stress level, before they were further loaded to σ'_v = 2 MPa. The purpose of this group of tests was to investigate the effect of thermal creep on the compression and swelling indices of slurry-deposited London clay.

(iii) Tests OED-RE-20 and OED-RE-40 were performed on specimens from a reconstituted London clay cake, at T = 20°C and 40°C, respectively. Specimens were loaded to σ'_v = 5 MPa or 7 MPa, with unloading/ reloading cycles performed

at $\sigma_v' = 500$ kPa and 1 MPa. The purpose of this group of tests was to investigate the effect of temperature on the compression characteristics of the specimens from a reconstituted London clay cake.

(iv) Test OED-RE-20-40-20-cycles was performed on a specimen from a reconstituted London clay cake, starting at $T = 20$°C and loaded to different vertical effective stress levels. At $\sigma_v' = 100$, 500 and 1000 kPa, the specimen was heated to $T = 40$°C and then cooled to $T = 20$°C. This heating-cooling cycle was repeated five times at each stress level, before the specimen was loaded to the next stress level. Similarly, test OED-RE-40-20-40-cycles started at $T = 40$°C. At $\sigma_v' = 100$, 500 and 1000 kPa, the specimen was cooled to $T = 20$°C and then heated to $T = 40$°C. This cooling-heating cycle was repeated five times at each stress level, before the specimen was loaded to the next stress level. Purpose of this group of tests was to investigate the effect of temperature cycles on the compression characteristics of the specimens taken from a reconstituted London clay cake.

(v) Test OED-RE-20-40-creep was performed on a specimen from a reconstituted London clay cake. It was loaded to $\sigma_v' = 300$ kPa at $T = 20$°C and then heated to $T = 40$°C, before it was further maintained at $\sigma_v' = 300$ kPa and $T = 40$°C to creep for three months. After the creep period, the specimen was further loaded to $\sigma_v' = 1000$ kPa under a constant temperature of 40°C and then maintained to creep for three and a half months, before it finally loaded to $\sigma_v' = 5$ MPa. The purpose of this test was to investigate the effect of thermal creep on the compression characteristics of specimens taken from a reconstituted London clay cake.

Table 6-1: Applied stress and temperature paths for tests in temperature-controlled oedometer apparatus

Group	Test	Material	Temperature and σ_v' stress paths
i	OED-SL-20	slurry-consolidated London clay	20°C, load to 3 MPa
	OED-SL-30		30°C, load to 7 MPa
	OED-SL-40		40°C, load to 7 MPa
	OED-SL-60		60°C, load to 7 MPa
ii	OED-SL-20-creep	slurry-consolidated London clay	20°C, creep at 100 kPa for 3 months, then load to 2 MPa
	OED-SL-40-creep		40°C, creep at 100 kPa for 3 months, then load to 2 MPa
iii	OED-RE-20	reconstituted London clay	20°C, load to 5 MPa
	OED-RE-40		40°C, load to 7 MPa

iv	OED-RE-20-40-20-cycles	reconstituted London clay	20-40-20°C. five temperature cycles at three different stress levels-100, 500 and 1000 kPa.
	OED-RE-40-20-40-cycles		40-20-40°C. five temperature cycles at three different stress levels-100, 500 and 1000 kPa.
v	OED-RE-20-40-creep	reconstituted London clay	20-40°C. At 300 kPa, heat to 40°C then leave for creep for 3 months. Then the specimen was kept at 40°C when it was loaded. At 1000 kPa, the specimen was left for creep for 3.5 months.

6.3 Behaviour of the slurry-deposited London clay in 1D compression under different temperature

This section presents the behaviour of slurry-deposited London clay specimens in 1D compression tests at temperatures of 20, 30, 40 and 60°C, as well as the effect of creep on the compression characteristics.

6.3.1 Effect of temperature on compression characteristics

Figure 6-1 shows intrinsic compression lines (ICLs) of slurry-deposited London clay at four temperature levels ranging from 20 to 60°C. When the vertical effective stress varied between 10 kPa and 1000 kPa, which corresponds to the depth where thermo-active piles are usually installed, normal compression lines at different temperature levels were practically parallel to each other, indicating that the compression index C_c was not sensitive to change in temperature. The initial void ratio when the specimens were first loaded was slightly different in the four tests. This was mainly due to the small difference in the mass of the slurry that was put in the oedometer cell. When the vertical effective stress was larger than 1000 kPa, normal compression lines at different temperature levels exhibited some divergence, possibly due to soil specimens becoming very thin. Compression indices at different temperature levels are summarised in Table 6-2, by linearly interpolating through the data points from vertical effective stress of 10 kPa to 1000 kPa. Values of C_c ranged from 0.451 to 0.467, with no clear trend of change with temperature. The small difference in C_c was due to experimental scatter. Data for all temperature levels were plotted in Figure 6-1 (b). A regression line was plotted through these data and the normal compression line can be represented by Equation 6-1. Since the 1D compression data were obtained from slurry, this normal compression line was also the intrinsic compression line (ICL) of the soil. The term 'intrinsic' is used to describe the properties of clays which have been reconstituted at a water content such that $w_L \leq w \leq 1.5w_L$ (preferably $1.25w_L$) and these properties are independent of the clays' natural state (Burland,

1990). The value of compression index C_c can be taken as 0.458 for a slurry-deposited London clay when the temperature varies between 20 and 60°C, as a result of the linear regression line plotted through all the data.

$$e = -0.458 log\sigma'_v + 1.959 \qquad 6\text{-}1$$

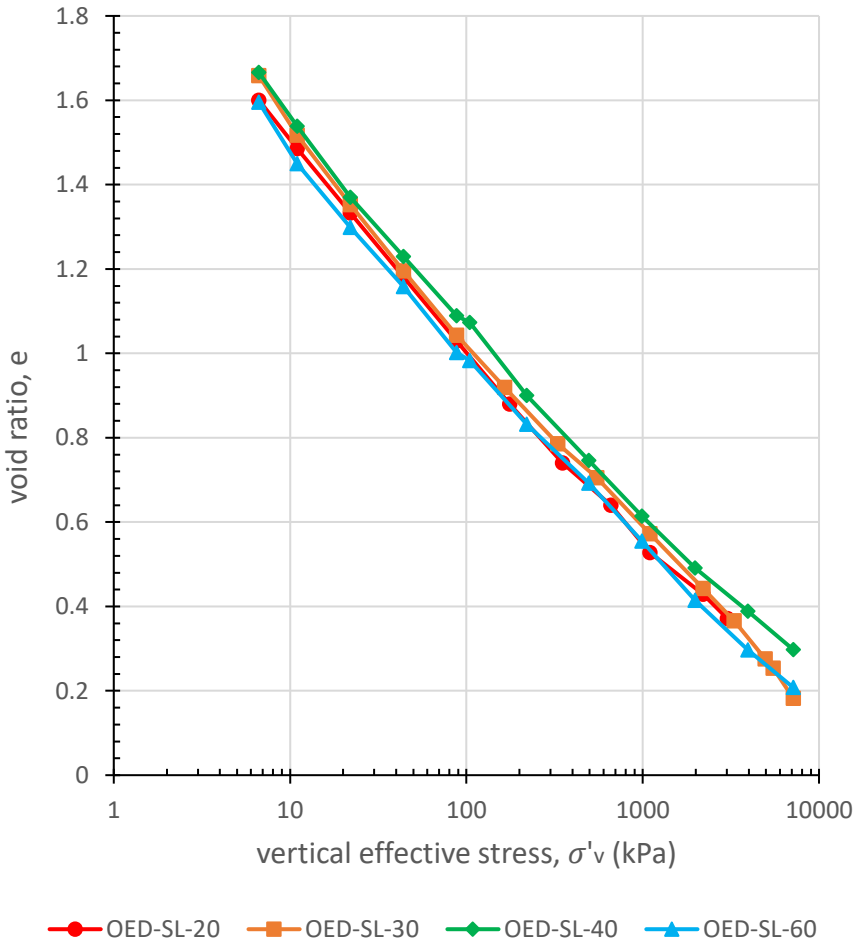

(a) For each temperature level

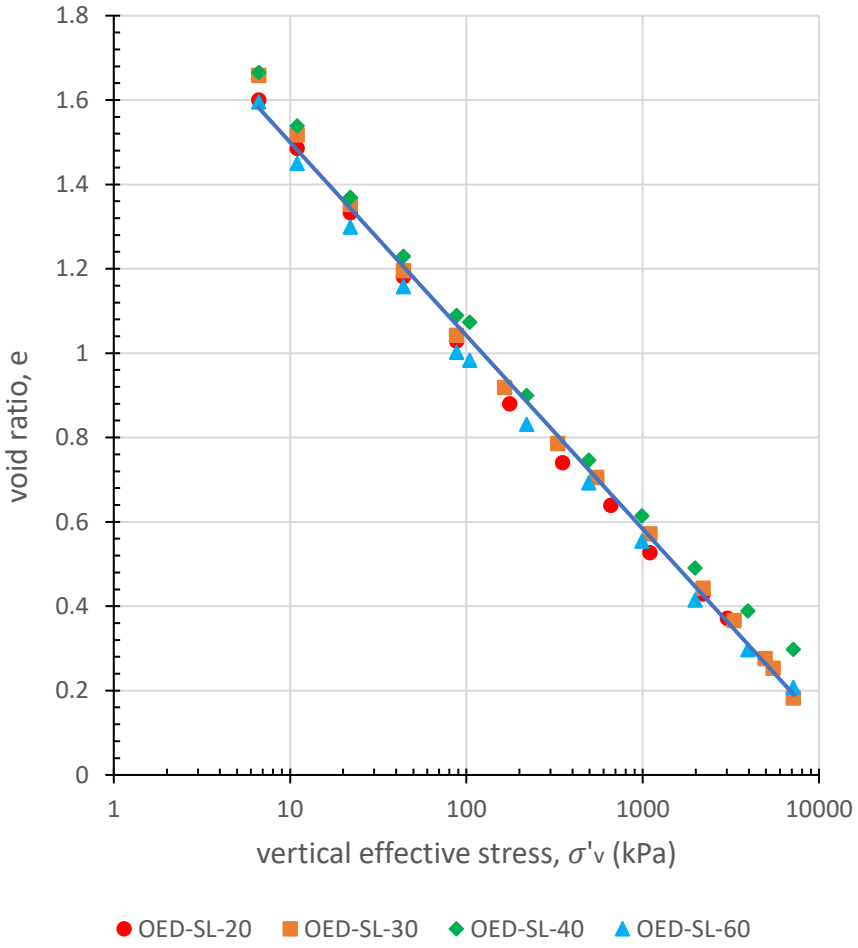

(b) For all temperature levels

Figure 6-1: One-dimensional compression of slurry-deposited London clay, with intrinsic compression lines only

Table 6-2: Compression and swelling indices for one-dimensional compressed slurry-deposited specimens

Temperature (°C)	C_c	C_s
20	0.465	0.110
30	0.467	-
40	0.451	0.103
60	0.452	0.118
Linear regression for all data	0.458	0.110

Void index, I_v, is used to normalise the curves in Figure 6-1 and is calculated using Equation 6-2.

$$I_v = \frac{e - e^*_{100}}{e^*_{100} - e^*_{1000}} = \frac{e - e^*_{100}}{C^*_c} \qquad 6\text{-}2$$

where e^*_{100} and e^*_{1000} are the intrinsic void ratios corresponding to σ'_v =100 kPa and 1000 kPa, respectively.

Using Equation 6-1, it can be found that $e^*_{100} = 1.043$ and $e^*_{1000} = 0.585$. Substituting these two parameters into Equation 6-2, the normalised ICL can be represented as

$$I_v = \frac{e - 1.043}{1.043 - 0.585} = \frac{-0.458 log\sigma'_v + 1.959 - 1.043}{1.043 - 0.585} = 2 - log\sigma'_v \qquad 6\text{-}3$$

Normalised intrinsic compression curve based on Equation 6-3 is plotted in Figure 6-2.

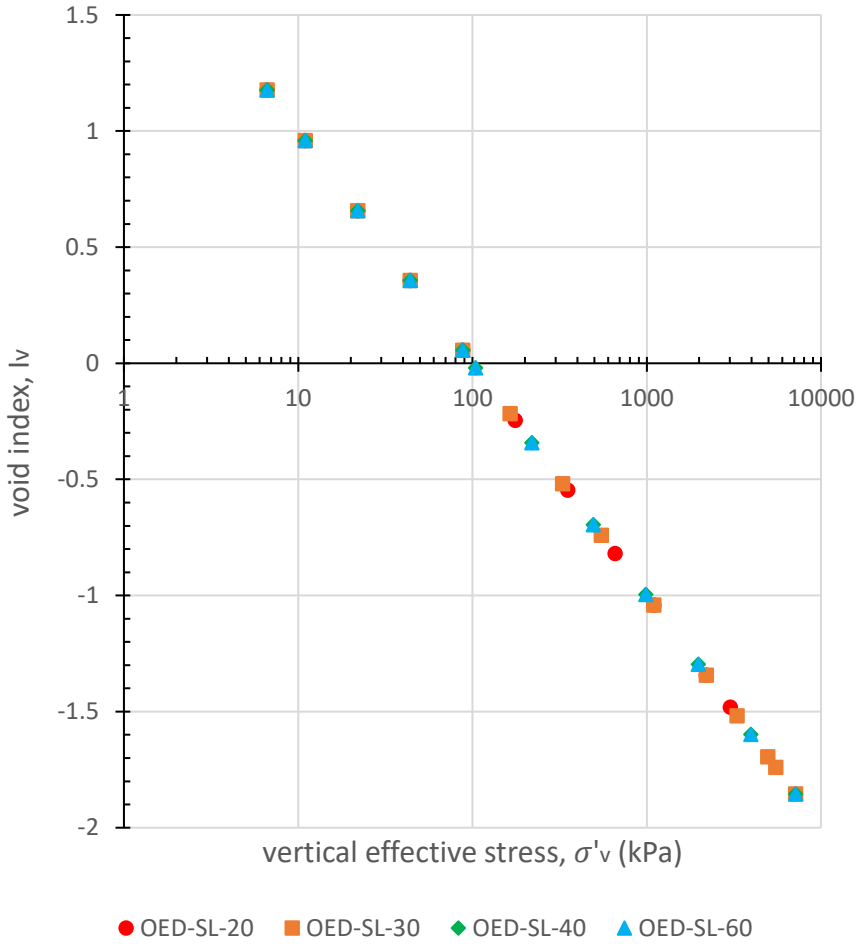

Figure 6-2: Normalised intrinsic compression curves

Figure 6-3 shows the results of the same 1D compression tests on slurry-deposited London clay but including the unloading/ reloading cycles. At 20°C, the unloading paths tended to be straight lines down to 10 kPa and then stayed relatively flat when soil specimens were unloaded from 10 kPa to 7 kPa. Upon reloading, the initial part of the path was relatively flat, then the curve became steeper as the vertical effective stress increased before it finally joined the intrinsic compression line. The shape of a typical unloading/ reloading path in consolidation tests can be approximated with the sketch in Figure 6-4. The initial gradient of the unloading curve from point A to B is equal to the initial gradient of the reloading curve from point D to

E. Hysteresis was observed in the unloading/ reloading process. At $T = 40$ and 60°C, the swelling lines were non-linear. Hysteresis was also observed at these two temperature levels.

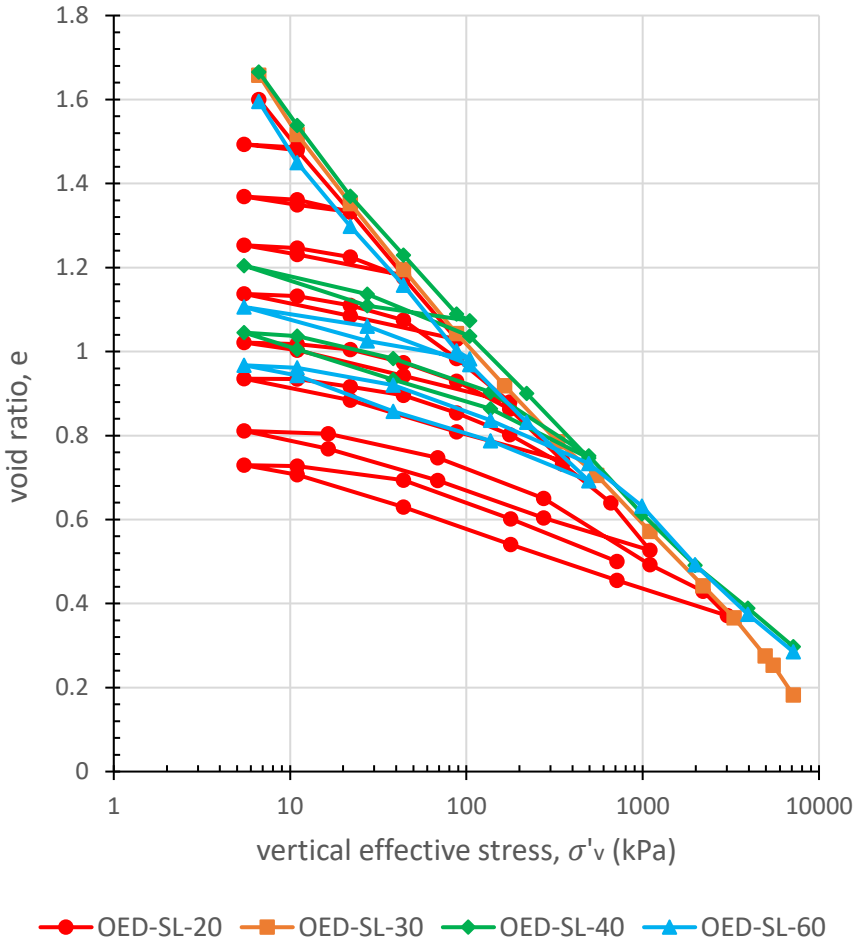

Figure 6-3: One-dimensional compression on slurry-deposited London clay, with normal compression lines and swelling lines

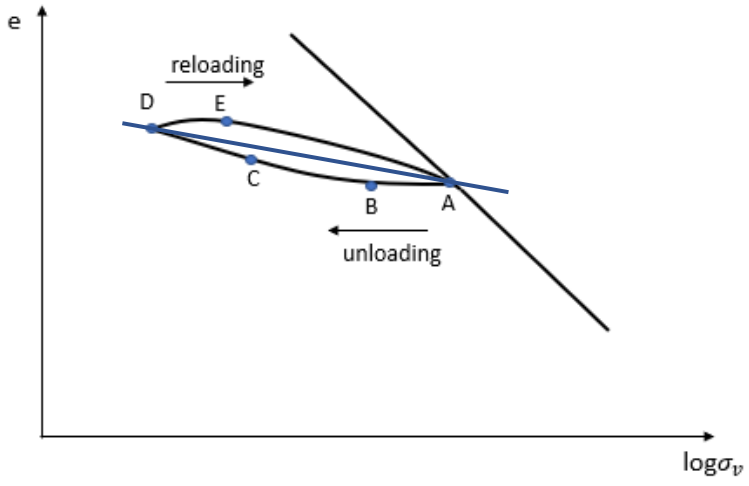

Figure 6-4: Typical unloading/ reloading path in consolidation tests

In Figure 6-5, secant gradients were determined for each of these unloading/reloading cycles and plotted as straight lines to approximate the swelling lines. These straight lines could be considered largely parallel to each other at each different temperature value and in the vertical effective stress range from 10 to 500 kPa. The values of swelling indices, C_s, are summarised in Table 6-2. They were not sensitive to changes in temperature or stress levels.

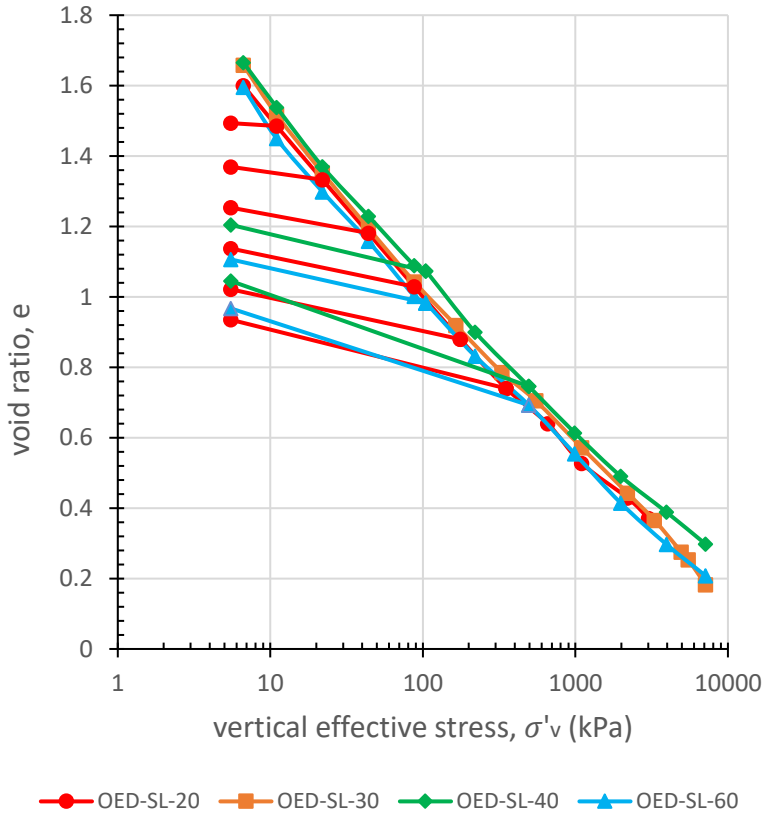

Figure 6-5: One-dimensional compression on slurry-consolidated London clay, with straight line approximation for swelling lines

6.3.2 Effect of creep on compression characteristics

Figure 6-6 shows the normal compression lines of tests on slurry-deposited London clay specimens, at $T = 20$ and 40 °C, which were subjected to a three-month creep period at 100 kPa. At the same temperature level, there was no visible change in void ratio as a result of the creep period, with the compression line parallel to the one obtained without the creep period. Compression indices were the same before and after the creep period for the same test. This observation could not be considered definitive as the creep period was limited by the time available for the entire experimental programme.

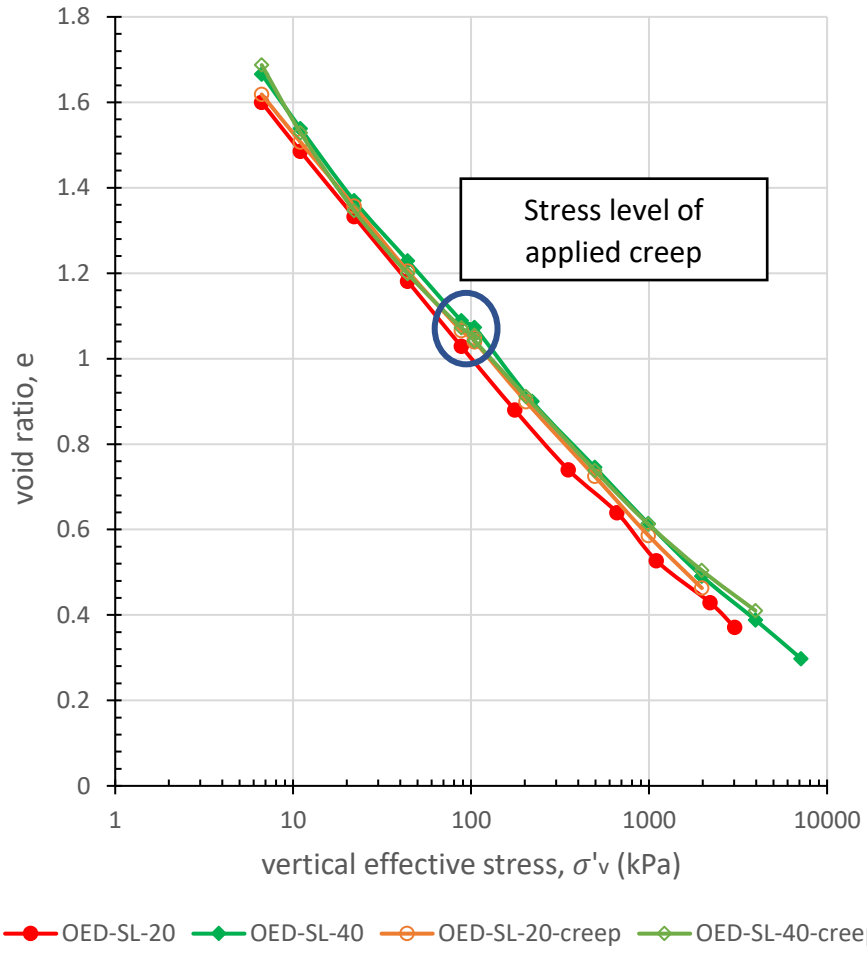

Figure 6-6: One-dimensional consolidation and thermal creep on slurry-deposited London clay

Four data points are plotted at $\sigma'_v = 100$ kPa in Figure 6-6, corresponding to void ratios at 1 day, 1 month, 2 months and 3 months creep period at $\sigma'_v = 100$ kPa. Change in void ratio with time at 20°C and 40°C is plotted in Figure 6-7 and Figure 6-8, with values at different stages of the creep period listed in Table 6-3. Change in void ratio in Table 6-4 is calculated between two consecutive data points selected in Table 6-3.

The number in the bracket shows the proportion of change in void ratio during each stage, to the total change in void ratio, from loading to 100 kPa until the end of the 3-month creep period. At 20°C, 72% of the change in void ratio occurred during the first 24 hours after loading, and 28% occurred over the first 1 month after loading. In the second and third month, no change in void ratio was measured, possibly because of the limited resolution of the linear variable differential transformer (LVDT) that was used to measure the vertical deformation of the specimen. At 40°C, 54.8% of the void ratio change occurred in the first day after loading, followed by 41.9% over the first month, negligible change over the second month and the third month. Under elevated temperature, it took longer for the creep deformation to develop. In this test, it seemed that more time should be allowed for soil to creep, before loading the soil

specimen to the next level, instead of the 24h period for each load step that was currently used. This may result in an offset in the void ratio and a shift in the location of the normal compression line, compared to the current results, but slopes of normal compression lines and swelling lines would not be affected. Compression and swelling indices calculated from current experimental data are still reliable.

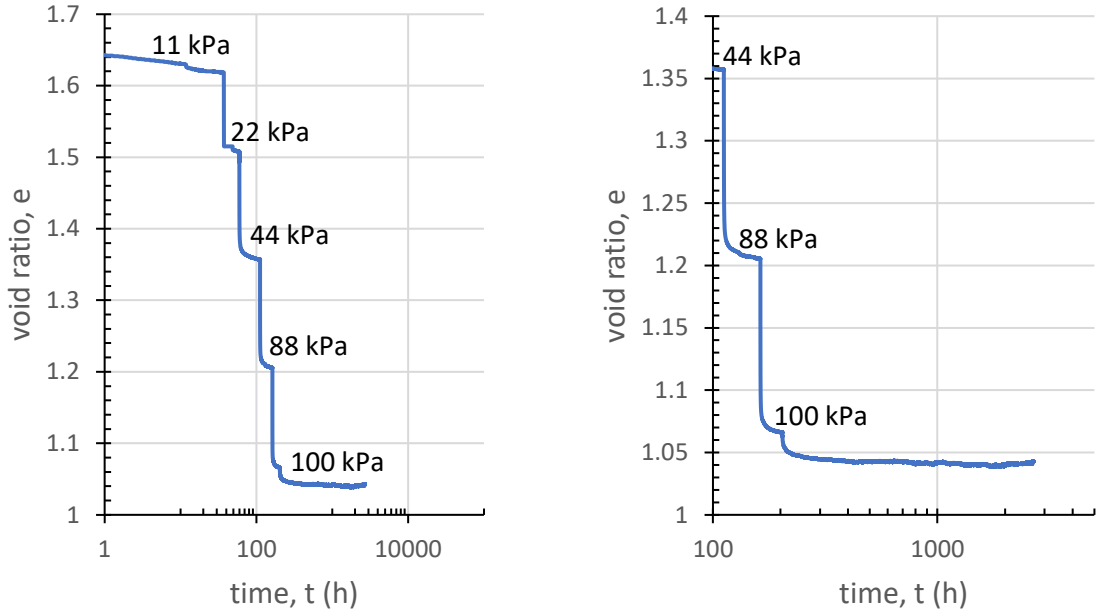

(a) at different stress levels (b) at 100 kPa

Figure 6-7: Change of void ratio with time for OED-SL-20-creep

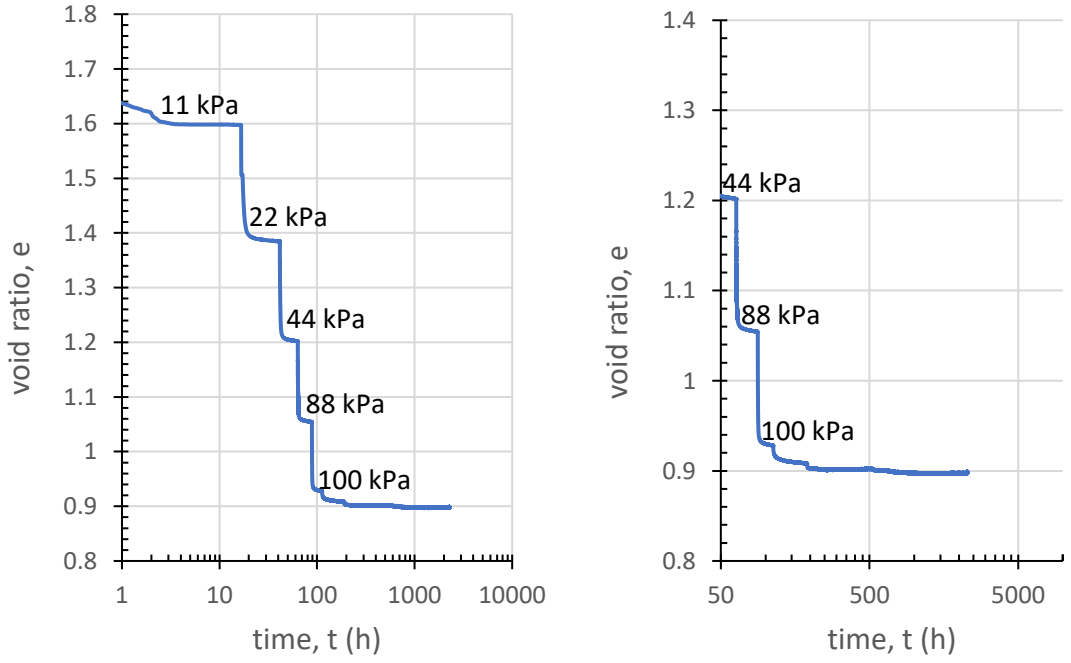

(a) at different stress levels (b) at 100 kPa

Figure 6-8: Change of void ratio with time for OED-SL-40-creep

Table 6-3: Void ratio during the creep period at $\sigma_v' = 100$ kPa

Temperature	Void ratio				
	At the end of previous loading stage	1 day after loading	1 month after loading	2 months after loading	3 months after loading
20°C	1.066	1.048	1.041	1.040	1.041
40°C	0.928	0.911	0.898	0.897	0.899

Table 6-4: Change in void ratio during the creep period at $\sigma_v' = 100$ kPa

Temperature	Change in void ratio			
	1 day after loading	1 month after loading	2 months after loading	3 months after loading
20°C	-0.018 (-72%)	-0.007 (-28%)	-0.001 (-4%)	0.001 (4%)
40°C	-0.017 (-54.8%)	-0.013 (-41.9%)	-0.001 (-3.2%)	0.002 (6.5%)

6.4 Behaviour of London clay specimens in compression under elevated temperatures, from reconstituted clay cake

6.4.1 Effect of temperature on compression characteristics under isothermal loading

Figure 6-9 shows the results of one-dimensional compression tests on specimens of London clay from a reconstituted clay cake at $T = 20$°C, 40°C and 60°C. The intrinsic compression line that was plotted in the figure was obtained from tests on slurry-deposited London clay at different temperature levels, as presented in Section 6.3. Compression characteristics are presented in Table 6-5. The initial part of the normal compression lines was flat, as London clay cakes from which the specimens were trimmed, were consolidated from slurry in a large consolidometer under a vertical effective stress of 200 kPa. In other words, clay specimens were pre-consolidated during the sample preparation process, as described in Chapter 3. Therefore, the initial parts of the compression curves corresponded to unloading / reloading paths before joining the virgin compression line at stress level that was higher than the pre-consolidation pressure. The normal compression lines at these three temperature levels were practically parallel to each other, hence giving similar gradients of the straight parts of the compression curves, independent of temperature level up to $\sigma_v' = 3000$ kPa (see Table 6-5). An average value of compression indices of 0.394 could be derived from data on London clay specimens taken from a reconstituted cake. This is a lower value compared to the intrinsic gradient $C_c^* = 0.458$, which may indicate a slight formation of structure in the London clay cake samples during the previous consolidation of the cake. Compression curves were plotted below the ICL when the vertical effective stress was below 200 kPa, which agreed with the value of pre-consolidation pressure of the reconstituted London clay cake. When the vertical

effective stress was larger than 200 kPa, the compression curves of the specimens taken from reconstituted London clay cake gradually merged towards the ICL. There was no obvious change in pre-consolidation pressure with change in temperature level.

The swelling lines at the three temperature levels were also parallel. Swelling indices are calculated in three different ways described as follows: 1) by taking the slope of the middle part of the unloading path; 2) by taking the slope of the middle part of the reloading path; 3) by taking the secant gradients of the unloading/ reloading loop. Values of swelling indices are presented in Table 6-5. Swelling indices calculated using the first and the second method were in the range of 0.090 to 0.109. They were not sensitive to changes in temperature level, stress level or whether they were taken from unloading path or reloading path. Swelling indices calculated using the third method were also insensitive to changes in temperature, although there was small variation due to experimental scatter. By comparing swelling indices calculated using different methods, it can be concluded that, the secant gradients of the unloading/ reloading curves were not affected by changes in temperature, and they were not affected by the stress level at which the unloading/reloading paths started from.

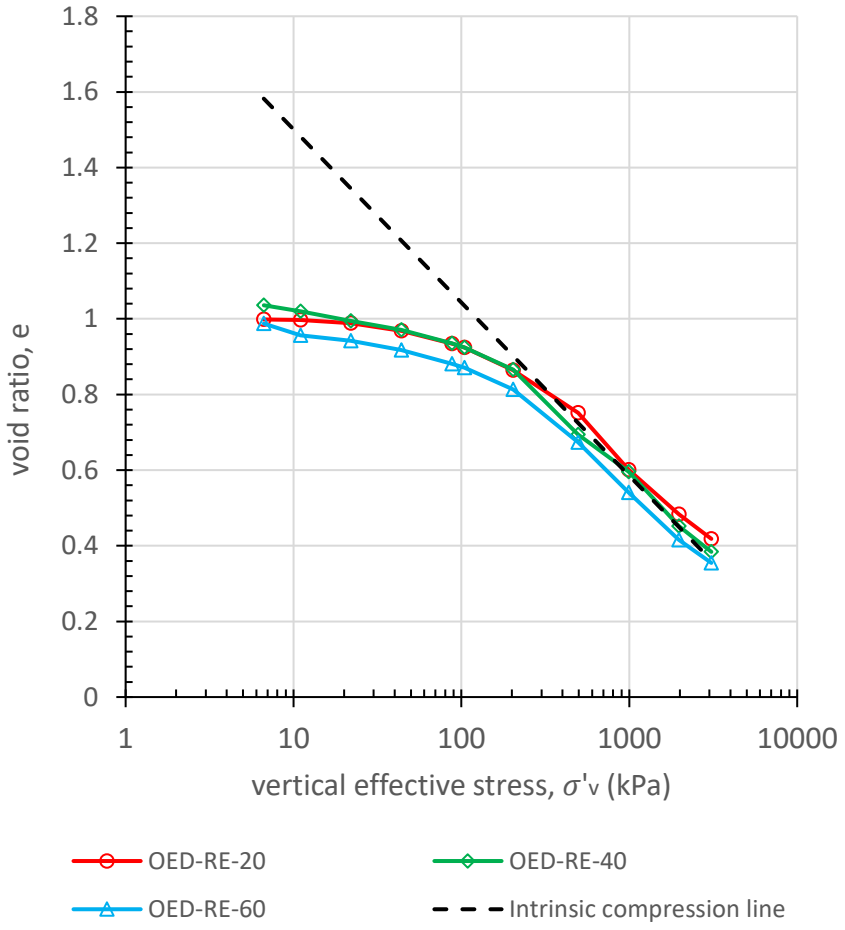

(a) with normal compression lines only

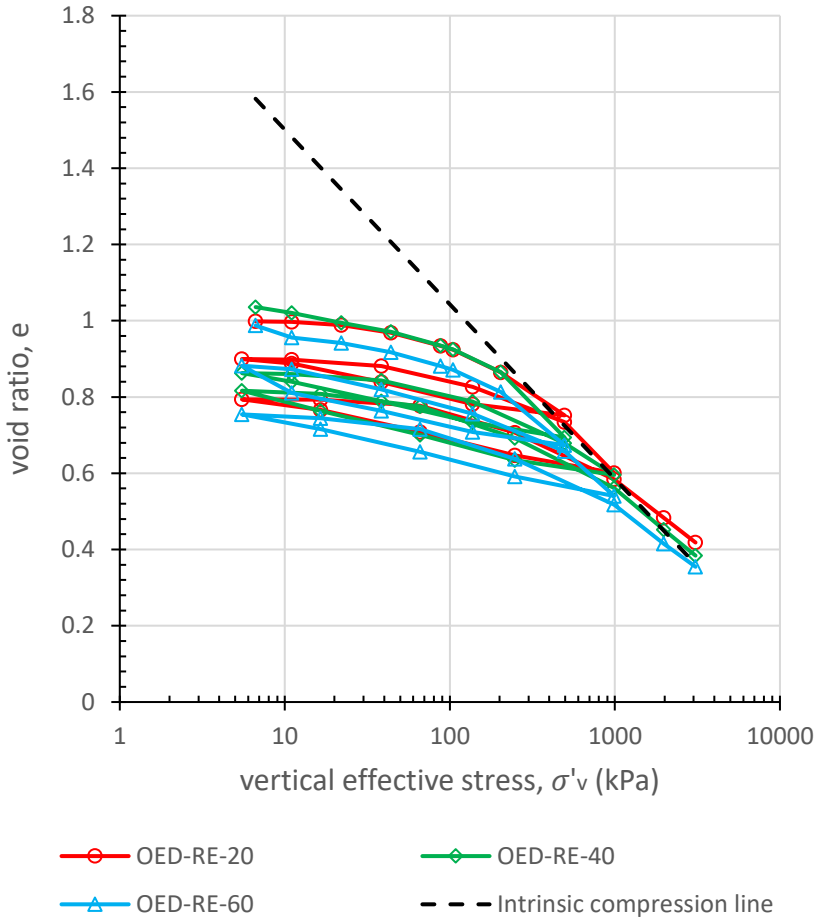

(b) with normal compression lines and swelling lines

Figure 6-9: One-dimensional compression of cake specimens of reconstituted London clay at 20°C, 40°C and 60°C

Table 6-5: Compression characteristics of one-dimensional compressed reconstituted specimens

Temperature (°C)	Vertical stress (kPa)	C_c	C_s			Pre-consolidation pressure (kPa)
			Unloading path	Reloading path	Secant gradient	
20	500	0.390	0.107	0.098	0.105	200
	1000		0.101	0.100	0.103	
40	500	0.403	0.098	0.100	0.104	200
	1000		0.109	0.099	0.108	
60	500	0.388	0.094	0.107	0.106	200
	1000		0.106	0.090	0.105	
Average		0.394	0.103	0.099	0.105	200

6.4.2 Effect of temperature cycles on compression characteristics

This section presents one-dimensional compression tests on reconstituted cake specimens of London clay, with temperature cycles at 100, 500 and 1000 kPa. Results were plotted in Figure 6-10, in comparison to tests performed at the same temperature level but without temperature

cycles. Compression characteristics were presented in Table 6-6. The gradients of compression curves did not change after the soil specimen went through temperature a cycle at 100, 500 and 1000 kPa of vertical effective stress. The maximum change in void ratio was calculated as a proportion of the maximum change in void ratio due to thermal cycles, to the initial void ratio before the specimen went through thermal cycles. For test OED-RE-20-40-20-cycles, at the same stress level, the maximum change in void ratio was 2.6%, as presented in Table 6-7. For test OED-RE-40-20-40-cycles, at the same stress level, the maximum change in void ratio was 1.0%, as presented in Table 6-8. It can be concluded that when the stress level remained unchanged, the void ratio was not sensitive to temperature cycles. Change in void ratio due to thermal cycles was negligible compared to that due to mechanical loading. For test OED-RE-20-40-20-cycles, soil specimen was kept at ambient temperature before it went through thermal cycles. Normal compression line of specimen at 20°C gradually moved towards the normal compression line of specimen tested under 40°C, after temperature cycles of 20-40-20 at three stress levels, while temperature cycles of 40-20-40 did not affect compression indices of soil specimen that was pre-heated to 40°C, as can be observed from Figure 6-10 (c). There was no obvious change of pre-consolidation pressure with temperature cycles.

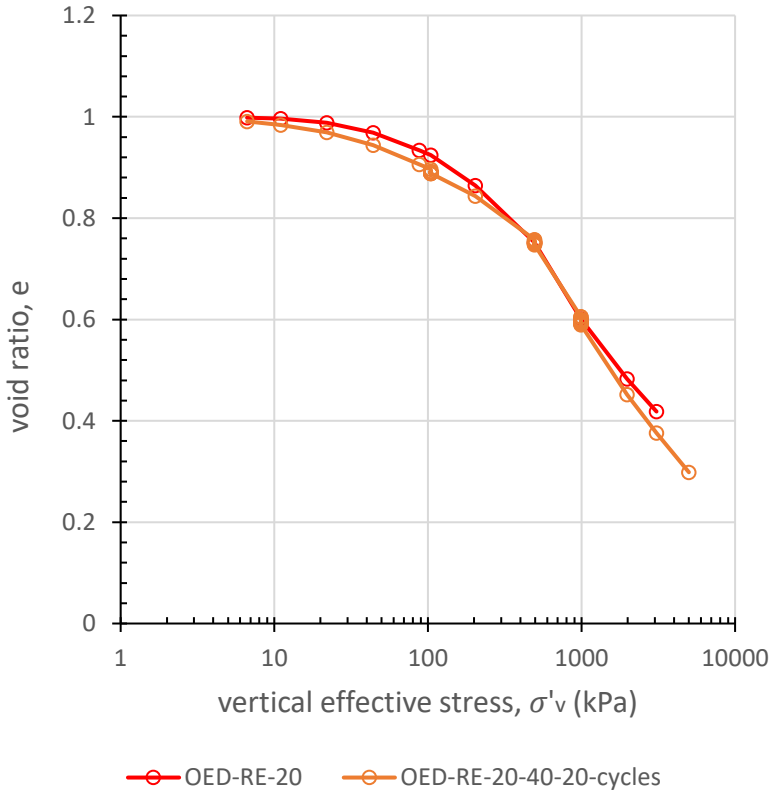

(a) 20°C

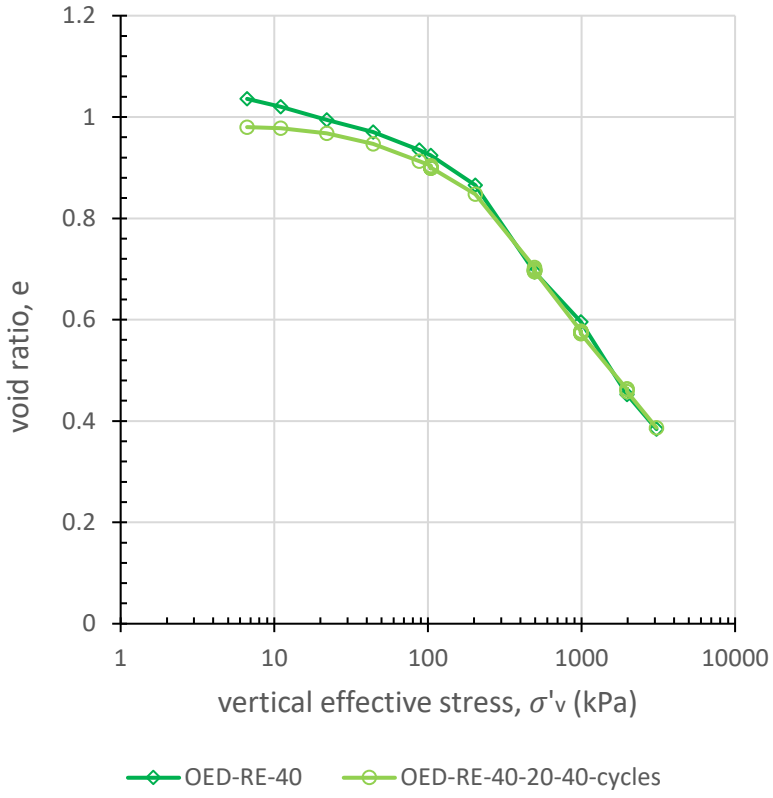

(b) 40°C

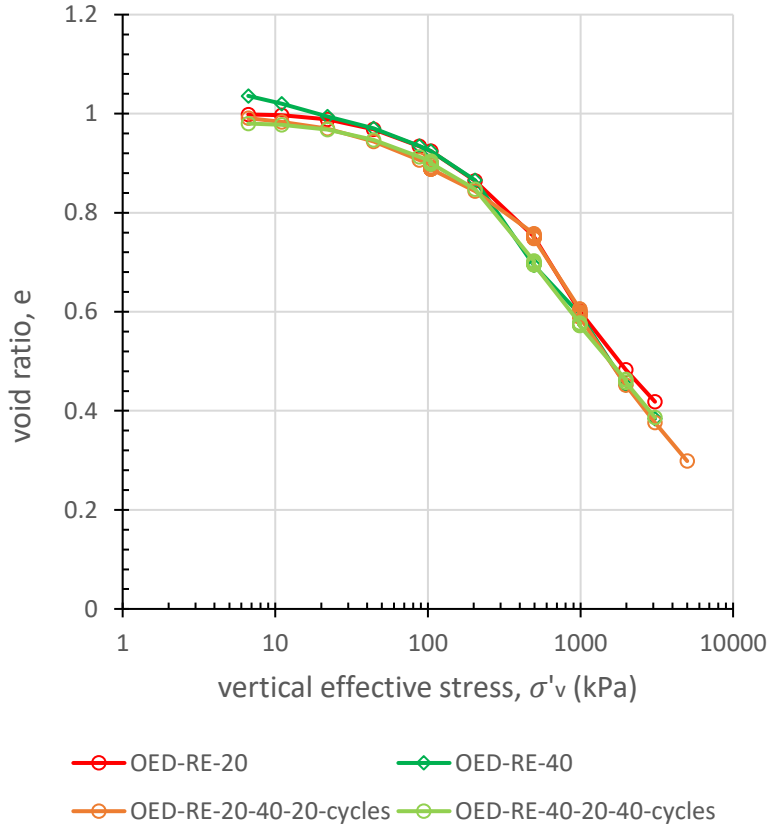

(c) 20°C and 40°C

Figure 6-10: One-dimensional compression tests on reconstituted cake specimens of London clay with temperature cycles a) 20°C; b) 40°C; c) 20°C and 40°C

Table 6-6: Compression characteristics of one-dimensional compressed specimens with temperature cycles

Test	C_c	Pre-consolidation pressure (kPa)
OED-RE-20-40-20-cycles	0.409	200
OED-RE-20	0.390	200
OED-RE-40-20-40-cycles	0.391	200
OED-RE-40	0.403	200

Table 6-7: Void ratio in each temperature cycle for test OED-RE-20-40-20-cycles

Stress level (kPa)	Number of cycles	Void ratio	
		at $T = 20^oC$	at $T = 40^oC$
100	Before loading	0.906	
	24h after loading	0.897	
	1st cycle	0.897	0.892
	2nd cycle	0.891	0.892
	3rd cycle	0.891	0.891
	4th cycle	0.890	0.891
	5th cycle	0.890	0.891
	6th cycle	0.889	0.890
	7th cycle	0.889	0.890
	8th cycle	0.889	0.890
	9th cycle	0.889	0.890
	10th cycle	0.889	0.890
	End of thermal cycle	0.890	
	Maximum change in void ratio	0.9%	
500	Before loading	0.843	
	24h after loading	0.758	
	1st cycle	0.758	0.756
	2nd cycle	0.752	0.754
	3rd cycle	0.751	0.753
	4th cycle	0.749	0.752
	5th cycle	0.749	0.751
	End of thermal cycle	0.748	
	Maximum change in void ratio	1.3%	
1000	Before loading	0.748	
	24h after loading	0.606	
	1st cycle	0.606	0.605
	2nd cycle	0.599	0.600
	3rd cycle	0.595	0.597
	4th cycle	0.593	0.594
	5th cycle	0.591	0.593
	End of thermal cycle	0.590	
	Maximum change in void ratio	2.6%	

Table 6-8: Void ratio in each temperature cycle for test OED-RE-40-20-40-cycles

Stress level (kPa)	Number of cycles	Temperature (°C)	
		40	20
100	Before loading	0.913	
	24h after loading	0.904	
	1st cycle	0.904	0.902
	2nd cycle	0.902	0.900
	3rd cycle	0.901	0.899
	4th cycle	0.900	0.899
	5th cycle	0.900	0.899
	End of thermal cycle	0.900	
	Maximum change in void ratio	0.4%	
500	Before loading	0.848	
	24h after loading	0.703	
	1st cycle	0.703	0.698
	2nd cycle	0.700	0.697
	3rd cycle	0.699	0.695
	4th cycle	0.698	0.695
	5th cycle	0.697	0.696
	End of thermal cycle	0.696	
	Maximum change in void ratio	1.0%	
1000	Before loading	0.696	
	24h after loading	0.577	
	1st cycle	0.577	0.574
	2nd cycle	0.577	0.574
	3rd cycle	0.576	0.573
	4th cycle	0.575	0.572
	End of thermal cycle	0.574	
	Maximum change in void ratio	0.5%	

6.4.3 Effect of creep on compression characteristics

Figure 6-11 shows the one-dimensional compression tests on reconstituted London clay with a long creep period, in comparison with those performed on the same material and at the same temperature levels. Test started at 20°C and then the specimen was heated to 40°C at 300 kPa, where the temperature and stress were kept at constant values for three months to allow for creep. Changes in void ratio during this creep period were negligible, with values presented in Table 6-9 and Table 6-10. The majority (71.4%) of the change in void ratio occurred during the first day after loading was applied, while a smaller amount (28.6%) of the change occurred during the second month after loading. In the first unloading/ reloading cycle that started at 300 kPa, the swelling index was similar to that of the test OED-RE-20, at 20°C without creep period. After reloading, the curve followed a similar trend as that of the test OED-RE-20, with similar compression index. At 1000 kPa, the specimen was left for three and a half months for creep, before another unloading/ reloading loop started. Similar to the case of creep under 300 kPa,

the majority (92.5%) of the change in void ratio occurred during the first day after loading was applied. The compression and swelling indices did not change with the elongated creep period, in the timeframe of 3.5 months tested in this research.

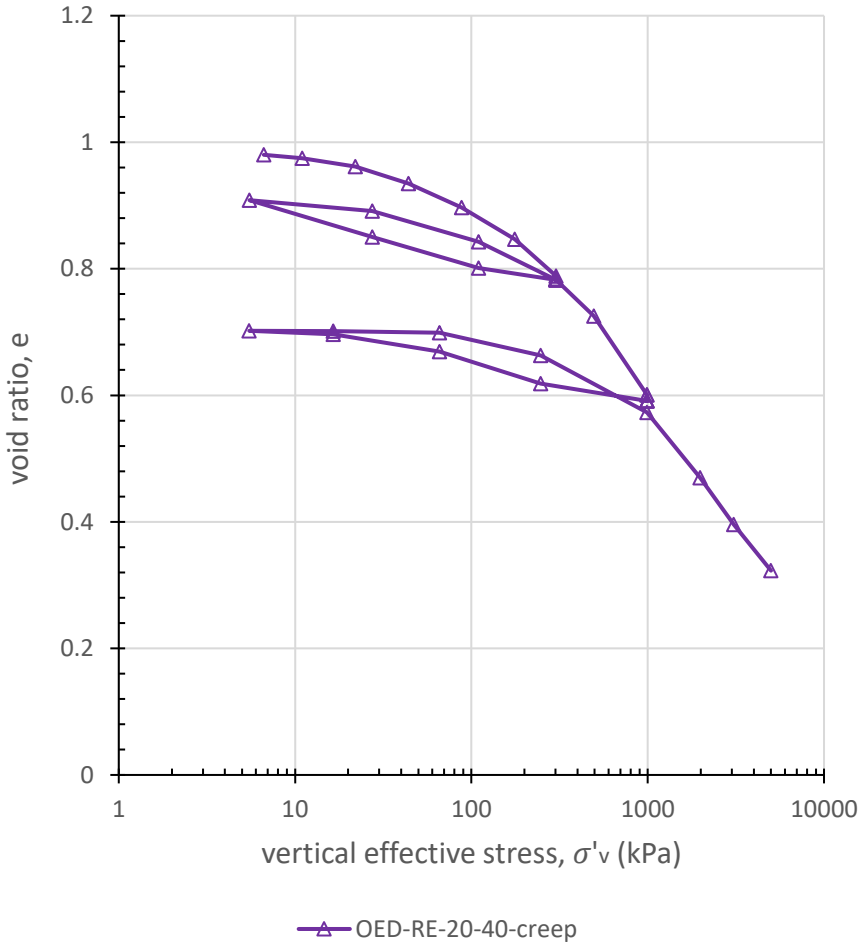

(a) OED-RE-20-40-creep

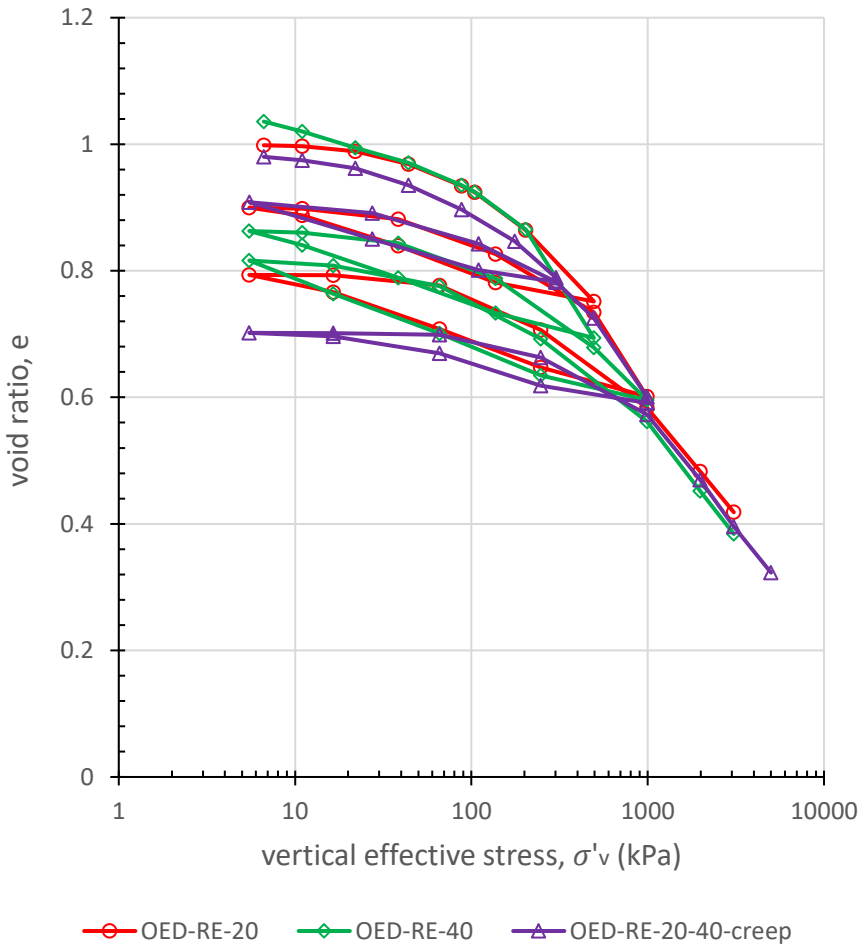

(b) comparison with other tests

Figure 6-11: One-dimensional compression tests on reconstituted London clay with creep

Table 6-9: Void ratio during the creep period

Stress level	Void ratio					
	At the end of previous loading stage	1 day after loading	1 month after loading	2 months after loading	3 months after loading	3.5 months after loading
300 kPa	0.789	0.784	0.784	0.782	0.782	-
1000 kPa	0.725	0.601	0.591	0.591	0.591	0.591

Table 6-10: Change in void ratio during the creep period

Stress level	Change in void ratio				
	1 day after loading	1 month after loading	2 months after loading	3 months after loading	3.5 months after loading
300 kPa	-0.005 (71.4%)	0	-0.002 (28.6%)	0	-
1000 kPa	-0.124 (92.5%)	-0.010 (7.5%)	0	0	0

6.5 Discussion

In this section, compression characteristics of London clay obtained from one-dimensional compression tests under ambient and elevated temperature are discussed and compared with results in the literature. Possible mechanisms that lead to observations from the results are also discussed.

6.5.1 Compression characteristics of London clay at ambient temperature

Compression characteristics of London clay at ambient temperature from tests performed in this research and from those in the literature are summarised in Table 6-11. Compression index of specimens from slurry-deposited London clay measured in this research was comparable to some of the results reported in the literature (Skempton, 1944; Som, 1968; Jardine, 1985), while it was smaller than the value presented by Gasparre (2005). Compression index for specimens taken from reconstituted London clay cakes was comparable to those presented by Gasparre (2005) and Martinez-Calonge (2007). Values of swelling indices were smaller than that presented by Gasparre (2005). Compression indices of slurry-deposited specimens were larger than those of reconstituted specimens. This is because for slurry-deposited specimens, the soil was not pre-loaded before and it had higher water content, which made it to be more compressible and softer, while the reconstituted specimens were consolidated to a London clay cake before they were trimmed and tested in oedometer apparatus. Swelling indices for slurry-deposited London clay and reconstituted London clay cake were practically the same. Similar observations were reported by Gasparre (2005).

Table 6-11: Compression characteristics of London clay at ambient temperature

Material tested	Stress level (kPa)	C_c	C_s	Reference
Slurry-deposited London clay, unit C_1	7-3000	0.458	0.110	This research
Slurry-deposited London clay	69-6865	0.490	-	Skempton 1944
Slurry-deposited London clay	-	0.494	-	Som 1968
Slurry-deposited London clay	-	0.446	-	Jardine 1985
Slurry-deposited London clay, unit B_{2c}	-	0.522	0.144	Gasparre 2005
Reconstituted London clay cake, unit C_1	7-3000	0.390	0.102	This research
Reconstituted London clay cake, unit C	5-1300	0.386	0.148	Gasparre 2005
Reconstituted London clay cake, unit B_2	5-2000			
	5-6000			
	5-1660			

Reconstituted London clay cake, unit A_3	5-7500			
Reconstituted London clay cake, unit A_2	5-1000			
Reconstituted London clay cake, unit C_1	-	0.419	-	Martinez-Calonge 2007

6.5.2 Effect of temperature on pre-consolidation pressure under isothermal loading condition

Pre-consolidation pressure (σ'_{vc}) is the maximum pressure that a soil has been subjected to. It is where the soil behaviour changes from that of an over consolidated (OC) soil to that of a normally consolidated (NC) soil. In a Casagrande graphical construction, the pre-consolidation pressure is estimated as the one where the OC compression line intersects with the NC compression line, shown by changes in the slopes of the lines. For conventional laboratory tests that are normally performed under ambient temperature, an overconsolidated soil is a soil that has experienced a higher effective stress than the current one. A normally consolidated soil is a soil that has never experienced a higher effective stress before. In other words, the current effective stress is the maximum effective stress that the soil has been subject to. In thermal testing, however, temperature can change the soil properties, including the pH and salt concentration, and make the soil behave as if it were over-consolidated, although it may not have experienced a higher effective stress before. Kirkham (2020) suggested that instead of using the definition of over and normally consolidated soils, it would be better to identify the normal compression line (NCL) first and then define the soil as normally consolidated if its behaviour plots on the NCL. If the soil behaviour is plotted below the NCL, it is defined as over consolidated. In some literature, the pre-consolidation pressure at elevated temperature is also referred to as 'apparent pre-consolidation pressure', and this value may be different from the pre-consolidation pressure at ambient temperature.

Some researchers found that the pre-consolidation pressure reduced with increase in temperature levels (Gray, 1936; Plum and Esrig, 1969; Eriksson, 1989; Tidfors and Šallfors, 1989; Moritz, 1995; Abuel-Naga et al., 2005; Fraņcois et al., 2007; Favero et al., 2016). Tidfors and Šallfors (1989) suggested that the relationship between pre-consolidation pressure and temperature was linear, while Eriksson (1989) and Moritz (1995) proposed that there was a non-linear relationship between pre-consolidation pressure and temperature and that a power function could be used. Normal compression lines shifted to the left (or described as 'shift down' in some literature) as temperature increased, leading to the reduction in pre-consolidation pressure (Gray, 1936; Finn, 1952; Plum and Esrig, 1969; Eriksson, 1989; Tidfors

and Šallfors, 1989; Moritz, 1995; Abuel-Naga et al., 2005; Franҫois et al., 2007; Favero et al., 2016).

There was no obvious change in pre-consolidation pressure with the change of temperature level in this research. Based on the stress and temperature range that was covered in the testing programme, it is difficult to draw a clear conclusion on how the pre-consolidation pressure changed with temperature. Various methods were proposed to estimate the pre-consolidation pressure from the analysis of one-dimensional compression curves in the $log\sigma'_v - e$ plot (Casagrande, 1936; Burmister, 1951; Schmertmann, 1955; Janbu, 1963; Laloui, 2020). The Casagrande method (1936), for example, considered the point of maximum curvature in the $log\sigma'_v - e$ plot as the pre-consolidation pressure. The point of intersection between the recompression and compression curves was identified and the corresponding vertical stress was the pre-consolidation pressure. However, this is very subjective, and it is also affected by experimental scatter, as the normal compression lines may not be completely linear in the $log\sigma'_v - e$ plot. This leads to ambiguity and uncertainty in the determination of pre-consolidation pressure. The discrepancy between observations in this research and those in literature can be explained by this.

A prolonged creep period did not show any effect on the pre-consolidation pressure, but this is probably because the creep period occurred at effective stresses that were higher than the pre-consolidation pressure and the length of the creep period was not extensive. Isothermal loading tests with a prolonged creep period at an effective stress that is lower than the pre-consolidation pressure are needed to confirm this.

6.5.3 Effect of temperature on the compression and swelling indices

Values of compression and swelling indices of the soil at ambient and elevated temperature are summarised in Table 6-12. For slurry-deposited specimens, compression and swelling indices were not affected when the temperature changed from 20 to 60°C. An average value of 0.458 for C_c and 0.110 for C_s can be used in design for simplicity. The author did not find similar tests in the literature on slurry-consolidated soils to compare to.

For reconstituted London clay cake specimens, compression indices were largely insensitive to the temperature levels examined. This agreed with findings by many researchers in the temperature range of 4.4 to 55 °C (Gray (1936) for a fine grained soil from 10 to 22°C, Finn (1952) for slightly organic silt or clay with high compressibility from 4.4 to 26.7°C, Eriksson (1989) for sulphite-rich silty clay from 5 to 55°C, Tidfors and Šallfors (1989) for B̈ackebol clay from 7 to 40°C). A few researchers observed a small effect of temperature on the

compressibility. Plum and Esrig (1969) found that the compression index changed with temperature (in the range of 24 to 50 °C) when the stress level was below 40 psi (275 kPa) and then remained constant at different stress levels when the stress level was above 40 psi (275 kPa) for illite. Some variations could be observed from Plum and Esrig (1969) data and the non-linear normal compression lines in their diagrams might contribute to the change in compression index with temperature at low stress levels. Ye et al. (2012) found that the critical state compressibility parameter λ, which is related to compression index, decreased with increase in temperature (from 20 to 80 °C), while the critical state compression parameter κ, which is related to swelling index, did not change with temperature for bentonite clay. This conclusion was not well supported by the limited data presented by Ye et al. (2012). Kirkham (2020) presented a comprehensive summary on the effect of temperature on compressibility of soils, with most of the findings in the literature agreeing with observations in this research.

Table 6-12: Compression characteristics of slurry-deposited and reconstituted London clay

Temperature (°C)	Slurry-deposited specimens		Reconstituted cake specimens	
	C_c	C_s	C_c	C_s
20	0.465	0.110	0.390	0.104
30	0.467	-	-	-
40	0.451	0.103	0.403	0.106
60	0.452	0.118	0.388	0.105
Linear regression for all data	0.458	0.110	0.394	0.105
Maximum difference	3.5%	14.6%	3.9%	1.9%

6.5.4 Effect of thermal cycling on the compression characteristics of soil

Regarding the effect of thermal cycling on pre-consolidation pressure, Plum and Esrig (1969) performed tests on a normally consolidated illite specimen which was subjected to a thermal cycle of 24-50-24°C. They found that temperature cycles, especially the cooling path, caused the illite to behave as if it were over consolidated, thus increasing the pre-consolidated pressure. The increase in over consolidation ratio due to temperature effect is referred to as 'thermally induced OCR', with the normal compression line shifted downwards, and the pre-consolidation pressure increased. Pre-consolidation pressure and the location of the normal compression line depends on the temperature history of the soil. This includes temperature level at which the test was performed at, under isothermal loading conditions, and temperature cycles that the soil was subjected to, even if there was no net change in temperature. These two factors can be treated in a way that are analogous to the effect of stress level and overconsolidation ratio, as in conventional one-dimensional compression tests at ambient temperature. The same effect

was observed by Gray (1936) where they reloaded the specimen after the cooling path. This contradicts with what was observed by Tidfors and Šallfors (1989), as they stated that the position of normal compression line and pre-consolidation pressure was only affected by temperature but did not change when there was no net change in temperature, as in the case of temperature cycles. Abuel-Naga et al. (2005) performed thermal cycling tests on soft Bangkok clay and found that thermally induced OCR did not change with stress level. For London clay specimen that went through temperature cycles of 20-40-20°C, pre-consolidation pressure did not change compared to that of the test performed at the same temperature but without temperature cycles. The discrepancy of the effect of thermal cycling on pre-consolidation pressure in this research and literature can be explained by reasons mentioned in Section 6.5.2.

6.6 Summary points

In this chapter, results from one-dimensional compression tests on slurry-deposited London clay and on specimens taken from a reconstituted London clay cake are presented. Specimens were tested under isothermal conditions, with thermal cycles, or with a prolonged creep period.

The following are the main observations:

- Compression and swelling indices of London clay were found insensitive to temperature levels when specimens were under isothermal loading conditions. This agrees with most of the observations from the literature.
- Normalised intrinsic compression curves obtained from one-dimensional compression tests on slurry-deposited London clay at different temperature levels agreed with the unique intrinsic compression line proposed by Burland (1990).
- Having a 3-month creep period did not change the compression characteristics of the clay, but this is probably because the length of the creep period was not extensive.
- For clay that was originally at ambient temperature but then subjected to thermal cycles of 20-40-20°C, the overall picture is that the compression and swelling indices were not affected by temperature cycles.
- Based on the stress and temperature range that was covered in this testing programme, it is difficult to draw a conclusion on how and whether the pre-consolidation pressure changed with temperature.

Chapter 7: Conclusions and recommendations for further work

7.1 Introduction

This research aims to study the thermo-hydro-mechanical behaviour of London clay, for the purpose of designing thermo-active structures. The main findings of this research are summarised in four sections, following the sequence that they are presented in this thesis. Recommendations for future work are proposed. These include improvement to the existing methodology and suggestions for future tests.

7.2 Methodology for thermal testing of saturated soils

Three pieces of equipment have been used for thermal testing of London clay in this research. A temperature-controlled isotropic apparatus was used for undrained heating tests, to investigate the effect of temperature on thermally-induced pore water pressures. It was designed by Martinez-Calonge (2017) at the ICGL and was enhanced with a mid-height pore pressure probe in the current research. This enables the measurement of pore water pressure at both the mid-height and the base of the specimen, and works as a back-up for pore pressure measurement, in case failure in the pressure transducer occurred in long-term testing that is normally associated with low permeability clay soils. The apparatus can supply a confining pressure of up to 800 kPa, and raising the temperature of cell water surrounding the specimen from 20 °C to 85 °C, with an accuracy of $\pm$0.5 °C.

A temperature-controlled triaxial apparatus with a double load-cell measuring system was developed to investigate the effect of temperature on thermal volumetric strains, strength and stiffness of saturated soils. This apparatus enables drained heating, followed by undrained shearing of London clay specimens at both ambient and elevated temperatures. It has the same capacity in temperature and pressure as the isotropic apparatus.

A temperature-controlled oedometer apparatus was developed for the determination of the compression characteristics of soils when subjected to changes in the applied vertical effective stress, under different temperature levels. Temperature of the specimen can be controlled from 20 to 70°C with an accuracy of $\pm$0.5°C. The soil specimens can be loaded to a maximum vertical stress of 7 MPa.

London clay was used as a testing material in this research. Its geological history, stratigraphy, details of how and where it was sourced, minerology were presented. Some basic classification tests were performed to characterise the material.

Mechanical and thermal calibrations were performed on the instrumentation and these calibrations were repeated at regular intervals, to ensure a satisfactory performance of the instrumentation. Consistent procedures for thermal testing of clays are developed and documented. Methods of calculating some of the quantities and corrections to the data are presented, including the equations and assumptions.

The design of the equipment, thermal and mechanical calibrations, testing procedures and corrections for data processing presented in this thesis serve as a reference to perform thermal testing on soils in the future, in an apparatus that has heaters installed internally into the top and bottom plates of the cell, as in the case of temperature-controlled triaxial and isotropic cell in this research.

7.3 Effect of temperature on the pore water pressures

For normally consolidated clays, thermally-induced pore water pressure increased with the increase of initial stresses, and most of the thermally-induced pore water pressure was reversible. Thermally-induced pore water pressure increased with the increase in the magnitude of temperature change but the relationship between the two was not linear.

For lightly overconsolidated clays (OCR=2 or 3), thermally-induced pore water pressure was a function of both the initial stresses and overconsolidation ratios. It increased with the increase of initial stresses but decreased with the increase of overconsolidation ratios.

Thermally-induced pore water pressure seemed to be less sensitive to stress level at high overconsolidation ratios (OCR=5 or 6). More laboratory evidence is necessary to confirm this observation. Amount of irreversible thermally-induced pore water pressure increased with the increase in overconsolidation ratios. This can be explained by the thermally-induced fabric change of clays, as this permanent disintegration of fabric was more obvious in overconsolidated clays.

Most of the irrecoverable pore water pressure was generated in the first thermal cycle. For the subsequent thermal cycles, most of the pore water pressure generated upon heating was recovered upon cooling. For tests with high OCR values, it took more thermal cycles for the change in pore water pressure to be repeatable compared to previous thermal cycles.

7.4 Effect of temperature on volume change, strength and stiffness

Normally consolidated London clay specimens exhibited contraction upon heating and thermally induced volumetric strains were irreversible upon cooling. Lightly overconsolidated (OCR=1.5 or 3) specimens contracted upon heating and the volumetric strains were reversible

when specimens were cooled to ambient temperature. Heavily overconsolidated (OCR=6) specimens dilated upon heating and the volumetric strains were reversible upon cooling. With increase in the OCR, the magnitude of contraction upon heating gradually decreased, until it turned to dilation at high OCR.

Peak strength and critical state stress ratio were insensitive to elevated temperature or a temperature cycle, in the stress range and temperature range tested in this research.

Both the short-term temperature intervention (one temperature cycle) and the long-term effect (holding the elevated temperature at a constant value) had influence on the soil stiffness. This is of particular importance when serviceability limit design is considered. It seemed that having one temperature cycle and elevated temperature had similar effect on the soil stiffness, but this is not conclusive based on the limited data from this research.

7.5 Effect of temperature on compression characteristics

For slurry-deposited specimens in a temperature-controlled oedometer apparatus, compression and swelling indices were not affected when the temperature changed from 20 to 60°C. For reconstituted London clay cake specimens, compression indices were largely insensitive to temperature levels examined. This agreed with most of the observations from literature in the temperature range of 4.4 to 55 °C on a range of clays.

Normalised intrinsic compression curves obtained from one-dimensional compression tests on slurry-deposited London clay at different temperature levels agreed with the unique intrinsic compression line proposed by Burland (1990).

Having a 3-month creep period did not show any effect on the compression characteristics. This is probably because the length of creep period was not extensive.

Having a thermal cycle of 20-40-20°C did not seem to affect the compression or swelling indices.

Based on the stress and temperature range that was covered in the testing programme, it is difficult to draw a conclusion on how the pre-consolidation pressure changed with temperature.

7.6 Recommendations for future work

7.6.1 Equipment improvement

Some potential modifications to the existing equipment are proposed below, to improve the performance and extend the capabilities of the equipment.

Temperature-controlled isotropic apparatus

In the current equipment, the maximum confining pressure that the cell can supply is 800 kPa. To avoid fluctuation at extreme pressures, the range of 50 kPa to 750 kPa was used in this research. To obtain a satisfactory degree of saturation before consolidation, the back pressure value was usually set at or above 250 kPa, which indicates that if the cell pressure was set to 750 kPa, the maximum mean effective stress that could be achieved is 500 kPa. This may not be sufficient for tests with high OCRs or high stress levels, in order to produce a larger range of initial stresses for testing at particular values of overconsolidation ratios. Increasing the maximum confining pressure that is allowed could further improve the capabilities of the equipment.

Temperature-controlled triaxial apparatus

In the current equipment, insulation was achieved by manually placing bubble wraps to cover the cell. An insulation chamber could be added to the equipment so that it would be more user friendly, and that would also ensure that heating could be achieved in a more controlled and consistent manner.

The maximum confining pressure can also be improved to allow tests with high OCRs or stress levels.

Since the triaxial cell is made of stainless steel, it is not straightforward to observe whether the load cell is in contact with the specimen or not. In the current configuration, the load cell was set to move towards the specimen at a very small displacement rate, until a small load (5 N) was measured, indicating that the load cell and the specimen was just in contact. This process could be improved by measuring the height of all the components in the cell, including the base pedestal, porous disc, friction reduction end and topcap, and then setting the location of the loading frame and load cell at a fixed location. This would improve the consistency of every test and avoid possible overload between the load cell and the specimen.

Temperature-controlled oedometer apparatus

In the current configuration, the confining ring is made of stainless steel. Other materials, for example, invar, could be used to minimise thermal deformation of the ring in the radial

direction. Installing displacement transducers in the radial direction could also be considered to quantify the thermal deformation of the apparatus. This measurement could be compared with the corrections applied to the data due to thermal deformation of the confining ring, as presented in Section 3.8.4.

An insulation chamber, or a soft shell made of foam, could be added to the cell, to reduce water evaporation and temperature fluctuation. The current configuration relies on manual topping up the cell with water, to compensate for the evaporation. This is not ideal especially for tests at high temperature levels, where water evaporates quickly. This could be improved by connecting the oedometer cell to a water tank that is at the same level as the water in the oedometer cell. In this way, water can be automatically topped up when the water in the cell is below the desired level.

7.6.2 Further testing

A number of additional tests on specimens with higher OCRs and different initial stress levels (for example, OCR=8 or 10, p'_{max} =300 or 450 kPa) could be performed in the temperature-controlled isotropic cell. If the maximum confining pressure of the isotropic cell can be improved, higher stress levels can also be applied. These additional tests aim to provide more information on whether the thermally-induced pore water pressure is stress level dependent at high OCRs.

Tests with multiple temperature cycles, or with larger change in temperature before undrained shearing could be performed in the temperature-controlled triaxial cell. The aim of this suite of tests would be to confirm whether the temperature cycle and elevated temperature have the same effect on the stiffness of clays, providing the maximum changes in temperature in both cases are the same.

One-dimensional compression tests with an extensive creep period under elevated temperature, for example, 6 months or even longer, could be performed. These tests would help to provide more information on the effect of creep period on compression characteristics.

The stress and temperature range covered in this research using the oedometer apparatus could be extended, to further explore the effect of temperature on the preconsolidation pressure.

References

Abuel-Naga, H. M., Bergado, D. T. and Bouazza, A. (2007a) Thermally induced volume change and excess pore water pressure of soft Bangkok clay. Engineering Geology, 89 (1-2), 144-154.

Abuel-Naga, H. M., Bergado, D. T., Bouazza, A. and Ramana, G. V. (2007b) Volume change behaviour of saturated clays under drained heating conditions: Experimental results and constitutive modeling. Canadian Geotechnical Journal, 44 (8), 942-956.

Abuel-Naga, H. M., Bergado, D. T. and Lim, B. F. (2007c) Effect of temperature on shear strength and yielding behavior of soft Bangkok clay. Soils and Foundations, 47 (3), 423-426.

Abuel-Naga, H. M., Bergado, D. T., Soralump, S. and Rujivipat, P. (2005) Thermal consolidation of soft Bangkok clay. Lowland Technology International. 7 (1), 13-21.

Abuel-Naga, H. M., Bergado, D. T., Ramana, G. V., Grino, L., Rujivipat, P. and Thet, Y. (2006) Experimental evaluation of engineering behavior of soft Bangkok clay under elevated temperature. Journal of Geotechnical and Geoenvironmental Engineering, 132 (7), 902-910.

ASTM (2004) ASTM D1776-04. Standard Practice for Conditioning and Testing Textiles. American Society for Testing and Materials, Pennsylvania.

Baldi, G., Borsetto, M. and Hueckel, T. (1987) Calibration of mathematical models for simulation of thermal, seepage and mechanical behaviour of Boom clay. Commission of the European Communities. Report number: EUR 10924.

Baldi, G., Hueckel, T., Peano, A. and Pellegrini, R. (1991a) Developments in modelling of thermo-hydro-geomechanical behaviour of Boom clay and clay-based buffer materials. Commission of the European Communities. Report number: EUR 13365/2.

Baldi, G., Hueckel, T., Peano, A. and Pellegrini, R. (1991b) Developments in modelling of thermo-hydro-geomechanical behaviour of Boom clay and clay-based buffer materials. Commission of the European Communities. Report number: EUR 13365/1.

Baldi, G., Hueckel, T. and Pellegrini, R. (1988) Thermal volume changes of the mineral-water system in low-porosity clay soils. Canadian Geotechnical Journal, 25 (4), 807-825.

Banks, D. (2012) An Introduction to Thermogeology: Ground Source Heating and Cooling. 2nd Edition. Chichester, Wiley-Blackwell.

Becker, D.R., Crooks, J.H.A, Been, K. and Jefferies, M.G. (1987) Work as criterion for determining in-situ and yield stresses clays. Can. Geotech. J. 24: 549-564.

Berry, F. G. (1979) Late Quaternary scour-hollows and related features in central London. Quarterly Journal of Engineering Geology. 12 (1), 9-29.

Bishop, A. W. and Henkel, D.J (1962) Measurement of Soil Properties in the Triaxial Test. Published by Edward Arnold.

Bishop, A. W., Webb, D. L. and Lewin, P. I. (1965) Undisturbed Samples of London Clay from the Ashford Common Shaft: Strength–Effective Stress Relationships. Géotechnique. 15 (1), 1-31.

Bishop, A.W. and Wesley, L.D. (1975) A hydraulic triaxial apparatus for controlled stress path testing. Géotechnique. 25 (4), 657-670.

Blitht, G.E., (1967) Effective stress evaluation for unsaturated soils. ASCE Journal of the Soil Mechanics and Foundations Division, 93 (SM2), 125-148.

Boudali, M., Leroueil, S., Srinivasa Murthy, B.R., (1994) Viscous behaviour of natural clays. In: Proceedings of the 13th International Conference on Soil Mechanics and Foundation Engineering, New Delhi, India, vol. 1, pp. 411–416.

Brandl, H. (2006) Energy foundations and other thermo-active ground structures. Geotechnique, 56 (2), 81-122.

British Geological Survey. (2016) The BGS Lexicon of Named Rock Units - London Clay Formation. Available from: http://www.bgs.ac.uk/Lexicon/lexicon.cfm?pub=LC [Accessed on 03 March 2022].

British Standard Institution. (1990) BS 1377: 1990 - Methods of test for soils for civil engineering purposes.

Burghignoli, A., Desideri, A. and Miliziano, S. (1992) Deformability of clays under non isothermal conditions. Rivista Italiana di Geotecnica, 4 227-236.

Burghignoli, A., Desideri, A. and Miliziano, S. (2000) A laboratory study on the thermomechanical behaviour of clayey soils. Canadian Geotechnical Journal, 37 (4), 764-780.

Burland, J. B. (1990) On the compressibility and shear strength of natural clays. Géotechnique. 40 (3), 329-378.

Burmister, D. (1951) The application of controlled test methods in consolidation testing. Fifty-Fourth Annual Meeting of the ASTM. Symposium on Consolidation Testing of Soils, Special Technical Publication 126, pp. 83-98. Atlantic City, NJ, 18 June 1951. Philadelphia, PA

Busby, J., Lewis, M., Reeves, H. and Lawley, R. (2009) Initial geological considerations before installing ground source heat pump systems. Quarterly Journal of Engineering Geology and Hydrogeology, 42 295-306.

Campanella, R. G. and Mitchell, J. K. (1963) Creep studies in saturated clays. ASTM-NRC of Canada, Symposium of Laboratory Shear Testing of Soils. September 1963, Ottawa, Canada. pp.90-103.

Campanella, R. G. and Mitchell, J. K. (1968) Influence of temperature variations on soil behaviour. Journal of the Soil Mechanics and Foundation Division. 94 (3), 709-734.

Casagrande, A. (1936) Determination of the pre-consolidation load and its practical significance, Proc. 1st Int. Conf. on Soil Mechanics and Foundation Engineering, Cambridge, Mass, Vol. 3: 60-64

Cekerevac, C. and Laloui, L. (2004) Experimental study of thermal effects on the mechanical behaviour of a clay. International Journal for Numerical and Analytical Methods in Geomechanics, 28 (3), 209-228.

Cekerevac, C., Laloui, L. and Vulliet, L. (2005) A Novel Triaxial Apparatus for Thermo-Mechanical Testing of Soils. Geotechnical Testing Journal. 28 (2), 161-170.

Çengel, Y. A., and A. J. Ghajar. (2011) Heat and mass transfer: Fundamentals and applications. 4th ed. New York: McGraw-Hill.

Chandler, R. J. (1966) The Measurement of Residual Strength in Triaxial Compression. Géotechnique, 16 (3), 181-186.

Chandler, R. J. (1968) A note on the measurement of strength in the undrained triaxial test. Géotechnique, 18, 261-266.

Chandler, R. J. and Apted, J. P. (1988) The effect of weathering on the strength of London Clay. Quarterly Journal of Engineering Geology. 21 (1), 59-68.

Cuccovillo T. and Coop M.R. (1997) The measurements of local axial strains in triaxial tests using LVDTs. Géotechnique, 47 (1), 167-171.

Cui, W., D. M. Potts, L. Zdravković, K. A. Gawecka, and D. M. G. Taborda. (2018) An alternative coupled thermo-hydro-mechanical finite element formulation for fully saturated soils. Comput. Geotech. 94 (Feb): 22–30.

Cui, Y.J., Sultan, N., Delage, P., (2000) A thermo-mechanical model for saturated clays. Canadian Geotechnical Journal 37, 607–620.

De Bruyn, D. and Thimus, J. F. (1996) The influence of temperature on mechanical characteristics of Boom clay: The results of an initial laboratory programme. Engineering Geology, 41 (1), 117-126

Delage, P., Sultan, N. and Cui, Y. J. (2000) On the thermal consolidation of Boom clay. Canadian Geotechnical Journal, 37 (2), 343-354.

Del Olmo, C., Fioravante, V., Gera, F., Hueckel, T., Mayor, J.-C., and Pellegrini, R. (1996) Thermo-mechanical properties of deep argillaceous formations. Engineering Geology, 41, 87–102.

Demars, K. R. and Charles, R. D. (1982) Soil volume changes induced by temperature cycling. Canadian Geotechnical Journal, 19 (2), 188-194.

Di Donna, A. and Laloui, L. (2015) Response of soil subjected to thermal cyclic loading: experimental and constitutive study. Engineering Geology, 190, 65–76.

Duffy, A. (2012) Essential physics [online]. Available from: https://www.webassign.net/question_assets/buelemphys1/chapter13/section13dash2.pdf [visited on March 2022].

Eriksson, L. G. (1989) Temperature effects on consolidation properties of sulphide clays. In: Proceedings of the 12th International Conference on Soil Mechanics and Foundation Engineering, 13-18 August 1989, Rio De Janeiro, Brazil. Rotterdam, Balkema Publishers. pp. 2087-2090.

Favero, V., Ferrari, A., and Laloui, L. (2016) Thermo-mechanical volume change behaviour of Opalinus clay. International Journal of Rock Mechanics and Mining Sciences, 90, 15–25.

Finn, F. (1952) The effect of temperature on the consolidation characteristics of remolded clay. Symposium on Consolidation Testing of Soils, New Jersey, USA, 65–71.

François, B. and Laloui, L. (2010) An oedometer for studying combined effects of temperature and suction on soils. Geotechnical Testing Journal, 33(2), 112–122.

François, B., Salager, S., El Youssoufi, M.S., Ubals Picanyol, D., Laloui, L., and Saix, C. (2007). Compression tests on a sandy silt at different suction and temperature levels. Geo-Denver: Computer Applications in Geotechnical Engineering, Denver, USA, 1–10.

Gasparre, A. (2005). Advanced laboratory characterisation of London clay. PhD thesis. Imperial College London, United Kingdom.

Gawecka, K.A., Taborda, D.M.G., Potts, D.M., Cui, W., Zdravkovic, L. and Kasri, M.S.H. (2017). Numerical modelling of thermo-active piles in London Clay. Proceedings of Institution of Civil Engineers. Geotechnical Engineering, 170, 201-219.

Gens, A. (1982). Stress-strain and strength characteristics of a low plasticity clay. PhD thesis. University of London, United Kingdom.

Ghahremannejad, B. (2003) Thermo-mechanical behaviour of two reconstituted clays. PhD thesis. University of Sydney, Australia.

Graham, J., Tanaka, N., Crilly, T., Alfaro, M., (2001). Modified Cam-Clay modeling of temperature effects in clays. Canadian Geotechnical Journal 38, 608–621.

Gray, H. (1936). Progress report on research on the consolidation of fine-grained soils. 1st International Conference on Soil Mechanics and Foundation Engineering, Massachusetts, USA, 138–141.

Hamada, Y., Saitoh, H., Nakamura, M., Kubota, H. and Ochifuji, K. (2007) Field performance of an energy pile system for space heating. Energy and Buildings, 39 (5), 517-24.

Head, K. H. (1998) Manual of soil laboratory testing. Volume 3, Effective stress tests. 3rd edition. Dunbeath, Whittles.

Hight D.W., McMillan, F., Powell, J.J.M., Jardine, R.J., Allenou, C.P. (2003) Some characteristics of London Clay. In: Tan, T. S. (ed.). Characterisation and Engineering Properties of Natural Soils, Volume 2. , CRC Press. 851-908.

Hueckel, T. and Baldi, G. (1990) Thermoplasticity of saturated clays: experimental constitutive study. ASCE Journal of Geotechnical and Geoenvironmental Engineering, 116 (12), 1778-1796.

Hueckel, T. and Pellegrini, R. (1991) Thermoplastic modeling of undrained failure of saturated clay due to heating. Soils and Foundations, 31 (3), 1-16.

Hueckel, T. and Pellegrini, R. (1992) Effective stress and water pressure in saturated clays during heating–cooling cycles. Canadian Geotechnical Journal, 29 (6), 1095-1102.

IAPWS (2007) Revised Release on the IAPWS Industrial Formulation 1997 for the Thermodynamic Properties of Water and Steam. Available at www.iapws.org.

Jaky, J. (1944). The coefficient of earth pressure at rest. In Hungarian (A nyugalmi nyomas tenyezoje). Journal of the Society of Hungarian Architects and Engineering, 355–358.

Janbu, N. (1963). Soil compressibility as determined by oedometer and triaxial tests. Proc. Euro. Conf. on Soil Mech. and Found. Eng. 1, 19-25.

Jardine R.J. (1985), Investigation of pile-soil behaviour with special reference to the foundations of offshore structures. PhD Thesis, University of London.

King, C. (1991) Stratigraphy of the London Clay (Early Eocene) in the Hampshire Basin. PhD Thesis. Kingston Polytechnic, UK.

King, C. (1981) The stratigraphy of the London Basin and associated deposits. Tertiary Research Special Paper 6 (Backhuys, Rotterdam).

Kirkham, A. (2020). Development of a new temperature-controlled oedometer. PhD thesis. Imperial College London, United Kingdom.

Kuntiwattanakul, P., Towhata, I., Ohishi, K. and Seko, I. (1995) Temperature effects on undrained shear characteristics of clay. Soils and Foundations, 35 (1), 147-147.

Lade, P. and Hernandez, S. (1977). Membrane Penetration Effects in Undrained Tests. Journal of the Geotechnical Engineering Division. 103, 109-125.

Laloui, L., Cekerevac, C., (2003). Thermo-plasticity of clays: an isotropic yield mechanism. Computer and Geotechnics 30 (8), 649–660.

Laloui, L. and Loria, A.F.R. (2020). Determination of design parameters for energy geostructures. Analysis and Design of Energy Geostructures, 821-932.

La Rochelle P., Leroueil S., Trak B., Blais-Leroux L. and Tavenas F. (1988), Observational approach to membrane and area corrections in triaxial tests. Advanced triaxial testing of soil and rock, Donaghe, Chaney Silver eds.

Li, C., Kong, G., Liu, H. and Abuel-Naga, H.M. (2018). Effect of temperature on behaviour of red clay–structure interface. Canadian Geotechnical Journal, 56 (1).

Lingnau, B. E., Graham, J. and Tanaka, N. (1995) Isothermal modeling of sand–bentonite mixtures at elevated temperatures. Canadian Geotechnical Journal, 32 (1), 78-88.

Lingnau, B. E., Graham, J., Yarechewski, D., Tanaka, N. and Gray, M. N. (1996) Effects of temperature on strength and compressibility of sand-bentonite buffer. Engineering Geology, 41 (1), 103-115.

Martinez-Calonge, D. (2017) Experimental investigation of the thermo-mechanical behaviour and thermal properties of London clay. PhD thesis. Imperial College London, United Kingdom.

Mitchell, J.K., (1993). Fundamental of Soil Behavior. J. Wiley and Sons, Inc., New York.

Moritz, L. (1995) Geotechnical properties of clay at elevated temperatures. Swedish Geotechnical Institute. Report number: 47.

Ng, C. W. W., Ma, Q. J. and Gunawan, A. (2016) Horizontal stress change of energy piles subjected to thermal cycles in sand. Computers and Geotechnics, 78 54-61.

Ng, C.W.W., Mu, Q., and Zhou, C. (2017). Effects of boundary conditions on cyclic thermal strains of clay and sand. Géotechnique Letters, 7(1), 73–78.

Paaswell, R.E. (1967). Temperature effects on clay soil consolidation. Journal of the Soil Mechanics and Foundations Division, 93(3), 9–22.

Plum, R. and Esrig, M. (1969). Effects of temperature on some engineering properties of clay soils. International Conference on Effects of Temperature and Heat on Engineering Behaviour of Soils, Washington, D.C., USA, 231–242.

Potts, D. M., and L. Zdravković. (1999). Finite element analysis in geotechnical engineering: Theory. London: Thomas Telford.

Potts, D. M., and L. Zdravković. (2001). Finite element analysis in geotechnical engineering: Application. London: Thomas Telford.

Pusch, R., Karnland, O., Hokmark, H., (1991). The nature of expanding clays as exemplified by the multifaced smectite mineral montmorillonite. Workshop on Stress Partitioning in Engineering Clay Barriers. Duke University, U.S.A.

Romero, E. (1999). Characterisation and thermo-hydro-mechanical behaviour of unsaturated Boom clay: an experimental study. Thesis (PhD). Universitat Politècnica de Catalunya.

Romero, E., Gens, A., and Lloret, A. (2001). Temperature effects on the hydraulic behaviour of an unsaturated clay. Geotechnical and Geological Engineering, 19(3-4), 311–332.

Romero, E., Villar, M.V., and Lloret, A. (2005). Thermo-hydro-mechanical behaviour of two heavily overconsolidated clays. Engineering Geology, 81(3), 255–268.

Roscoe, K.H. and Burland, J.B. (1968). On the generalized stress-strain behaviour of 'wet' clay, in: J. Heyman, F. Leckie (Eds.), Engineering plasticity, Cambridge University Press, Cambridge, 535-609.

Roscoe, K.H., Schofield, A.N. and Thurairajah, A. (1963). Yielding of Clays in States Wetter than Critical. Géotechnique, 13 (3), 211-240.

Sailer, E., Taborda, D.M.G., Zdravkovic, L., Potts, D.M. (2018). Factors affecting the thermo-mechanical response of a retaining wall under non-isothermal conditions. 9th European Conference on Numerical Methods in Geotechnical Engineering, 741-749.

Sandroni, S.S. (1977). The strength of London clay in total and effective stress terms. PhD thesis, Imperial College, University of London, United Kingdom.

Savvidou, C. and Britto, A. M. (1995) Numerical and experimental investigation of thermally induced effects in saturated clay. Soils and Foundations. 35 (1), 37-44.

Schmertmann, J.H. (1955). The undisturbed consolidation behavior of clay. Trans. ASCE, 120, 1201-1233

Shariatmadari, N. and Saeidijam, S. (2011). The effect of elevated temperature on compressibility and swelling of bentonite-sand mixtures. Electronic Journal of Geotechnical Engineering, 16, 137–146.

Sittidumrong, J., Jotisankasa, A., and Chantawarangul, K. (2019). Effect of thermal cycles on volumetric behavior of Bangkok sand. Geomechanics for Energy and the Environment, 20, 100-127.

Skempton A.W. (1944), Notes on the compressibility of clays. Q.J. Geological Soc. No.100, 119-135.

Skempton, A. W. (1961) Horizontal stresses in an overconsolidated Eocene clay. Proceedings of the 5th ICSMFE, Paris. 351-357

Som, N. N. (1968) The effect of stress path on the deformation and consolidation of London clay. PhD thesis, Imperial College, University of London, United Kingdom.

Sultan, N., Delage, P. and Cui, Y. J. (2002) Temperature effects on the volume change behaviour of Boom clay. Engineering Geology, 64 (2-3), 135-145.

Tanaka, N., Graham, J. and Crilly, T. (1997) Stress-strain behaviour of reconstituted illitic clay at different temperatures. Engineering Geology, 47 (4), 339-350.

Tidfors, M. and Šallfors, G. (1989). Temperature effect on preconsolidation pressure. Geotechnical Testing Journal, 12(1), 93–97.

Toll, D. (1999) A Data Acquisition and Control System for Geotechnical Testing. In: Kumar, B. & Topping, B. H. V. (eds.) Computing Developments in Civil and Structural Engineering. Edinburgh, 237-242.

Towhata, I., Kuntiwattanaku, P., Seko, I., and Ohishi, K. (1993). Volume change of clays induced by heating as observed in consolidation tests. Soils and Foundations, 33(4), 170–183.

Vega, A. and McCartney, J.S. (2015). Cyclic heating effects on thermal volume change of silt. Environmental Geotechnics, 2(5), 257–268.

Villar, M.V. and Lloret, A. (2004). Influence of temperature on the hydro-mechanical behaviour of a compacted bentonite. Applied Clay Science, 26(1-4), 337–350.

Webb D. L. (1964), The mechanical proprieties of undisturbed samples of London Clay and Pierre shale. PhD. Thesis, University of London.

Wood, C. J., Liu, H. and Riffat, S. B. (2009) Use of energy piles in a residential building, and effects on ground temperature and heat pump efficiency. Geotechnique, 59 (3), 287-290.

Yavari, N., Tang, A. M., Pereira, J.-M. and Hassen, G. (2014) A simple method for numerical modelling of mechanical behaviour of an energy pile. Géotechnique Letters, 4 (2), 119-124.

Yavari, N., Tang, A. M., Pereira, J.-M. and Hassen, G. (2016) Effect of temperature on the shear strength of soils and the soil–structure interface. Canadian Geotechnical Journal, 53 (7), 1186-1194.

Ye, W.-M., Zhang, Y.-W., Chen, B., Zheng, Z.-J., Chen, Y.-G., and Cui, Y.-J. (2012). Investigation on compression behaviour of highly compacted GMZ01 bentonite with suction and temperature control. Nuclear Engineering and Design, 252(1), 11–18.